UNIVERSITA' DEGLI STUDI DI PALERMO
Dottorato in Scienze della Terra e del Mare
Dipartimento di Scienze della Terra e del Mare
GEO/01

Paleoclimatic and Paleoceanographic reconstruction of the Pleistocene-Holocene through the study of planktonic foraminifera of two sedimentary cores collected in North Atlantic Ocean, southwest of the Azores Islands.

IL DOTTORE
Alessandro Bonfardeci

IL COORDINATORE
Prof. Alessandro Aiuppa

IL TUTOR
Prof. Antonio Caruso

CO TUTOR
Prof.ssa Annachiara Bartolini (MNHN-Parigi)

CICLO - XXIX
ANNO CONSEGUIMENTO TITOLO - 2016/2017

UNIVERSITÀ DEGLI STUDI DI PALERMO

Dottorato in Scienze della Terra e del Mare
Dipartimento di Scienze della Terra e del Mare
GEO/01

Paleoclimatic and Paleoceanographic reconstruction of the Pleistocene-Holocene through the study of planktonic foraminifera of two sedimentary cores collected in North Atlantic Ocean, southwest of the Azores Islands.

IL DOTTORE
Alessandro Bonfardeci

IL COORDINATORE
Prof. Alessandro Aiuppa

IL TUTOR
Prof. Antonio Caruso

CO TUTOR
Prof.ssa Annachiara Bartolini (MNHN-Parigi)

CICLO - XXIX
ANNO CONSEGUIMENTO TITOLO - 2016/2017

UNIVERSITÀ DEGLI STUDI DI PALERMO

Index

ACKNOWLEDGEMENTS

Firstly, I would like to express my sincere gratitude to all those responsible of my Ph.D. project, my tutor Prof. Antonio Caruso, my co-tutor Annachiara Bartolini and Dr. Marie-Madelaine Blanc-Valleron, for the continuous support, their knowledge, their motivation and, above all, for their patience. Their guidance helped me in all the phases of the research project, from the initial laboratory step, up to the final one, represented by the writing of this thesis.

I would also to thank the director of the Ph.D. school of the DiSTeM of Palermo, Prof. Alessandro Aiuppa, as well as the director of the Ph.D. school of the Muséum National d'Histoire Naturelle (MNHN), Prof. Nathalie Machon. I would also thank to the colleagues of the DiSTeM of Palermo and of the MNHN of Paris, who made possible the configuration and the realization of this Ph.D. project in joint-supervision. Thanks to this organization I had the opportunity to spend one year of my Ph.D. course at the MNHH of Paris.

Besides, I would particularly Dr. Slah Boulila, Dr. Franck Bassinot and Prof. Giuseppe Siani for their insightful comments and encouragement, but also for the hard question which incented me to widen my research from various perspectives.

I would also to thank very much Dr. Gulay Isguder and Fabien Dewilde, as well as all the research team of the Laboratoire des Sciences du Climat et de l'Environnement, where I carried out the isotope analyses.

I would to thank Ravi Dalliah who provided me an enormous help for laboratory analysis, without they precious support it would not be possible to conduct this research. I also thank very much to Dr. Sylvain Pont for its competence and its support to Scanning Electron Microscope analyses on planktonic foraminifera.

I would like to thank Prof. Francisco Sierro and Dr. Fabrizio Lirer for thorough and constructive comments that significantly improved the manuscript, as well as Dr. Nicola Pelosi for its support on data treatment.

Finally, I want to thank very much Dr. Francis Lucazeau, responsible of the OCEANOGRAFLU 2013 research project, during which the two sedimentary cores studied were collected. Moreover I would to thank to Dr. Francis Lucazeau for its financial support to AMS analyses, essential for the project.

Paleoclimatic and paleoceanographic reconstruction of Pleistocene-Holocene through the study of planktonic foraminifera of two sedimentary cores collected in the North Atlantic Ocean, southwest of the Azores Islands.

Introduction

This PhD project regards the "Paleoclimatic and paleoceanographic reconstruction of Pleistocene-Holocene through the study of planktonic foraminifera of two sedimentary cores collected in the North Atlantic Ocean, southwest of the Azores Islands" and has been performed in joint-supervision between the Departimento di Scienze della Terra e del Mare (DiSTeM) of University of Palermo (IT) and the Muséum National d'Histoire Naturelle of Paris, Centre de recherche sur la paléobiodiversité et les paléoenvironnements, CR2P, (FR).

The aim of this project was to do a high-resolution study of two sedimentary cores collected during the Oceanograflu cruise, carried out in June 2013, on board of the Atalante vessel. The cruise was supported by grants of IPGP (Institut de Physique du Globe de Paris), IFP (Institut Français du Pétrole), CNRS (Centre National de la Recherche Scientifique) and UPMC (Université Pierre et Marie Curie, Paris) to study the variable heat-flow patterns and hydrothermal processes near the Mid-Atlantic Ridge (MAR), south-west of the Azores archipelago.

During this cruise many (>200) heat-flow measurements were performed, 31 cores were sampled by means of a Küllenberg corer near the Oceanographer fracture zone (Fox et al., 1969). Thereafter the cores were stored at the core repository of the Muséum national d'Histoire Naturelle, Paris.

Two cores were selected, ATA13-OF-KT1 and ATA13-OF-KT18, collected respectively on the western and eastern side of the MAR.

1. Background and PhD proposal

Research on marine sediments and ice cores has demonstrated cyclical alternation of glacial and interglacial periods during the Quaternary. These climatic changes depend upon astronomical parameters (eccentricity, obliquity and precession), as explained by the Milankovitch theory (Milankovitch, 1948; Hays et al., 1976; Shakleton and Opdyke, 1977).

The astronomical forcing, joined to tectonic reorganization of the Earth's plates, induced the intense Neogene climatic changes.

The closure of Panama isthmus (3.1-2.5 Ma) induced the Gulf Stream formation, which is responsible of the intense moisture introduction at high latitudes of North Atlantic ocean and of the North Atlantic Deep Water (NADW) formation (Haug and Tiedemann, 1988; Duplessy, 1999), which favoured the Northern Hemisphere ice sheet growing and the global thermohaline circulation.

Some authors (Heinrich, 1988; Bond et al., 1993; Dansgaard et al., 1993; Broecker, 1994) have demonstrated the presence, in late Quaternary marine sediments, of rapid climatic variations caused by changes in solar output. D-O events (20) consist of an abrupt warming to near-interglacial conditions that occurred in a matter of decades, followed by a gradual cooling. (Dansgaard et al., 1993; Bond et al., 1993). Related to some of the coldest intervals between D-O events were six distinctive events, named after paleoclimatologist Hartmut Heinrich, that are recorded further North in Atlantic marine sediments as layers with a large amount of coarse-grained sediments derived from land (Heinrich, 1988; Bond et al. 1993; Broecker, 1994). These climatic fluctuations have a global imprint and radically modify oceanic circulation. In particular, Heinrich and Dansgaard-Oeschger events have been related to oscillations in NADW formation, with its weakening or shutdown during coldest phases (Alley, 1998).

All of these rapid millennial climatic variations are well registered by the diversity of planktonic foraminifera assemblages from oceanic down-core sediments. Relative abundances in the planktonic foraminiferal assemblages, and variations in the test isotope composition, represent powerful tool to study the Neogene climatic changes (Emiliani, 1955; Shackleton and Opdyke, 1977; Kucera et al., 2005). Their rapid and precise response to climatic changes gives also an evidence of periodic fluctuations in extension and strength of oceanic currents and gyres (Kucera, 2007).

Therefore, the pattern of surface and sub-surface currents in the North Atlantic Ocean has been modified, in response to climatic changes occurring during the Pleistocene and Holocene, affecting the planktonic foraminifera distribution. For the late Quaternary high amplitude (low-frequency) climatic cycles, such as glacial/interglacials alternations (Milankovian cycles), have been widely studied.

However high frequency (low periodicity) climatic changes are poorly studied in the central sector of the Atlantic Ocean. In the Azores sector few studies on living and recent planktonic foraminiferal assemblages (Ottens, 1991; Schiebel et al., 2002b; Storz et al., 2009)

have been performed to analyze the changes in strength and latitudinal position of the Azores Current (AC) (an eastward branch of Gulf Stream) and of the related Azores Front (AF).

This work has been focused on the North Atlantic climatic and hydrographic variability reconstruction during middle Pleistocene to Holocene through the analysis of planktonic foraminifera of two cores, collected south-westward of the Azores archipelago.

The aim is to obtain a high detailed eco-biozonation of the central North Atlantic and to appreciate if there are some differences in planktonic foraminiferal assemblages east and west of the Mid-Atlantic Ridge in the Azores region.

2. Geological setting of Azores region and cores location

The Azores archipelago is composed by seven volcanic islands, two of which are located in the western side of the Mid-Atlantic Ridge (MAR). This area is characterized by the presence of the Azores Plateau (Kurase and Watkins, 1970; Lourenço et al., 1998; Beier et al. 2015) and the Azores Triple Junction (Searle, 1980; Lourenço et al., 1998). The Azores Triple Junction (ATJ) is the point where the North American, Eurasian and African lithospheric plates meet (Fig.1). In this area several transform faults interrupt and displace the Mid-Atlantic ridge. Hipolito et al. (2013) suggested the existence of the Nubian (Azores) microplate, delimitated by three tectonic discontinuities: the Terceira Rift (Beier et al., 2008), to the north-east, East-Azores Fracture Zone to the south and a segment of the MAR to the west (Kurase and Watkins, 1970).

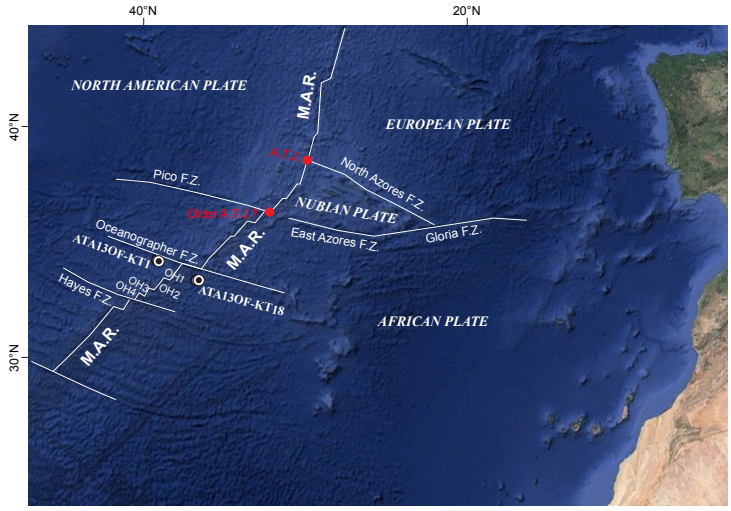

Figure 1. Geological setting of the Azores region with location of the studied cores. M.A.R.=Mid-Atlantic Ridge; A.T.J.=Azores Triple Junction.

Yang et al. (2006) consider the area around the Azores archipelago as the result of the interaction between a hotspot with a mid oceanic ridge (Mid-Atlantic Ridge). The presence of positive gravity and residual depth anomaly has been interpreted as the expression of a mantle plume (White et al. 1976; Guest et al. 1999). Moreover, Beier et al. (2010) interpreted the highest number of islands in the eastern side of the MAR, as due to the asymmetry of this mantle plume. In the outer parts of the Azores Plateau are present several basins formed by transform faults, which interrupt and displace the Mid-Atlantic Ridge. The study area is located between two of these important tectonic structures, the Oceanographer and Heyes transform faults (Fig. 2). For this reason, the sector was labelled ~~as~~ "Oceanographer-Heyes Fracture Zone" (OH) and subsequently subdivided into four minor segments (OH1 to OH4), from north to south (Detrick et al., 1995; Rabain et al., 2001).

Both cores were recovered in the northern part of OH1 (Bougault and Cande, 1982; Bideau et al. 1998; Rabain et al. 2001): ATA13-OF-KT1 on the western side of the MAR, ATA13-OF-KT18 on its eastern side (Fig.2). The estimated age of the oceanic crust at coring sites is ≈ 8.1 Ma, for ATA13-OF-KT1, and ≈ 9.7 Ma for ATA13-OF-KT18 (Rabain et al. 2001).

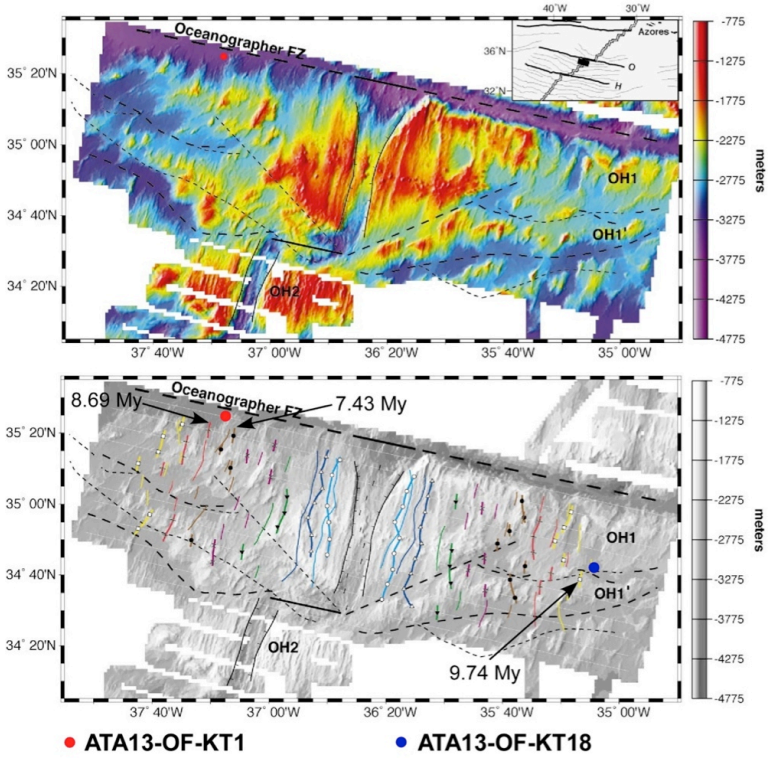

Figure 2. Core location as regards to the Oceanographer Fracture Zone (Modified by Rabain et al., 2001). The age of the oceanic crust below the sedimentary column, has been estimated, starting from the data of Rabain et al. (2001).

3. Materials and methods

3.1. ATA13-OF-KT1 and ATA13-OF-KT18 cores

Amongst the 31 cores collected during the Oceanograflu cruise, two of the longest and less bioturbated ones were selected, at different depths: ATA13-OF-KT1 core (35°24.956'N - 37°15.749'W; bathymetry=3,431 m; length=4.03 m) on the western side and ATA13-OF-KT18 (34°42.206'N - 35°07.334'W; bathymetry=2,801m; length=4.45 m) on the eastern side.

3.2. Cores sub-sampling and sedimentological analyses

ATA13-OF-KT1 and ATA13-OF-KT18 cores were sub-sampled at MNHN laboratories, using U-channels (1.8 cm width). Two U-channels were collected for each core, one for micropaleontology, the other for bulk sediment analysis (carbonatometry, mineralogy). Each U-channel was then sampled with 1 cm resolution, in order to obtain continuous data records. Each sample was weighed before and after being dried at 50°C to obtain its H_2O content, then washed over a 63-µm sieve. Afterward, the remaining part of the samples (> 63 µm) was oven dried at 50°C and weighed again to obtain the sand wt.%. This "sand fraction" usually corresponds to foraminifers, radiolarians and/or diatoms as there is almost no detrital components issued from the land. Micropaleontological and geochemical analyses were conducted on fraction greater than 63 µm, whilst carbonate content analysis on the bulk sediment. For the detailed description of carbonate content analysis see chapter 6.

On the basis of the preliminary onboard description of the cores, joined to carbonate H_2O and sand fraction contents, the lithologic logs of ATA13-OF-KT1 (Fig. 3) and ATA13-OF-KT18 (Fig. 4) cores have been produced.

The ATA13-OF-KT1 proxy records show cyclical oscillations with an evident negative correlation between carbonate and H_2O contents. This evidence confirms the assumption that the H_2O content may represent the non-carbonate aliquot of sediments, probably due to the increase of the clayey and/or biosiliceous fraction. Moreover, in ATA13-OF-KT1 core record a positive correlation between carbonate content and sand fraction is well discernable.

ATA13-OF-KT18 core also presents a cyclical trend of $CaCO_3$ and H_2O content variations, as well as a negative correlation between these sedimentary proxies. However,

unlike ATA13-OF-KT1 record, no correlation is evident between the carbonate and the sand fraction (Fig. 4).

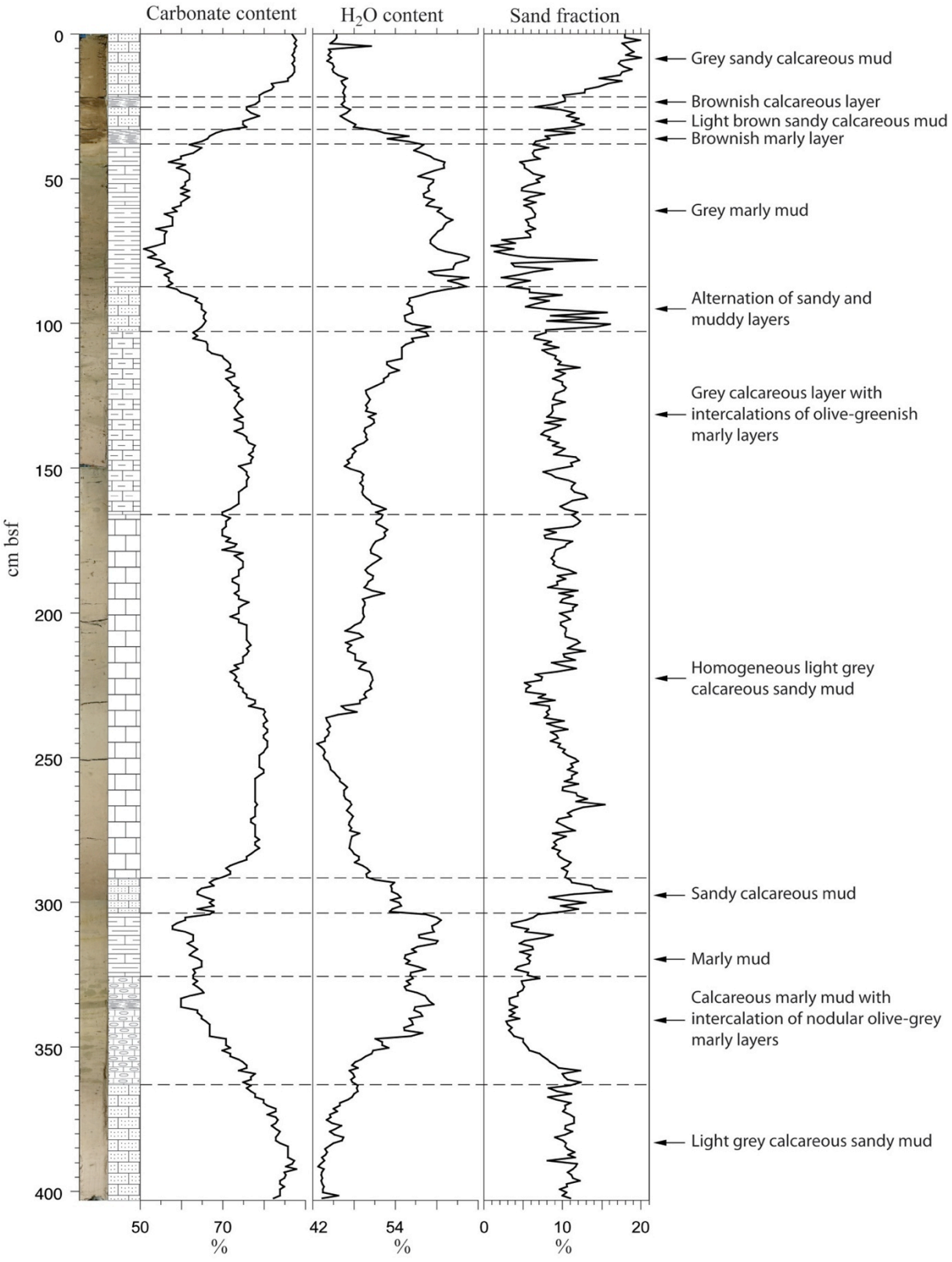

Figure 3. Lithologic log of ATA13-OF-KT1 core

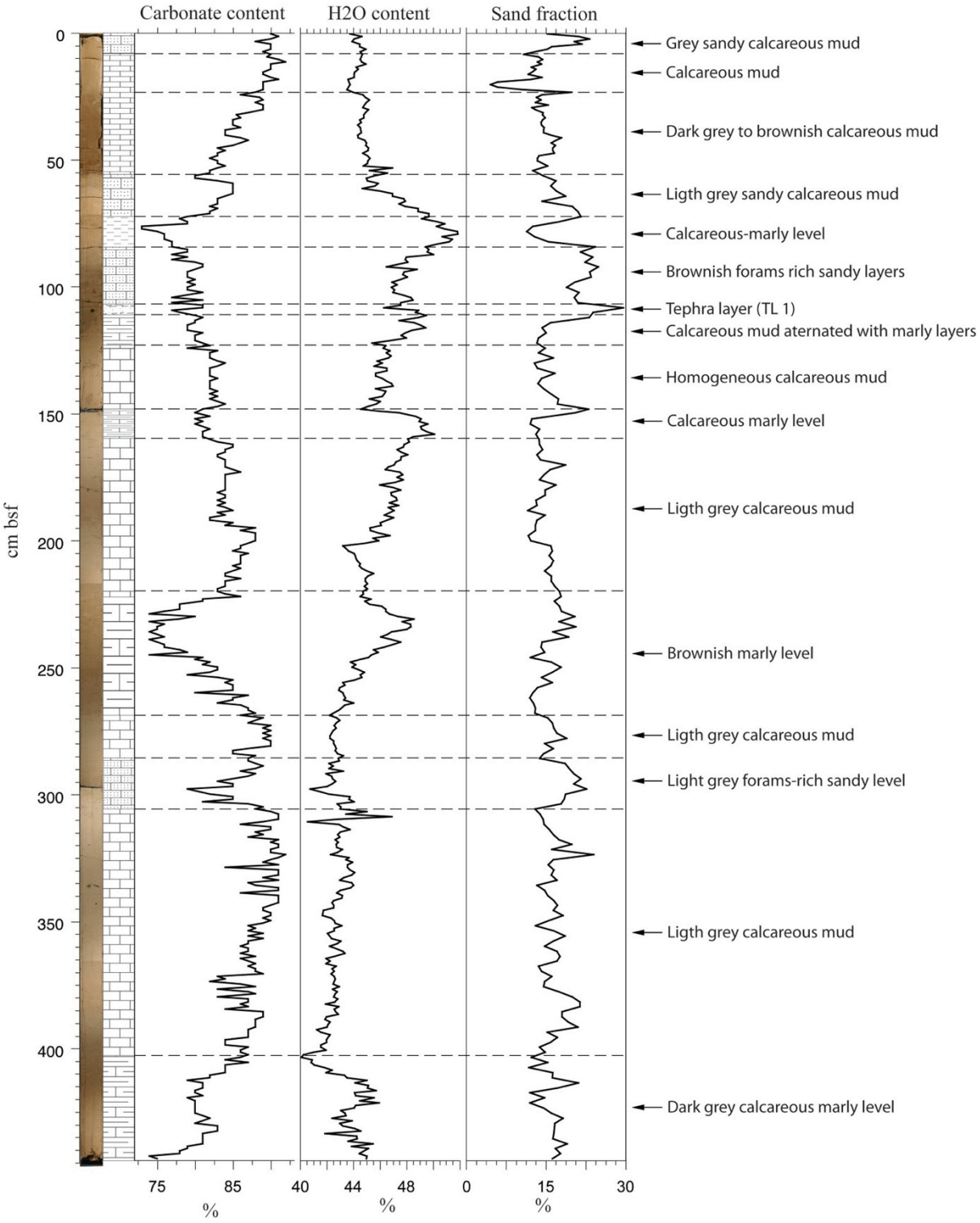

Figure 4. Lithologic log of ATA13-OF-KT18 core

3.3. ATA13-OF-KT18 tephra layer 1

At depth comprised between 108.5 and 110.5 cm bsf a tephra layer was found (TL 1).

In the size-fraction > 63 μm, a large amount of glass fragments was observed, together with some rare crystals of pyroxenes, olivine and plagioclase. Moreover at 109.5 cm bsf a pumice fragment of 1 cm width was recovered.

CAMECA® SX FIVE Electron microprobe analyses of glass and pumice fragments were performed at the CAMPARIS platform at the UPMC – ISTeP, in collaboration with Benoit Caron. These analyses revealed, in terms of major elements, a highly homogeneous chemically composition. Considering the chemical composition of the analysed glasses and the characteristics in terms of morphology, dimension and density of fragments, the volcanic products of TL 1 are considered belonging to the same eruption. The mean values obtained are around 62.9 % for SiO_2, 18 % for Al_2O_3, 13.2 % for total alkali, 7.4 % for Na_2O constantly more abundant than K_2O (5.9 %) and 3.1 % for $Fe_2O_{3(T)}$. The signature of the total alkali versus silica (Fig. 5) revealed a trachytic composition for TL 1.

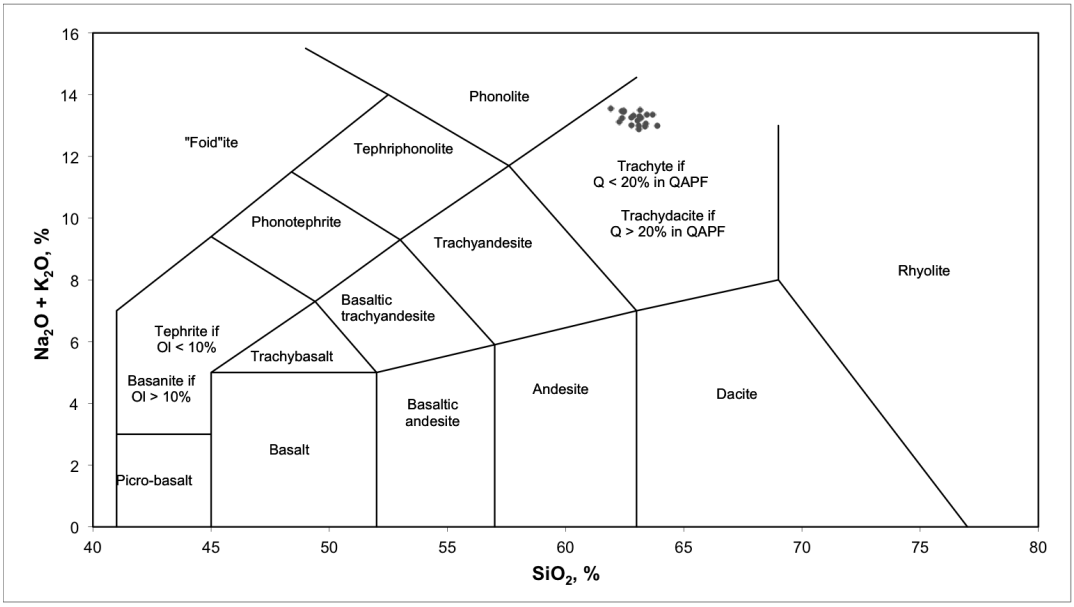

Figure 5. Total Alkali vs. Silica plot with classification of La Maitre et al. (1989). Results show as the chemic composition of the TL1, in terms of major elements, is highly homogeneous and that is trachytic in composition.

Based on published data related to nearby glass samples (submarine or inland), a preliminary correlation with eruptions studied in the Azores archipelago has been hypothesized. The chemical composition and the stratigraphic position of the TL 1 event

suggest the Furnas Volcano, São Miguel Island, as a possible source of the studied eruption. According to Guest et al. (1999) and Duncan et al. (1999), two high magnitude trachytic eruptions may be related to the range of TL 1: the Provoação Ignimbrite Fmn, dated at ~30 ka and the Tufo Fmn at ~27 ka. Further analyses on this tephra layer are in progress. The origin and timing of this eruption are important to add another tie point for ATA13-OF-KT18 calibration, as well as to provide more informations on the atmospheric setting of the Azores region during the past.

4. Planktonic foraminiferał in central North Atlantic

The microplaeontological and geochemical analyses have been conducted on planktonic foraminifera. Their identification and classification is based on Rögl & Bolli (1973), Saito et al. (1981), Kennett & Srinivasan (1983), Bolli et al. (1985), Hemleben et al. (1989) and BouDagher-Fadel (2013).

In total, 61 taxa have been identified and counted, including species, sub-species, specimens identified only at genus level, here labelled as $sp._n$, and also morphotypes and chromotypes of certain species.

The distribution and relative abundance of each taxon in the planktonic foraminiferal assemblages are controlled by several limiting factors, even if the sea surface temperature (SST), is probably the main controller (Kucera, 2007). Living planktonic foraminifera are the best indicators for hydrographic properties, such as temperature, salinity, nutrient content and therefore they are widely used for paleoceanographic reconstructions (Kucera, 2007). Many authors developed biogeographic distributional zonation of planktonic foraminifera (Bé & Torderlund, 1971; Bé, 1977; Vincent & Berger, 1981). These latter distributions reflect the ecological preferences of planktonic foraminifera, in terms of limiting factors of the water masses in which they live. Moreover, if almost all species could tolerate considerable range of SST, maximum abundance is restricted to their optimum range (Bé & Torderlund, 1971; Kucera, 2005). Therefore, the dependence of these species for determinate water masses, is responsible for their horizontal and vertical distribution in modern ocean domains and minor basins (Bé and Torderlund, 1971; Bé, 1971; Hemleben et al., 1989).

According to Bradshaw (1959), Bé and Torderlund (1971), Bé (1977), and Vincent and Berger (1981), the recent planktonic foraminifera are distributed in five zoographic provinces. The layout of these five faunal provinces depends on the temperature of surface water masses and then they are differentiated in specific latitudinal belts (Fig. 6).

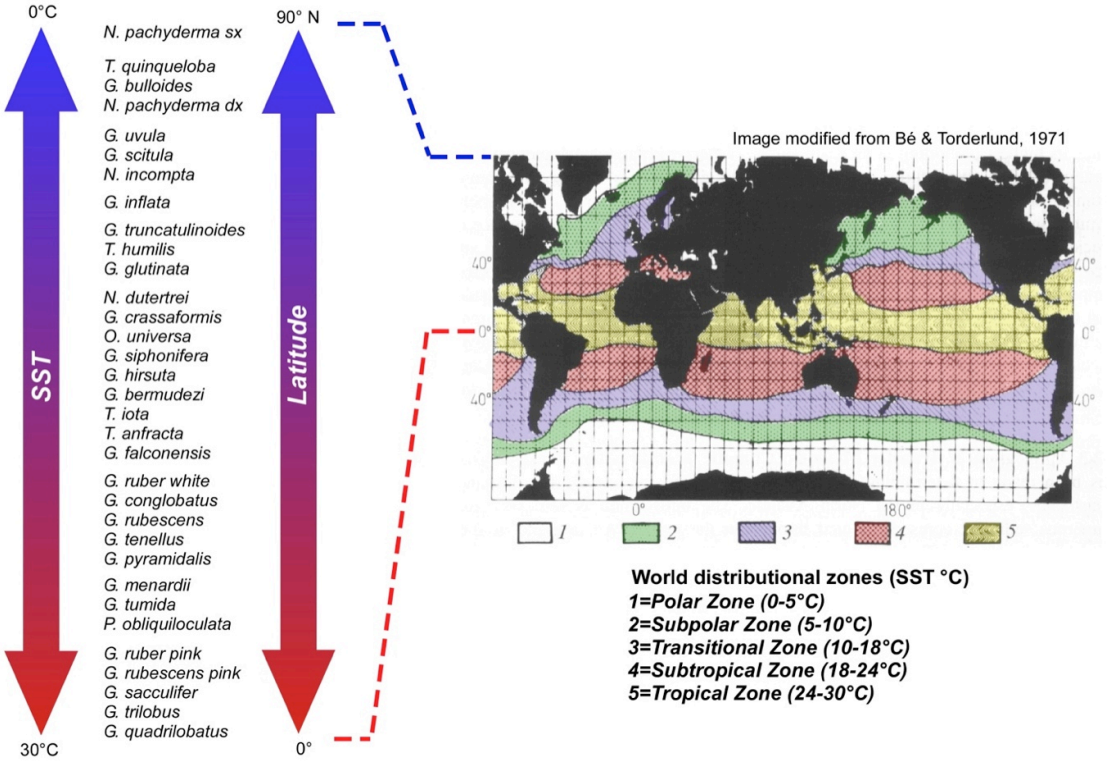

Figure 6. World distributional zones of planktonic foraminifera (Modified from Bé and Torderlund, 1971). The species planktonic foraminiferal species, recognised in ATA13-OF-KT1 and ATA13-OF-KT18 core records, are reported on the left of this plot. Depending on their ecological preferences, each species occupies a specific position as regards to the latitude and the SST, in the North Atlantic Ocean.

If the temperature of seawater masses forces their distribution within these provinces, other factors, such as salinity, nutrient availability, turbidity, presence of predators and/or competitors, influence as well their relative abundance in the assemblage (Torderlund and Bé, 1971; Bijma et al., 1990b; Schiebel et al., 1991; Schiebel and Hemleben, 2005). On average, the specific richness and the population density decreases toward the higher latitudes, in each oceanic realm.

Kucera (2007) proposed an alternative zoogeographical zonation, also based on the relative abundance of species in the assemblages (Fig. 7).

Moreover, planktonic foraminiferal species dwell at specific depth in water column, related to their ecological preferences, such as temperature, salinity, food availability, turbidity, reproduction strategies (Schiebel et Kucera, 2005). During the seasonal alternations the planktonic foraminiferal assemblages are subject to changes in water column depth position and abundance of species (Bé and Torderlund, 1971, Bé, 1977; Schiebel et al., 2002b). During the summer the PF assemblage is composed of a larger number of species and

some species reach deeper positions, due to higher temperature of the water column. On the contrary, a reduced faunal diversity has been observed during the winter.

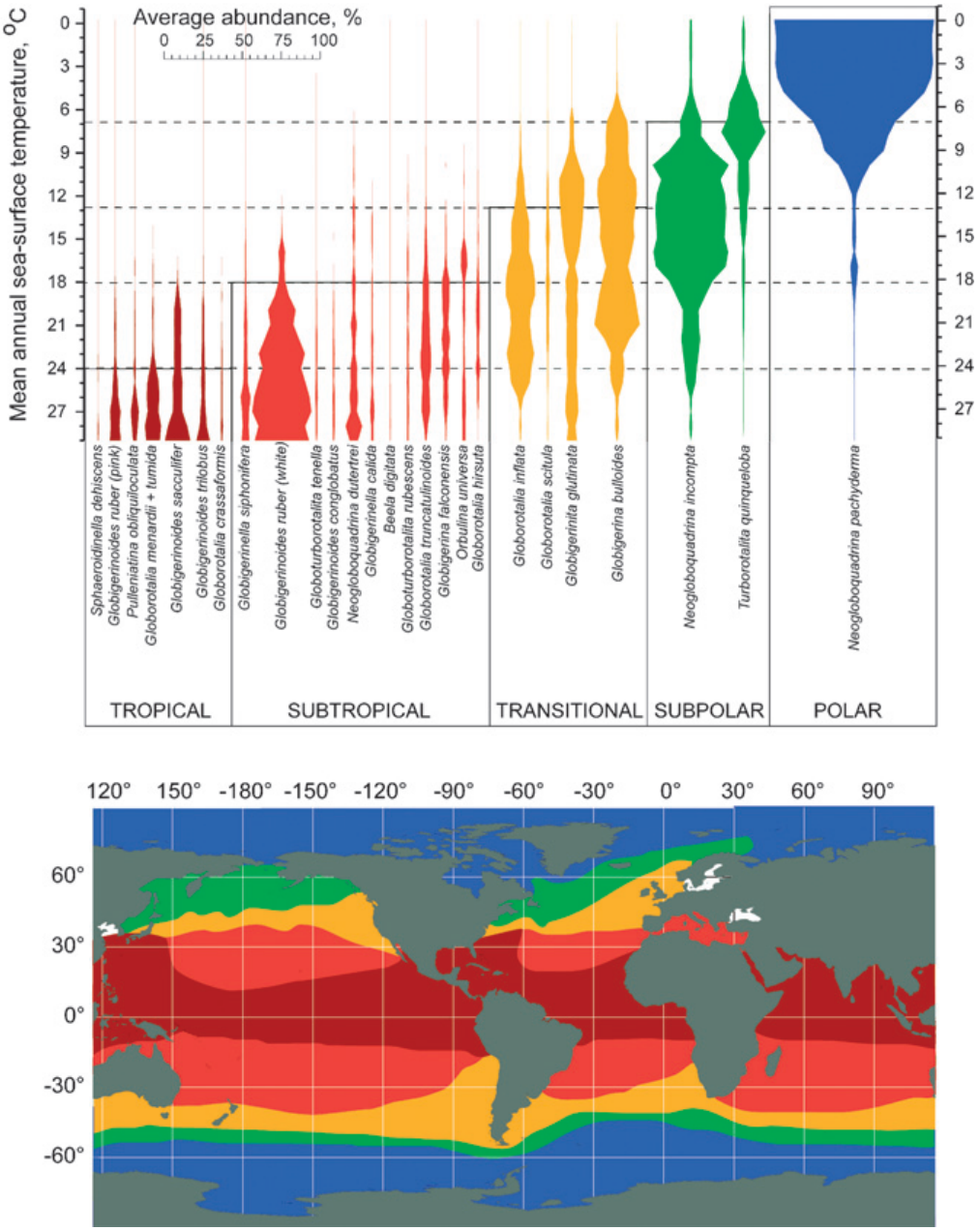

Figure 7. Planktonic foraminiferal provinces of the modern oceans (modified from Kucera, 2007). Each zoogeographic province is characterised by specific association, increasing in diversity toward the equator.

Moreover, the specific depth habitat is reduced, with almost all taxa dwelling in surface and sub-surface waters.

In figure 8 and 9 the seasonal habitat depth and distribution of the principal species or group of species dwelling in the Azores region, are shown.

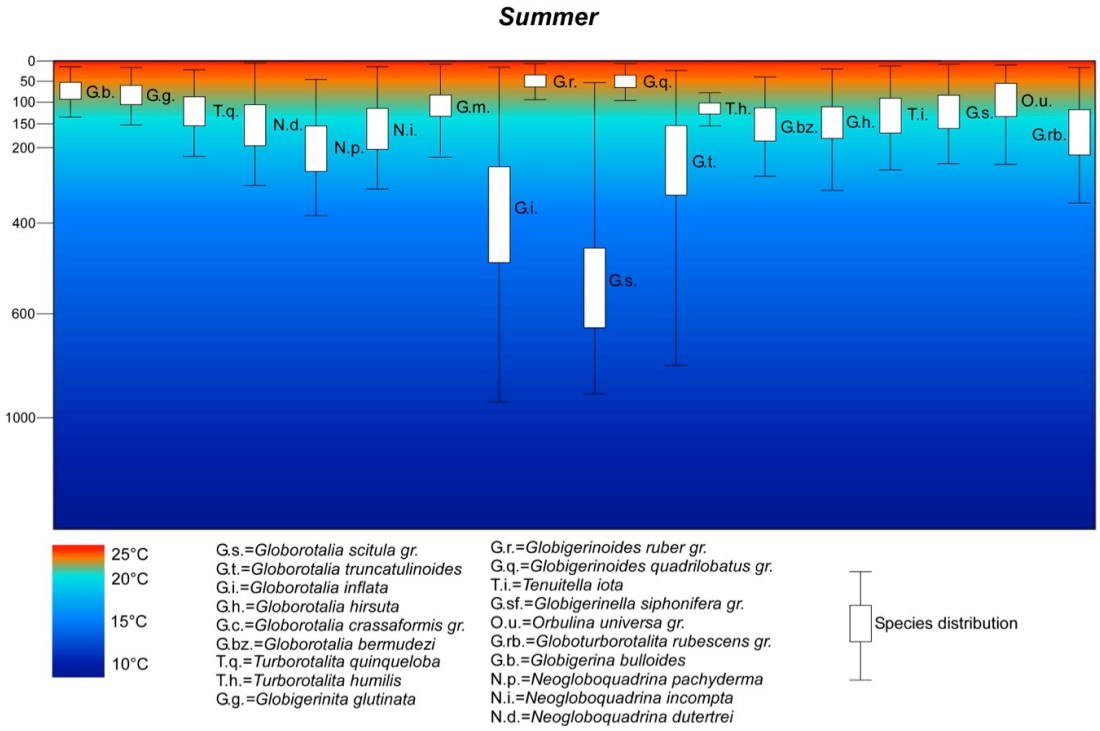

Figure 8. Planktonic foraminifera vertical positions and distributions in the Azores region, during the summer, starting from the data published by Schiebel et al. (2001 and 2002a-b).

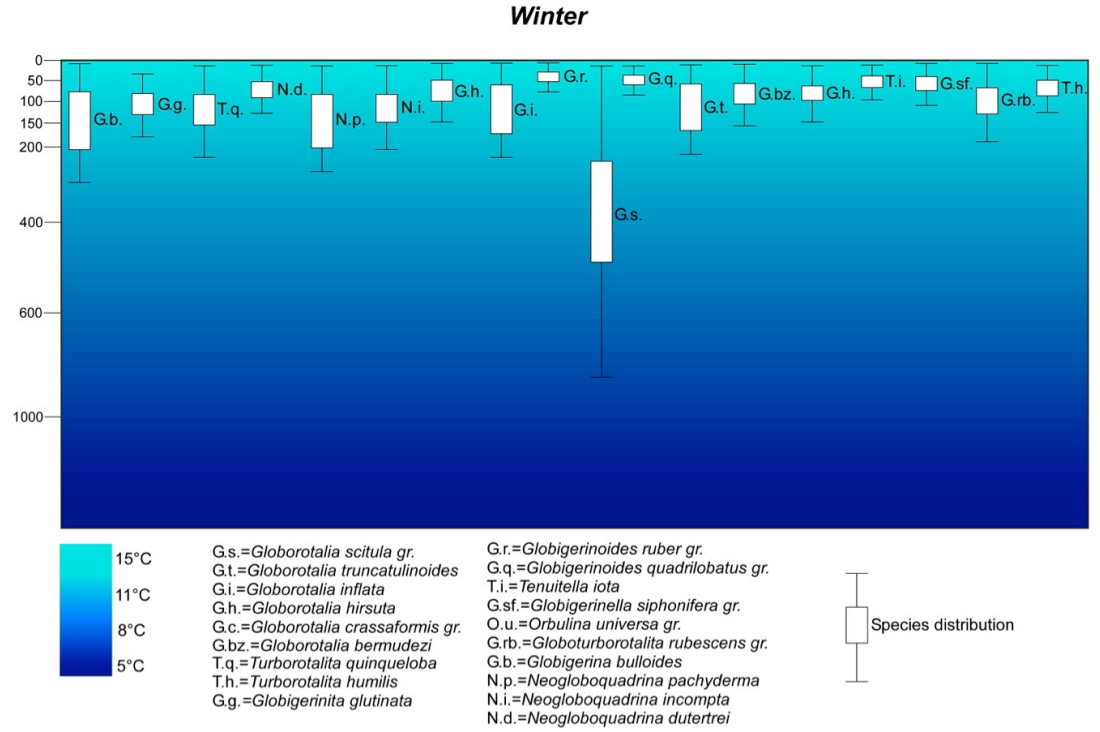

Figure 9. Planktonic foraminifera vertical positions and distributions in the Azores region, during the winter, starting from the data published by Schiebel et al. (2001 and 2002a-b).

5. Thesis manuscript structure

The manuscript is structured in three interconnected articles-chapters presenting the major results and their interpretation.

1) The main objectives of the first article-chapter, intituled "*Palaeoclimatic reconstruction and carbonate content of two sedimentary cores from the central North Atlantic (Azores region) during middle Pleistocene-Holocene*", were to i) establish the most precise possible age-model for the two studied cores, and ii) reconstruct the carbonate production/preservation history in the Azores area during the last glacial cycle (0-150 kys). To achieve these objectives, high-resolution carbonate content and $\delta^{18}O_{G.\ ruber}$ down core data were analysed. Moreover, planktonic foraminiferal assemblage census combined with Modern Analog Technique (SST-mat) allowed finely reconstructing Sea Surface Temperature (SST) variations. The curves of planktonic foraminiferal dissolution resistant and susceptible species were traced to depict eventual intervals of increasing dissolution. For the uppermost interval of both the two cores, mass spectrometry (AMS) ^{14}C ages have been also performed on planktonic foraminiferal tests. Two different approaches have been compared to establish the best possible age model for the two studied cores: the insolation-based astronomical tuning and the stratigraphic alignment with the high-resolution North Atlantic MD95-2042 $\delta^{18}O_{G.\ bulloides}$ record (Shackleton et al. 2000), recently recalibrated using the LS16 global $\delta^{18}O$ stack (Lisiecki and Stern 2016). Once established the age model, it was possible to highlight how orbital and sub-orbital forcing strongly controlled the stable isotope and carbonate content oscillations of the Azores region, during the last 144 ka. In particular, the high-frequency fluctuations observed in the $\delta^{18}O_{G.\ ruber}$ and carbonate content record, have been well correlated with the quasi-periodic rapid climatic oscillations linked to Heinrich and Dansgaard-Oeschger related events. The comparison of the carbonate and dissolution resistant species abundance curves between the two cores, situated at different bathymetries, allows tracing the vertical displacements of the calcite lysocline during the last 144 ka. Then the carbonate production/preservation history of Azores area was related to the Atlantic Meridional Overturning Circulation strengthening/weakening phases at orbital and millennial time scale.

2) The second article-chapter, intituled "*Planktonic foraminifera as tracers of central North Atlantic (Azores region) hydrographic changes during the last 144 kyr*" unravels the complex central North Atlantic surface hydrographic and paleoproductivity variability history, during the last 144 kyr. In this work, high-resolution census analyses on planktonic foraminiferal assemblages, combined with Modern Analog Technique sea surface temperatures reconstructions have been used to reconstruct the last 144 ka hydrographical and climatic variability of the central North Atlantic. Some selected species, which, at present, characterize specific water masses and surface front/current systems of the North Atlantic, have been used as paleoceanographic tracers. Therefore, the relative abundance fluctuations of these species have been used as indexes of the position occupied by these water masses. The adopted approach aims to evaluate the latitudinal/longitudinal migration of Azores Front/Current System, during the late Quaternary, as well as of the other fronts and currents characterising the central North Atlantic hydrographic pattern.

3) The third article-chapter, intituled "*Distribution and ecology of the G. ruber – G. elongatus eco-morphotypes in the Azores region during Late Pleistocene-Holocene*", is focused on *G. ruber* gr. variability, in the Azores region. Through its test chemistry and stable isotopic composition it is extensively used for reconstructing past sea-surface temperature and salinity variations. However, the taxonomic of this species has changed as *G. ruber* was considered as *plexus* regrouping several species and sub-species previously defined. More recently, molecular and geochemical studies evidenced the presence of different genotypes within *G. ruber plexus*, implying different habitats of calcification and ecological preferences and so different species. So, despite a large number of works in the last years on the *G. ruber-G. elongatus* plexus, the link between genotype, morphological variants and ecological preferences and their calcification habitat, is still not well understood. Here an "alternative" approach is presented to test the relationship between *G. ruber-G. elongatus* morphological variability and environmental conditions at glacial-interglacial scale, through high resolution quantitative micropaleontological and geochemical analyses of the last 85.3 kyr downcore sediments from the Azores region. A fine identification and characterization of each eco-morphotype/morphospecies has been adopted, adding even more poorly studied forms, such as *G. pyramidalis* and *G. cyclostomus*.

Finally, this study allowed to recognise several eco-morphotypes in the *G. ruber – G. elongatus* population of the central North Atlantic, which were used as tracers of Subtropical Gyre and Azores Front Current System displacements.

6. Paleoclimatic reconstruction and carbonate content of two sedimentary cores from the central North Atlantic (Azores region) during middle Pleistocene-Holocene

Bonfardeci A.[1-2], Caruso A.[1], Boulila S.[3], Blanc-Valleron M.M.[2], Bartolini A.[2], Bassinot F.[4], Siani. G.[5]

1- Dipartimento di Scienze della Terra e del Mare, Università degli studi di Palermo, via Archirafi 20-22, 90123 Palermo, Italy

2- CNRS – UMR 7207 CR2P, MNHN, 8, rue Buffon, 75005 Paris, France

3- Université Paris VI, CNRS – UMR 7193, ISTeP Institut des Sciences de la Terre-Paris, case 117, 4, place Jussieu, 75252 Paris, France

4- LSCE-IPSL, Unité Mixte CEA-CNRS, Domaine du CNRS, Gif sur Yvette, 91190, France

5- LSCE, Domaine du CNRS, Avenue de la Terrasse, F-91118 Gif sur Yvette, France

Keywords: North Atlantic, Azores, Stable isotopes, Carbonate content, orbital- and millennial-scale climatic phases, last climate cycle

6.1 Abstract

High-resolution carbonate content and $\delta^{18}O_{\ G.\ ruber}$ records from two cores (ATA13-OF-KT1 and ATA13-OF-KT18) recovered south-westward of the Azores archipelago, provide powerful tools to reconstruct the carbonate production/preservation history, by relating it to the palaeoclimatic and hydrographic variability at orbital and millennial time scales, for the last 144 kyr. Two different approaches have been compared to establish the best possible age model for the two studied cores: the insolation-based astronomical tuning and the stratigraphic alignment with the high-resolution North Atlantic MD95-2042 $\delta^{18}O_{G.\ bulloides}$ record (Shackleton et al. 2000), recently recalibrated using the LS16 global δ18O stack (Lisiecki and Stern 2016). The spectral analysis and the wavelet treatment of the time series, produced with these two different approaches, indicated that the tuning strategy based on the correlation with the MD95-2042 $\delta^{18}O_{G.\ bulloides}$ record, is the most plausible. The adopted age model permits to establish that the ATA13-OF-KT1 core spans the interval between 2.75 and 81.94 ka (from MISs 1 to 5.1), and ATA13-OF-KT18 the interval between 3.36 and 143.8 ka (from MISs 1 to 6).

The spectral analysis of the $\delta^{18}O_{\ G.\ ruber}$ and carbonate signals, for the last 144 kyr, show periodicities of 23.5 (ATA13-OF-KT18) and 21.2 ka (ATA13-OF-KT1) coherent with the precessional band. Furthermore, the high-frequency fluctuations observed are well correlated with the quasi-periodic climatic oscillations related to Heinrich and Dansgaard-Oeschger events.

The data suggest that $\delta^{18}O_{\ G.\ ruber}$ fluctuations, carbonate production and its preservation are controlled by glacial/interglacial variations that strongly modified the paleoceanograhic circulation of the Northern Atlantic in this Azores region. This area is indeed a very sensitive region to understand the Atlantic Meridional Overturning Circulation (AMOC) system in the North Atlantic, which was likely weaker during glacials, whereas it shows an opposite behaviour during the strongest interglacials (i.e. MIS 5.5 and 1). We highlighted that during some of the more extreme Heinrich related cold climatic events, the AMOC shut down might have caused important shallowing of the calcite lysocline in the central North Atlantic and enhanced deep dissolution of the carbonate fraction: at 22.1 kyr (LGM) the lysocline was probably positioned around 1,000 m above its actual position (3,431 mbsf instead of 4,500 m bsf in the Azores area).

6.2 Introduction

Paleoclimatic proxies, such as stable isotopes, biomarker fluctuations and carbonate content of marine sediments contain the evidence of the Earth's orbital forcing (Hays et al. 1976). Starting from this assumption, the paleoclimatic indicators have been widely used to understand the mechanisms and the periodicities of these orbital-forced climatic fluctuations and represent a powerful tool to develop highly accurate geochronologies (Imbrie et al. 1984; Shackleton et al. 1990; Tiedemann et al., 1994; Bassinot et al. 1994; Grutzner et al. 2002). Moreover, Martinson et al. (1987) demonstrated that the tuning approach based on insolation rate, ice volume models, precession and/or obliquity, produces equivalent results.

In the global climatic system, the North Atlantic Ocean is considered as a highly sensitive region, which plays a crucial role in the Northern Hemisphere dynamics. Moreover, the pioneer of the astronomical theory of Earth's climate (Milankovitch, 1930), realised that the first response to orbital forcing is likely registered in the high latitudes of the North Atlantic (Berger, 2013). To understand the complexity of climate dynamics, it is necessary to integrate the studies of the atmospheric and oceanic spheres.

Starting from the end of the '60s to the present, DSDP and then ODP and IODP

projects, have provided a lot of data to shed light on the geologic history of the Atlantic domain. Furthermore, other North Atlantic deep-sea sampling and relative studies have been carried out during Marion Dufresne and Meteor expeditions. Several paleoclimatic studies have been performed at the low and medium latitudes of the North Atlantic Ocean, in particular as regard to the eastern North American area (Hagen and Keigwin, 2002; Grutzner et al. 2002; Billups and Scheinwald, 2014; Billups et al. 2016) and Iberian margins (de Abreu et al. 2003; Shackleton et al. 2004; Martrat et al. 2007; Hodell et al., 2013). However, in the North Atlantic Ocean south-west of the Azores archipelago only few researchers have carried out paleoenvironmental reconstructions, based on sedimentological and micropaleontological proxies (Chapman and Shackleton, 1998; Chapman et al. 2000; Schiebel et al. 2002b). High-resolution studies have regarded only the last 16 ka (Schwaab et al. 2012; Repschläger et al. 2015).

Many authors tuned sedimentary records to oxygen isotope records provided by GRIP (Greenland Ice-Core Project members, 1993), GISP2 (Greenland Ice Sheet Project, Grootes et al., 1993) and NGRIP (North Greenland Ice Core Project members, 2004) ice cores. This approach has provided accurate information as regard to glacial/interglacial cycles and millennial-scale variability, describing in detail the climatic oscillations (Chapman and Shackleton, 1998; Bond et al., 1993; Dansgaard et al., 1993; Broecker, 1994; Chapman et al. 2000; Eynaud et al., 2009; Martrat et al., 2007).

Recently, Lisiecki and Stern (2016) aligning North Atlantic SST, IRD stack, Greenland ice core record and millennial variability in speleothems, produced an age model for the global benthic foraminifera $\delta^{18}O$. These authors revised the model proposed by Lisiecki and Raymo (2004), as regards to the last climate cycle (the last 150 kyr). Furthermore, the use of $\delta^{18}O_{G.\ bulloides}$ record of the MD95-2042 core (LS16), as reference time series for developing the age model, is justified by the fact that the Iberian margin sediments have a very high sedimentation rate and are very sensitive to climate changes at both orbital- and millennial-scale (Lisiecki and Stern, 2016; Hodell et al., 2013 and reference therein). Moreover, many authors showed as the $d^{18}O_{G.\ bulloides}$ and SST records of that core are perfectly correlated to the Greenland $\delta^{18}O_{ice}$, whereas the benthic $\delta^{18}O$ record fluctuations are coherent with the temperature record of Antarctica (Lisiecki and Stern, 2016; Hodell et al., 2013; Martrat et al., 2007; Shackleton et al., 2004; Shackleton et al., 2000).

In this work we propose a robust age model for the last climate cycle, based on the accurate correlation of the oxygen isotope and carbonate content records of two deep

sedimentary cores of the Azores region to the $\delta^{18}O_{G.\ bulloides}$ record of the MD95-2042 core (LS16), testing the response of the studied proxies to the astronomical forcing. Hence, this calibration could provide new insights to obtain a precise chronology for the paleoclimate events occurring in this region during the late Quaternary.

Moreover, the great climate sensitivity of the chosen proxies (carbonate content, $\delta^{18}O_{G.\ ruber}$), their high resolution sampling and fine analysis treatment, allow to analyse the high frequency cyclic fluctuations, linked to sub-Milankovitch periodicities, likely related to the rapid climatic Heinrich and Dansgaard-Oeschger events. The comparison of the carbonate and dissolution resistant species abundance curves between the two cores, situated at different bathymetries, allows traking the vertical displacements of the calcite lysocline during the last 144 ka, and so the carbonate production/preservation history of Azores area at orbital and millennial time scale.

6.3 North Atlantic oceanographic setting

The complex North Atlantic climate system primarily depends on the exchanges between atmosphere and ocean. These exchanges regulate the delicate balance between surface and deep seawater circulation in oceanic realms.

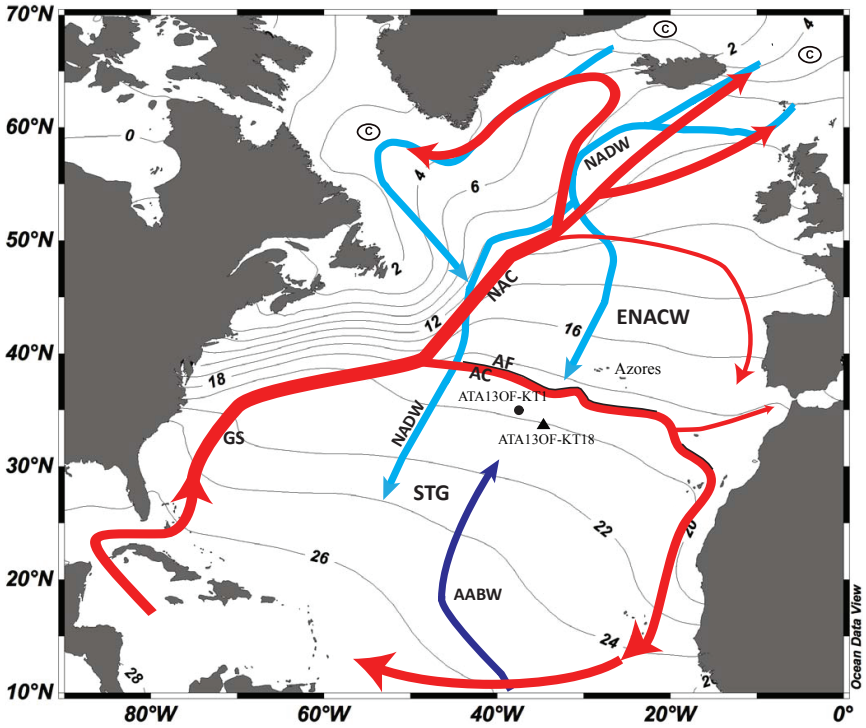

Figure 1. Modern surface water circulation of the North Atlantic overlayed on contour map of spring

(April– June) sea surface temperatures (SSTs) (modified from Schwab et al., 2012, Repschlager et al., 2015; Locarnini et al., 2010). STG=SubTropical Gyre; ENACW=Eastern North Atlantic Central Water; NADW=North Atlantic Deep Water; AABW=Antarctic Bottom Water; GS=Gulf Stream; NAC=North Atlantic Current; AC=Azores Current; AF=Azores Front;. ©=NADW formation sites. Numbers are referred tosea surface temperatures of North Atlantic (°C). Red arrows indicate the surface water currents direction and intensity. Light blue arrows indicate the NADW, whereas the dark blue arrows are referred to AABW.

In particular, the North Atlantic region is dominated by the so-called Atlantic Meridional Overturning Circulation (AMOC) system (Lynch-Stieglitz et al., 2007). It represents the main mechanism regulating a complex system of surface and deep-water masses circulation in the North Atlantic Ocean (Fig. 1). Therefore, the AMOC system represents an enormous circulation cell in the North Atlantic. It is composed by warm and salty waters that flow northward in the shallowest part of the Atlantic basin, as North Atlantic drift. It reaches northern latitudes and causes the formation of southward flowing cold deep waters, known as North Atlantic Deep Water (NADW) (Repschläger et al., 2015 and reference therein).

The wind-driven Gulf Stream represents the trigger for the Northern Hemisphere climate system (Fig. 1). It constitutes the main carrier of heat and moisture for high northern latitudes, which together control the North Atlantic ice sheet (Haug and Tiedmann, 1998; Duplessy, 1999; Billups et al., 2016). The Gulf Stream, in its east to north-east flowing, is responsible for the origin of the Azores Anticyclone and the Azores Front/Current System (AFCS) (Schiebel et al., 2002b; Storz et al., 2009; Repschläger et al., 2015). AFCS, together with air mass movements, influence the climatic setting of low-medium latitude of the North Atlantic Ocean and Europe region, respectively. Furthermore, the Azores Front/Current System nowadays represents the major sea surface water that feeds the Mediterranean basin (Gould, 1985; Schwaab et al., 2012).

The Azores Front/Current System actually lies just South of the Azores archipelago and constitutes an important gear of the AMOC system (Fig. 1). Here, the Azores Front/Current System acts as the boundary between 18°C oligotrophic mode waters (Harvey and Arhan, 1988; Schiebel et al. 2002b; Bashmachnikov et al., 2015), belonging to the Subtropical Gyre (STG) and the Eastern North Atlantic Central Water (ENACW) cool/transitional waters (Repschläger et al. 2015).

Hence, the Azores region, given its particular position, could be considered as the sensor for the North Atlantic climatic variability. Studies on marine cores have demonstrated that, during the past, factors controlling AMOC system considerably varied (Lynch-Stieglitz et

al. 2007; Repschläger et al. 2015). In particular, during the late Quaternary glacial/interglacial oscillations, controlled by orbital parameters, were responsible of latitudinal shifts of hydrographic/atmospheric frontal systems, in the Atlantic Ocean (Bond et al., 1993; Dansgaard et al., 1993; Broecker, 1994; Eynaud et al., 2009; Barker et al., 2009; Hodell et al., 2010).

6.4 Materials and methods

6.4.1 Cores location and description

During the Oceanograflu cruise (2013), conducted around the Azores archipelago on board the Atalante vessel, 31 sedimentary cores using a Kullenberg gravity corer were collected. Two of the longest and less bioturbated cores were selected, one on each side of the MAR at different depths: ATA13-OF-KT1 core (35°24.956'N - 37°15.749'W; bathymetry=3,431 m; length=4.03 m) on the western side and ATA13-OF-KT18 (34°42.206'N - 35°07.334'W; bathymetry=2,801m; length=4.45 m) on the eastern side.

The ATA13-OF-KT1 core is constitutes by light grey carbonate ooze, alternating with olive-brownish marly levels. The sedimentary record appears to be continuous and slightly to moderately bioturbated, especially in the deeper part.

The ATA13-OF-KT18 core, results also composed by light grey carbonate ooze, with rare intercalations of greenish-yellowish layers. Some bioturbated intervals have been recognised, particularly in the deeper part of the core.

6.4.2 Sample preparation

Both cores have been sampled using U-channels (1.8 cm width) and then sampled continuosly (each sample 1 centimetre thick) in order to have a continuous and high-resolution record. Each sample has been dried at 50°C, weighed, and washed over a 63-mm sieve. Micropaleontological and geochemical analyses have been performed on size-fraction grater than 125 μm, in both cores.

6.4.3 Radiocarbon dating

To obtain a correct age model and to calibrate the studied cores, ten accelerator mass spectrometry (AMS) ^{14}C ages have been performed on planktonic foraminiferal tests, at Poznan Radiocarbon Laboratory (Tab. 1).

By considering the minimum sample weight required by Poznan Laboratory (20 mg), the analyses on planktonic foraminifera monospecific samples were not possible. Therefore, to minimize the errors (Mekik, 2014), we have selected species living today in the Azores region at around the same depth in water column (Bé and Torderlund, 1971; Bé, 1977, Ottens, 1991; Schiebel et al., 2002a; Schiebel et al., 2002b; Schiebel and Hemleben, 2005; Repschläger et al., 2015).

Lab. number	Core	Depth (cm bsf)	AMS ^{14}C (yr BP)	R_{surf} (yr)	2σ-calibrated ages (yr BP)	Median probability (yr BP)
Poz-79832	ATA13OF-KT18	0-1	12030 ± 60	-400	13449 ± 124	13462
Poz-79833	ATA13OF-KT18	12-13	5090 ± 35	-400	5399 ± 80	5401
Poz-79834	ATA13OF-KT18	25-26	7170 ± 40	-400	7625 ± 51	7623
Poz-79861	ATA13OF-KT18	50-51	11290 ± 60	-400	12797 ± 109	12764
Poz-79862	ATA13OF-KT18	64-65	13900 ± 70	**-800**	**15689 ± 289**	**15714**
Poz-79863	ATA13OF-KT18	84-85	17840 ± 100	-400	21066 ± 322	21059
Poz-79864	ATA13OF-KT1	0-2	3020 ± 30	-400	2752 ± 27	2752
Poz-79865	ATA13OF-KT1	17-18	9370 ± 50	-400	10174 ± 70	10131
Poz-79866	ATA13OF-KT1	29-30	12720 ± 60	-400	14377 ± 308	14299
Poz-79867	ATA13OF-KT1	39-40	13710 ± 70	**-800**	**15443 ± 252**	**15426**

Table 1. Radiocarbon ages calibration.

Surface-dwelling species such as *G. ruber* gr. (including morphotypes and chromotypes), *G. pyramidalis*, *G. elongatus*, *G. sacculifer*, *G. quadrilobatus*, *and G. trilobus* have been selected, whilst in the cases where it was not possible, subsurface-dwelling species such as *G. bulloides*, *G. falconensis*, *G. calida*, *G. obesa*, *G. siphonifera* (=*G. aequilateralis*) have been also selected. A number of 2500-4500 tests have been handpicked for each sample in the fraction >150 mm.

Before calibration, ^{14}C values have been corrected considering the difference between the ^{14}C age of the sea surface and that of the atmosphere (R_{surf}=Reservoir age of surface seawaters). According to Bard (1988) and Siani et al. (2001) ^{14}C ages have been corrected using a reservoir age of ≈ 400 yr, except for the levels at 39-40 cm bsf of the ATA13-OF-KT1 core and at 64-65 cm bsf of the ATA13-OF-KT18 core. We have assumed that these levels were deposited in correspondence of the Heinrich event 1 (H1) and then we applied an R_{surf} of ≈ 800 yr (Siani et al., 2001).

One AMS ^{14}C analysis, at 0-1 cm bsf of ATA13-OF-KT18 core, yielded an unreasonable age and therefore has been discarded (Table 1).

All the ^{14}C ages have been successively converted in calibrated ages using the Calib 7.1 online version software (Stuiver and Reimer, 1993), with IntCal13 calibration curve (Reimer

et al., 2013). The ^{14}C ages calibration produces two values for each analysed sample, comprised in the range of sigma-2. To avoid biases in the interpretation of these analyses and to uniform the data, the median probability values has been preferred to the 2-s (Table 1). Moreover in the median probabilities are included the uncertainties of measurements.

6.4.4 Carbonate content analysis (carbonatometry)

To determinate the carbonate content, supplementary U-channels have been collected, continuously sampling every cm (402 samples for ATA13-OF-KT1 core and 445 for ATA13-OF-KT18 core). Dried bulk samples have been grounded in an agate mortar. The carbonate content is performed using a ManoCalcimeter Mélières apparatus (MCM) derived from the "carbonate bomb" (Müller and Gastner, 1971). The total carbonate content (in weight %) has been calculated from CO_2 volume evolved from the reaction of 100 mg of finely crushed sediment with 8 N HCl. The precision of the measurement has been estimated at around ± 1 wt. %.

6.4.5 Stable isotope analyses

The oxygen isotopic composition of carbonate is expressed in the conventional d notation, which corresponds to the relative difference in parts per mille (‰) between the isotopic ratio R ($^{18}O/^{16}O$) of the sample (s) and of the reference (r) V-PDB (Vienna Peedee Belemnitella) defined by Craig (1965) and revised by Gonfiantini et al. (1995).

$$\delta = [(Rs/Rr) - 1] \times 1000$$

The isotopic measurements were realized on six to ten specimens of *G. ruber* s.s. (white variety), handpicked in the size fraction between 250-315 mm, to minimize size effects on the isotopic values (Billups and Spero, 1995). Prior to analysis the foraminifers have been cleaned in a methanol ultrasonic bath for 10 seconds and then naturally dried in fume hood. For this analysis the sampling rate was 1 sample every 2 cm in both cores (201 samples for ATA13-OF-KT1 core and 223 for ATA13-OF-KT18 core).

The oxygen stable isotopes have been analyzed at LSCE (Laboratoire des Sciences du Climat et de l'Environnement – Gif sur Yvette) using an Elementar Isoprime mass spectrometer.

The used standard (UCD-SM92) is a Carrara marble, prepared at the beginning of 1990s for the University of California. The adopted values of this standard are –1.91 ‰ (V-PDB) for $\delta^{18}O$ and +2.09 ‰ (V-PDB) for $\delta^{13}C$. The analytical precision and the reproducibility for

repeated measurements of the laboratory reference calcite is ± 0.05 ‰ for $\delta^{18}O$ and ± 0.03 ‰ for $\delta^{13}C$.

6.4.6 Planktonic foraminifera identification and dissolution effect

Planktonic foraminifera have been analysed in the fraction greater than 125 mm. All the 403 samples of ATA13-OF-KT1 core have been analysed whereas 248 samples for ATA13-OF-KT18 (one every cm between 0-50 cm, and then one every 2 cm).

The taxonomic classification of the planktonic foraminiferal species has been based on the original description of type species specimens and on subsequent revisions by Saito et al. (1981), Kennett and Srinivasan (1983), Bolli and Saunders (1985), Hemleben et al. (1989). Quantitative analyses have been performed on 300-400 individuals in each sample.

In order to evaluate the dissolution effects on carbonate fraction of both cores, the comparison between the abundance of resistant and susceptible species to dissolution has been analysed. According Haddam et al. (2016), as resistant species percentages (RSP) group have been added together *Globorotalia inflata*, *G. menardii* gr., *G. tumida* gr., *Neogloboquadrina dutertrei* and *Pulleniatina obliquiloculata*. Whilst, as sensitive species group (SS), the percentages of *Globigerinoides ruber* gr., *Globigerina bulloides* and *Globigerinita glutinata*, have been summed.

Two threshold corresponding to RSP > 40% and RSP > 30% (Haddam et al., 2016), have been used to individuate the samples affected by dissolution.

6.4.7 Sea Surface Temperature reconstruction

Sea Surface Temperature (SST) is the main factor influencing planktonic foraminifera species distribution in the present and past oceans (Chapman et al., 2000; de Abreu et al., 2003; Kucera et al. 2005). Thus the assemblage census data, especially if combined with Modern Analog Technique (SST-mat), is considered one of the finest tools for SST palaeotemperatures reconstructions (Hutson, 1980; Prell, 1985; Kucera et al., 2005a; Caley et al. 2014; Haddam et al. 2016).

The MAT measures the distance between the planktonic foraminiferal faunal composition of a fossil sample with the assemblages from a modern core-top database, and identifies the best set of modern analogs (Prell, 1985). The peculiarity of MAT respect with other transfer function methods, is that it takes into account not only the most abundant species, but also the rare ones. MAT method has been applied to reconstruct the mean annual SST-mat (aSST-mat)

variations in the last 144 ka of the Azores region, using PaleoAnalogs 2.0 software (Theron et al., 2004). 15 best analogs have been selected for analysis.

The adopted database for MAT calibration, was provided by "Paléocéans" research team of LSCE (Gif sur Yvette), and it consists of planktonic foraminifera census data coming from North Atlantic Ocean 615 core-tops, where the corresponding SSTs are known. Thirty taxa were considered for this analysis, according to software input data constrains. Following Haddam et al. (2016), certain species, sub-species and chromotypes were combined, whilst other taxa have not been considered, because not present in the database (see the list in the supplementary material). The adopted LSCE North Atlantic Ocean database was performed in the fraction greater than 150 μm.

However, quantitative data used in this study have been carried out in the size-fraction > 125 μm. Therefore, in order to compare the SST-mat reconstruction between the two different size-fractions, 20 supplementary quantitative analyses were carried out in fraction > 150 μm, selecting levels considered as representatives of both warm and cold climatic conditions. SST-mat values from 150 μm fraction resulted to be slightly higher than those from 125 μm, with average values of 0.77 °C of ΔT (ΔT=Ti_150μm – Ti_125μm, with i=sample), for February-SSTs and 0.7°C for August-SSTs. Higher derived ΔT values (1.8 – 2.4 °C) between the two fractions have been calculated in correspondence with cold-climatic related intervals, while for warm-climatic related intervals the derived ΔT values (-0.37 – 0.8 °C) are negligible. Such bigger derived ΔT values between the two fractions in cold intervals are ascribable to a major occurrence of cold affinity small-size species (Bé, 1977), whose abundance is likely underestimated using the fraction > 150 μm.

6.5 Age model

6.5.1. Insolation-based age model

The astronomical tuning of ATA13-OF-KT1 and ATA13-OF-KT18 cores (Fig. 2) is based on the correlation of carbon radiometric ages, tuning carbonate content and oxygen isotopic composition with the 21 June insolation at 35°N.

The daily summer insolation curve corresponds to the rate of the Northern Hemisphere insolation calculated at 35°N of latitude, during the June solstice. The reference curve of the Laskar et al. (2004) solution has been obtained through the software AnalySeries 2.0.8 (Paillard et al., 1996), which has allowed to extrapolate accurate ages of daily summer insolation minima/maxima. The insolation curve calculated at the latitude of the coring sites

(35°N) allows to reconstruct the exact solar forcing to the past climate system of the Azores region.

Firstly, the age model have been separately derived for the two records, through the application of several age control points that have allowed to convert the depth in time.

For the upper part of the ATA13-OF-KT18 core, between 12 and 85 cm bsf, 5 calibrated ^{14}C ages have been utilized, whereas, for the ATA13-OF-KT1 core, between the top and 40 cm bsf, 4 calibrated ^{14}C ages have been utilized.

As regards to the remaining part of the sedimentary records, control age points have been obtained through the tuning of carbonate content and oxygen isotopic composition with 21 June insolation at 35°N of Laskar et al. (2004) solution. Moreover, the weighted average curves (10%) of carbonate content and $d^{18}O_{G.\ ruber}$ have been allowed to better individuate minima/maxima and then to produce the best match with the insolation/precessional cycles of the late Quaternary (Fig. 2).

As suggest by several authors (Broecker, 1994; Keiwing and Jones, 1994; Hodell et al., 2001; Grutzner et al., 2002; Hagen and Keigwin, 2002; Sexton and Barker, 2012), the orbital tuning of carbonate content and oxygen isotopic composition has been made by aligning summer insolation minima with minima percentages in carbonate content and heavier values of $\delta^{18}O_{G.\ ruber}$, respectively (Schiebel et al. 2002b; Hagen and Keigwin 2002; Billups and Scheinwald, 2014; Billups et al., 2016). Vice versa insolation maxima have been tuned to highest percentages in carbonate content and lighter values of $\delta^{18}O_{G.\ ruber}$, respectively (Fig. 2). Therefore, according to the insolation-based age model, the ATA13-OF-KT1 core record was deposited during about 3.5 precessional cycles, whereas the ATA13-OF-KT18 during 6 precessional cycles (Fig. 2). Furthermore, other control tie points have been added in order to ameliorate the chronology. Particularly, for insolation-based age model of the ATA13-OF-KT1 core, the base of the Younger Dryas has been recognized at 24.5 cm bsf. Here, the age of 12.76 ka, has been added as tie point. This value has been established on the basis of the correlation with the radiocarbon dating at 50.5 cm bsf of ATA13-OF-KT18 core.

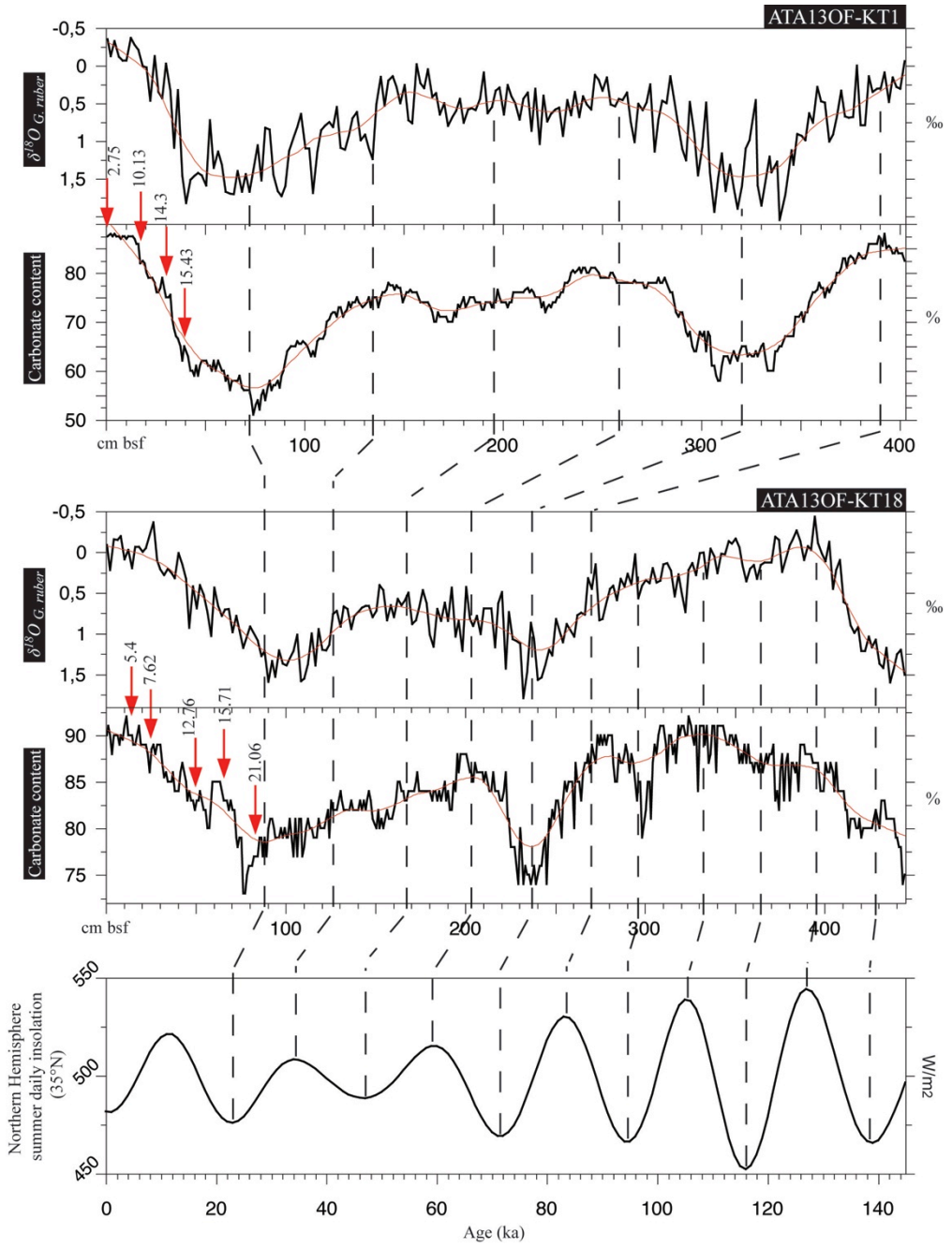

Figure 2. Astronomical tuning of the ATA13-OF-KT1 and ATA13-OF-KT18 records. For each studied core the carbonate content, $\delta^{18}O_{G.\ ruber}$, are plotted. Large dashed black lines=main age control points, based on the correlation with the 21 June insolation record at 35°N (Laskar et al., 2004); continue red line=weighted curve fit (10%). The values in correspondence of the short red arrows indicate the calibrated radiocarbon ages (ka).

Event	Depth (cm bsf)	Assigned age (ka)	Reference
ATA13OF-KT18			
Core top	0	3.35	This study
Poz-79833	12	5.4	-
Poz-79834	25	7.62	-

Base Holocene	45	11.74	This study
Poz-79861 / Base Younger Dryas	50	12.76	-
Base Bolling/Allerod /	59	14.66	This study - 2*, 3*, 4*, 5*
Poz-79862	64	15.71	-
Poz-79863	84	21.06	-
Insolation minimum 1	88	23	1*
Insolation maximum 2	126	34	1*
Insolation minimum 2	167	47	1*
Insolation maximum 3	203	59	1*
Insolation minimum 3	237	72	1*
Insolation maximum 4	270	83	1*
Insolation minimum 4	301	95	1*
Insolation maximum 5	332	105	1*
Insolation minimum 5	364	116	1*
Insolation maximum 6	395	127	1*
Insolation minimum 6	428	139	1*
Core bottom	444	144.82	This study
ATA13OF-KT1			
Poz-79864 / Core top	0	2.75	-
Poz-79865	17	10.13	-
Base Holocene	21	11.64	This study
Base Younger Dryas	24	12.76	This study (derived from Poz-79861)
Poz-79866	29	14.3	-
Base Bolling/Allerod	32	14.64	This study - 2*, 3*, 4*, 5*
Poz-79867	39	15.43	-
Insolation minimum 1	72	23	1*
Insolation maximum 2	134	34.5	1*
Insolation minimum 2	195	47	1*
Insolation maximum 3	257	59.5	1*
Insolation minimum 3	320	71.5	1*
Insolation maximum 4	390	83.5	1*
Core bottom	402	85.64	This study

Table 2. Chronostratigraphic model for ATA13-OF-KT18 and ATA13-OF-KT1 cores. List of the selected age control points. 1* 21 June insolation at 35°N. (Laskar et al., 2004); 2* Ruddiman (1977); 3* Bond et al. (1993); 4* Barker et al. (2011); 5* Repschlager et al. (2015); 6* de Abreu et al. (2003); 7* Billups et al. (2016).

According to the obtained age model, the ATA13-OF-KT18 core spans the interval from the 144.8 to 3.35 ka. However, it must be taken into account that the ages of the top and the bottom of ATA13-OF-KT18 core have been extrapolated, considering the sedimentation rate calculated in the adjacent intervals. The ATA13-OF-KT1 core record

instead spans the interval from 85.6 to 2.75 ka. In Table 2 the tie points adopted for the development of the insolation-based age model are shown.

The age model indicates mean sedimentation rates at the core sites ATA13-OF-KT1 and ATA13-OF-KT18 respectively of 4.84 and 3.06 cm/kyr across the entire time span, which at a sampling interval of 1 cm yields a temporal resolution of 207 up to 321 years between samples.

To obtain ages for all data point of both cores, a linear interpolation between the selected age control points was adopted. Through this approach the variations in the sedimentation rate, during the different climatic stages, were analysed.

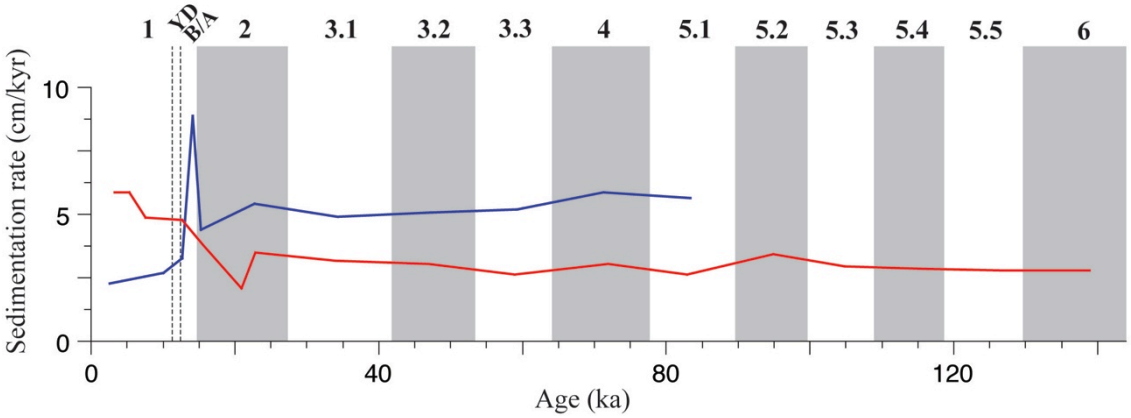

Figure 3. Sedimentation rate between the selected tie points (Tab.2), obtained through the insolation-based tuning. The blue line is relative to the ATA13OF-KT1 core, whereas the red line represents the sedimentation rate of the ATA13OF-KT18 core. Numbers above are referred to the Marine Isotope Stages (Lisiecki and Raymo, 2005) and sub-Stages (Martinson et al., 1987). Light gray vertical bars refer to the glacial stages (MIS 2, 4 and 6) and cool-temperate periods (MIS 3.2, 5.2 and 5.4). YD=Younger Dryas stadial; B/A=Bølling/Allerød interstadial.

Mean sedimentation rate reflects typical pelagic conditions, even if it shows some variations during glacial/interglacial transitions (Fig. 3). However, ATA13-OF-KT1 and ATA13-OF-KT18 sedimentation rates are lower than those observed by Schwab et al. (2012) and Repschlager et al. (2105) to the north of the Azores archipelago (4-122 cm/kyr). Moreover, at similar latitudes but close to the eastern North American margin, Billups and Scheinwald, (2014) and Hodell et al. (2010) obtained sedimentation rates of 7-90 cm/kyr and 20-100 cm/kyr, respectively.

The orbital forcing dominates the carbonate content and $d^{18}O_{G.\ ruber}$ fluctuations. Furthermore, a similar orbital-tuning was adopted to develop the chronology of sedimentary cores, in the eastern North American margin (Billups and Scheinwald, 2014). These latter

authors recognised the robust correlation between the northern summer insolation and $d^{18}O_{G.\ ruber}$, even if with slightly lower values (from -2 to 1 ‰), respect to those observed in this study (-0.5 to 2 ‰). The difference is probably due to the influx of the warm Gulf Stream in the North American margin characterised by higher SSTs than the Azores region.

Comparing the obtained age model with others based on the study of North Atlantic downcore sediments, some discrepancies have been highlighted. The largest difference regards the timing of the MIS 4. The orbital-tuning age model, proposed in this work, is not in agreement with the age models proposed by Chapman et al. (2000), Hagen and Keigwin (2002), de Abreu et al. (2003), Kandiano et al. (2004), Martrat et al. (2007). The above cited authors suggested ages variable between ~60 and 74 ka, whereas in our reconstruction MIS 4 spans the interval from 64.7 to 78.4 ka. On the other hand, Ruddiman (1997) estimated an age between 70 and 80 ka, slightly older than those proposed in this study.

6.5.2 LS16-based age model: synchronization with $d^{18}O_{G.\ bulloides}$ record of MD95-2042 core

The LS16-based age model has been developed correlating the $\delta^{18}O_{G.\ ruber}$ records of both cores to the $\delta^{18}O_{G.\ bulloides}$ record of the MD95-2042 core. This latter oxygen isotope record, firstly tuned by Shackleton et al. (2000), has recalibrated and realigned by Lisiecki and Stern (2016), in order to provide a global δ18O stack (LS16). In order to reinforce the age model, it has been also used the global benthic δ18O stack and the IRD stack chronology, proposed by Lisiecki and Stern (2016), to derive supplementary age control points. The global benthic δ18O stack represents an important paleoclimate record for stratigraphic correlations, taking into account the ice volume and related sea level variations (Lisiecki and Stern, 2016). The global benthic δ18O stack has been used better identify in the analysed proxies glacial/interglacial transitions, related to the last climate cycle.

The IRD stack (LS16) has allowed to identify, both in the ATA13OF-KT1 and ATA13OF-KT18 $\delta^{18}O_{G.\ ruber}$ records, intervals correspondent to the Heinrich events 1 to 12 (Heinrich, 1988; Lisiecki and Stern; 2016). Furthermore, the high frequency fluctuations in the $\delta^{18}O_{G.\ ruber}$ records, linked to Dansgaard-Oeschger interstadials (Dansgaard-Oeschger et al., 1993; Bond et al., 1933), have been correlated to those reported by Barker et al. (2011) in the 800,000-year Greenland synthetic record.

The age model has been obtained separately for the two studied cores, using the calibrated AMS ^{14}C ages and some strategic age control points. In particular, $\delta^{18}O_{G.\ ruber}$

minima and maxima peaks of both cores have been aligned to MD95-2042 $\delta^{18}O_{G.\ bulloides}$ (LS16) minima and maxima (Fig. 4 and 5).

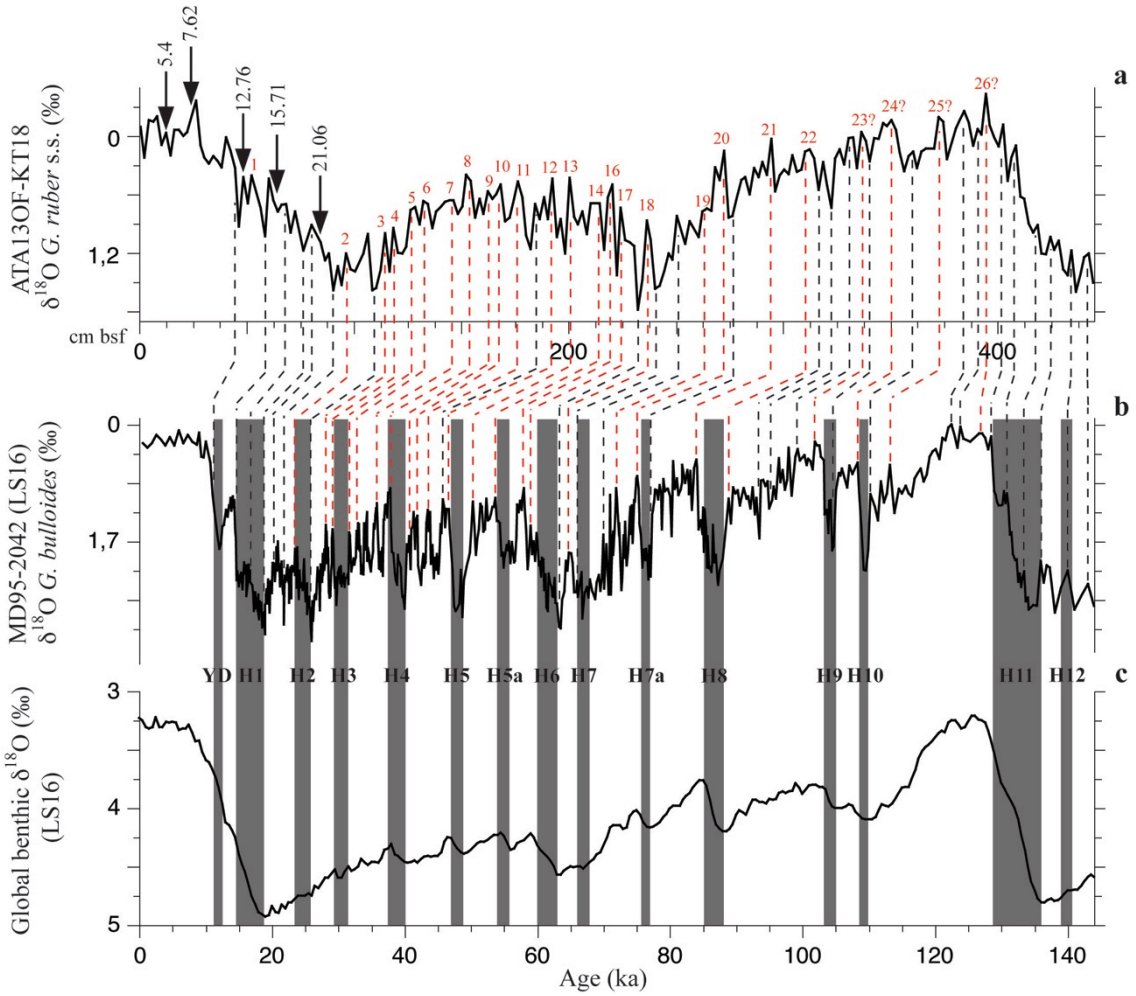

Figure 4. Alternative age model developing for ATA13-OF-KT18 core (a). The (c) global benthic $d^{18}O$ stack (LS16) and the (b) MD95-2042 $d^{18}O_{G.\ bulloides}$ (LS16) have been used as reference curve for the age model developing. Black arrows indicate the depth correspondent to the AMS ^{14}C analyses performed in the $d^{18}O_{G.\ ruber}$ record. Black numbers above these arrows indicate the calibrated ^{14}C adopted (ka). Black dashed lines are relative to the correlation points between the ATA13OF-KT18 $d^{18}O_{G.\ ruber}$ and the MD95-2042 $d^{18}O_{G.\ bulloides}$ (LS16) records. Red dashed lines are referred to the correlation points correspondent with the Dansgaard/Oeschger (D/O) events, labelled with red numbers 1 to 22 (Barker et al., 2011; Billups et al., 2016). The warming events labelled with the red numbers 23 to 26 are not present in literature. Dark gray vertical bars identify the interval correspondent to the Heinrich events, proposed by Lisiecki and Stern (2016), here labelled as H1 to H12. YD=Younger Dryas cold period.

The synchronization of the ATA13OF-KT18 $d^{18}O_{G.\ ruber}$ with the MD95-2042 $d^{18}O_{G.\ bulloides}$ (LS16), have been performed using forty-nine correlation points and five calibrated ^{14}C ages (Table 3). The developed age model has allowed to establish that the ATA13-OF-

KT18 core record spans between 3.36 and 143.8 ka. According to the adopted tuning strategy, the D/O interstadial events 1 to 22, occurred in the upper Pleistocene, have been recognised in the $d^{18}O_{G.\ ruber}$ record. Only the D/O 15 has not been recognised in the isotope record of this core. In particular the D/O 1 corresponds to the Bølling/Allerød warm climate phase (Barker et al., 2011). Hence, in the ATA13-OF-KT18 core record the entire last climate cycle has been recognised.

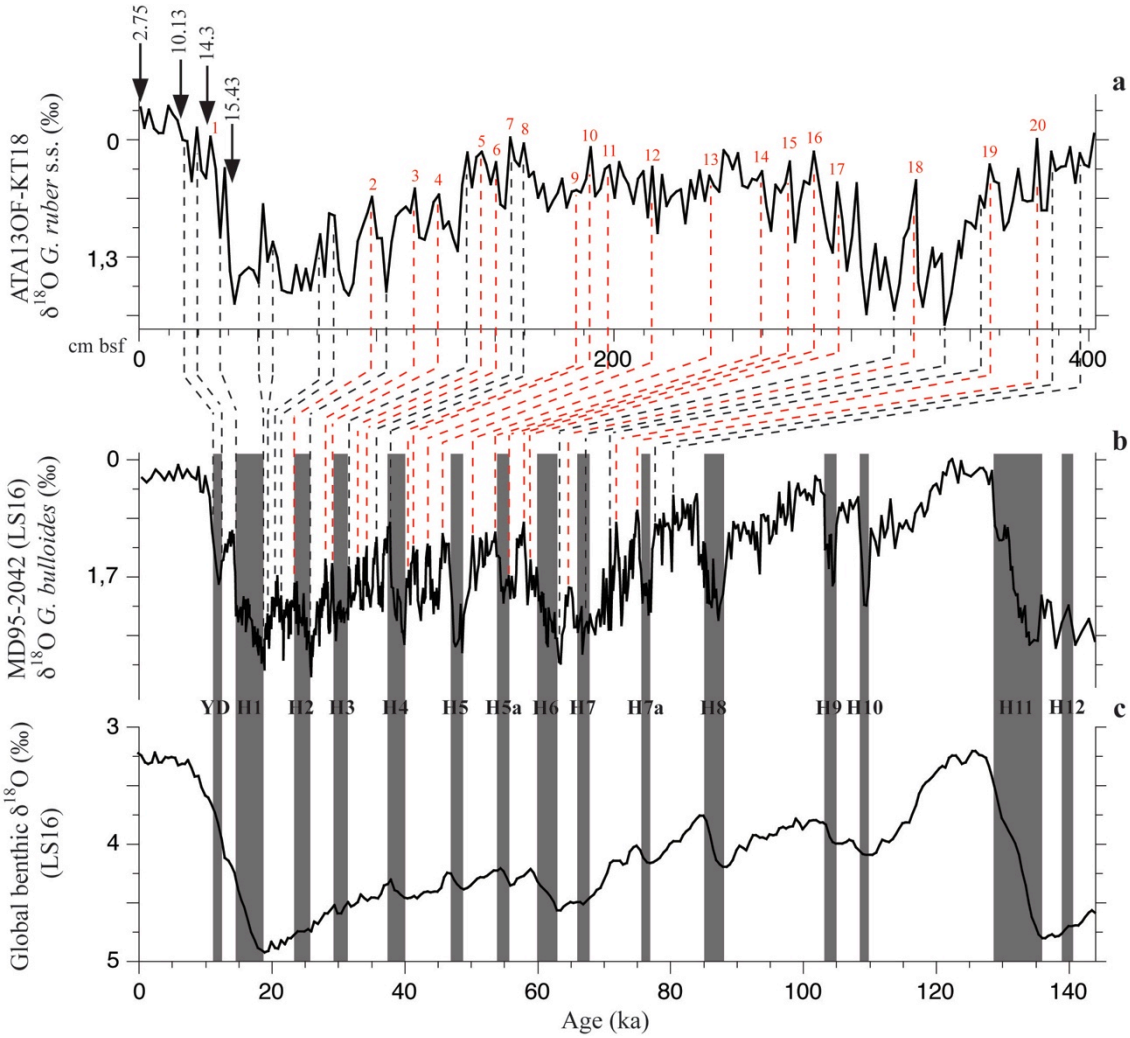

Figure 5. Alternative age model developing for ATA13-OF-KT1 core (a). The (c) global benthic $\delta^{18}O$ stack (LS16) and the (b) MD95-2042 $\delta^{18}O_{G.\ bulloides}$ (LS16) have been used as reference curve for the age model developing. Black arrows indicate the depth correspondent to the AMS ^{14}C analyses performed in the $\delta^{18}O_{G.\ ruber}$ record. Black numbers above these arrows indicate the calibrated ^{14}C adopted (ka). Black dashed lines are relative to the correlation points between the ATA13OF-KT18 $\delta^{18}O_{G.\ ruber}$ and the MD95-2042 $d^{18}O_{G.\ bulloides}$ (LS16) records. Red dashed lines are referred to the correlation points correspondent with the Dansgaard/Oeschger (D/O) events, labelled with the red numbers 1 to 22 (Barker et al., 2011; Billups et al., 2016). Dark gray vertical bars identify the interval correspondent to the Heinrich events, proposed by Lisiecki and Stern (2016), here labelled as H1 to H12.

The ATA13-OF-KT18 $\delta^{18}O_{G.\ ruber}$ trend is very similar to those of the Iberian margin records, such as the MD95-2042 $\delta^{18}O_{G.\ bulloides}$ (Cayre et al., 1999; Shackleton et al., 2000; Pailler et al., 2002; de Abreu et al., 2003; Lisiecki and Stern, 2016) and the MD01-2443-44 $d^{18}O_{G.\ bulloides}$ (Martrat et al., 2007; Hodell et al., 2013), and those of the eastern North American margin, such as the KNR140-37PC $\delta^{18}O_{G.\ ruber}$ (Hagen and Keigwin, 2002; Billups and Scheinwald, 2014; Billups et al., 2016).

The alternative age model for ATA13OF-KT1 core record has been developed aligning the $\delta^{18}O_{G.\ ruber}$ record with the MD95-2042 $\delta^{18}O_{G.\ bulloides}$ (LS16) and using four calibrated ^{14}C ages (Table 3). In order to synchronise the ATA13OF-KT1 $\delta^{18}O_{G.\ ruber}$ record, thirty-three additional age control points have been adopted. According to the age model, the D/O events 1 to 20, have been recognised in the high frequency oscillations of $\delta^{18}O_{G.\ ruber}$ record. The time interval recorded by this sedimentary record resulted between 2.75 and 81.94 ka.

The ages for all data points in the sedimentary records of both cores have been obtained linearly interpolate between the age control points.

The average sedimentation rate for ATA13OF-KT18 core resulted 3.12 cm/kyr, whereas reaches the values of 5.08 cm/kyr for ATA13OF-KT1 core. Considering the sampling interval of 1 cm, a temporal resolution of 197 up to 320 years between samples resulted.

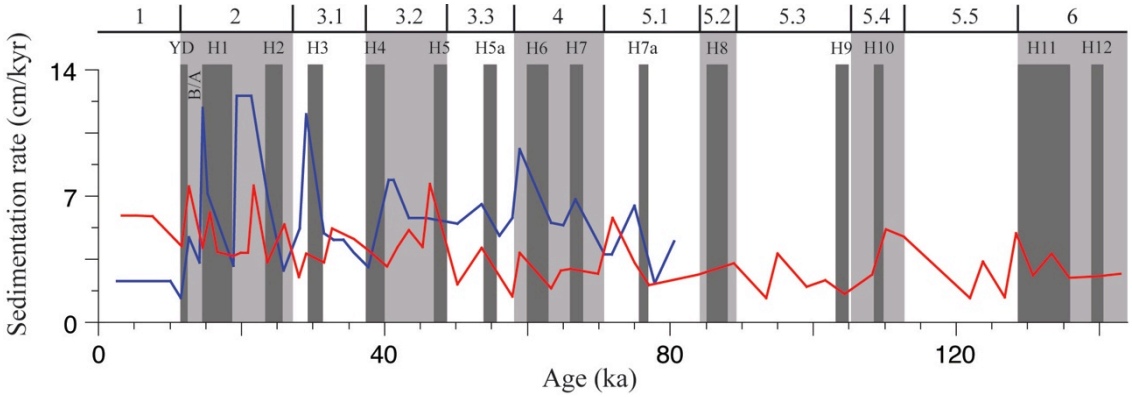

Figure 6. Sedimentation rate between the selected age control points, obtained through the synchronization with MD95-2042 $\delta^{18}O_{G.\ bulloides}$ (LS16) record. The blue line is relative to the ATA13OF-KT1 core, whereas the red line represents the sedimentation rate of the ATA13OF-KT18 core. Numbers above are referred to the Marine Isotope Stages (Lisiecki and Raymo, 2005) and sub-Stages (Martinson et al., 1987). Light gray vertical bars refer to the glacial stages (MIS 2, 4 and 6) and cool-temperate periods (MIS 3.2, 5.2 and 5.4). Dark gray vertical bars are relative to the Heinrich event intervals proposed by Lisiecki and Stern (2016), labelled as H1 to H12. YD=Younger Dryas stadial; B/A=Bølling/Allerød interstadial.

According to the adopted age model for both cores, the sedimentation rate between the age control points have been calculated. The sedimentation rate, for the ATA13OF-KT18 core record, resulted between 1.3 and 7.64 cm/kyr, whereas for the ATA13OF-KT1 one, this rate varies between a minimum of 1.28 cm/kyr and a maximum of 12.53 cm/kyr. In general the sedimentation rates have shown an increasing trend starting from the MIS 4 to the top of the cores. The highest sedimentation rate have been observed in correspondence of the cold-cool climate phases, whereas resulted lower during warm climate periods. In particular for ATA13OF-KT18 core record, the lowermost sedimentation rate verified during MIS 5.5. On the contrary, for ATA13OF-KT1 core the depositional rate increased at the end of the "Heinrich" related events 3 (29.2 ka), 1 (14.7 ka) and above all during the Last Glacial Maximum (~23-19 ka). The sedimentation rate instead clearly decreased during MIS 5.1 and 1.

6.5.3 Spectral analysis

Spectral analyses studied records have been carried out in order to provide a statistical control on the developing of the two age models and to validate them. The $\delta^{18}O_{G.\ ruber}$ and carbonate content records of non-stationary and non-linear signals have been analysed to study the characteristic periodicities. The signals have been analysed without interpolation, keeping the original unevenly sampling intervals. The temporal resolution (1 sample each cm) considered for the insolation-based age model was 0.207 ka, for ATA13-OF-KT1 core, and 0.321 ka, for ATA13-OF-KT18 core (§ 6.6.1). For the LS16-based age model, the temporal resolution adopted was 0.197 ka for ATA13-OF-KT1 core, and 0.316 ka for ATA13-OF-KT18 core (§ 6.6.1). It is important to precise that for $\delta^{18}O_{G.\ ruber}$ record spectral analysis of both cores, the sampling rate was one sample every two centimetre.

The spectral analyses have been performed using the REDFIT software (Schulz and Mudelsee, 2002). This software analyses the time series through an evolution of the Lomb-Scargle periodogram (Lomb, 1976; Scargle, 1982; Schulz and Mudelsee, 2002). This method allowed to observe the "red-noise" in the carbonate content and $\delta^{18}O_{G.\ ruber}$ signals. The "red-noise" in time-series consists in the continuous decrease of spectral amplitude with increasing frequency (Schulz and Stattegger, 1997; Schulz and Mudelsee, 2002; Bonomo et al., 2016). The Schulz and Mudelsee (2002) analysis uses an implemented first-order autoregressive AR(1) process (Hasselmann, 1976) to adapt the distribution function to red-noise signals (Bonomo et al., 2016).

In order to test the age models and to improve the investigation of dominant periodicities in analysed time-series, the Wavelet analysis has been carried out. This latter analysis uses the Foster's (1996) weighted wavelet Z-transform (WWZ) and, in this work, it has been performed to examine the frequency distribution of the non-stationary carbonate content and $\delta^{18}O_{G.\ ruber}$ signals. The wavelet analysis uses a set of fully scalable modulated windows, which have compact support in time and are band-limited in the frequency domain (Bonomo et al., 2016).

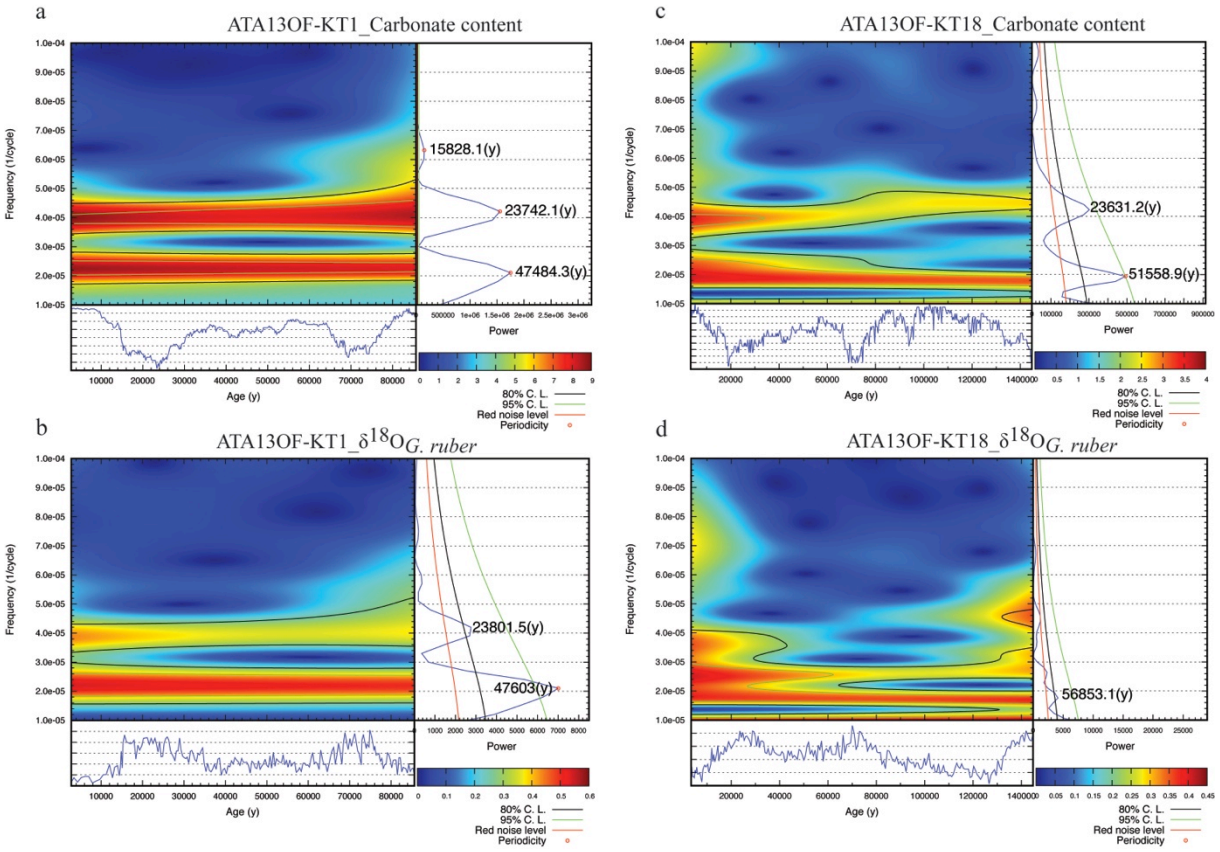

Figure 7. Wavelet analysis of the carbonate content and $\delta^{18}O_{G.\ ruber}$ signals, relative to the insolation-based age model. a) ATA13OF-KT1 carbonate content; b) ATA13OF-KT1 $d^{18}O_{G.\ ruber}$; c) ATA13OF-KT18 carbonate content; d) ATA13OF-KT18 $d^{18}O_{G.\ ruber}$. C.L.=Confidence Level.

Therefore, the spectral and the wavelet analyses have been used to examine the dominant periodicities in the carbonate content and $\delta^{18}O_{G.\ ruber}$ records of both cores. These analyses have been repeated on studied proxies, using the insolation-based and LS16-based age model respectively. Only the low-frequency periodicities are discussed in this work.

Spectral analysis carried out from tuning insolation ATA13-OF-KT1 core age model highlighted that carbonate content oscillations are mainly controlled by 47.48, 23.74 and

15.83 kyr cycles (Fig. 7 a), whereas those of $\delta 18O_{G.\ ruber}$ by 47.6 and 23.86 cycles (Fig. 7 b). The peaks at 23.74-23.86 kyr, together with that at 15.83 kyr, are coherent with the precessional periodicity. The periodicities in the band 47.6-47.48 kyr are linked to the obliquity band.

Likewise, the spectral analyses carried out for the ATA13-OF-KT18 core have highlighted that carbonate content oscillations are mainly controlled by periodicities centred at 51.56 and 23.63 kyr (Fig. 7 c). In the $\delta^{18}O_{G.\ ruber}$ power spectrum, only the periodicity at 56.85 kyr exceeds the 80 % confidence level (Fig. 7 d). No other periodicities have been evidenced, because the remaining signal stays under the red noise level.

In general, the 23.63 peak lies in the precessional band, whereas the peaks at 56.85-51.56 kyr are probably linked to the obliquity signal.

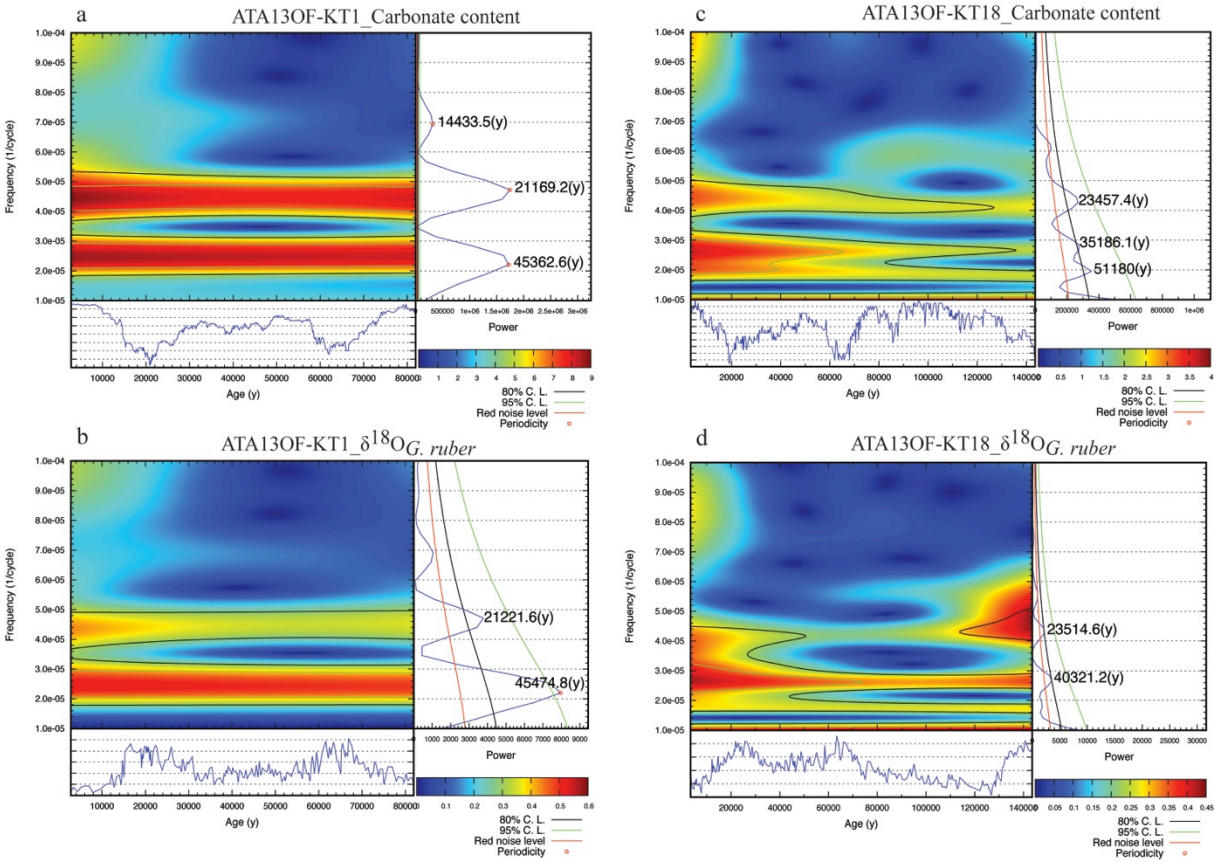

Figure 8. Wavelet analysis of the carbonate content and $\delta^{18}O_{G.\ ruber}$ signals, relative to the alternative, LS16-based, age model. a) ATA13OF-KT1 carbonate content; b) ATA13OF-KT1 $d^{18}O_{G.\ ruber}$; c) ATA13OF-KT18 carbonate content; d) ATA13OF-KT18 $\delta^{18}O_{G.\ ruber}$. C.L.=Confidence Level.

The wavelet analysis has shown that the dominant periodicities, linked to the precessional and obliquity forcing, are better represented and uniformly distributed in the carbonate

content and $\delta^{18}O_{G.\ ruber}$ records of ATA13-OF-KT1 core, rather than the ATA13-OF-KT18 core.

According to the ATA13-OF-KT1 core age model, based on the $\delta^{18}O_{G.\ ruber}$ synchronization with the MD95-2042 $\delta^{18}O_{G.\ bulloides}$ (LS16), the observed dominant periodicities in the carbonate content record are centred at 45.36, 21.17 and 14.43 kyr (Fig. 8 a). Concerning the $\delta^{18}O_{G.\ ruber}$ record, the periodicities of 45.48 and 21.22 kyr have been recognised (Fig. 8 b). The periodicities centred at 21.17 and 21.22 kyr are consistent with the precession cycles. Moreover, in the carbonate content spectrum, a periodicity of 14.43 kyr is also evident. ATA13-OF-KT18 core carbonate content power spectra highlighted the dominance of periodicities centred at 51.18, 35.19 and 23.46 kyr (Fig. 8 c), while those of $\delta^{18}O_{G.\ ruber}$ signal showed periodicities in correspondence with 40.32 and 23.51 kyr cycles (Fig. 8 d). However, it is important to precise that these two latter periodicities just reach the 80 % confidence level without exceeding it.

The periodicities of 51.18-35.19 and 40.32 kyr are related to the obliquity band, whereas the peaks at 23.51-23.46 kyr are clearly relative to the precessional (insolation) forcing.

As observed in the time-series developed with the insolation-based age model, the dominant periodicities, linked to the precessional and obliquity forcing, are much more evident and uniformly distributed in the carbonate content and δ18OG. ruber records of ATA13-OF-KT1 core, than in ATA13-OF-KT18 core.

In order to calculate the possible time lag between the insolation forcing and the relative registration of climatic proxies (Imbrie an Imbrie, 1980; Bassinot et al., 1994), the time-series developed with the two different age models have been analysed. The difference in time, between maxima/minima of the insolation curve and oscillations in $\delta^{18}O_{G.\ ruber}$ and carbonate content have been measured.

According to the insolation-based age model, the curves filtered at 23.8 kyr (ATA13OF-KT1) for $\delta^{18}O_{G.\ ruber}$ and the curves filtered at 23.74 kyr (ATA13OF-KT1) and at 23.63 kyr (ATA13OF-KT18), for the carbonate content, have been used to calculate the time lag to the 21 June insolation signal at 35°N (Laskar et al., 2004). In both the cores, the time lag has been calculated solely for the ^{14}C dated uppermost part interval. For the rest, the lag is evidently zero because the $CaCO_3$ and $\delta^{18}O_{G.\ ruber}$ curves have been *a priori* aligned to insolation maxima/minima. A time lag of 2.46 and of 2.28 kyr have been respectively obtained for carbonate content signals of ATA13OF-KT1 and ATA13OF-KT18 cores. A time lag of 2.57 kyr for $\delta^{18}O_{G.\ ruber}$ record has been calculated for ATA13OF-KT1 core record. In ATA13OF-KT18 $\delta^{18}O_{G.\ ruber}$ spectrum the precessional-related periodicity is not observable.

The insolation-tuned records should be considered not affected by consistent time lag. Alternatively the time lag could be considered constant over the time interval studied and thus omitted (Shackleton et al., 1995; Billups and Scheinwald, 2014).

Concerning the LS16 tuning age model, the $\delta^{18}O_{G.\ ruber}$ curves filtered at 21.22 kyr (ATA13OF-KT1) and 23.51 kyr (ATA13OF-KT18), and the CaCO3 curves filtered at 21.17 kyr (ATA13OF-KT1) and at 23.46 kyr (ATA13OF-KT18), have been used to calculate the time lag to the 21 June insolation both at 65°N and 35°N (Laskar et al., 2004). The 21 June insolation at 65°N has also been taken into account because it was used by Lisiecki and Stern (2016) to test the sensitivity of their age model (Tab. 3).

The average values of the lag between $\delta^{18}O_{G.\ ruber}$ record and 21 June insolation minima/maxima at 65°N and 35°N, resulted 4.72 and 4.6 kyr , respectively, for the ATA13OF-KT1 core, and 2.3 kyr and 2.18 kyr, respectively, for the ATA13OF-KT18 core (Tab. 3). Respect with 65°N and 35°N 21 June insolation forcing, the climatic response of ATA13OF-KT1 carbonate content resulted lagged of 4.8 and 4.68 kyr, respectively, and those of ATA13OF-KT18 of 4.94 and 4.82 kyr, respectively (Tab. 3).

According to the spectral and wavelet analysis the LS16-based age model have been adopted for both ATA13OF-KT1 and ATA13OF-KT18 proxy records interpretation. The carbonate content and $\delta^{18}O_{G.\ ruber}$ power spectra evidenced more accurate and more uniformly distributed periodicities, as regard to the insolation-based age model. Furthermore, this latter approach underestimates the time lag between the astronomical forcing and the climatic response, which, on the contrary, is included in the model proposed by Lisiecki and Stern (2016). Moreover, this latter model is based on the study of several oceanic cores, collected from marginal to deep ocean domains and thus it appears more indicated to establish better stratigraphic correlations.

ATA13OF-KT1 $\delta^{18}O_{G.\ ruber}$	21 June insolation (65°N)	Lag (ka)	ATA13OF-KT1 $\delta^{18}O_{G.\ ruber}$	21 June insolation (35°N)	Lag (ka)
9.09	11.14	2.05	9.09	11.39	2.31
20.17	23.89	3.71	20.17	22.86	2.69
31.26	37.76	6.50	31.26	34.39	3.14
42.74	44.74	2.00	42.74	46.78	4.04
54.22	57.74	3.51	54.22	59.46	5.23
64.91	71.38	6.47	64.91	71.57	6.65
75.21	84.00	8.79	75.21	83.33	8.12
Average value		**4.72**	**Average value**		**4.60**
ATA13OF-KT1 Carbonate content	21 June insolation (65°N)	Lag (ka)	ATA13OF-KT1 Carbonate content	21 June insolation (35°N)	Lag (ka)
7.28	11.14	3.85	7.28	11.39	4.11
19.49	23.89	4.39	19.49	22.86	3.37

31.12	37.76	6.64	31.12	34.39	3.28
42.35	44.74	2.39	42.35	46.78	4.44
53.57	57.74	4.16	53.57	59.46	5.88
65.39	71.38	5.99	65.39	71.57	6.17
77.80	84.00	6.19	77.80	83.33	5.53
Average value		**4.80**	**Average value**		**4.68**
ATA13OF-KT18 $\delta^{18}O_{G.\ ruber}$	21 June insolation (65°N)	Lag (ka)	ATA13OF-KT18 $\delta^{18}O_{G.\ ruber}$	21 June insolation (35°N)	Lag (ka)
8.63	11.14	2.50	8.63	11.39	2.76
21.82	23.89	2.07	21.82	22.86	1.04
34.35	37.76	3.41	34.35	34.39	0.05
45.55	44.74	-0.82	45.55	46.78	1.23
56.76	57.74	0.97	56.76	59.46	2.69
67.31	71.38	4.07	67.31	71.57	4.26
79.18	84.00	4.82	79.18	83.33	4.15
91.05	94.80	3.75	91.05	94.56	3.51
102.25	104.82	2.56	102.25	105.33	3.08
114.12	115.71	1.59	114.12	115.98	1.86
125.99	127.48	1.49	125.99	127.16	1.17
138.52	139.66	1.15	138.52	138.87	0.36
Average value		**2.30**	**Average value**		**2.18**
ATA13OF-KT18 Carbonate content	21 June insolation (65°N)	Lag (ka)	ATA13OF-KT18 Carbonate content	21 June insolation (35°N)	Lag (ka)
8.42	11.14	2.71	8.42	11.39	2.97
19.49	23.89	4.40	19.49	22.86	3.37
30.88	37.76	6.88	30.88	34.39	3.52
42.26	44.74	2.48	42.26	46.78	4.52
53.33	57.74	4.40	53.33	59.46	6.12
64.09	71.38	7.30	64.09	71.57	7.48
74.84	84.00	9.15	74.84	83.33	8.49
85.91	94.80	8.89	85.91	94.56	8.65
97.61	104.82	7.20	97.61	105.33	7.72
114.06	115.71	1.65	114.06	115.98	1.92
125.76	127.48	1.72	125.76	127.16	1.40
137.15	139.66	2.51	137.15	138.87	1.72
Average value		**4.94**	**Average value**		**4.82**

Table 3. Time lag estimation for ATA13OF-KT1 and ATA13OF-KT18 cores. According to the age model, based on proxies synchronization with MD95-2042 $\delta^{18}O_{G.\ bulloides}$ (LS16), the time lag has been calculated as regard to the 21 June insolation forcing at 65°N and 35°N. In the $\delta^{18}O_{G.\ ruber}$ and Carbonate content columns of both cores are reported the ages (ka) of the minima/maxima peaks. In the 21 June insolation columns are listed the ages of the minima/maxima peaks at 65°N and 35°N. In the grey rows are reported the ages correspondent to the $\delta^{18}O_{G.\ ruber}$ maxima, carbonate content minima and insolation minima.

6.6 Results

6.6.1 Stable isotopes

In general, $\delta^{18}O$ stable isotope curves of the two studied cores show comparable trends in the time equivalent interval, showing typical interglacial-glacial fluctuations with lighter-higher values respectively.

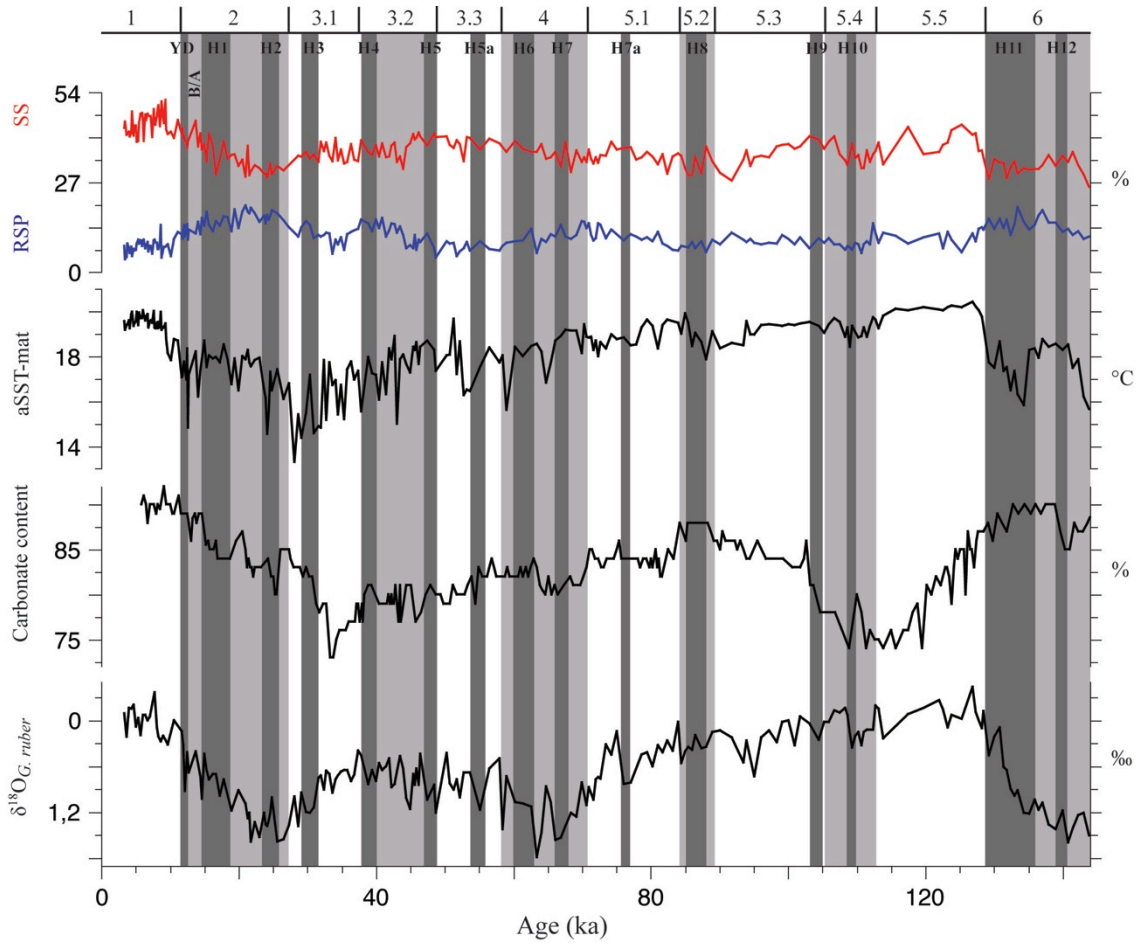

Figure 9. Carbonate content, $\delta^{18}O_{G.\ ruber}$, aSST-mat and Resistant Species Percentages (RSP) vs. Sensitive Species (SS) records of ATA13-OF-KT18 core. Light gray vertical bars refer to the glacial stages (MIS 2, 4 and 6) and cool-temperate periods (MIS 3.2, 5.2 and 5.4). Dark gray vertical bars are relative to the Heinrich event intervals proposed by Lisiecki and Stern (2016), from H1 to H12. YD=Younger Dryas stadial; B/A=Bølling/Allerød interstadial.

However, on average, the values are lighter in ATA13-OF-KT18 core (0.62 ‰), rather than in ATA13-OF-KT1 (0.75 ‰). In the ATA13-OF-KT18 core, $\delta^{18}O_{\ G.\ ruber}$ values oscillate from -0.45 and 1.8‰, whereas heavier values have been measured during MISs 6, 4, and 2 (1.6-1.8 ‰) (Fig. 9). Lighter values in $\delta^{18}O_{\ G.\ ruber}$ composition have been measured in MISs 5

and 1. During MIS 3, $\delta^{18}O_{\text{G. ruber}}$ ranges between 0.4 and 1.2 ‰. As regards to the ATA13-OF-KT1 record, $\delta^{18}O_{\text{G. ruber}}$ values vary from -0.4 and 2.06 ‰, and as described for the previous core, heavier values (2.1 - 0.8 ‰) have been measured in correspondence of the MISs 4 and 2 (Fig. 10). On the contrary, lighter values have been measured during MISs 1, 3 and 5.1. The interval of MIS 1 is characterised by the lightest values comprise between -0.4 and 0.5 ‰.

6.6.2 Carbonate content oscillations

As previously described by Hodell et al. (2001) and Sexton and Barker (2012), a typical "Atlantic-style" has been recognised with high percentages of carbonate during interglacial periods, and minima during glacial phases.

The carbonate content of both cores shows similar trends, although the absolute values are lower in ATA13-OF-KT1 during the glacial MIS 4 and 2. These discrepancies are considerably reduced in the interglacial stages or in warmer periods (Figs 9 and 10).

The carbonate content of the ATA13-OF-KT18 core shows higher values of carbonate (72-92 %), with an evident cyclical trend (Fig. 9). The lowest percentages occurred during MISs 2 (73-80 %), 4 (74-86 %) and 6 (74-87 %), respectively. On the contrary, it reaches the highest values during MISs 1 (80-92 %), 3.3 (82-88%), 5.1 (80-90 %), 5.3 (84-92 %) and 5.5 (83-89 %). Two sub-stages, characterised by sharp decreases were recognised during MISs 5.2 and 5.4.

The percentage of carbonate of the ATA13-OF-KT1 core varies between 51 and 88 of the total weight (Fig. 10), lower values correspond to the last two glacial periods (MISs 4 and 2), whereas higher percentages have been measured in correspondence of MISs 1 and 5.1 (75-88 %). Two peaks of carbonate content have been measured at the MISs 3.1 and 3.3, and it slightly decreased during MIS 3.2.

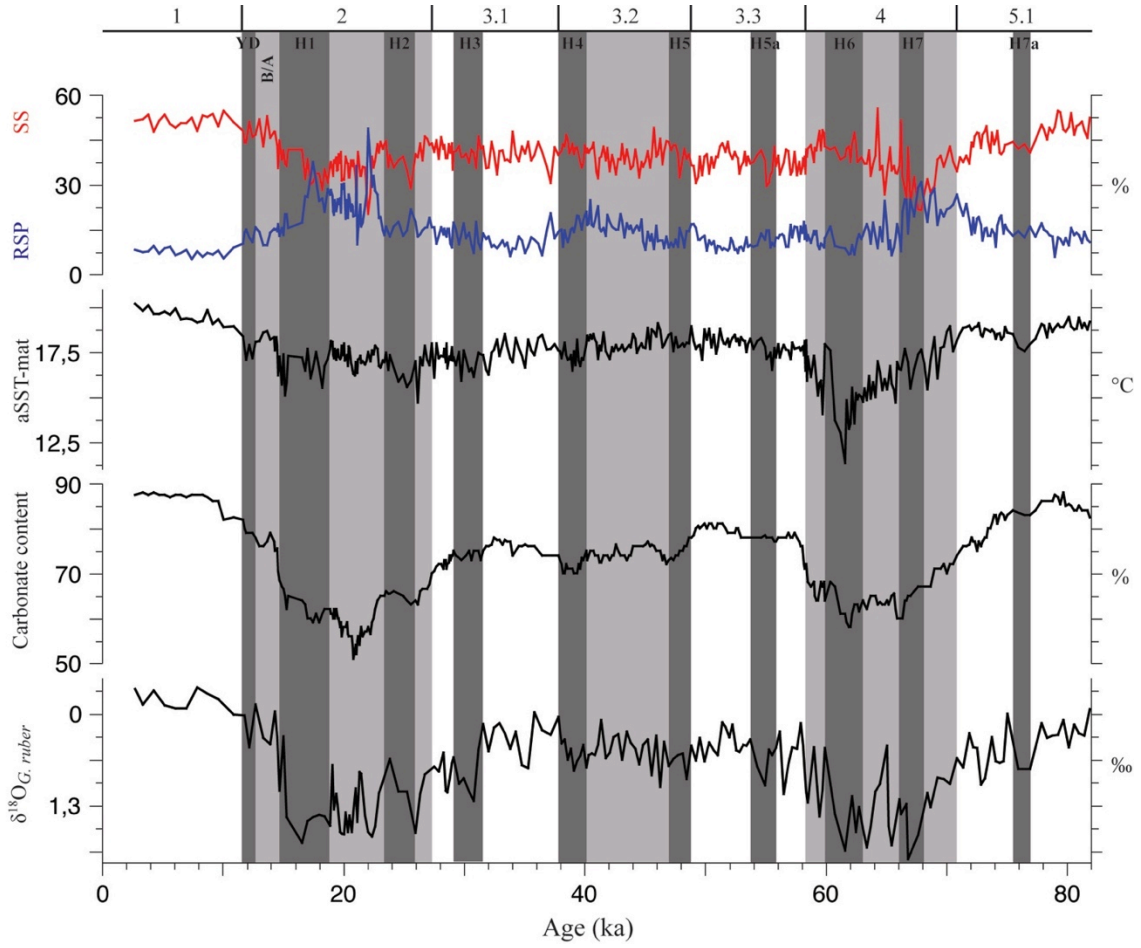

Figure 10. Carbonate content, $\delta^{18}O_{G.\ ruber}$, aSST-mat and Resistant Species Percentages (RSP) vs. Sensitive Species (SS) records of ATA13-OF-KT1 core. Numbers above are referred to the Marine Isotope Stages (Lisiecki and Raymo, 2005) and sub-Stages (Martinson et al., 1987). Light gray vertical bars refer to the glacial stages (MIS 2, 4 and 6) and cool-temperate periods (MIS 3.2). Dark gray vertical bars are relative to the Heinrich event intervals proposed by Lisiecki and Stern (2016), from H1 to H7a. YD=Younger Dryas stadial; B/A=Bølling/Allerød interstadial.

6.6.3 Resistant Species Percentages vs Sensitive Species

To analyse the dissolution effect in the studied records the RSP group has been plotted versus the SS (Fig. 9, 10 and 11). The signal of RSP is dominated by *G. inflata* and in the core ATA13-OF-KT18 shows an opposite trend to SS. These latter species are generally more abundant than RSP (Fig. 9 and 11 b). The increase in percentages of RSP and the contemporaneous decreasing of SS occurs during MISs 6, 4, 3.2 and 2.

In the ATA13-OF-KT1 core, the RSP reaches higher values than the other core, with percentages varying from 5 to 48.5 % (Fig. 10 and 11 a). The amount of SS shows similar percentages (20-55.5 %) to those of the ATA13-OF-KT18 core. The highest percentages of RSP occur during the early MIS 4, MIS 3.2 and mostly during MIS 2. On the contrary, the

highest percentages of SS occur during MISs 5.1 and 1 as well as in the central/later part of MIS 4.

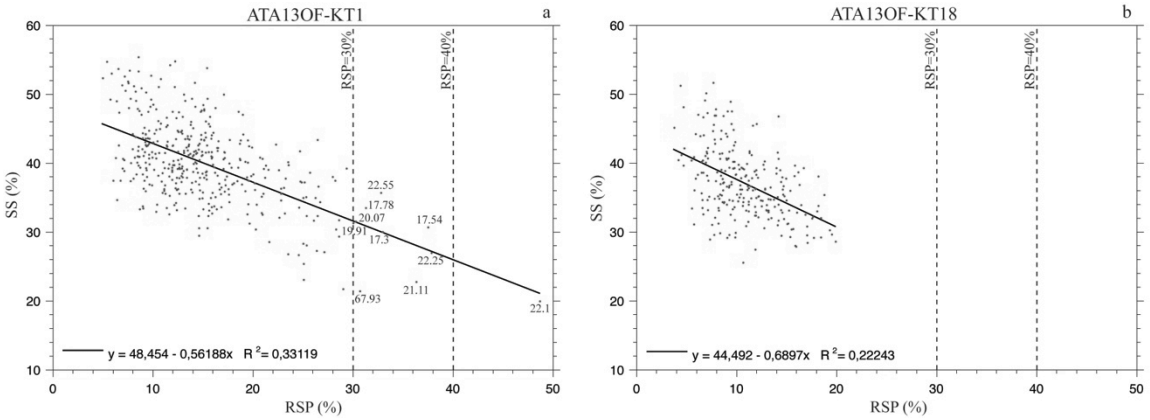

Figure 11. Resistant Percentage Species (RSP) vs. Sensitive Species (SS) for ATA13-OF-KT1 (a) and ATA13-OF-KT1 (b) cores. The black line represents the RSP vs. SS tendency line. The equations and R^2 related to RSP vs. SS is shown. According to Haddam et al. (2016), two RSP values (30% and 40%) have been selected as thresholds as dissolution effect sensors.

As regard the ATA13-OF-KT18 core, dissolution effects can be not relevant, because the RSP values stay generally lower than 20 %, whilst some samples of the ATA13-OF-KT1 core exceed 30-40 %, implying enhanced dissolution (Fig. 11 a). In particular, at 22.1 ka RSP reached value of 48.5% testifying a strong dissolution on carbonate fraction.

6.6.4 Sea Surface Temperature reconstruction

Mean aSST-mat results higher (18.28 °C) in ATA13-OF-KT18 than in ATA13-OF-KT1 core (17.5 °C). In ATA13-OF-KT18 core record, interglacials stages MIS 5.5 and MIS 1 are characterised by remarkable similar maxima aSST-mat values around 17.5-20 °C (Fig. 9). Minima aSST-mat values have been observed during the last part of glacial MIS 6 (coinciding with the H12) and in the transition MIS 3.1/2, where aSST-mat decreases to lowermost values of the core record (13.3 °C). During MIS 4 a stepwise cooling trend is observable, with values decreasing from 19.4 to 15.6 °C. The MIS 3.3 is marked by an increase in aSST-mat, followed by a long term cooling trend culminating with the lowest values at the end of MIS 3.1. During the entire MIS 3 several minor oscillations, probably linked to millennial-scale climate variability, are present. The glacial stage of MIS 2 (14.4-18.6 °C) instead is characterised by a gradual warming trend toward the top. During the early MIS 1 the aSST-

mat values decrease again, especially at the Bølling/Allerød / Younger Dryas transition (14.7 °C).

Some important differences are discernable between the aSST-mat records of ATA13-OF-KT1 and ATA13-OF-KT18 cores (Fig. 10). In ATA13-OF-KT1 core also highest aSST-mat values characterize MIS 5.1 (17.5-19.4 °C) and MIS 1 (17-20.2 °C), whereas a sharp aSST-mat decreasing marks the glacial MIS 4 culminating in coincidence of the "H" 6 with the lowest values at that site record (11.2°C). Then aSST-mat values increase in the MIS 4/3.3 transition, followed by a gradual cooling from the MIS 3.2 to the top of MIS 3.1, and a rapid temperature decreasing to 14.6 °C in coincidence with the "H" 3. The MIS 2 is characterised by a gradual and slight climate warming, interrupted by rapid cooling events in correspondence with the "H" 2 (16.2 °C) and especially the "H" 1 (15.1-17.4 °C). The last deglacial is characterised by an aSST-mat increase during the Bølling/Allerød (17.4-18.6 °C), followed by a rapid cooling episode in correspondence of the Younger Dryas (16.9-17.8 °C).

6.7 Discussion

6.7.1 Carbonate content and $\delta^{18}O_{G.\ ruber}$ records response to orbital forcing

According to the adopted LS16 age model, the time lags between the orbital forcing and the response of the studied sedimentary palaeoclimatic proxies (carbonate and $\delta^{18}O_{G.\ ruber}$) are well in agreement with those estimated by several Authors in others North Atlantic palaeoclimatic records (Imbrie and Imbrie, 1980; Bassinot et al., 1994; Chapman and Shackleton, 1998; de Abreu et al. 2003; Martrat et al. 2007; Billups et al. 2016; Lisiecki and Stern, 2016).

This time lag of the proxy response to the insolation forcing resulted higher for ATA13-OF-KT1 core and it is in the order of magnitude close to that (~4-5 kyr) measured in the precessional band by Imbrie and Imbrie (1980). This time lag might depend on the delayed ice volume response to the Northern Hemisphere insolation forcing at 65°N (Imbrie and Imbrie, 1980; Imbrie et al., 1984; Bassinot et al., 1994; Billups and Scheinwald, 2014).

Despite the low sedimentation rate of the two studied Azores region cores, it is important to note that the carbonate content and the $\delta^{18}O_{G.\ ruber}$ fluctuations recorded the same orbital- and millennial-scale variability, observed by higher-sedimentation records along the eastern (Shackleton et al., 2000; de Abreu et al., 2003; Martrat et al., 2007; Hodell et al., 2013; Lisiecki and Stern, 2016) and the western (Hagen and Keigwin 2002; Billups

and Scheinwald, 2014; Billups et al., 2016) margins of the North Atlantic. Thus, the Azores region is extremely sensitive indeed to the climatic oscillations occurred in the last glacial cycle. According to the LS16-based age model, the carbonate and $\delta^{18}O_{G.\ ruber}$ data from the ATA13-OF-KT18 core recorded the last 6 insolation cycles, and those from the ATA13-OF-KT1 core the last 4. The Azores region sedimentary record is also high sensitive to millennial-scale climatic variabilities. These latters are much more evident in $\delta^{18}O_{G.\ ruber}$ record of both cores, due to the rapid and frequent oscillations, related to the AMOC variations (Repschlager et al., 2015). On the contrary, the spectral and the wavelet analyses showed as the maxima/minima of the 21 June insolation both at 65°N and 35°N, are more evident in carbonate content record. The less noisy signal of carbonate content allows to better appreciate climatic variability linked to low-frequency periodicity (precession- and obliquity-related), sometimes masked in the $\delta^{18}O_{G.\ ruber}$ record of the studied cores.

In correspondence of the north-westernmost coring site (ATA13OF-KT1), twenty rapid warming phases, recorded in the $\delta^{18}O_{G.\ ruber}$ curve, have been correlated with the D/O interstadials (Dansgaard et al., 1993; Bond et al., 1993; Barker et al., 2011). Likewise, at the latitude of the south-easternmost site (ATA13OF-KT18), the D/O events from 1 to 22 have been observed. Furthermore, the MD95-2042 $\delta^{18}O_{G.\ bulloides}$ (LS16) tuning strategy ha allowed to recognise four events more, in which rapid climate warming and AMOC strengthening, may have been responsible for ATA13OF-KT18 $\delta^{18}O_{G.\ ruber}$ lightening (D/O 23? to D/O 26?).

6.7.2 Carbonate production and preservation

In both KT1 and KT18 sites, carbonate content show the typical "Atlantic-style" relative to maxima abundances during interglacial and minima during glacial periods. This behaviour, during the last 144 ka is closely related to the Northern Hemisphere summer insolation cycles (Fig. 12). The carbonate content depends by the balance between production, dissolution and dilution effects. In the studied sites, very distal from continents, the sedimentary continental input was extremely low, excluding therefore this dilution effect. Thus carbonate content fluctuations may have been driven mainly by variations in sea surface water calcareous plankton production (coccolithoforids and planktonic foraminifera), which was likely higher during glacial/interglacial transitions and interglacial periods (MISs 5.5 and 1), in coincidence with maxima insolation, than during the glacial stages of MISs 4 and 2, in coincidence with minima insolation. The dissolution and the

variations of the calcite compensation depth (CCD) during glacial/interglacial periods may have also influenced the amount of carbonate content in deep sea sediments, especially if the sea-bottom was close to lysocline depth. Today, in the central sector of the North Atlantic, the calcite compensation depth (CCD) lies at ~ 5,000-5,500 m depth (Berger and Winterer, 1974; Sexton and Barker, 2008), and in the Azores region at 35 °N the calcite lysocline depth lies at 4,500 m bsf (Schiebel et al. 2002b), much deeper than the present day sea-bottom depth of ATA13OF-KT1 (3,431 m bsl) and ATA13OF-KT18 (2,801 m bsl). However, the depth of lysocline can be strictly tied to changes in deep-ocean circulation, and it was probably less deep during glacial periods. From the last 82 ka, the depth fluctuations of the lysocline in the Azores area can be traced comparing the carbonate content and resistant species percentages (RSP) records between the ATA13OF-KT18 and ATA13OF-KT1 cores situated at different sea level bottom depth (Fig. 12).

In the south-easternmost shallower ATA13OF-KT18 site (2,801 m bsl), significantly above the lysocline, RSP percentages stay generally below 20%, excluding an important impact of dissolution on carbonate produced by planktonic foraminifera (Fig. 12). On the contrary, in the northern-most deeper ATA13OF-KT1 site (3,431 m bsl), RSP percentages exceeds 30-40 % in some peculiar interval, implying increased carbonate deep-water dissolution during the “H” 7 event in the MIS 4, and especially during the LGM and “H” 1 in the MIS 2 (Fig. 11).

Very rapid change in lysocline depth may have been occurred during these cooling climate phases, with an acme during the Last Glacial Maximum (22.1 ka), when the lysocline depth in the Azores area was probably shallowing up to 1000 m respect with the present day depth, reaching a depth less than 3,431 m (Fig. 12).

Some Authors argued that in the Central-North Atlantic the shallowing of the lysocline may be caused by an increasing of Antartic Bottom Water (AABW) circulation with a shallowing of 200-700 metres during the glacial periods (Gardner, 1975). Thus, AABW intensified during glacial periods, balancing the reduction of NADW formation and reaching higher latitudes in the North Atlantic basin. The 1.9 °C isotherm in the deep equatorial Atlantic marks the top of the AABW (Gardner, 1975) and today lies below NADW. The interplay between these two water masses control carbonate dissolution rate in the deep-sea sediments, because AABW normally is older and much more corrosive than NADW (Berger, 1973; Hodell et al., 2001; Sexton and Barker, 2012).

Thus, it may be plausible that during the H7, and especially during the H2 and H1, the reduced NADW formation allowed the more corrosive AABW to invade the deepest part of central north Atlantic until 35°N and therefore induced the shallowing of the lysocline.

6.7.3 Astronomical control of AMOC in the Azores area

In response of the insolation forcing, transition from glacial/interglacial conditions and above all, during the onset of glacial maxima and "Heinrich" related events, the Azores climate system rapidly reacted modifying the pattern of surface/deep water circulation (Fig. 12). The results of that have been well recorded in the planktonic oxygen isotope records. Usually, during cold periods (insolation minima) the $\delta^{18}O_w$ and $\delta^{18}O_{G.ruber}$ increase linked to enhanced in ^{16}O concentration in the ice sheets reducing the AMOC intensity (Kuhlbrodt et al., 2007). On the contrary, during the warm climatic intervals (insolation maxima) the surface water masses resulted more diluted and the $\delta^{18}O_w$ reduced inducing the AMOC restoration.

The heaviest $\delta^{18}O_{G.\ ruber}$ and the consequent SST-mat decreasing during the glacial stages (MISs 6, 4 and 2), testified the AMOC weakening, whereas during interglacial stages (MIS 5 and 1), the $\delta^{18}O_{G.\ ruber}$ lightening and the correlated SST-mat increasing were mainly linked to the AMOC strengthening (Fig. 12).

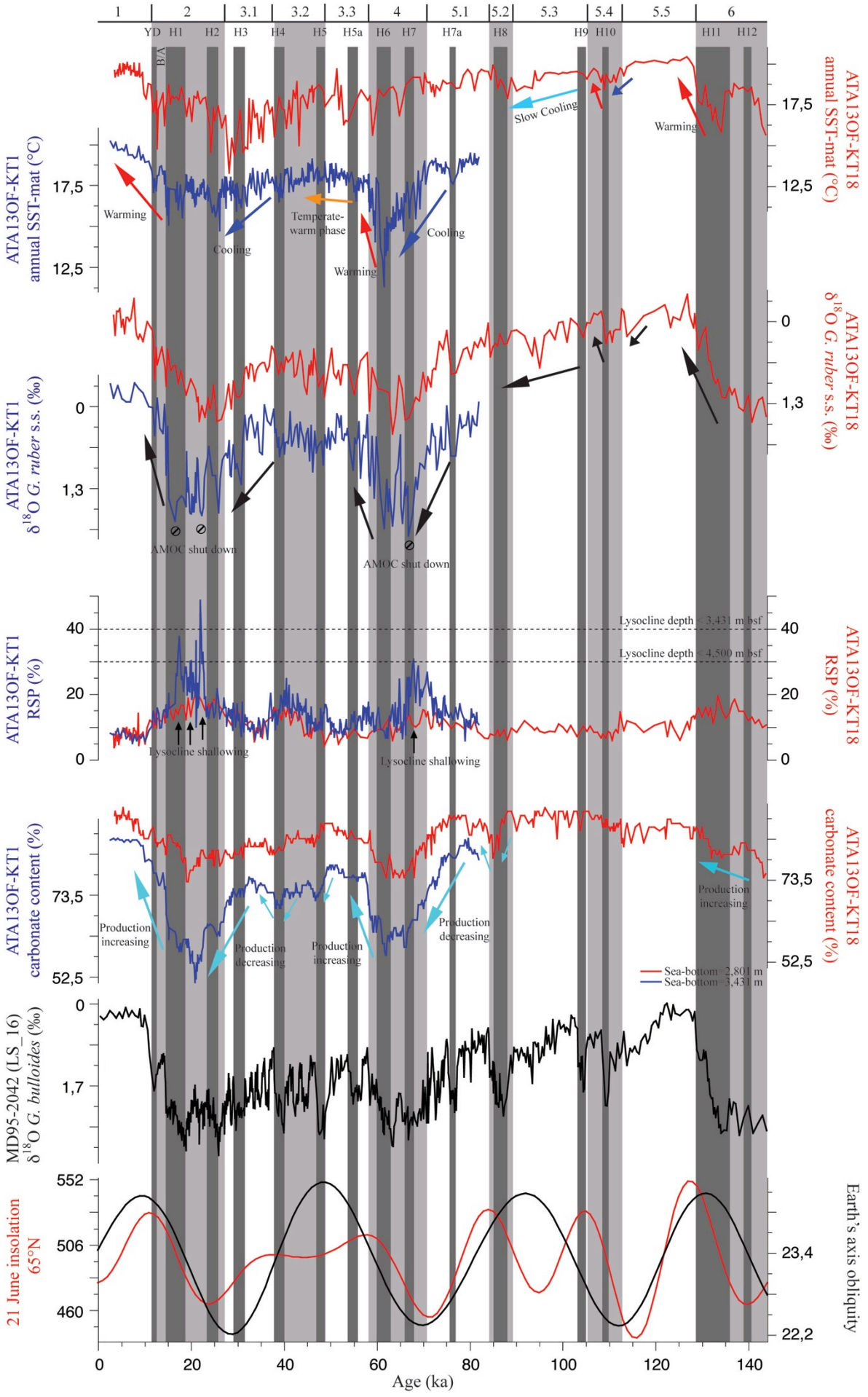
1
2
3.1
3.2
3.3
4
5.1
5.2
5.3
5.4
5.5
6
YD
H1
H2
H3
H4
H5
H5a
H6
H7
H7a
H8
H9
H10
H11
H12
B/A
ATA13OF-KT1
annual SST-mat (°C)
ATA13OF-KT18
annual SST-mat (°C)
Warming
Cooling
Temperate-
warm phase
Warming
Cooling
Slow Cooling
Warming
17,5
12,5
ATA13OF-KT1
δ18O G. ruber s.s. (‰)
ATA13OF-KT18
δ18O G. ruber s.s. (‰)
0
1,3
AMOC shut down
AMOC shut down
ATA13OF-KT1
RSP (%)
ATA13OF-KT18
RSP (%)
40
20
0
Lysocline depth = 3,431 m bsf
Lysocline depth = 4,500 m bsf
Lysocline shallowing
Lysocline shallowing
ATA13OF-KT1
carbonate content (%)
ATA13OF-KT18
carbonate content (%)
73,5
52,5
Production
increasing
Production
decreasing
Production
increasing
Production
decreasing
Production
increasing
Sea-bottom = 2,801 m
Sea-bottom = 3,431 m
MD95-2042 (LS_16)
δ18O G. bulloides (‰)
0
1,7
21 June insolation
65°N
552
506
460
Earth's axis obliquity
23,4
22,2
0
20
40
60
80
100
120
140
Age (ka)

Figure 11. Paleoeclimatic and paleoceanographic reconstruction of the Azores region. The carbonate content, RSP, $\delta^{18}O_{G.\ ruber}$ and aSST-mat records of the ATA13-OF-KT1core are plotted with blue lines. The carbonate content, RSP, $\delta^{18}O_{G.\ ruber}$ and SST-iso anomaly records of the ATA13-OF-KT18 record are plotted with red lines. In this figure, also the 21 June insolation at 65°N (red curve) and Earth's axis obliquity (black curve) signals are plotted. Light gray vertical bars refer to the glacial stages (MIS 2, 4 and 6) and cool-temperate periods (MIS 3.2, 5.2 and 5.4). Dark gray vertical bars are relative to the Heinrich event intervals proposed by Lisiecki and Stern (2016), from H1 to H12. YD=Younger Dryas stadial; B/A=Bølling/Allerød interstadial.

Usually, at the high latitudes of the North Atlantic seawater masses are characterised by low $\delta^{18}O_w$ due to the meltwater input from the ice sheet. Moreover, the meltwater input caused the periodic AMOC shut down, recorded in the high-medium latitudes of the North Atlantic. Considering that, the study area is far from continents, freshwater input can be attributed only to the North Atlantic iceberg calving, due to periodic collapses of the Laurentide ice sheets (MacAyeal, 1993), Greenland, Icelandic and Fennoscandinavian (Stanford et al., 2011). During the late Quaternary, these conditions, were met during the Heinrich events, in the North Atlantic (Heinrich, 1988; Bond et al., 1993; Broecker, 1994; Rohling et al., 2003; Eynaud et al., 2009). According to Cortijo et al. (2005) and Eynaud et al. (2009), during the "H" 1 and "H" 2 events the iceberg discharges, coming from the Laurentide ice sheet, Greenland and eastern Canadian continental margin, caused the $\delta^{18}O_w$ lightening. Consequently, strong sea surface cooling occurred as well as documented by drastic decreases of ~ 4 °C, and the AMOC almost completely shot down (Fig. 12).

However, observing the $\delta^{18}O_{G.\ ruber}$ records it is evident that the contribution of freshwaters did not affect these latitudes of the central North Atlantic, except during the Younger Dryas in correspondence of the ATA13-OF-KT1 coring site (Fig. 12). The difference in temperature between the two cores was probably due to the effect of meltwater input that may have covered the $\delta^{18}O_{G.ruber}$ signal of more northern-western core. According to Broecker et al. (1989), during the Younger Dryas meltwater inputs from the southwestern margin of the Laurentide Ice Sheet turned off the normal circulation system in the Atlantic Ocean.

Although Eynaud et al. (2009) suggested that during the Heinrich events the southern boundary of the so-called "Ruddiman belt" (Ruddiman, 1977, Hodell et al., 2010) was placed south of 40° N, there are no evidences of freshwater inputs in the $\delta^{18}O_{G.\ ruber}$, as well as any trace of ice rafted debris in the studied cores. These evidences suggest that the periarctic ice sheet was not so large to affect the Azores region, neither during millennial-

scale climatic cooling as "Heinrich" related events. The excursions in the $d^{18}O_{G.\ ruber}$ signals should be linked mainly to the temperature of surface waters and the global ice volume variations ($\delta^{18}O_w$). In the Azores region, the AMOC shut down clearly occurred during the "H" 7, LGM and "H" 1, well documented in the rapid $d^{18}O_{G.\ ruber}$ increases and SST-iso drops, between 2 and 5°C. Besides, these events are much more evident in the north-westernmost core, confirming local differences in the pattern of surface water masses between the two coring sites.

From a climatic-paleoceanographic point of view, the insolation and especially when in phase with obliquity minima caused the weakening of the AMOC system. On the contrary, the climatic warming induced by insolation maxima triggered the AMOC restoration (Fig. 12).

6.8 Conclusions

The wavelet analysis performed on carbonate content and $\delta^{18}O_{G.\ ruber}$ time-series of both cores revealed as the periodicities related to insolation forcing (precessional band) are the main trigger of the climatic and oceanographic changes of the Azores region. The cyclical fluctuations of the carbonate content and of the $\delta^{18}O_{G.\ ruber}$ records clearly show in which way the climate of the Azores region reacted to the variations of the Northern Hemisphere insolation rate.

In this study we compare an insolation-based tuning of studied records with a age model developed on the basis of the $\delta^{18}O_{G.\ ruber}$ calibration to the MD95-2042 $\delta^{18}O_{G.\ bulloides}$ (LS16) record. This latter approach allowed to estimate a time lag of 4.72-2.3 kyr, for $\delta^{18}O_{G.\ ruber}$, and of 4.94-4.8 kyr, for carbonate content, to summer insolation at 65°N.

According to the selected age model (LS16-based) the ATA13-OF-KT1 core records the time interval between 2.75 and 81.94 ka (MIS 1 to 5.1), whereas the other one was deposited between 3.36 and 143.79 ka (MIS 1 to 6). The dominant forcing of both record was related to the precession cycles and produced the periodicities at 21.17 and 23.46 kyr for ATA13OF-KT1 and ATA13OF-KT18 carbonate content records. Likewise, for ATA13OF-KT1 and ATA13OF-KT18 $\delta^{18}O_{G.\ ruber}$ records, the response to insolation forcing it has been recorded into 21.22 and 23.51 kyr cycle, respectively.

In the Azores region, over the last 144 ka, the highest percentages in the carbonate content and lower values in the $\delta^{18}O_{G.\ ruber}$ were forced by the Northern Hemisphere summer

insolation maxima. These conditions marked the onset of climatic warm/interglacial phases of MIS 5.5 and 1. On the contrary, insolation minima induced cold climatic conditions well marked by minima percentages in the carbonate content and heavier $\delta^{18}O_{G.\ ruber}$ values.

According to the age model, based on MD95-2042 $\delta^{18}O_{G.\ bulloides}$ (LS16) record, high-frequency climatic fluctuations have been recognised in the $\delta^{18}O_{G.\ ruber}$ signals. In ATA13OF-KT1 oxygen isotope record the D/O interstadials phases (Barker et al., 2011) from 1 to 20 have been recorded. In the ATA13OF-KT18 coring site signal instead, the D/O events 1 to 22 were recorded into the $\delta^{18}O_{G.\ ruber}$ signal. Likewise, the "Heinrich" related events from 1 to 7a (Lisiecki and Stern, 2016) have been recognised in the ATA13OF-KT1 studied proxies, whereas in the ATA13OF-KT18 coring site, the "Heinrich" related events 1 to 12 (Lisiecki and Stern, 2016) have been traced through the $\delta^{18}O_{G.\ ruber}$ high-frequency fluctuations.

The carbonate content shows the typical "Atlantic-Style" behaviour and reflects the interplay between surface biogenic production and deep dissolution. In particular, using the Resistant Species Percentage of the deepest core (ATA13OF-KT1) have been traced the vertical displacements of the lysocline of calcite during the last 144 ka. During interglacials the lysocline lied at 4,500 m depth, in central North Atlantic, reaching shallower positions during glacial phases. In particular, we estimated that the lysocline reached shallowest positions in central North Atlantic, during "Heinrich" related events 7and 1, as well as during the Last Glacial Maximum. In fact, during the LGM the lysocline was likely 1000 m shallower than today. The rise in lysocline corresponds probably to the AMOC system shut down.

Finally, different paleoenvironmental conditions resulted in the two coring sites despite their proximity and this study has permitted to interpret the complex North Atlantic paleoclimate history and paleoceanographic circulation during the last glacial cycle.

References

Alley, R., 1998. Icing the north Atlantic. Nature 392, 335-337.

Barker, S., Diz, P., Vautravers, M.J., Pike, J., Knorr, G., Hall, I.R., Broecker, W. S., 2009. Interhemispheric Atlantic seesaw response during the last deglaciation. Nature 457(7233), 1097-1102.

Barker, S., Knorr, G. Edwards, R.L., Parrenin, F. Putnam, A.E., Skinner, L.C., Wolff, E.,

Ziegler, M., 2011. 800,000 years of abrupt climate variability. Science 334(6054), 347–351.

Bashmachnikov, I., Nascimento, Neves, F., Menezes, T., Koldunov, N. V., 2015. Distribution of intermediate water masses in the subtropical northeast Atlantic. Ocean Sci. 11, 803–827.

Bassinot, F.C., Labeyrie, L.D., Vincent, E., Quidelleur, X., Shackleton, N.J., Lancelot, Y., 1994. The astronomical theory of climate and the age of the Brunhes-Matuyama magnetic reversal. Earth and Planetary Science Letters 126, 91–108.

Bé, A.W.H., 1977. An ecological, zoogeographic and taxonomic review of recent planktonic foraminifera, in: A.T.S. Ramsey (Eds.), Oceanic micropaleontology. London: Academic Press, Vol. 1, pp. 1–100.

Bé, A.W.H., Tolderlund, D.S., 1971. Distribution and ecology of living planktonic foraminifera in surface waters of the Atlantic and Indian Oceans. In The Micropalaeontology of the Oceans (eds. B. H. Funnell and W. R. Riedel). Cambridge Univ. Press, London, pp. 105–149.

Beier, C. Turner, S., Plank, T., White, W., 2010. A preliminary assessment of the symmetry of source composition and melting dynamics across the Azores plume. Geochemistry Geophysics Geosystems 11(2), Q02004.

Berger, W.H., 1973. Deep-sea carbonates: Pleistocene dissolution cycles. J. Foraminifer. Res. 3, 187-195.

Berger, W.H., 2013. On the Milankovitch sensitivity of the Quaternary deep-sea record. Climate of the Past 9, 2003–2011.

Billups, K., Spero, H.J., 1995. Reconstructing the stable isotope geochemistry and paleotemperatures of the equatorial Atlantic during the last 150,000 years: Results from individual foraminifera. Paleoceanographyv 11(2), 217-238.

Billups, K., Scheinwald, A., 2014. Origin of millennial-scale climate signals in the subtropical North Atlantic. Paleoceanography 29, 612–627.

Billups, K., Hudson, C. Kunz, H., Rew, I., 2016. Exploring Globorotalia truncatulinoides coiling ratios as a proxy for subtropical gyre dynamics in the northwestern Atlantic Ocean during late Pleistocene Ice Ages. Paleoceanography 31, 553–563.

Bolli, H.M., Saunders, J.B., 1985. Oligocene to Holocene low latitude planktic foraminifers, in: Bolli, H.M., Saunders, J.B., Perch-Nielsen, K., Plankton Stratigraphy, Cambridge Earth Sciences Series, Cambridge University Press, pp. 165-262.

Bond, G., Broecker, W., Johnsen, S., McManus, J., Labeyrie, L., Jouzel, J., Bonani, G., 1993. Correlations between climate records from North Atlantic sediments and Greenland ice. Nature 365, 143-147.

Bonomo, S., Cascella, A., Alberico, I., Sorgato, S., Pelosi, N., Ferraro, L., Lirer, F., Vallefuoco, M., Bellucci, L., Agnini, C., Pappone, G., 2016. Reworked Coccoliths as runoff proxy for the last 400 years: The case of Gaeta Gulf (central Tyrrhenian Sea, Central Italy). Paleogeography, Paleoclimatology, Paleoecology 459(1), 15-28.

Broecker, W.S., Peteet, D.M., Rind, D., 1985. Does the ocean–atmosphere system have more than one stable mode of operation? Nature 315, 21-26.

Broecker, W.S., 1994. Massive iceberg discharges as trigger for global climate change. Nature 372, 421-424.

Chapman, M.R., Shackleton, N.J., 1998. Millennial-scale fluctuations in North Atlantic heat flux during the last 150,000 years. Earth and Planetary Science Letters 159, 57–70.

Chapman, M.R., Shackleton, N.J., Duplessy, J.C., 2000. Sea surface temperature variability during the last glacial-interglacial cycle: assessing the magnitude and pattern of climate change in the North Atlantic. Palaeogeography, Palaeoclimatology and Palaeoecology 157, 1-25.

Coplen, T.B., 1988. Normalization of oxygen and hydrogen isotope data. Chemical Geology (lsot. Geosci. Sect.) 72, 293-297.

Cortijo, E., Duplessy, J.C., Labeyrie, L., Duprat, J., Paillard D., 2005. Heinrich events: Hydrological impact, C. R. Geosci. 337(10–11), 897-907.

Craig, H., 1965. The measurement of oxygen isotope paleotemperatures, in: Stable Isotopes in Oceanographic Studies and Paleotem- peratures, Tongiorgi, E. (eds), Consiglio Nazionale delle Ricerche, Laboratorio di Geologia Nucleare, Pisa, 1-24.

Dansgaard, W., Johnsen, S.J., Clausen, H.B., Dahl-Jensen, D., Gundestrup, N.S., Hammer, C.U., Hvidberg, C.S., Steffensen, J.P., Sveinbjörnsdottir, A.E., Jouzel, J., Bond, G., 1993. Evidence for general instability of past climate from a 250-kyr ice-core record. Nature 364, 218-220.

de Abreu, L., Shackleton, N., Schönfeld, J., Hall, M., Chapman, M., 2003. Millenial-scale oceanic climate variability off the western Iberian margin during the last two glacial periods. Marine Geology 196, 1–20.

Duplessy, J.C., 1999. Climate and the Gulf Stream. Nature 402, 593-595.

Eynaud, F., de Abreu, L., Voelker, A., Schoenfeld, J., Salgueiro, E., Turon, J.L., Penaud, A.,

Toucanne, S., Naughton, F., Goni, M.F.S., Malaize, B., Cacho, I., 2009. Position of the Polar Front along the western Iberian margin during key cold episodes of the last 45 ka. Geochem. Geophys. Geosyst. 10, Q07U05.

Foster, G., 1996. Wavelets for period analysis of unevenly sampled time series. Astron. J. 112, 1709–1729. Frankcombe,

Gardner, J.V., 1975. Late Pleistocene carbonate dissolution cycles in the eastern Equatorial Atlantic, in: Sliter, W.V., Bé, A.W.H., Berger, W.H. (Eds.), Cushman Found: Foraminiferal Res. Spec. Publ. 13, pp. 129–141.

Gonfiantini, R., Stichler, W., Rozanski, K., 1995. Standards and inter-comparison materials distributed by the International Atomic Energy Agency for stable isotope measurements, IAEA-TECDOC-825. Int. At. Energy Agency, Vienna.

Gould, W.J., 1985. Physical oceanography of the Azores front. Progress in Oceanography 14, 167-190.

Greenland ice-core project (GRIP) members, 1993. Climate instability during the last interglacial period recorded in the GRIP ice core. Nature 364, 203-207.

Grootes, P.M., Stuiver,M., 1997. Oxygen 18/16 variability in Greenland snow and ice with 10-3 to 10-5 year time resolution. Journal of Geophysical Research 102, 26,455–26,470.

Grutzner, J., Giosan, L., Franz, S.O., Tiedemann, R., Cortijo, E., Chaisson, W.P., Flood, R.D., Hagen, S., Keigwin, L.D., Poli, S., Rio, D., Williams, T., 2002. Astronomical age models for Pleistocene drift sediments from the western North Atlantic (ODP Sites 1055-1063). Marine Geology 189, 5-23.

Haddam N. A. Haddam, E. Michel, G. Siani, G. Cortese, H. C. Bostock, J. M. Duprat, and G. Isguder, 2016. Improving past sea surface temperature reconstructions from the Southern Hemisphere oceans using planktonic foraminiferal census data. Paleoceanography 31(6), 822–837.

Hagen, S., Keigwin, L.D., 2002. Sea-surface temperature variability and deep water reorganization in the subtropical North Atlantic during Isotope Stage 2–4. Marine Geology 189, 145-162.

Harvey, J. and Arhan, M., 1988. The water masses in central North Atlantic in 1983-84, J. Phys. Oceanogr. 18, 1855–1875.

Haug, G.H., Tiedemann, R., 1998. Effect of the formation of the Isthmus of Panama on Atlantic Ocean thermohaline circulation. Nature 393, 673-676.

Hays, J.D., Imbrie, J., Shackleton, N.J., 1976. Variations in the Earth's Orbit: Pacemaker of

the Ice Ages. Science 194 (4270), 1121-1132.

Heinrich, H., 1988. Origin and consequences of cyclic ice rafting in the northeast Atlantic Ocean during the past 130,000 years. Quaternary Research 29, 142-152.

Hemleben, C., Spindler, M., Anderson, O.R., 1989. Modern Planktonic Foraminifera. New York, Springer.

Hodell, D.A., Charles, C.D., Sierro, F.J., 2001. Late Pleistocene evolution of the ocean's carbonate system. Earth and Planetary Science Letters 192 (2), 109–124.

Hodell, D., Evans, H.F., Channell, J.E.T., Curtis, J.H., 2010. Phase relationships of North Atlantic ice-rafted debris and surface-deep climate proxies during the last glacial period. Quaternary Science Reviews 29, 3875-3886.

Hodell, D., Crowhurst, S., Skinner, L., Tzedakis, P.C., Margari, V., Channell, J.E.T., Kamenov, G., MacLachlan, S., Rothwell, G., 2013a. Response of Iberian Margin sediments to orbital and suborbital forcing over the past 420 ka. Paleoceanography 28, 185-199.

Imbrie, J., Imbrie, J.Z., 1980. Modeling the climatic response to orbital variations. Science 207, 943-953.

Imbrie, J., Hays, J.D., Martinson, D.G., McIntyre, A., Mix, A.C., Morley, J.J., Pisias, N.G., Prell, W.L., Shackleton, N.J., 1984. The orbital theory of Pleistocene climate: support from a revised chronology of the marine d18O record, in: Berger, A., Imbrie, J., Hays, J., Kukla, G., Saltzman, B. (Eds.), Milankovitch and Climate, Part I., D. Reidel, Dordrecht, pp. 269-305.

Kandiano, E.S., Bauch, H.A., Müller, A., 2004. Sea surface temperature variability in the North Atlantic during the last two glacial-interglacial cycles: comparison of faunal, oxygen isotopic, and Mg/Ca-derived records. Palaeogeography, Palaeoclimatology, Palaeoecology 204, 145-164.

Kennett, J.P., Srinivasan, M.S., 1983. Neogene planktonic foraminifera: a phylogenetic atlas. Hutchinson Ross Publishing Company. Stroudsburg, Pennsylvania.

Keigwin, L. G., and G. A. Jones (1994), Western North Atlantic evidence for millennial-scale changes in ocean circulation and climate, J. Geophys. Res. 99, 397-410.

Kuhlbrodt, T., Griesel, A., Montoya, M., Levermann, A., Hofmann, M., Rahmstorf. S., 2007. On the driving processes of the Atlantic Meridional Overturning Circulation. Reviews of Geophysics, 45, RG2001.

Laskar, J., Robutel, P., Joutel, F., Gastineau, M. Correia, A.C.M., Levrard, B., 2004. A long

term numerical solution for the insolation quantities of the Earth, Astron. Astrophys. 428, 261-285.

LeGrande, A., Schmidt, G., 2006. Global gridded data set of the oxygen isotopic composition in seawater. Geophys. Res. Lett. 33 (12), L12604.

Lynch-Stieglitz, J., Adkins, J.F., Curry, W.B., Dokken, T., Hall, I.R., Herguera, J.C., Hirschi, J.J. M., Ivanova, E.V., Kissel, C., Marchal, O., Marchitto, T.M., McCave, I.N., McManus, J.F., Mulitza, S., Ninnemann, U., Peeters, F., Yu, E.-F., Zahn, R., 2007. Atlantic meridional overturning circulation during the Last Glacial Maximum. Science 316, 66-69.

Lisiecki, L.E., Raymo, M.E., 2005. A Pliocene-Pleistocene stack of 57 globally distributed benthic d18O records. Paleoceanography 20 (PA1003).

Lisiecki, L.E., Stern, J.V., 2016. Regional and global benthic d18O stacks for the last glacial cycle. Paleoceanography 31, 1368-1394.

Locarnini, R. A., Mishonov, A. V., Antonov, J. I., Boyer, T. P., Garcia H. E., 2010, in: S. Levitus, U.S. Gov. Print. Off., Washington, D.C, World Ocean Atlas 2009, 1: Temperature, NOAA Atlas NESDIS, 68.

Lomb, N.R., 1976. Least-square frequency analysis of unequally spaced data. Astrophys. Sp. Sci. 29, 447–462.

Long, J. Stoy, P., 2013. Quantifying the periodicity of Heinrich and Dansgaard-Oeschger events during Marine Oxygen Isotope Stage 3. Quaternary Research (United States) 79 (3), 413-423.

MacAyeal, D.R., 1993. Binge/purge oscillations of the Laurentide Ice Sheet as a cause of the North Atlantic's Heinrich events, Paleoceanography 8, 775-784.

McIntyre, A., Molfino, B., 1996. Forcing of Atlantic equatorial and subpolar millenial cycles by precession. Science 274, 1867-1870.

Martinson, D.G., Pisias, N.G., Hays, J.D., Imbrie, J., Moore, T.C., Shackleton, N.J., 1987. Age dating and the orbital theory of the ice ages: development of high-resolution 0 to 300,000-year chronostratigraphy Quaternary Research 27, 1-29.

Martrat, B., Grimalt, J.O., Shackleton, N.J., de Abreu, L., Hutterli, M.A., Stocker, T.F., 2007. Four climate cycles of recurring deep and surface water destabilizations on the Iberian Margin. Science 317, 502-507.

Mekik, F., 2014. Radiocarbon dating of planktonic foraminifer shells: A cautionary tale. Paleoceanography 29 (1), 13-29.

Milankovitch, M., 1930. Mathematische Klimalehre und astronomische Theorie der Klimaschwankungen, in: Handbuch der Klimatologie, edited by: Köppen, W. and Geiger, R., Vol. 1, Gebrüder Bornträger, Berlin 1-176.

Müller, P. J., Gastner, M., 1971. The "Karbonate-Bombe," a simple device for the determination of the carbonate content in sediments, soils and other materials. N. Jahrb. Mineral. Monatsch. 10, 466-469.

North Greenland Ice Core Project members, 2004. High-resolution record of Northern Hemisphere climate extending into the last interglacial period. Nature 431 (7005), 147-151.

Ottens, J.J., 1991. Planktic foraminifera as North Atlantic water mass indicators. Oceanol. Acta 14(2), 123–140.

Paillard, D., Labeyrie, L., Yiou, P., 1996. Macintosh program performs time-series analysis. EOS. Trans. Am. Geophys. Union 77, 379 (http://www.lsce.cnrs-gif.fr/soft-lsce/indexen.html).

Pailler, D., Bard, E., 2002. High frequency palaeoceanographic changes during the past 140,000 yrs recorded by the organic matter in sediments of the Iberian Margin. Palaegeography Palaeoclimatology Palaeoecology 181, 431-452.

Ravelo, C., Hillaire-Marcel, C., 2007. The Use of Oxygen and Carbon Isotopes of Foraminifera in Paleoceanography, in: Hillaire-Marcel, C., de Vernal, A., Methods in Late Cenozoic Paleoceanography, Elsevier (Eds), Amsterdam (NL).

Reimer, P.J. et al. 2013. Intcal13 and Marine13 radiocarbon age calibration curves 0–50,000 years cal BP. Radiocarbon 55(4), 1869-1887.

Repschläger, J., Weinelt, M., Kinkel, H., Anderesen, N., Garbe-Schönberg, D., 2015. Response of the subtropical North Atlantic surface hydrography on deglacial and Holocene AMOC changes. Paleoceanography 30 (5), 456-476.

Rohling, E.J., Mayewski, P.A., Challenor, P., 2003. On the timing and mechanism of millennial-scale climate variability during the last glacial cycle. Climate Dynamics 20, 257-267.

Ruddiman, W.F., 1977. Late Quaternary deposition of icerafted sand in the sub-polar North Atlantic (lat. 40°N to 65°N), Geol. Soc. Am. Bull. 88, 1813-1821.

Saito, T., Thompson, P. R., and Breger, D., 1981. Systematic Index of Recent and Pleistocene Planktonic Foraminifera. University of Tokyo Press.

Scargle, J.D., 1982. Studies in astronomical time series analysis, II statistical aspects of

spectral analysis of unevenly spaced data. Astrophys. J. 263, 835-853.

Schulz, M., Mudelsee, M., 2002. REDFIT: estimating red-noise spectra directly from unevenly spaced paleoclimatic time series. Comput. Geosci. 28, 421-426.

Schulz, M., Stattegger, K., 1997. Spectrum: spectral analysis of unevenly spaced paleoclimatic time series. Comput. Geosci. 23, 929-945.

Schiebel, R., and Hemleben, C., 2005. Modern planktic foraminifera. Pala¨ontologische Zeitschrift 79, 135–148

Schiebel, R., Waniek, J., Zeltner, A., Alves, M., 2002a. Impact of the Azores Front on the distribution of planktic foraminifers, shelled gastropods, and coccolithophorids. Deep Sea Res. Part II 49(19), 4035–-4050.

Schiebel, R., Schmuker, B., Alves, M., Hemleben, C., 2002b. Tracking the recent and late Pleistocene Azores front by the distribution of planktic foraminifers, J. Mar. Syst. 37(1-3), 213-227.

Schwab, C., Kinkel, H. Weinelt, M., Repschläger, J., 2012. Coccolithophore paleoproductivity and ecology response to deglacial and Holocene changes in the Azores Current System, Paleoceanography 27, PA3210.

Sexton, P.F., Barker, S., 2012. Onset of 'Pacific-style' deep-sea sedimentary carbonate cycles at the mid-Pleistocene transition. Earth and Planetary Science Letters 321-322, 81-94.

Shackleton, N.J., Berger, A., Peltier, W.R., 1990. An alternative astronomical calibration of the Lower Pleistocene timescale based on ODP Site 677. The Late Cenozoic Ice Age. Transactions of The Royal Society of Edinburgh, Earth Sciences 81, 251-261.

Shackleton, N.J., Hall, M.A., Pate, D., 1995. Pliocene stable isotope stratigraphy of Site 846, Proc. ODP Sci. Results 138, 337-356.

Shackleton, N.J., Hall, M.A., Vincent, E., 2000. Phase relationships between millennial-scale events 64,000-24,000 years ago. Paleoceanography 115(6), 565–569.

Shackleton, N.J., Fairbanks, R.G., Chiu, T.-C., Parrenin, F., 2004. Absolute calibration of the Greenland time scale: Implications for Antarctic time scales and for Δ14C, Quat. Sci. Rev., 23, 1513–1522.

Siani, G., Paterne, M., Michel, E., Sulpizio, R., Sbrana, A., Arnold, M., Haddad, G., 2001. Mediterranean sea-surface radiocarbon reservoir age changes since the last glacial maximum, Science 294, 1917-1920.

Stanford, J.D., Rohling, E.J., Bacon, S., Roberts, A.P., Grousset, F.E., Bolshaw, M., 2011. A new concept for the paleoceanographic evolution of Heinrich event 1 in the North

Atlantic. Quaternary Science Reviews 30, 1047-1066.

Storz, D., Schulz, H. Waniek, J.J. Schulz-Bull, D.E., Kuçera M., 2009. Seasonal and interannual variability of the planktic foraminiferal flux in the vicinity of the Azores Current, Deep Sea Research Part I 56(1), 107-124.

Stuiver, M., Reimer, P.J., Braziunas, T.F., 1993. High-precision radiocarbon age calibration for terrestrial and marine samples. Radiocarbon 40(3), 1127-1151.

Tiedemann, R., Samthein, M., Shackleton, N.J., 1994. Astronomical timescale for the Pliocene Atlantic d18O and dust flux records of ODP site 659. Paleoceanography 9 619-638.

White, W.M., Schilling, J.G., Hart, S.R., 1976. Evidence for the Azores mantle plume from strontium isotope geochemistry of the Central North Atlantic. Nature 263, 659-663.

7. Planktonic foraminifera as tracers of central North Atlantic (Azores region) hydrographic changes during the last 144 kyr

Bonfardeci A.[1-2], Caruso A.[1], Bartolini A.[2], Blanc-Valleron M.M.[2]

1- Dipartimento di Scienze della Terra e del Mare, Università degli studi di Palermo, via Archirafi 20-22, 90123 Palermo, Italy

2- CNRS – UMR 7207 CR2P, MNHN, 8, rue Buffon, 75005 Paris, France

Keywords: North Atlantic, Azores region, planktonic foraminifera, paleoceanography, paleoproductivity, climatic changes, late Quaternary

7.1 Abstract

Planktonic foraminifera census data combined with Modern Analog Technique sea surface temperatures reconstructions, from two sedimentary cores collected southwest of the Azores archipelago, have been used to truck the complex central North Atlantic surface hydrographic and palaeoproductivity variability history, during the last 144 kyr. Although the two cores were collected in relatively close (200 Km) distance and, at the present, are both situated near the northern boundary between the North Atlantic Subtropical Gyre (STG) and the Azores Front Current System (AFCS), the data highlighted very contrasting sea surface temperatures and productivity patterns between the two coring sites, especially during extreme glacial periods. This may imply that during such periods, the north-westernmost coring site was likely under the influence of North Atlantic Subpolar Gyre (SPG) water mass, while the south-easternmost site was still limbed by the warmer and oligotrophic North Atlantic STG water mass, or at least by the transitional Eastern North Atlantic Central Water system (ENACW). Furthermore, during the extreme rapid climate variations linked to the "Heinrich" related events, "normal" temperature decreases of 2-5 °C have been observed in the north-westernmost core record, whereas in the south-easternmost core "anomalous" increases of temperature of 2-4 °C have been estimated. Finally, the downcore fluctuations of key planktonic foraminifera taxa, typically mass-water tracers in the Azores area, has allowed to truck the displacement of the ACFS and of the SPG-STG-ENACW system in the Azores region at glacial/interglacial and millennial scales, and demonstrated their strong connection with the orbital-forced AMOC weakening/strengthening.

7.2 Introduction

General oceanic circulation in the Atlantic Ocean results in a complex overturning of surface and deep-water masses, known as the Atlantic Meridional Overturning Circulation (AMOC).

The central North Atlantic Ocean, in particular the Azores region, represents a very climate sensitive region, crucial to test the interplaying between variations in extension and strength of the North Atlantic Subtropical Gyre (STG) and Subpolar Gyre (SPG), the AMOC strengthening/weakening, and climatic astronomical orbital forcing during the late Quaternary (Chapman et al., 2000; Schwaab et al., 2012; Repschlager et al., 2015). Today, in the Azores area, important atmospheric phenomena (Azores Anticyclone) and surface water currents (Azores Current/Front System) originate, influencing the climate of low-medium latitude of the North Atlantic Ocean and the Mediterranean region (Schiebel et al., 2002b, Rogerson et al., 2004, Storz et al., 2009; Repschläger et al., 2015).

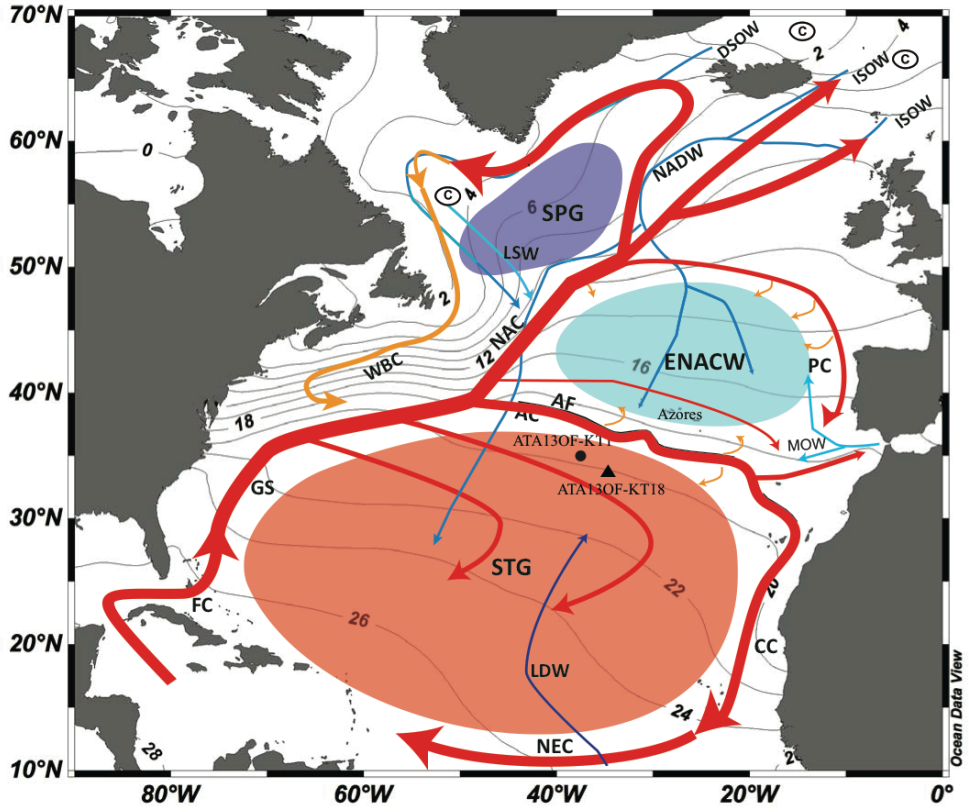

Figure 1. Modern surface water circulation of the North Atlantic overlayed on contour map of spring (April–June) sea surface temperatures (SSTs) (modified from Schwab et al., 2012, Repschlager et al., 2015; Locarnini et al., 2010). STG=SubTropical Gyre; ENACW=Eastern North Atlantic Central Water; SPG=SubPolar Gyre; NADW=North Atlantic Deep Water; ISOW= Iceland Scotland Overflow Water; DSOW=Denmark Strait

Overflow Water; LDW=Lower Deep Water; ©=NADW formation sites; WBC=Western Boundary Current; LSW=Lower Sea Water; NEC=North Equatorial Current; FC=Florida Current; GS=Gulf Stream; NAC=North Atlantic Current; AC=Azores Current; AF=Azores Front; PC=Portugal Current; CC=Canary Current; MOW=Mediterranean Outflow Water. Numbers are referred to sea surface temperatures of North Atlantic (°C).

Several studies on living planktonic foraminifera in the Azores region revealed as some species are intimately linked with peculiar mass waters and current fronts (Ottens, 1991; Schiebel et al., 2002b; Storz et al., 2009). Downcore fluctuations of such key taxa can be therefore used as fine tracers of mass waters and current fronts displacements and intensification (Ottens, 1991; Schiebel et al., 2002b; Repschläger et al., 2015). Thus it became possible to truck in such sensitive Azores area the interplaying between the hydrographical and climatic variability at the glacial/interglacial scale, as well as up to millennial-centennial to decadal scale. In particular, some Authors focused on the link between Azores Front/Current System latitudinal shifts and late Quaternary glacial/interglacial climate changes (Schiebel et al., 2002 a-b; Rogerson et al., 2004). Schiebel et al. (2002b) demonstrated indeed a more southern position of the Azores Front during last four glacial as compared to the interglacials. Schwab et al. (2012) and Repschläger (2015) reported latitudinal shifts of phyto- and zooplankton taxa during the last deglacial and Holocene (0-16 kyr B.P.), related to changes in SST of water masses close to the Azores Current/Front System. However, Rogerson et al. (2004) argued that the AFC system has not changed its position during the last deglacial period, in the Gulf of Cadiz.

In this work, high-resolution census analyses on planktonic foraminiferal assemblages, combined with Modern Analog Technique sea surface temperatures reconstructions, from two sedimentary cores, collected south-westward of the Azores islands, have been used to reconstruct the last 145 ka hydrographical and climatic variability of the central North Atlantic. Some selected species, which, at present, characterize specific water masses and surface front/current systems of the North Atlantic, have been used as paleoceanographic tracers. Therefore, the relative abundance fluctuations of these species have been used as indexes of the position occupied by these water masses. The adopted approach aims to evaluate the latitudinal/longitudinal migration of Azores Front/Current System, during the late Quaternary, as well as of the other fronts and currents characterising the central North Atlantic hydrographic pattern. Finally, the high-resolution sampling strategy adopted in this work, allowed to explore in the Azores region, the interactions between SST variations, the displacement of the ACF and of the SPG-STG-ENACW systems, and the climatic orbital forcing.

7.3 Hydrographic setting

The Gulf Stream represents one of the most important surface currents in the North Atlantic Ocean (Schmitz & McCarthy, 1993). The wind-driven Gulf Stream current originates in the Gulf of Mexico and constitutes the trigger for the activation of Atlantic Meridional Overturning Circulation (AMOC) system (Kuhlbrodt et al., 2007; Delworth et al., 2008; Parker at al., 2015) (Fig. 1). This warm water flows out through the Florida strait along the American eastern margin (Repschläger et al., 2015) and then, at 38-42° N of latitude, divides in two branches. One of these, known as North Atlantic Current (NAC), continues toward the high latitudes of North Atlantic, bringing heat in these regions (Crowley, 1981; LeGrande and Lynch-Stieglitz, 2007; Repschläger et al., 2015). The heat transfer from the surface waters to atmosphere, at high latitudes of North Atlantic, causes an inverse density contrast and triggers the sinking of cold and salty surface waters. Finally, these denser waters form the southward flowing North Atlantic Deep Water (NADW). Three major site of NADW formation are present in the North Atlantic: the Nordic (Greenland-Iceland), the Norwegian and the Labrador Seas (Hagen and Keigwin, 2002). The second branch of the Gulf Stream, the Azores Current (AC), flows toward the east at transitional-subtropical latitudes (Schiebel et al., 2002a; Rogerson et al., 2004; Schwab et al., 2012). Part of this current continues toward the Gulf of Cadiz, while a second portion moves towards the Canary Islands (Rogerson et al., 2004) and forms the Canary Current (CC). These latter current (CC) flows southward along the western African margin and reaches the low latitudes of North Atlantic, where it generates the North Equatorial Current (NEC). The present front/currents setting causes the formation of tree important superficial-gyres, in the North Atlantic Ocean (Fig. 1): the Sub Polar Gyre (SPG), with a cyclonic surface waters rotation, in North-western sector, the Subtropical Gyre (STG), characterized by an anticyclonic movement of water masses and the Eastern North Atlantic Central Water (ENACW), also known as North Atlantic Transitional Water (NATW) (Schwab et al., 2012).

7.3.1 The Azores Front/Current system

The Azores region hydrographic pattern is dominated by the Azores Front/Current system (AFCS). The Azores current (AC), as eastern branch of the Gulf Stream Current (Schiebel et al., 2002a; Rogerson et al., 2004; Schwab et al., 2012), is present throughout the year (Schiebel et al., 2002a), even if it is stronger in spring (Alves & DeVerdière, 1999; Rogerson et al., 2004). Today, the Azores Current, 50 km wide, is centred at 34°N and reaches the depth

of about 1 km (Klein and Siedler, 1989; Schiebel et al., 2002a). In its eastward flowing, this surface meandering current causes presence of mesoscale eddies, that locally induce upwelling/downwelling movements (Siedler et al., 1985; McClain & Firestone, 1993; Alves & DeVerdière, 1999; Rogerson et al., 2004).

The northern boundary of the Azores Current (AC), is constituted by the so-called Azores Front (AF), which separates African and European surface water masses (Rogerson et al., 2004). According to Schiebel et al. (2002a-b), this Azores Front separates the saltier southern (originated in the Sargasso Sea), that characterise the Subtropical Gyre, from colder and fresher northern water masses, belonging to the Eastern North Atlantic Central Water (Gould, 1985; Schiebel et al., 2011; Schwab et al., 2012). Therefore, in the Azores region, the AFCS represents the northern boundary of North Atlantic Subtropical Gyre (Repschlager et al., 2015). Macedo et al. (2000), suggested as the Azores Front Current System lies between the 18°C Mode Water (to the south) and 15°C Mode Waters (to the north).

According to Gould (1985) and Schiebel et al. (2002a), the position of the AF, in the Azores region, corresponds to the zone of strongest dipping 15°C isotherm, identified in the central zone of the AF between 200 and 300 m depth.

The prosecution of the Azores Front is clearly identifiable south of the Azores Islands between Madeira and Canary Islands (Kase et al., 1985; Johnson & Stevens, 2000; Rogerson et al., 2004). However, in the literature there is not consensus about the fate of the AC toward the Gulf of Cadiz: according Johnson & Stevens (2000) its prosecution is not at all evident, while for Rogerson et al. (2004),the AC would transform in the Gulf of Cadiz and penetrate into the Mediterranean basin through the Strait of Gibraltar (Rogerson et al., 2004). Furthermore, some authors attributed to the sub-surficial current outgoing from the Mediterranean basin, known as Mediterranean Outflow Water (MOW), a main control factor on the Azores Current dynamic (Volkov and Fu, 2010; Schwab et al., 2012).

7.4 Materials and methods

7.4.1 Core location

ATA13-OF-KT1 and ATA13-OF-KT18 cores were collected during Oceanograflu cruise (2013), with a 5 meter Küllenberg gravity corer. In particular ATA13-OF-KT1 core (35°24.956'N - 37°15.749'W; bathymetry=3,431 m; length=4.03 m) was collected north-west of the Mid-Atlantic Ridge, whereas ATA13-OF-KT18 core was (34°42.206'N -

35°07.334'W; bathymetry=2,801m; length=4.45 m) recovered on the eastern side (Bonfardeci et al., this thesis) (Fig.1).

Both cores are characterised by homogeneous and continuous records of carbonate oozes, alternated with calcareous-marly layers, slightly bioturbated in some levels.

7.4.2 Planktonic foraminifera as paleoceanographic tracers

For planktonic foraminifera census data, samples were analysed in fraction greater than 125 μm. In ATA13-OF-KT1 core, micropaleontological studies have been carried out analysing every centimetre (403 samples). For ATA13-OF-KT18 core the sampling resolution was of 1 sample every cm in the interval 0-50 cm bsf and 1 sample every 2 cm for the rest of the core (248 samples in total).

As described by Bonfardeci et al. (this thesis), for taxonomic classification of the planktonic foraminiferal species has been used the revisions proposed by Rögl & Bolli (1973), Saito et al. (1981), Kennett & Srinivasan (1983), Bolli et al. (1985), Hemleben et al. (1989). Seventy-seven taxa have been distinguished and identified. The totality of censed taxa includes species, sub-species, specimens identified only for genera, as well as the morphotypes and chromotypes of certain species. Quantitative analyses were performed counting 300-400 individuals in each sample. Thanks to duplicate analyses for some samples, an assumed error of 5 % has been estimated. Where necessary, samples were split into suitable aliquots.

Palaeoclimatic and palaeoceanographic reconstructions have been performed using a restrict number of recognised taxa. Following Ottens (1991), Pflaumann et al. (1996), Schiebel et al. (2002b), Rogerson et al. (2004) and Repschläger et al. (2015), we chose key species that can track in the Azores region hydrographic fronts and surface mass water displacements at glacial-interglacial scale.

Globigerinoides ruber gr. (d'Orbigny, 1839) white is surface-dwelling warm-water indicator, considered as Sub Tropical Gyre typical (Bé & Torderlund, 1971; Bé, 1977; Storz et al., 2009). In the Azores region its abundance variations can trace latitudinal shifts of the AFCS (Schiebel et al., 2002b; Repschläger et al., 2015; Bonfardeci et al., this thesis). In *G. ruber* (white) group all *G. ruber* morphotypes, *G. elongatus* (d'Orbigny, 1839) and *G. pyramidalis* (van den Broeck, 1976) have been added together.

Globorotalia truncatulinoides (d'Orbigny, 1839) is a deep-dwelling subtropical species, reaching maximum abundance during winter (Bé & Torderlund, 1971). It presents maxima

abundances south of Azores Front (Bé, 1977; Pujol, 1980) and its juvenile form is transported from Sargasso Sea into the Azores region through the Azores Current (Billups et al., 2016). Thus the fluctuations of its relative abundance have been used as indicator of the Azores Current intensity variations (Schiebel et al., 2002a; Repschläger et al., 2015).

Globorotalia scitula (Brady, 1882) is a deep-dwelling subpolar to temperate species (Bé & Torderlund, 1971; Bé, 1977, Hemleben et al., 1989), reaching maximum abundance north of 35-40°N (Prell et al., 1999; Rogerson et al., 2004). Essentially *G. scitula* is most frequent in surface water north of the Azores Front, although it has also been founded below the thermocline south of but the AF (Schiebel et al., 2002b). Schiebel et al. (2002b) observed peaks in abundance of *G. scitula* north of and within the present Azores Front, where eddies, linked to cyclonic recirculation, cause enhanced vertical mixing (upwelling). Thus this species, typical of Eastern North Atlantic Central Water (ENACW), should be considered as tracer of Azores Front position and so of its latitudinal shifts in the past.

Globorotalia inflata (d'Orbigny, 1839) is a temperate-cool species, typical of transitional waters (Bé & Torderlund, 1971) and increases its abundance in high food levels and during winter overturning, in temperate regions (Lourens et al., 1992; Schiebel et al., 2002a). It seems to be most abundant in central western North Atlantic and is used to trace North Atlantic Current position and intensity (Ottens, 1991; Repschläger et al., 2015).

Neogloboquadrina incompta (Cifelli, 1961) right coiling (dx), considered as a cool-temperate affinity species, dwells in slightly warmer and shallower waters than *N. pachyderma* dx (Ottens, 1991; Pflaumann et al., 1996; Kuroyanagi & Kawahata, 2004; Haddam et al., 2016). Ottens (1991) showed that this species is most abundant south of the boundary between Subpolar Gyre (SG) and North Atlantic Current (NAC), along with *G. inflata*. Therefore it may be considered as tracer of the northern boundary of NAC.

Neogloboquadrina pachyderma (Ehrenberg, 1861) right coiling (dx) is a cold-affinity species, reaching maximum abundance in subpolar-transitional waters (Bé & Torderlund, 1971) and in correspondence of Deep Chlorophyll Maximum, within or at the base of the thermocline (Cullen, 1982). It's widely demonstrated that best indicator for glacials and Heinrich events is the *Neogloboquadrina pachyderma* left coiling (Bé & Torderlund, 1971; Bond et al., 1993; Broecker 1994). However, in this work *N. pachyderma* right coiling has been considered as Heinrich events indicator, because the *N. pachyderma* left coiling is very rare at these latitudes (34-35°N).

N. pachyderma right coiling morphotype is considered now as distinct species genetically separates from the right coiling variety, which should be named *Neogloboquadrina incompta*

(see Darling et al., 2006). However, we have distinguished *N. pachyderma* right coiling by *Neogloboquadrina incompta*, based on their morphological and ecological differences in the north Atlantic Ocean (Ottens, 1991; Haddam et al., 2016).

N. pachyderma dx could be used to trace the southward expansion of Subpolar Gyre and the related Subpolar Front (SPF) during glacial phases and millennial-scale cold climatic events (Heinrich and Bond events). Such events have been associated with AMOC weakening or shut down (Duplessy et al., 1988; Alley, 1994; Broecker, 1994; Eynaud et al., 2009; Barker et al., 2009; Hodell et al., 2010; Stanford et al., 2011; Repschläger et al., 2015; Billups et al., 2016).

In order to trace and quantify the primary productivity variations in the Azores region, over the last 145 kyr, some key planktonic foraminiferal species have been selected.

Globigerina bulloides d'Orbigny, 1826, is a typical subpolar to transitional species, dwelling in the subsurface water masses, till 300-400 m of depth (Bé and Torderlund, 1971; Bé, 1977; Hemleben et al., 1989), more abundant in the first 100 m bsf (Schiebel et al., 2001). This species is also abundant in lower latitude upwelling systems and is considered opportunistic, feeding in particular microalgae (Schiebel et al., 1997), but also any other organic matter (Schiebel and Hemleben, 2005; Rigual-Hernández et al., 2012). According to Schiebel et al. (2001) and Schiebel et al. (2004), *G. bulloides* may be used as primary productivity indicator, most abundant in ENACW gyre (Schiebel et al., 2002b). Ottens (1991) demonstrated as, north of the Azores region, large size *G. bulloides* are most abundant in Subpolar waters, whereas smaller size specimens are mostly associated with North Atlantic Current.

Globigerinita glutinata (Egger, 1893) is the most ubiquitous planktonic foraminifer, distributed from tropical/subtropical water masses (Bé and Torderlund, 1971; Hemleben et al., 1989). According to Schiebel and Hemleben (2000), *G. glutinata* increases in abundance during mixed layer deepening phases, associated with temperature decreases and nutrient supply toward the upper limb of water column. Hemleben et al., (1989) suggest as its diet consists essentially in diatoms. Schiebel et al. (2001) highlighted as the increase in abundance of *G. glutinata* is clearly linked to the enhanced nutrient (NO^3-) concentration in surface waters during early spring, which triggers the diatoms blooms. Therefore, *G. glutinata* can be used as proxy of diatoms productivity. Moreover, Ottens (1991) suggested as, in the Azores region, *G. glutinata* is most abundant in along the Azores Current waters..

Turborotalita quinqueloba (Natland, 1938) is a typical cold-water species, abundant between 80 and 100 m (Schiebel et al., 2001), but present till about 200 m bsl (Schiebel et al.,

2002b). Lirer et al. (2014) consider *T. quinqueloba* as herbivorous-opportunistic species and high surface productivity indicator. In the Azores region, *T. quinqueloba*, has been associated with depending of high productivity surface water masses, showing likely different trophic strategy than *G. bulloides* (Schiebel et al., 2001). However, Ottens (1991) observed that *T. quinqueloba* increases north of the North Atlantic Current system, similarly to *G. bulloides*.

Following the zoogeographic provinces classifications, developed by Bé & Torderlund (1971), Bé (1977), Vincent & Berger (1981), Ottens (1991) and Kucera (2007), species relative abundances have been used to identify five distinctive groups, based on the faunal distribution in the central North Atlantic: Polar-Subpolar sp., Temperate-Cold sp., Cold-Subtropical sp., Warm-Subtropical sp. and Tropical sp. (see table 1).

Afterwards, in order to better highlight the response of planktonic foraminiferal assemblages to climatic changes, the Warm/Cold sp. ratio has been calculated as:

Warm/Cold sp. = Warm sp. / (Warm sp. + Cold sp.) %,

with, Warm sp.= Warm-Subtropical sp. + Tropical sp. and Cold sp.= Polar-Subpolar sp.

The species we used as paleoceanographic and paleoproductivity tracers are illustrated in Plate 1 and 2 (see appendix).

7.4.3 *Sea Surface Temperature reconstruction*

The Sea Surface Temperature (SST) reconstruction of the Azores region, during the last 144 ka, has been produced using the Modern Analog Technique (SST-mat). This technic allows to estimate the SST directly from the plancktonic foraminifera census data and is considered one of the most reliable tools for SST reconstructions (Hutson, 1980; Prell, 1985; Kucera et al., 2005a; Caley et al. 2014; Haddam et al. 2016).

PaleoAnalogs 2.0 software (Theron et al., 2004) has been used to reconstruct the summer (sSST-mat) and winter SST-mat (wSST-mat) variations, selecting 15 best analogs for analysis.

In this work the annual SST-mat, here labelled aSST-mat, has been used as mean SST values. The aSST-mat reconstruction for ATA13OF-KT1 and ATA13OF-KT18 was already performed by Bonfardeci et al. (this thesis) in their study.

7.5 Chronostratigraphy

The age model for ATA13OF-KT1 and ATA13OF-KT18 cores (Bonfardeci et al., this thesis) is based on AMS ^{14}C analyses, combined with the $\delta^{18}O_{G.\ ruber}$ synchronization with the MD95-2042 $\delta^{18}O_{G.\ bulloides}$ record, re-tuned by Lisiecki and Stern (2016).

In table 1 are listed the age control points used to develop the age model for each core record (Bonfardeci et al., this thesis). For ATA13-OF-KT1 core chronology (Fig. 2) has been obtained using four calibrated ^{14}C ages, whereas for ATA13-OF-KT18 core age model developing (Fig. 3) five calibrated ^{14}C ages have been taken into account (Bonfardeci et al., this thesis).

Event	Depth (cm bsf)	Age (ka)	Reference
Poz-79864 / Core top	1.00	2.75	-
Poz-79865	17.50	10.13	-
Base Holocene	19.50	11.69	*1, *2
Base Younger Dryas	24.50	12.76	*1, *2
Poz-79866	29.50	14.30	-
D/O 1	30.50	14.39	*1, *2, *3
Base Bolling/Allerod	34.50	14.72	*1, *2
Poz-79867	39.50	15.43	-
$d^{18}O$ maximum - Base H1	50.50	18.95	*1, *2
$\delta^{18}O$ minimum	56.50	19.43	*1
$\delta^{18}O$ minimum	76.50	21.03	*1
$\delta^{18}O$ minimum	82.50	21.51	*1
D/O 2	98.50	23.88	*1, *2, *3
$d^{18}O$ maximum - Base H2	104.50	26.01	*1
D/O 3	116.50	28.33	*1, *2
D/O 4	126.50	29.19	*1, *2
$\delta^{18}O$ minimum	138.50	31.65	*1
D/O 5	144.50	32.98	*1, *2
D/O 6	150.50	34.30	*1, *2
D/O 7	156.50	35.87	*1, *2
D/O 8	162.50	37.87	*1, *2, *3
D/O 9	184.50	40.66	*1, *2
D/O 10	190.50	41.42	*1, *2
D/O 11	202.50	43.51	*1, *2, *3
D/O 12	216.50	45.95	*1, *2, *3
D/O 13	240.50	50.35	*1, *2, *3
D/O 14	262.50	53.73	*1, *2, *3

D/O 15	274.50	56.24	*1, *2
D/O 16	284.50	57.98	*1, *2, *3
D/O 17	294.50	59.03	*1, *2, *3
$d^{18}O$ maximum	318.50	63.41	*1
D/O 18	327.50	65.09	*1, *2, *3
$d^{18}O$ maximum	339.50	66.87	*1
$\delta^{18}O$ minimum	354.50	70.88	*1
D/O 19	358.50	71.95	*1, *2, *3
D/O 20	378.50	75.06	*1, *2, *3
$\delta^{18}O$ minimum	384.50	77.91	*1
$\delta^{18}O$ minimum	396.50	80.59	*1
Core Bottom	402.50	81.94	This study (extrapolated)

Table 1. Chronostratigraphic model for ATA13-OF-KT1 core. List of the selected age control points. 1* Lisiecki and Stern (2016); *2 Barker et al. (2011); *3 Billups et al. (2016).

Furthermore, minima and maxima in $\delta^{18}O_{G.\ ruber}$ signal of both cores, have been correlated with minima and maxima peaks in MD95-2042 $\delta^{18}O_{G.\ bulloides}$ (LS16) record (Lisiecki and Stern, 2016). In Order to improve the age model and to better observe the glacial/interglacial transition and ice volum effect on analysed oxygen isotope records, these have also been compared to the global benthic $\delta^{18}O$ stack, proposed by Lisiecki and Stern (2016) (Fig. 2 and 3).

Event	Depth (cm bsf)	Age (ka)	Reference
Core top	0.50	3.36	This study (extrapolated)
Poz-79833	12.50	5.40	-
Poz-79834	25.50	7.62	-
Base Holocene	42.50	11.70	*1, *2
Poz-79861 / Base Younger Dryas	50.50	12.76	-
D/O 1	52.50	13.80	*1, *2, *3
Base Bolling/Allerod	58.50	14.73	*1, *2
Poz-79862	64.50	15.71	-
$\delta^{18}O$ minimum	68.50	16.75	*1
$d^{18}O$ maximum - Base H1	76.50	18.96	*1
$\delta^{18}O$ minimum	80.50	20.01	*1
Poz-79863	84.50	21.06	-
$d^{18}O$ maximum	90.50	21.86	*1
D/O 2	96.50	23.69	*1, *2, *3
$d^{18}O$ maximum - Base H2	109.50	26.10	*1
D/O 3	114.50	28.13	*1, *2
D/O 4	118.50	29.19	*1

D/O 5	126.50	31.63	*1, *2
D/O 6	132.50	32.79	*1, *2
D/O 7	146.50	35.85	*1, *2
D/O 8	154.50	37.88	*1, *2, *3
D/O 9	162.50	40.48	*1, *2
D/O 10	168.50	41.93	*1, *2
D/O 11	176.50	43.51	*1, *2, *3
$\delta^{18}O$ minimum	184.50	45.44	*1
D/O 12	192.50	46.49	*1, *2, *3
D/O 13	200.50	50.33	*1, *2, *3
D/O 14	214.50	53.73	*1, *2, *3
D/O 16	220.50	57.98	*1, *2, *3
D/O 17	224.50	59.03	*1, *2, *3
$d^{18}O$ maximum	232.50	63.42	*1
D/O 18	236.50	64.84	*1, *2, *3
$d^{18}O$ maximum - Top H7	240.50	66.20	*1, *2
$\delta^{18}O$ minimum	250.50	69.97	*1
D/O 19	262.50	72.05	*1, *2, *3
D/O 20	272.50	75.08	*1, *2, *3
$d^{18}O$ maximum - Base H7a	276.50	77.08	*1
D/O 21	294.50	83.97	*1, *2, *3
D/O 22	310.50	88.95	*1, *2, *3
$d^{18}O$ maximum	316.50	93.49	*1
$d^{18}O$ maximum	322.50	95.08	*1
$\delta^{18}O$ minimum	330.50	99.22	*1
D/O 23?	336.50	101.84	*1, *2, *3
$d^{18}O$ maximum	340.50	104.48	*1
D/O 24?	350.50	108.30	*1, *2, *3
$\delta^{18}O$ minimum	360.50	110.25	*1
D/O 25?	372.50	112.79	*1
$\delta^{18}O$ minimum	384.50	122.03	*1, *2, *3
$\delta^{18}O$ minimum	390.50	123.84	*1
D/O 26?	394.50	126.84	*1, *2, *3
$\delta^{18}O$ minimum	402.50	128.48	*1
$\delta^{18}O$ minimum	408.50	130.84	*1
$\delta^{18}O$ minimum	418.50	133.47	*1
$\delta^{18}O$ minimum - Base H11	424.50	135.96	*1
$\delta^{18}O$ minimum	434.50	139.98	*1
$\delta^{18}O$ minimum	442.50	143.03	*1
Core Bottom	444.50	143.79	This study (extrapolated)

Table 2. Chronostratigraphic model for ATA13-OF-KT18 core. List of the selected age control points. 1* Lisiecki and Stern (2016); *2 Barker et al. (2011); *3 Billups et al. (2016).

Twenty minima peaks have been correlated to the D/O insterstadials, reported in the studies of Barker et al. (2011) and Billups et al. (2016), for ATA13-OF-KT1 tuning, whereas the age of twenty-two of these events (D/O) have been used to obtain additional age control points. Also the Heinrich events 1 to 12 have been used to add as age control points for chronology of the studied records.

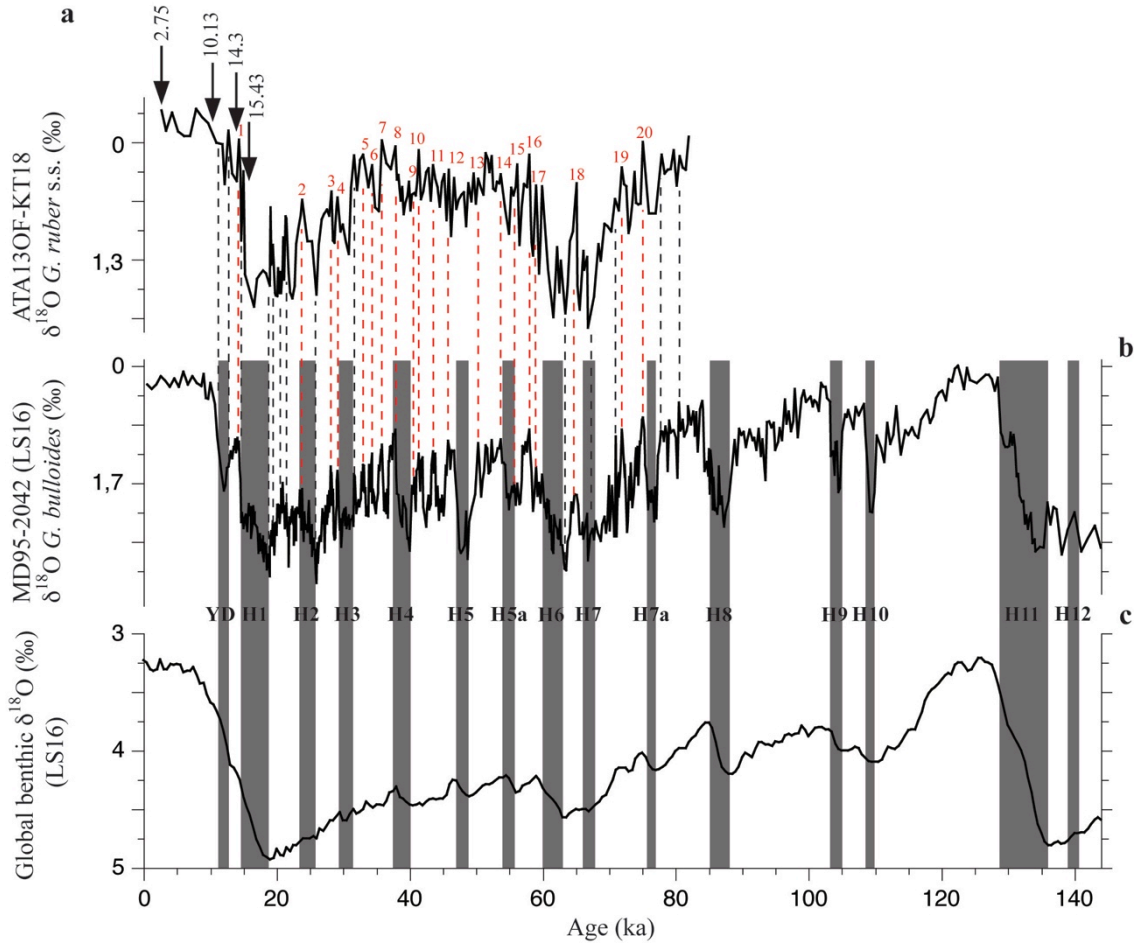

Figure 2. ATA13OF-KT1 $\delta^{18}O_{G.\ ruber}$ time-series synchronizated with the LS16 model (Lisiecki and Stern, 2016) (a). The (c) global benthic $\delta^{18}O$ stack (LS16) and the (b) MD95-2042 $\delta^{18}O_{G.\ bulloides}$ (LS16) have been used as reference curve for the age model developing. Black arrows indicate the depth correspondent to the AMS ^{14}C analyses performed in the $\delta^{18}O_{G.\ ruber}$ record. Black numbers above these arrows indicate the calibrated ^{14}C adopted (ka). Black dashed lines are relative to the correlation points between the ATA13OF-KT18 $\delta^{18}O_{G.\ ruber}$ and the MD95-2042 $\delta^{18}O_{G.\ bulloides}$ (LS16) records. Red dashed lines are referred to the correlation points correspondent with the Dansgaard/Oeschger (D/O) events, labelled with the red numbers 1 to 22 (Barker et al., 2011; Billups et al., 2016). Dark gray vertical bars identify the interval correspondent to the Heinrich events, proposed by Lisiecki and Stern (2016), here labelled as H1 to H12.

According to the developed age model, the ATA13-OF-KT1 core record spans from 2.75 to 81.94 ka, whereas the ATA13-OF-KT18 stratigraphic record covers the interval between 3.36 to 143.79 ka (Bonfardeci et al., this thesis).

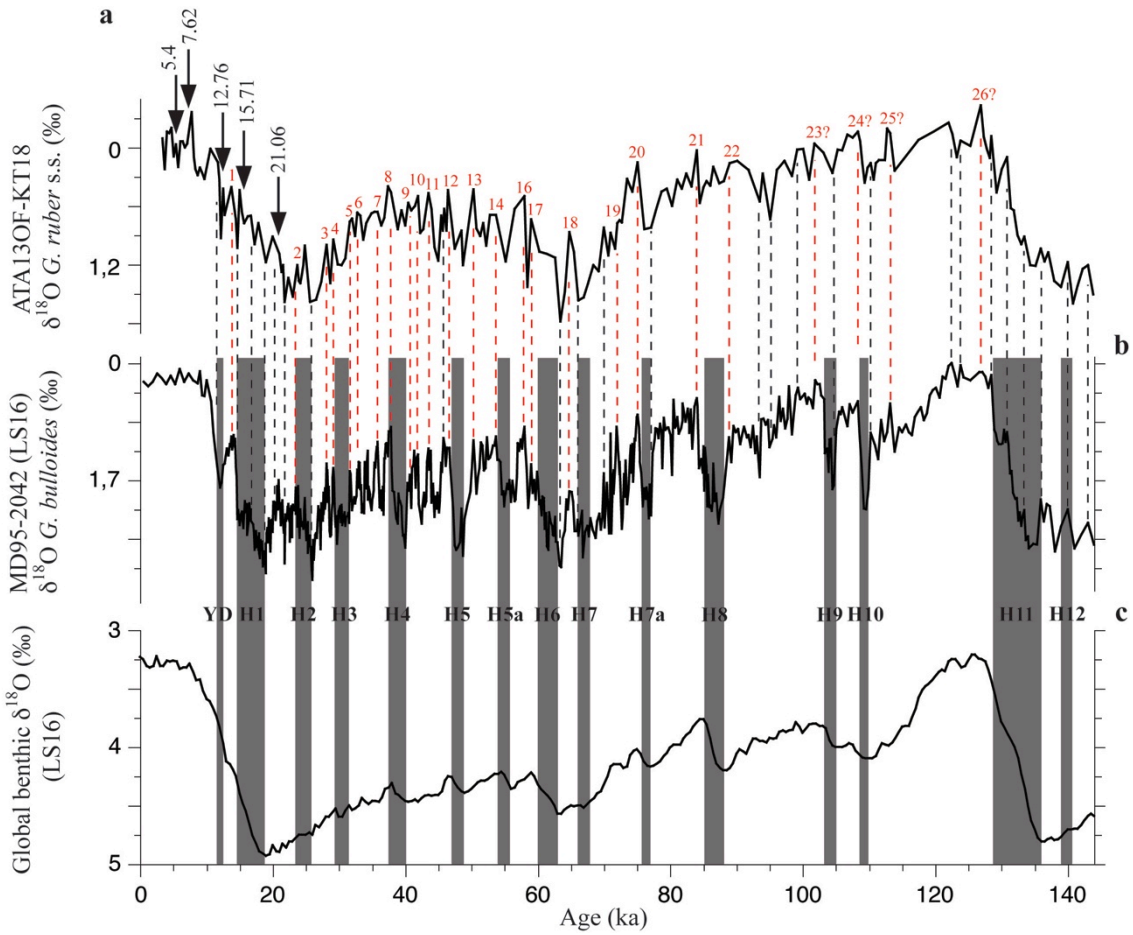

Figure 3. ATA13-OF-KT18 $\delta^{18}O_{G.\ ruber}$ record tuned according to LS16 model (Lisiecki and Stern, 2016) (a). The (c) global benthic $\delta^{18}O$ stack (LS16) and the (b) MD95-2042 $\delta^{18}O_{G.\ bulloides}$ (LS16) have been used as reference curve for the age model developing. Black arrows indicate the depth correspondent to the AMS ^{14}C analyses performed in the $\delta^{18}O_{G.\ ruber}$ record. Black numbers above these arrows indicate the calibrated ^{14}C adopted (ka). Black dashed lines are relative to the correlation points between the ATA13OF-KT18 $\delta^{18}O_{G.\ ruber}$ and the MD95-2042 $\delta^{18}O_{G.\ bulloides}$ (LS16) records. Red dashed lines are referred to the correlation points correspondent with the Dansgaard/Oeschger (D/O) events, labelled with red numbers 1 to 22 (Barker et al., 2011; Billups et al., 2016). The warming events labelled with the red numbers 23 to 26 are not present in literature. Dark gray vertical bars identify the interval correspondent to the Heinrich events, proposed by Lisiecki and Stern (2016), here labelled as H1 to H12. YD=Younger Dryas cold period.

The mean sedimentation rates for ATA13OF-KT1 and ATA13OF-KT18 core resulted 5.08 and 3.12 cm/kyr respectively. Considering the sampling interval of 1 cm, a temporal resolution of 197 up to 320 years between samples have been calculated (Bonfardeci et al.,

this thesis). In figure 4 is shown the sedimentation rate calculated (Bonfardeci et al., this thesis) in the intervals between two following age control points (Tab. 1 and 2), for both core records.

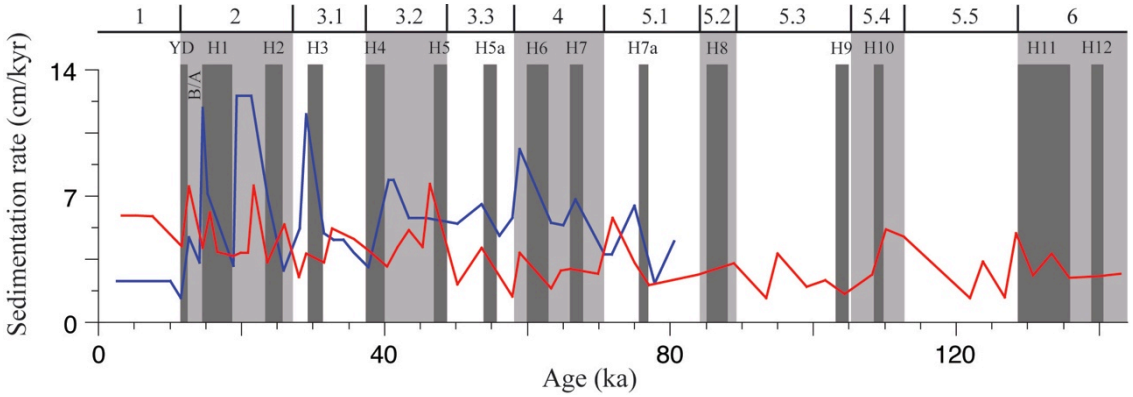

Figure 4. Sedimentation rate between the selected age control points (modified from Bonfardeci et al., this thesis), obtained through the synchronization with MD95-2042 $\delta^{18}O_{G.\ bulloides}$ (LS16) record (Lisiecki and Stern, 2016). The blue line is relative to the ATA13OF-KT1 core, whereas the red line represents the sedimentation rate of the ATA13OF-KT18 core. Numbers above are referred to the Marine Isotope Stages (Lisiecki and Raymo, 2005) and sub-Stages (Martinson et al., 1987). Light gray vertical bars refer to the glacial stages (MIS 2, 4 and 6) and cool-temperate periods (MIS 3.2, 5.2 and 5.4). White vertical bars are related to the interglacials (MIS 1, 5.1, 5.3 and 5.5) and temperate-warm periods (MIS 3.1 and 3.3). Dark gray vertical bars identify the intervals correspondent to the Heinrich events, proposed by Lisiecki and Stern (2016), here labelled as H1 to H12. YD=Younger Dryas stadial; B/A=Bølling/Allerød interstadial.

7.6 Results

7.6.1 Palaeoproductivity proxies

The sum of the average relative abundaces of *G. bulloides*, *G. glutinata* and *T. quinqueloba* results higher in ATA13-OF-KT1 record (36.4 %), than in the ATA13-OF-KT18 core (30.2 %), considering the time interval covered by both core records (3.36-81.94 ka). The curves of the three palaeoproductivity proxies show remarkable similar patterns between the two cores, a part in the MSIs 5.1 and 1 where highest values (up to > 30 %) of *G. bulloides* are present only in the ATA13-OF-KT1 record (Fig. 5). It is also evident a general anti-correlated trend between *G. bulloide*s and *G. glutinata* curves, especially during the MSI 3.

In planktonic foraminiferal assemblages of ATA13-OF-KT18 core, *G. bulloides* varies between 6.7 to 24.3 % (Fig. 5). In general, this species shows increases in abundance during

warm sub-stages MIS 5.3, 5.1, 3.1 and in correspondence of the deglacial transition MIS 4/3.3 and of MIS 2/1. After the YD it shows a stepwise decreasing during the Holocene.

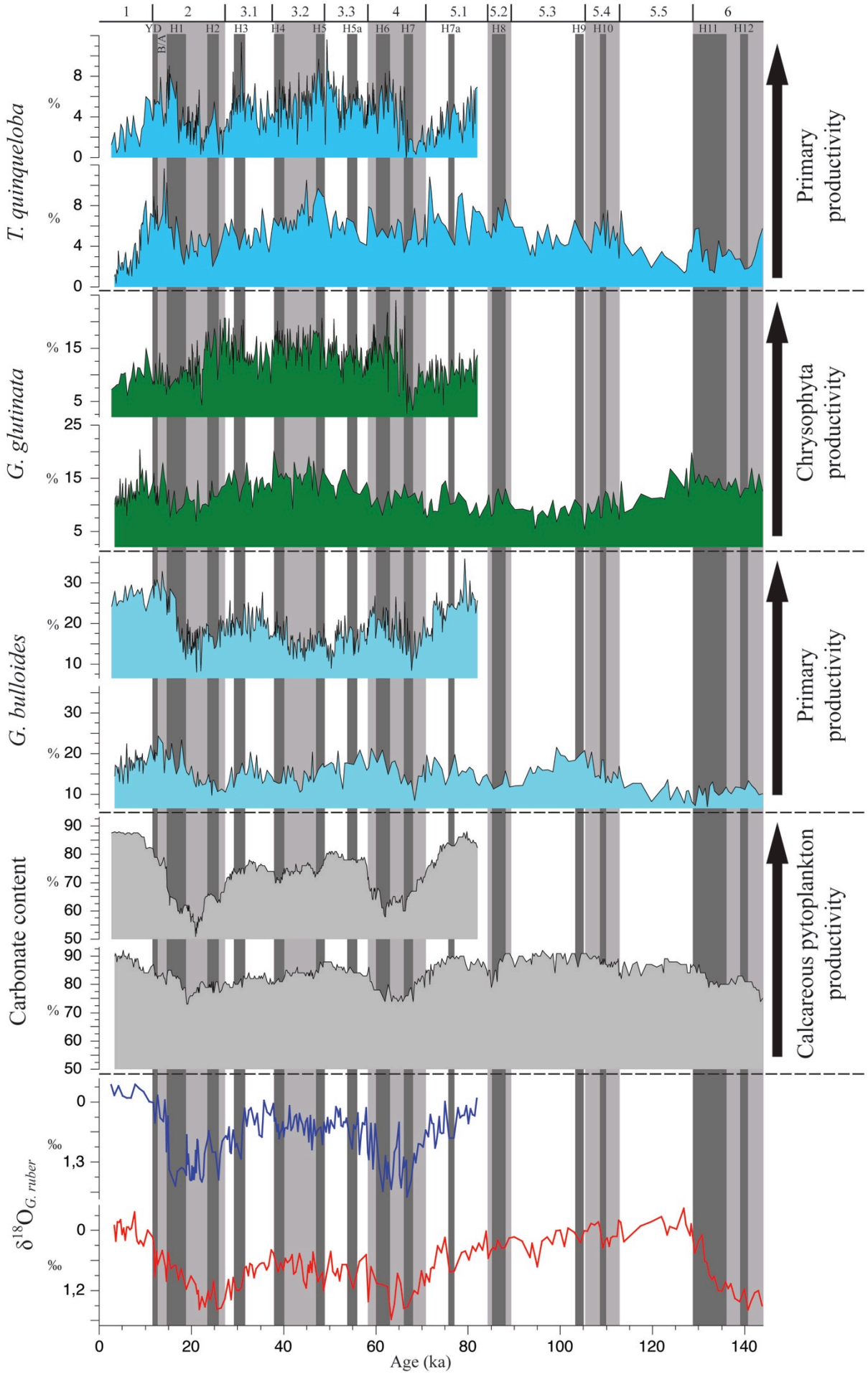
1
2
3.1
3.2
3.3
4
5.1
5.2
5.3
5.4
5.5
6
YD
H1
H2
H3
H4
H5
H5a
H6
H7
H7a
H8
H9
H10
H11
H12
B/A
T. quinqueloba
%
8
4
0
G. glutinata
15
5
25
G. bulloides
30
20
10
Carbonate content
90
80
70
60
50
δ18OG. ruber
‰
0
1,3
1,2
Primary productivity
Chrysophyta productivity
Calcareous pytoplankton productivity
0
20
40
60
80
100
120
140
Age (ka)

Figure 5. Paleoproductivity (PP) tracers of ATA13OF-KT1 and ATA13OF-KT18 cores. The shorter time-series are referred to the ATA13OF-KT1 proxy records (2.75 – 81.94 ka), whereas the longer time-series are relative to the ATA13OF-KT18 proxy records (3.36 – 143.79 ka). The curves with grey fill refer to the carbonate content of both cores (modified from Bonfardeci et al., this thesis). The curves with light blue fill are relative to the *G. bulloides* record of both cores; the curves with green fill are referred to the *G. glutinata* variability; the curve with dark blue fill are relative to the *T. quinqueloba* variability. On the right, is indicated the kind of productivity traced by the selected species. The $\delta^{18}O_{G.\ ruber}$ records of the ATA13-OF-KT1 (blue line) and ATA13-OF-KT18 (red line) were modified from Bonfardeci et al. (this thesis). Light gray vertical bars refer to the glacial stages (MIS 2, 4 and 6) and cool-temperate periods (MIS 3.2, 5.2 and 5.4). White vertical bars are related to the interglacials (MIS 1, 5.1, 5.3 and 5.5) and temperate-warm periods (MIS 3.1 and 3.3). Dark gray vertical bars identify the intervals correspondent to the Heinrich events, proposed by Lisiecki and Stern (2016), here labelled as H1 to H12. YD=Younger Dryas stadial; B/A=Bølling/Allerød interstadial.

The lowermost values of *G. bulloides*, in the ATA13-OF-KT18 assemblage, are in correspondence of MIS 6, lower part of MIS 5.5, lower part of MIS 4 ("H" 7) and of the transition MIS 3.1/2.

In the ATA13-OF-KT1 core *G. bulloides* is generally more abundant (8-35.7 %) than in the KT18 core, and it shows sharp increases particularly during MIS 5.1 and MIS 1 (Fig. 5). *G. bulloides* decreases in abundance at the beginning of MIS 4 ("H" 7), during MIS 3.2 and MIS 2.

In ATA13-OF-KT18 core *G. glutinata* relative abundance fluctuates between 5 and 20 % (Fig. 5). It was abundant during MIS 6, MIS3 and first half of MIS1, whereas it decreased during glacial stages 4, 2 and especially during MIS 5, where it shows a completely opposite trend compared to carbonate content curve. In ATA13-OF-KT1 core record, *G. glutinata* relative abundance varies between 3 and 24 %, (Fig. 5), showing the highest values during part of penultimate glacial (MIS 4) and great part of MIS 3, and lowest values during the MIS 5.1 and the early MIS 4 and also during the interval between the LGM and the late MIS 1 (Fig. 5).

T. quinqueloba relative abundances oscillate between 0.5 and 11.6 % in the ATA13-OF-KT18 record (Fig. 5), showing maxima values from MIS 5.2 to 3.1, and the late MIS 2, especially during the Bølling/Allerød and the Younger Dryas. Minima values characterize the MIS 5.5, the first half of MIS 2, and the upper Holocene, where a sharp decreasing trend is evident upward core. In ATA13-OF-KT1 core *T. quinqueloba* relative abundances fluctuate also between 0 and 11.6 %, reaching the highest values in the interval from MIS 4 to 3.1 (Fig. 5), and the latest part the MIS 2. Minima abundances have been observed at the early stage of MIS 4 and at the MIS 3.1/2 transitions. In general this species shows abrupt increases during

the “Heinrich” related events correspondent to those recognised by Lisiecki and Stern (2016), except for the “H” 7. This is much more evident in the ATA13-OF-KT1 than in ATA13-OF-KT18, probably also due to the different sampling resolution between the two cores.

7.6.2 Sea Surface Temperature reconstruction

As already described by Bonfardeci et al. (this thesis), average value of annual SST-mat results higher in ATA13-OF-KT18 record (18.28 °C) than in ATA13-OF-KT1 core (17.5 °C), according to the difference is due to a higher proportion of warm species in the southern east ATA13-OF-KT18 core, than in the northern west KT1 core (Fig. 6).

In ATA13-OF-KT18 core record, interglacials stages MIS 5.5 and MIS 1 are characterised by remarkable similar maxima aSST-mat values around 17.5-20 °C (Fig. 6). Minima aSST-mat values have been observed during the last part of glacial MIS 6 (coinciding with the “H”11) and in the at the end of MIS 3.1, where aSST-mat decreases to lowermost values of the core record (13.3 °C). During MIS 4 a stepwise cooling trend is observable, with values decreasing from 19.4 to 15.6 °C. The MIS 3.3 is marked by an increase in aSST-mat, followed by a long term cooling trend culminating with the lowest values at the end of MIS 3.1. The glacial stage of MIS 2 (14.4-18.6 °C) instead is characterised by a gradual warming trend toward the top. During the early Younger Dryas aSST-mat values decreased (14.7 °C). It is important to note that in this site during the interval correspondent to the Heinrich events, proposed by Lisiecki and Stern (2016), rapid fluctuations of aSST-mat with increasing of about 2-4 °C have been observed, with except for the “H” 11 and “H” 2, when two abrupt cold events were recorded (Fig. 6).

Some important differences are discernable between the aSST-mat records of ATA13-OF-KT1 and ATA13-OF-KT18 cores (Fig. 6). In the KT1 core also highest aSST-mat values characterize MIS 5.1 (17.5-19.4 °C) and MIS 1 (18-20.2 °C), whereas a sharp aSST-mat decreasing marks the glacial MIS 4 culminating in coincidence of the “H” 6 with the lowest values at that site record (11.2°C). Then aSST-mat values increase in the MIS 4/3.3 transition, followed by a gradual cooling from the MIS 3.2 to the top of MIS 3.1, and a rapid temperature decreasing to 14.6 °C just before the the base of “H” 2. The MIS 2 is characterised by a gradual and slight sea surface warming during the LGM, in this sector of Azores region. This phase was interrupted by rapid cooling events in correspondence with the “H” 2 (16.2 °C) and especially the “H” 1 (15.1-17.4 °C). The last deglacial is characterised by an aSST-mat increase during the Bølling/Allerød (17.4-18.6 °C), followed by a rapid cooling episode in correspondence of the Younger Dryas (16.9-17.8 °C).

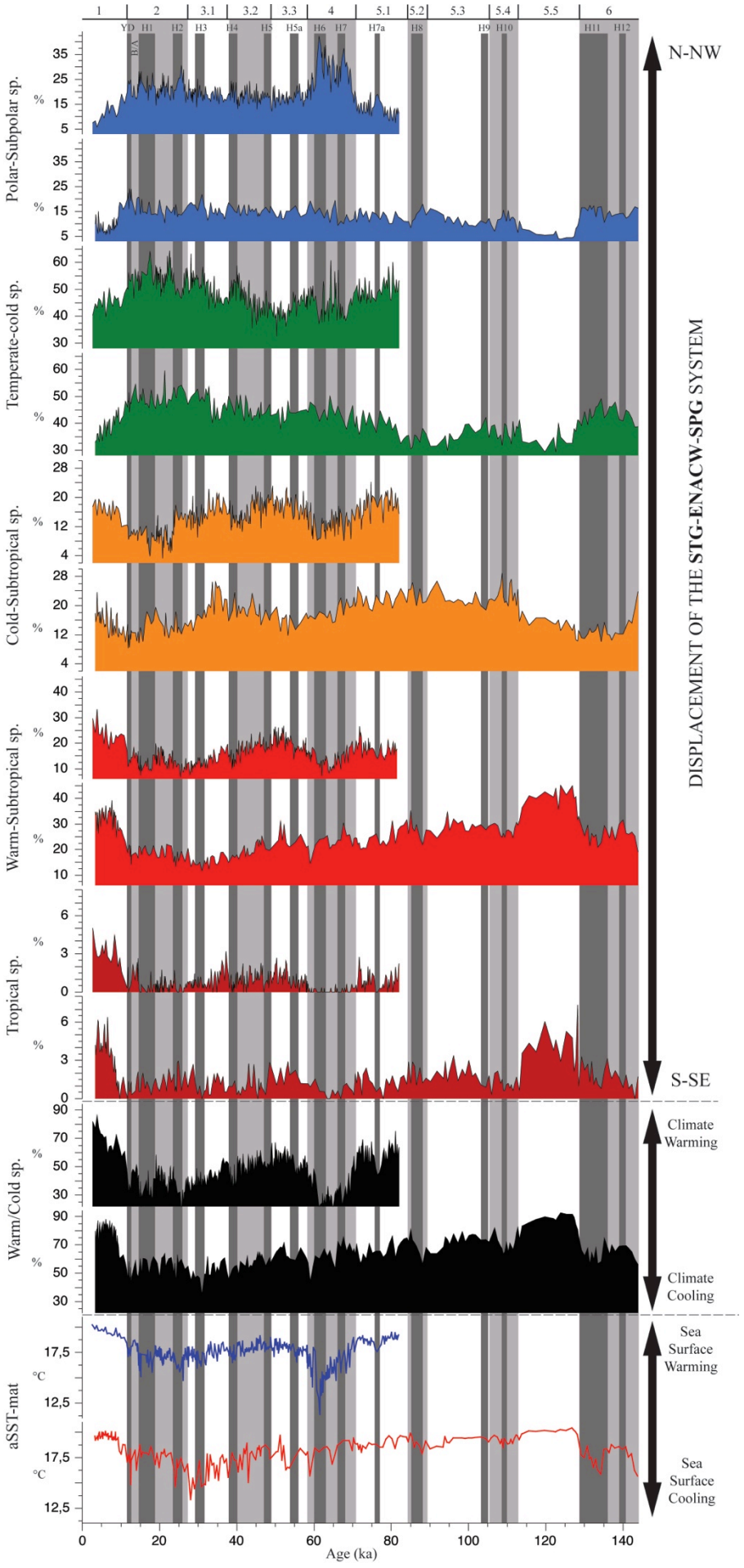
1
2
3.1
3.2
3.3
4
5.1
5.2
5.3
5.4
5.5
6
YD
H1
H2
H3
H4
H5
H5a
H6
H7
H7a
H8
H9
H10
H11
H12
BA
Polar-Subpolar sp.
Temperate-cold sp.
Cold-Subtropical sp.
Warm-Subtropical sp.
Tropical sp.
Warm/Cold sp.
aSST-mat
%
°C
N-NW
S-SE
DISPLACEMENT OF THE STG-ENACW-SPG SYSTEM
Climate Warming
Climate Cooling
Sea Surface Warming
Sea Surface Cooling
Age (ka)

Figure 6. Paleoceanographic proxies oscillations of ATA13OF-KT1 and ATA13OF-KT18 core record. The shorter time-series are referred to the ATA13OF-KT1 proxy records (2.75 – 81.94 ka), whereas the longer time-series are relative to the ATA13OF-KT18 proxy records (3.36 – 143.79 ka). The red curve are referred to the aSST-mat record of ATA13OF-KT18 core, whereas the blue line to the ATA13OF-KT1 aSST-mat record. These two curves indicate the phases of sea surface warming/cooling in the Azores region during the last 144 ka. The curves with black fill are relative to the Warm/Cold sp. records of both cores, indicating Azores region climate warming/cooling. The curves with dark red fill are relative to the Tropical sp. records; the curves with light red fill are relative to the Warm-Subropical sp. records; the curves with orange fill are relative to the Cold-Subropical sp. records; the curves with green fill are relative to the Temperate-Cold sp. records; curves with blue fill are relative to the Polar-Subpolar sp. records. All these latters are used as indicators of Subtropical Gyre (STG) – Eastern North Atlantic Central Water (ENACW) – Subpolar Gyre (SPG). Light gray vertical bars refer to the glacial stages (MIS 2, 4 and 6) and cool-temperate periods (MIS 3.2, 5.2 and 5.4). White vertical bars are related to the interglacials (MIS 1, 5.1, 5.3 and 5.5) and temperate-warm periods (MIS 3.1 and 3.3). Dark gray vertical bars identify the intervals correspondent to the Heinrich events, proposed by Lisiecki and Stern (2016), here labelled as H1 to H12. YD=Younger Dryas stadial; B/A=Bølling/Allerød interstadial.

In ATA13-OF-KT1 aSST-mat record the minima values correspond to the "Heinrich" related events, testifying abrupt climatic cooling of about 2-5 °C during these episodes, in contrast to that observed in more of those recorded in ATA13-OF-KT18 aSST-mat.

7.6.3 Planktonic foraminifera fluctuations

The major difference between the Warm/Cold sp. curves in figure 6 is the higher percentages of Warm sp. during glacial periods (especially during MIS 4) in southern eastern ATA13-OF-KT18 core than in the northern western ATA13-OF-KT1 core. Moreover, Cold-Subtropical fauna is also more abundant in ATA13-OF-KT18 record than in those of ATA13-OF-KT1, in which, on the contrary, the contribution of Temperate-Cold and Polar-Subpolar species is much more significant (Fig. 6).

During MIS 6 the planktonic foraminiferal assemblage is characterised by high percentage of Temperate-Cold and Polar-Subpolar fauna and moderate abundance of Subtropical species (both Warm- and Cold-) (Fig. 6). The species that mostly characterize the association are *N. pachyderma* dx (1-5.5 %), *N. incompta* dx (1-5.5 %), *G. inflata* (9-18 %) and *G. scitula* gr. (1-5.5 %). "H" 12 and especially the "H" 11 are marked by peaks in abundance of these species. On the contrary, warm water taxa *G. ruber* gr. and *G. truncatulinoides* are scarce, especially during the "H" 12 and "H" 11 intervals (Fig. 7).

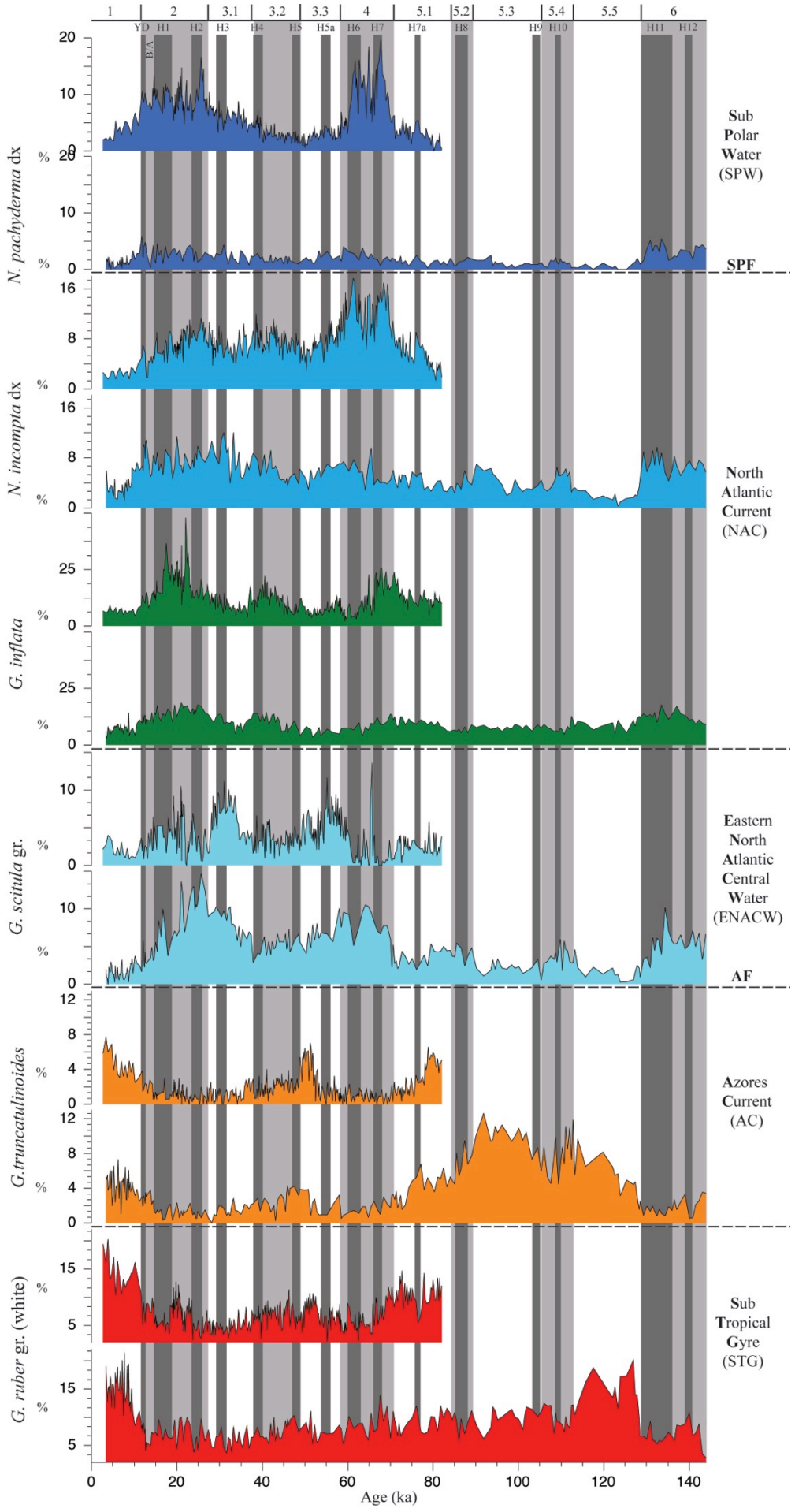
1
2
3.1
3.2
3.3
4
5.1
5.2
5.3
5.4
5.5
6
YD
H1
H2
H3
H4
H5
H5a
H6
H7
H7a
H8
H9
H10
H11
H12
BA
N. pachyderma dx
%
Sub Polar Water (SPW)
SPF
N. incompta dx
North Atlantic Current (NAC)
G. inflata
Eastern North Atlantic Central Water (ENACW)
AF
G. scitula gr.
G.truncatulinoides
Azores Current (AC)
G. ruber gr. (white)
Sub Tropical Gyre (STG)
Age (ka)

Figure 7. Paleoceanographic proxies of ATA13OF-KT1 and ATA13OF-KT18 cores. The shorter time-series are referred to the ATA13OF-KT1 proxy records (2.75 – 81.94 ka), whereas the longer time-series are relative to the ATA13OF-KT18 proxy records (3.36 – 143.79 ka). The curves with red fill are relative to the *G. ruber* gr. (white) records; the curves with orange fill are relative to the *G. truncatulinoides* records; the curves with light blue fill are relative to the *G. scitula* gr. records; the curves with green fill are relative to the *G. inflata* records; the curves with blue fill are relative to the *N. incompta* dx records; the curves with dark blue fill are relative to the *N. pachyderma* dx records. On the right panel are indicated the surface water masses and front/current systems of the central North Atlantic, traced through the selected species fluctuations. Light gray vertical bars refer to the glacial stages (MIS 2, 4 and 6) and cool-temperate periods (MIS 3.2, 5.2 and 5.4). White vertical bars are related to the interglacials (MIS 1, 5.1, 5.3 and 5.5) and temperate-warm periods (MIS 3.1 and 3.3). Dark gray vertical bars identify the intervals correspondent to the Heinrich events, proposed by Lisiecki and Stern (2016), here labelled as H1 to H12. YD=Younger Dryas stadial; B/A=Bølling/Allerød interstadial.

The interglacial stage correspondent with MIS 5 is widely dominated by Warm-Subtropical and, Cold-Subtropical species, whereas Polar-Subpolar and Temperate-Cold taxa are very low abundant. During MIS 5.5 Tropical and Warm-Subtropical species largely dominate the association, whereas Polar-Subpolar sp. are near to absent (Fig. 6). Warm and stable climatic conditions during this period are also documented by the highest abundance (9-20 %) of *G. ruber* gr. (white) (Fig. 7). *G. ruber* gr. (white) acme during this phase, has been also documented by Chapman et al. (2000) northwest of Azores Islands, where this species reached a similar relative abundance in the association (~20 %).

The interval MIS 5.4-5.1 is dominated by Cold-Subtropical fauna in ATA13-OF-KT18 coring site, whereas the Warm-Subtropical sp. gradually decrease toward the MIS 5.1 (Fig. 6). On the contrary, Polar-Subpolar and Temperate-Cold species show a slow gradual increase, during the MIS 5.4-5.1 interval. The two cool-climate phases, correspondent to MIS 5.4 and 5.2, are both marked by the increase in abundance of *G. scitula* gr. (2.5-6 %), whereas *G. truncatulinoides* (7-12.5 %) significantly increases in abundance during MIS 5.3 (Fig. 7). The last sub-stage (MIS 5.1) in ATA13-OF-KT18 core is represented by a trend of slow cooling, especially in the latest part, marked by the increase in abundance of temperate-cold species, such as *G. inflata* (8.5-12.5 %) (Fig. 7). In ATA13-OF-KT18 core record instead, the MIS 5.1 is carachterised by the gradual increase of *N. incompta* dx and *G. inflata* (Fig. 7).

MIS 4, in ATA13-OF-KT18 record, is characterised by a high abundance of Warm-Subtropical and Cold-Subtropical fauna, in the lower part, which decrease in the upper part, balanced by an increase of Polar-Subpolar and mainly Temperate-Cold species (Fig. 6). The lower part was characterised by high abundance of *G. inflata* (4.5-13 %) and *G. ruber* gr.

(white) (6.5-14%), whereas during the upper part *N. pachyderma* dx (1.5-4 %) and *N. incompta* dx (3-9.5 %) and especially *G. scitula* (2-10,5 %), increase in abundance (Fig. 7). The two "Heinrich" related events within the MIS 4 ("H" 7 and "H" 6), are marked by peaks in abundance of Cold-Subtropical and Warm-Subtropical species (Warm/Cold sp. increases), especially *G. ruber* gr. (white) (Fig. 7).

As observed in ATA13-OF-KT18 record, the end of glacial stage and the onset of MIS 3, is marked by the increasing of Cold-Subtropical fauna, which then gradually decreases at the end of MIS 3.1, surmounted by Temperate-Cold species (Fig. 6). The MIS 3.3 is also characterised by high abundance of warm water species, with increasing of *G. truncatulinoid*es and *G. ruber* gr. (white) and contemporary decreasing of cold and temperate species (Fig. 7), especially at the MIS 3.3/3.2 transition. The MIS 3.2 is marked by an increase of *N. incompta* dx (5-9 %) and *G. inflata* (6-14.5 %). In the MIS 3.1 planktonic foraminiferal assemblages clearly show an increase of cold and cool-temperate species toward the top, such as *N. pachyderma* dx (1-4.3 %), *N. incompta* dx (4-12 %) and *G. scitula* gr. (5-10.2) (Fig. 7). In particular, the rapid climate cooling of "H" 3 event is well represented by an increase in Polar-Subpolar sp. (especially *N. incompta* dx) together with Temperate-Cold sp. (especially *G. scitula* gr.) (Fig. 6 and 7).

Glacial period of MIS 2 is characterised by an increase in abundance of Warm-Subtropical and Temperate-Cold fauna, respect to the previous MIS 3.1 (Fig. 6), documented by the maxima abundances of *G. inflata* (10-18.5 %), *G. scitula* gr. (4-14.7 %) (Fig. 7). The significant abundance of warm water taxa during MIS 2, has been also observed by de Abreu et al. (2003) in the Iberian offshore. Furthermore, the *G. ruber* gr. (white) increasing (4-10 %) in the glacial MIS 2 (especially during the LGM) has been also reported by Rogerson et al. (2004) in the gulf of Cadiz. In ATA13-OF-KT18 core record, the "H" 2 is marked by an increase of Temperate-Cold fauna, especially *G. scitula* gr., whereas during the "H" 1 a slight increase in abundance of Subtropical taxa (both Warm- and Cold-) has been observed. The Bølling/Allerød, in ATA13-OF-KT18 core, last is characterized by an increasing in abundance of Tropical and Warm-Subtropical sp., followed by an evident increasing of Polar-Subpolar fauna during the Younger Dryas (Fig. 6), marked by the peaks in abundance of *N. pachyderma* dx (2.5-4.5 %), *N. incompta* dx (6-10.5 %) and *G. inflata* (9.5-13 %) (Fig. 7). Finally, the Holocene period results to be dominated by Tropical, Cold-Subtropical and Warm-Subtropical fauna, in particular *G. ruber* gr. (white) (7.5-21.5 %). However, *G. truncatulinoides* (1-7.3 %) reached values lower than those registered during previous interglacial (MIS 5), as also recognised by Chapman et al. (2000).

In ATA13-OF-KT1 core record is evident as the glacials, especially the MIS 4, are widely dominated by Polar-Subpolar sp., as also evident in the Warm/Cold sp. curve. On the contrary Warm water fauna dominate the assemblage during the interglacial periods (Fig. 6).

In particular, during MIS 5.1 Warm-Subtropical and mostly Cold-Subtropical species dominated the assemblage (Fig. 6), marked by increases in abundance of *G. ruber* gr. (white) (6-15 %) and *G. truncatulinoides* (1.5-8%) (Fig. 7). On the contrary, low abundance of Polar-Subpolar sp. characterizes this interval (Fig. 6). However, Temperate-Cold species such as *G. inflata* and *G. scitula* gr., maintain medium-low abundances (Fig. 7).

The transition to MIS 4 is clearly marked by the abrupt increase of Polar-Subpolar fauna and the contemporaneous decrease of Warm-Subtropical and Tropical fauna, which is near to absent in this glacial stage (Fig. 6). *N. pachyderma* dx (2.5-20 %) and N. *incompta* dx (6.5-17.5 %) reach the maxima abundances observed in the ATA13-OF-KT1 record (Fig.4). *G. inflata* (2.5-26 %) increases particularly during the early phase of MIS 4, whereas *G. scitula* gr. is extremely rare, with the exception of an evident peak (13.6 %) at 66 ka (Fig. 7). In ATA13-OF-KT1 faunal record, the intervals of the "H" 7 and "H" 6 are clearly carachterised by peaks in abundance of Polar-Subpolar sp., especially with abrupt increases of *N. incompta* dx and *N. pachyderma* dx (Fig. 6 and 7).

Marine Isotope Stage 3 is marked by the initial increase of Warm-Subtropical and Cold-Subtropical taxa, which gradually decrease toward the top, balanced by Temperate-Cold species, which show the opposite trend (Fig. 6). The rapid warming to gradual cooling trend of MIS 3 is also evident in the Warm/Cold sp. record (Fig. 6). In particular, during MIS 3.3 the initial high relatives abundances of *G. scitula* gr. and *N. incompta* dx, are followed by an abrupt increase of warm affinity species such as *G. ruber* gr. (white) and *G. truncatulinoides* (Fig. 7). MIS 3.2 instead is characterized by relatively high abundances of *N. incompta* dx and *G. inflata* and the decrease in abundance of *G. scitula* gr. and *G. truncatulinoides*. The transition to MIS 3.1 testifies a cooling trend, marked by the increase in abundance of cool-temperate species and mostly of subpolar *N. pachyderma* dx (7-16.5 %). *N. incompta* dx represents the better marker for "Heinrich" related stadials occurred during the MIS 3 (Fig. 7).. However, *G. scitula* gr. shows increases in abundance during the "H" 5a and "H" 3 (Fig. 7).

The last glacial stage (MIS 2) is dominated by *N. pachyderma* dx (5-14 %) and especially *G. inflata* (10-48 %). However warm species showed no substantial changes in abundance compared to MIS 3.1 (Fig. 6). However, during the Last Glacial Maximum *G. ruber* gr. (white) reaches higher percentages than MIS 3.1, whereas it strongly decreases during

millennial-scale cooling event "H" 2 and "H" 1. These two latter events are well marked by peaks in abundance of *N. pachyderma* dx and *N. incompta* dx, together with *G. inflata* for the early phase of "H" 1 (Fig. 7).

The last deglacial period is perfectly represented by planktonic foraminiferal fluctuations of ATA13-OF-KT1 core, in each phase, as also it is well observable in the Warm/Cold sp. curve (Fig. 7). The well distinguished Bølling/Allerød is dominated by Tropical and Warm-Subtropical sp., especially by *G. ruber* gr., whereas the onset of Younger Dryas cold stage, is marked by abrupt increases of *N. incompta* dx, *N. pachyderma* dx and *G. inflata* (Fig. 6 and 7).

Also in ATA13-OF-KT1 core record, the Holocene period (MIS 1) is characterized by the dominance of Tropical, Cold-Subtropical and Warm-Subtropical fauna, especially *G. ruber* gr. (white) (5-21 %) and by the strong decrease of Polar-Subpolar and Temperate-Cold species.

7.7 Discussion

Quantitative data on planktonic foraminifera and sea surface temperatures (aSST-mat) reconstructions, have represented important tools to reconstruct the complex hydrographic and palaeoproductivity history of the Azores region, during the last 144 ky. These proxies relieved some remarkable differences in surface water masses and paleoproductivity between the two coring sites, although the north-westernmost ATA13OF-KT1 was collected 210 km far from the easternmost ATA13OF-KT18 (~ 1° of latitude and ~ 2° of longitude). Thus, even if this distance could be considered as not significant in an oceanic domain, the two cores recorded North Atlantic climatic phases in a very different way.

7.7.1 Paleoproductivity in the Azores region

G. *bulloides*, *G. glutinata* and *T. quinqueloba* abundance fluctuations in both cores have been used as primary productivity tracers of the Azores region. G. *bulloides* is considered opportunistic, feeding in particular microalgae (Schiebel et al., 1997), and it is particularly abundant in modern ENACW gyre (Schiebel et al., 2002b). *T. quinqueloba* is also herbivorous-opportunistic species (Lirer et al., 2014) but, at difference of *G. bulloides,* in the Azores region it has been associated with depending of high productivity surface water masses (Schiebel et al., 2001). *G. glutinata* diet consists essentially in diatoms (Hemleben et al., 1989), therefore, *G. glutinata* can be used as proxy of diatoms productivity (Schiebel et al.

2001). Concerning the two studied core records, in general, higher percentages of *G. bulloides*, *G. glutinata* and *T. quinqueloba* are present in ATA13OF-KT1 (Fig. 5), implying more fertility and high productivity surface waters in the north-westernmost sector of the Azores region. Furthermore, the difference in percentages among these three species, suggests different environmental conditions between the two cores, in terms of surface nutrients concentrations and source of primary producers. The most high productivity periods were the MIS 4 and the following MIS 3, especially in the north-westernmost sector of Azores area (ATA13OF-KT1 core). The marked increase of *G. glutinata* in these periods are likely linked to enhanced diatoms productivity, which, at least, reached the latitude of ATA13OF-KT1 coring site (35°N), and/or to a southernward displacement of the Azores Current waters. In the Azores region, *G. glutinata* is indeed most abundant in along the Azores Current waters (Ottens 1991). *G. bulloides* shows similar trend to *T. quinqueloba* only in the south-easternmost coring site (ATA13OF-KT18), whereas in the north-westernmost sector site (ATA13OF-KT1) the two species are not correlated. In the north-westernmost sector, the sub-polar *T. quinqueloba* increases likely in response to decreased SST and diatoms availability. Therefore, the generally low abundance of this species is probably linked to the fact that it prefers higher latitudes in north Atlantic and reaches the study area during southernmost AFCS positions linked to AMOC weakening.

Furthermore, the contribution of *G. glutinata* and *T. quinqueloba* in terms of carbonate content percentage is low, considering their very thin and small test.

Hence, the higher discrepancy (10-20%) between carbonate content values of the two cores observed during cold and high-productivity intervals of MIS 4 and 3 respectively, could be interpreted as due to differences in sea surface productivity with at the the north-westernmost site (ATA13OF-KT1) a decreasing of coccolithophores and contemporaneous increasing of biosiliceous biota, as well of small size planktonic foraminifera with small potential of carbonate production. The deglacial MIS 5.5 was the lowermost primary productivity period and the high carbonate content is probably due to the expansion of STG and related enhanced coccolithopores productivity, as well as species richness in planktonic foraminiferal assemblages of the Azores region (Fig. 5). In general the largest contributors for the carbonate content, in open ocean, are coccolithophores, which have high affinity for oligotrophic, warm and stable surface waters (Brand, 1994; Stolz and Baumann, 2010; Schwab et al. 2012; Marino et al., 2014).

As suggested by Bonfardeci et al. (this thesis), in general maxima in carbonate content of sediments during summer insolation maxima (MIS 5.5, 5.3, 5.1, 3.3, 3.1 and 1) are probably

due to the enhanced coccolithofore productivity and warm larger size planctonic foraminifera, whereas minima (MIS 5.4, 5.2, 4 and 2) have been probably characterised by an increase in bio-siliceous organisms proliferation, such as chrysophyta (especially diatoms) and cold small size planktonic foraminifera.

7.7.2 SST reconstruction

In general the aSST-mat oscillations of the two core records are very similar to those observed in Warm/Cold sp. records, suggesting that this last approach based on ratio between Tropical-Warm-Subtropical vs. Polar-Subpolar fauna may be used to reconstruct the temperature variations in the Azores surface waters (Fig. 6). Interglacials and temperate periods have been similarly recorded in both cores by increased SSTs due to the intensification of AMOC system. However, the lowermost SSTs in the Azores region during MIS 4 have been well registered only in the north-westernmost coring site, testifing the AMOC weakening, as suggested by Schiebel et al. (2002b). On the contrary during the glacial stage of MIS 2 the SSTs showed similar trends between the two cores, even if with lower values in the north-westernomost sector of study area. This behaviour is linked to the higher abundance of Polar-Subpolar and Temperate-Cold taxa, due to the AMOC reduction and southernmost position reached by Subtropical Gyre, in the central North Atlantic.

However the most important difference between the two aSST-mat and Warm/Cold sp. records occurred during the "Heinrich" related events and thus at the time of AMOC strong weakening or shut down (Heinrich, 1988; Bond et al., 1993; Broecker, 1994; Rohling et al., 2003; Cortijo et al., 2005; Kuhlbrodt et al., 2007; Eynaud et al., 2009; Lisiecki and Stern, 2016). In the northernmost sector of the Azores region these events have been marked by decreases in SSTs of 2-5 °C, whereas in the south-easternmost sector an increase of 2-4 °C occurred (Fig. 6), except for "H" 11 and "H" 3. As suggested by Naafs et al. (2013b), the surface water warming at mid-latitude of North Atlantic (41°N; 32°W) was probably due to the expansion and intensification of Subtropical Gyre and the contemporaneous strong cooling at higher latitudes of the North Atlantic. These Authors argued that these mechanisms were triggered by the Laurentide ice sheet collapse and highest abundance of meltwater input that blocked the normal AMOC system, during the Heinrich events. Moreover, as suggested by Billups et al. (2016) the position of the Gulf Stream appears to be remained the same during glacial stages, although reduced in intensity (Lynch-Stieglitz et al., 1999).

All these evidences testified as the two studied sectors have been interested by different water masses during at the time of near complete shut down of AMOC system ("Heinrich"

related events), that represent the most extreme climatic and hydrographic condition in the North Atlantic. Therefore we argue that, during the almost of the coldest climatic phases, in the Azores region, the northernmost ATA13OF-KT1 coring site, was under the influence of Subpolar Gyre Water masses, whereas the southern-easternmost ATA13OF-KT18 site was still limbed by warmer water masses (Subtropical Gyre and/or Eastern North Atlantic Central Water) (Fig. 8).

7.7.3 Orbital-forcing on the hydrographic pattern variability of the Azores region

The interpretation of the planktonic foraminiferal records allowed to obtain a model to reconstruct the complex climatic and hydrographic variability of Azores region between the late part of MIS 6 and the Holocene (Fig. 8). In this region planktonic foraminiferal abundance fluctuations well recorded AMOC weakening/strengthening phases. The curves of Warm/Cold sp. represented a useful tool to evaluate in which way planktonic foraminiferal assemblages of both coring sites, reacted to orbital-scale and also millennial-scale climatic fluctuations. It is important to precise that in the adopted age model, for both core records, is considered the time lag (4.9-2.3 ka) between the 21 June insolation (65°N) forcing and the relative response of the analysed proxies (Bonfardeci et al., this thesis).

Each of the six elected species was used to trace a specific part of the AMOC system, in terms of superficial currents, fronts and gyres. *N. pachyderma* dx, as discussed above, well marked southeastward shifts of SPF. *N. incompta* dx and *G. inflata* maxima abundances, in Azores region, have been associated with south-easternmost shifts of the NAC (Ottens, 1991; Pflaumann, 1996; Schiebel et al., 2002a; Repschlager et al., 2015). Furthermore, *N. incompta* dx has shown more affinity with water masses just south to the SPF, in the Azore region. *G. scitula* well marked latitudinal shifts of the AFCS, reaching maxima abundances north of Azores Front and so it was considered as dominant species in the ENACW (Ottens, 1991; Prell et al., 1999; Schiebel et al., 2002a; Rogerson et al., 2004; Repschlager et al., 2015). Subtropical species *G. truncatulinoides* reached highest abundance in correspondence of the Azores Current, attesting changes in position and strength of these water masses (Schiebel et al., 2002a; Repschläger et al., 2015). Finally, *G. ruber* gr. (white) maxima abundances have been associated with northward expansion of STG, bordered to the north by AFCS (Schiebel et al., 2002b; Repschläger et al., 2015).

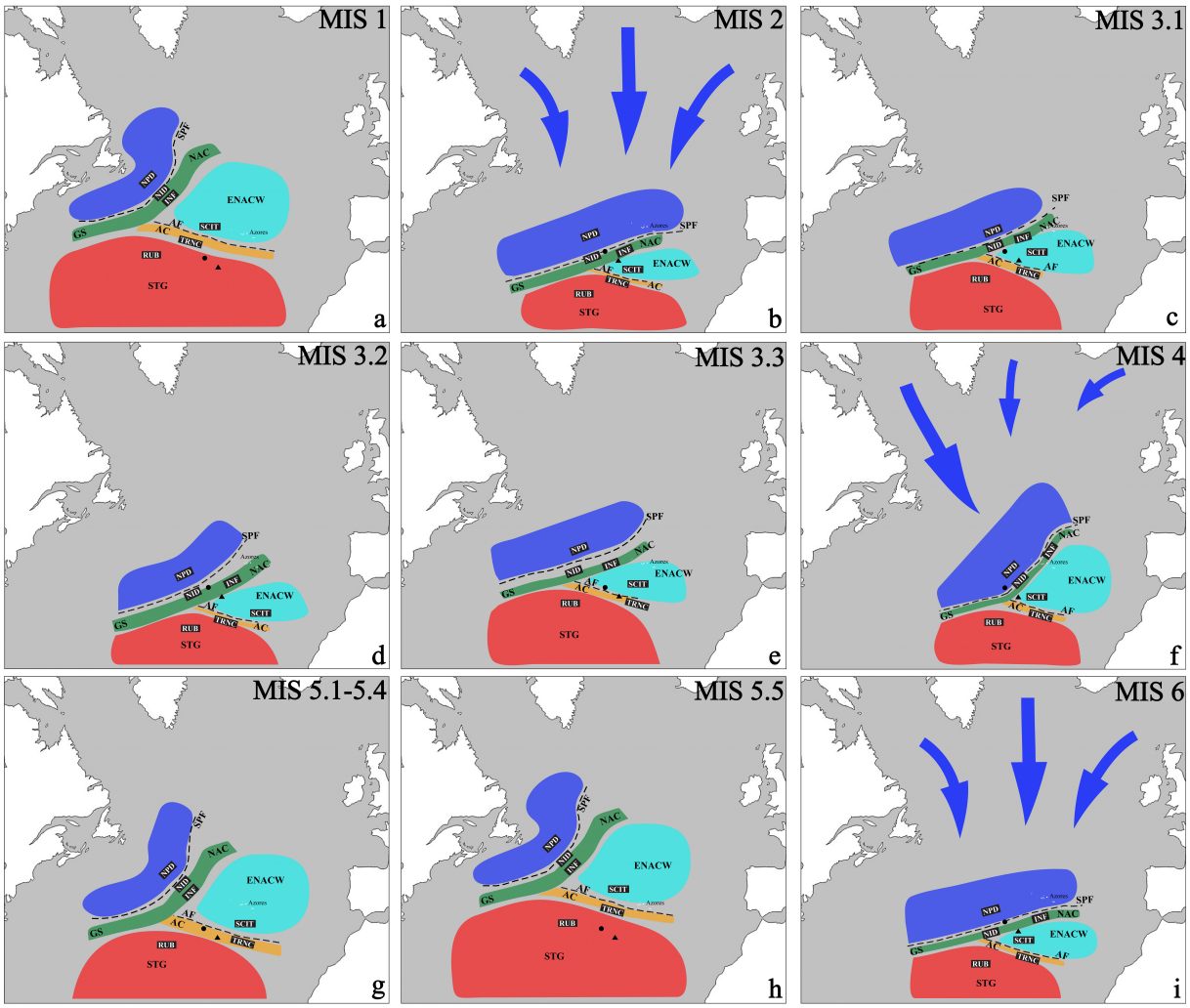

Figure 8. Paleoceanographic reconstruction of the North Atlantic, focused on the Azores region. This model shows the latitudinal and longitudinal variations of the surface water masses and front/current systems of the central North Atlantic, traced through the relative position of the six selected species, related to the different climatic phases. STG=Subtropical Gyre; ENACW=Eastern North Atlantic Central Water; SPG=Subpolar Gyre; GS=Gulf Stream; NAC=North Atlantic Current; AC=Azores Current; AF=Azores Front; SPF=Subpolar Front; NPD= *N. pachyderma* dx; NID= *N. incompta* dx; INF= *G. inflata*; SCIT= *G. scitula* gr.; TRNC= *G. truncatulinoides*; RUB= *G. ruber* gr. (white). Figures from 8.a to 8.i are referred to the central North Atlantic hydrography during MIS 1 to MIS 6.

The two coring sites are located in proximity of the actual northern boundary of STG (Fig. 8). Our model shows how the climatic forcing has triggered the displacements of the "triple junction", correspondent with the point where the Gulf Stream separates into North Atlantic Current and Azores Current. Hence, this mechanism controlled the weakening/strengthening of the central North Atlantic gyres (SPG, STG and ENACW) and their displacement from north-northwest toward south-southeast. In general, orbitally-forced climatic changes (Bonfardeci et al., this thesis) caused south-southeastward shifts of this seawater system

during insolation minima and relative AMOC weakening, whereas climatic warming, induced by insolation maxima and AMOC strengthening, have triggered north-northeastward displacements of that system.

In our model we reconstructed environmental variations of Azores region between 143.8 and 2,75 ka, although phases corresponding to MIS 6 to MIS 5.2 have been registered only on the southeasternmost coring site (ATA13OF-KT18). In the following discussion, the link between the astronomical forcing on climate and the response of planktonic foraminiferal assemblages of the Azores region, is analysed (Figs. 6, 7 and 8)

The MIS 6 represents the last part of a glacial period, coincident with an insolation minimum, ended at 129 ka (Billups & Scheinwald, 2014; Lisiecki and Stern, 2016; Bonfardeci et al., this thesis). This climatic cold period was distinctively documented, although it was not so extreme in Azores region, as other glacials, probably due to interference of eccentricity and obliquity signals on climate system. AMOC weakening resulted in a southward shift of polar water masses and related SPF, contemporary with STG reduction, in Azores region. The observed increase of *G. inflata* and *N. incompta* dx clearly testify the southward shift of NAC, around to 34°N in central North Atlantic (Fig. 8.i). During MIS 6 *G. scitula* abundance attested that AFCS was confined southernmost related to actual position. Subpolar gyre and related Subpolar Front during MIS 6 probably extended from the western North American to Iberian margin, compressing and slowing down the entire circulation system. This mechanism was responsible of the narrowing the distance between NAC and AFCS. We also recognised the two "Heinrich" related events ("H" 11 and "H" 12) due to southward expansion of SPF.

MIS 5.5 in Azores region has been clearly recorded by all proxy records of ATA13OF-KT18 core. As shown in figure 8.h, during this interval occurred the maximum expansion of AMOC system, with northern boundary of STG that reached higher latitude than today, as also suggested by Irval et al. (2012). In the Azores region mean annual SSTs were enough stable for the entire period, around 20°C. As also observed by Chapman et al. (2000), *G. ruber* gr. (white) dominated the planktonic foraminiferal assemblages and the "triple junction" system formed by GS, NAC and AFCS was constrained slightly north-westward than the actual position. This Northern Hemisphere climatic optimum, warmer than today, coincided with a moment in which insolation and obliquity maxima were nearly in phase.

During the interval between MIS 5.4 – 5.1, in the Azores region, a gradual and slow cooling trend toward glacial conditions has been observed (Fig. 8.g). In a period characterised by generally high and stable SST, two cool-temperate phases (MIS 5.4 and 5.2) occurred,

forced by two insolation minima. During warm sub-stages of MIS 5.3 and 5.1, dominance of subtropical species and especially of *G. truncatulinoides* provide the evidences that AC were positioned between 35-34 °N, whereas during MIS 5.4 and 5.2 the increases of *G. scitula* marked the further southward shift of AFCS.

Starting from 70.9 to 58.3 ka (MIS 4), in Azores region persisted extreme glacial conditions. The orbital forcing on Northern Hemisphere climatic system resulted in an insolation minimum, perfectly in phase with obliquity signal. These conditions imposed strong cooling in central North Atlantic, resulting in a southeastward shift of the "triple junction" system formed by GS, NAC and AFCS (Fig. 8.f). The difference in the proxy records between the two coring site, attests that principal source for Polar and Subpolar surface waters, for the Azores region, was the zone between Greenland and eastern Canadian continental margin. This site was probably the source area of diatoms-rich waters, testified by the increase in abundance of paleoproductivity tracers, especially *G. glutinata* (Fig 5). The highest abundance of *N. pachyderma* dx and *N. incompta* dx in the northwesternmost site, here considered as the tracer of SPF, may confirm this hypothesis. *G. inflata* was more abundant in the earlier phase of that glacial stage in both records, whereas *G. scitula* was near absent in the northwesternmost site and clearly present in the other one. AMOC system pattern during this phase, as shown in figure 8.f, was very different rather than other glacial stages. Subpolar water masses dominated the northwesternmost site, whereas ENACW system was present in correspondence of the southeasternmost one. Reduced and weakened NAC lied between the two sites. Moreover during this glacial period we recognised two phases of maximum expansion of Subpolar Gyre, correspondent with two "Heinrich" related events, the "H" 7 and "H" 6 respectively. Furthermore, during these two events the STG and ENACW dominated in the south-easternmost sector of Azores region, whereas the SPG was active at the north-westernmost site. The surface water masses between these two coring sites were separated by the SW-NE flowing North Atlantic Current.

After this complex glacial stage, Azores region was characterised by temperate-warm climatic conditions, during the MIS 3. From MIS 3.3 to 3.1 we observed a gradual cooling trend toward glacial conditions of the last glacial. In particular during MIS 3.3, insolation maximum caused a northwestward shift of surface currents system, related to previous glacial stage, with ENACW that dominated Azores region across the two sites (Fig. 8.e). The following substage MIS 3.2 instead occurred during a modest insolation minimum, in phase with the strongest eccentricity minimum of the last 144 kyr. The phase opposition of these two signal with obliquity, probably maked this climatic phase transitional, with mean annual

SSTs approximately stable and close to the other two substages. However, during MIS 3.2 NAC was the main surface current system that influenced the Azores region hydrography (Fig. 8.d). The gradual decrease of SSTs, coeval with increase in abundance of cold species, characterised the substage 3.1. Progressive increase in abundance of *N. pachyderma* dx, *N. incompta* dx and *G. inflata* and the contemporaneous decrease of subtropical taxa, signed southeastward shifting of the GS-NAC-AFCS "triple junction" system (Fig. 8.c). The decrease in abundance of *G. scitula* in northwesternmost site, toward the end of the substage and, on the contrary, the increase in southeasternmost one, may attest that ENACW and its southern boundary represented by the ACFS, were more influent toward est-southeast, in the Azores region. Furthermore, at the end of MIS 3.1, the very intense Heinrich related event "H" 3, marked a rapid expansion of Subpolar Gyre. Recognised by several Authors in North Atlantic (Heinrich, 1988; Bond et al., 1993; Broecker, 1994; Bond & Lotti, 1995; Chapman et al., 2000; Rohling et al., 2003; de Abreu et al., 2003; Hulbe at al., 2004; Hodell et al., 2008b; Hodell et al., 2010), this abrupt climatic cooling was much more intense in correspondence of northwesternmost studied site.

Last glacial stage, correspondent with MIS 2, has been clearly registered in Azores region, especially in the north-westernmost sector. The expansion of SPG caused at these latitudes the central North Atlantic cooling and ice sheets expansion, between 27.3 and 11.7 ka, induced the AMOC weakening and slowing down, with the result of south-southeastward displacement of the GS-NAC-AFCS "triple junction" system (Fig. 8.b). During this phase, in Azores region, south-southeastward displacement of SPF, attested through the high abundance of N. pachyderma dx. This hydrographic pattern caused the weakening and southward shift of NAC and AFCS, that flowed much closer to each other than today. In the northwesternmost site, Neogloboquadrinids and especially *G. inflata* dominated the association, whereas slightly to southeast *G. scitula* high abundance confirm the ENACW and associated AFCS was the main surface water masses system. However we observed that *G. ruber* gr. (white) was slightly more abundant, especially during the Last Glacial Maximum, than the previous MIS 3.1 and previous glacial. The reason could reside in the summer northward shift of northern boundary of STG, linked with more marked seasonality and warmer water inflow just below or within the Azores region. A similar behaviour was recognised by Cayre et al. (1999) and de Abreu et al. (2003) along the Iberian margin and by Rogerson et al. (2004) in the Gulf of Cadiz. The aSST-mat reconstruction confirm this tendency and also show a gradual increase, after the minimum between 12 and 13 °C at the MIS 3.1/MIS 2 boundary. The MIS 2 occurred during an insolation minimum, but also during

rising parts of obliquity and eccentricity signals. During the warm climatic phase of the Bolling/Allerod (14.7-12.7 kyr BP), Azores region was characterized by the STG and AFCS northward shifted and NAC northwestward displaced. The onset of following climatic cooling, correspondent with Younger Dryas (12.7-11.7 kyr BP), was marked, in study area, by decreases in SSTs and coeval *N. pachyderm*a dx and *N. incompta* dx increases in abundance, that traced the southeastward shifts of SPF and NAC. Hydrographic pattern during this period was similar to that of Heinrich related events.

The current interglacial stage (MIS1), in Azores region, was marked by gradual increase in SSTs that caused the rapid increase in abundance of Tropical Warm-Subtropical taxa (Fig. 8.a). In this phase, a climate system restoration characterised the study region, well marked by increase in abundance of *G. ruber* gr. (white) and in general of all warm water affinity species. The culmination of the insolation maxima, in phase with other orbital parameters, in the early stage of Holocene, forced the northward expansion of STG and AMOC strengthening. The minor eccentricity, even if in a positive phase, rather than MIS 5.5 can explain why this latter period in the Northern Hemisphere was warmer than the Holocene.

7.8 Conclusions

High-resolution census analyses on planktonic foraminifera assemblages of two sedimentary cores, collected southwestward of the Azores archipelago, have provided powerful tools to reconstruct climatic and hydrographic variability in the Azores area, during the last 144 Ka. In particular, we have traced surface sea-water temperatures, hydrographic and palaeoproductivity variations and demonstrated their strong connection with the orbitally-forced AMOC weakening/ strengthening, during late Quaternary.

G. bulloides, *T. quinqueloba* and *G. glutinata* relative abundances have been used as paleoproductivity proxies, showing that more high-productivity surface water masses have characterized the north-westernmost coring site. During glacial MIS 4 and, in less extent during MIS 3, high abundances of *G. glutinata* may suggest diatom dominated primary productivity. Such highest siliceous biogenic productivity, especially during extreme glacials, was probably fed by Polar-Subpolar water masses.

SSTs reconstruction based on Modern Analog Technique, together with Warm/Cold species index, highlighted that in the two coring sites, the climatic and hydrographic variability of the last 144 kyr have been recorded with different mode. In general during colder climatic phases, the AMOC system slowed down, inducing a decrease in SST, well

recorded in ATA13OF-KT1 planktonic foraminiferal record. Contemporaneously, the persistent activity of Gulf Stream and the activity of STG and ENACW induced warming of the surface water masses in correspondence with the ATA13OF-KT18 coring site, together with increases in abundance of Warm-Subtropical and Cold-Subtropical taxa. This contrasting reaction between the two coring sites was particularly evident during the most extreme "Heinrich" related events.

Downcore abundance fluctuations of key species, marking specific water masses and surface front/current systems in the central North Atlantic, have been used to trace the latitudinal and longitudinal migrations of these water masses and current fronts, as well their intensification linked to climatic orbital forcing.

N. pachyderma dx, has been used to trace a south-southeastern shift of Subpolar Gyre and the related Subpolar Front, linked to Laurentide-Greenland ice sheets expansion, during glacials MIS 6 and 2. The temperature and productivity effects related to this southeastern displacement of SPG resulted much more evident in the north-westernmost sector of the study area. This substantial difference, between the two core records, especially during glacial stages and millennial-scale cold events ("Heinrich" related events), may indicate that the main polar-subpolar water source was positioned between Canadian and Greenland margins (Hudson area).

N. incompta dx and *G. inflata* have been recognized as good proxies of the northeast-flowing North Atlantic Current (NAC) position and strength, linked to Gulf Stream fluctuations. Moreover we suggested that *N. incompta* dx probably occupied preferentially northwestern part of NAC, whereas *G. inflata* was most abundant in correspondence of the central body of that current. Hence, they together marked the period in which NAC was reduced and located south-easternmost, respect to the actual position. These conditions, in Azores region, marked the onset and the persistence of cold climate phases, in correspondence of MIS 6, 4, 3.2 and 2.

In order to trace the extension of the ENACW water masses and therefore the AF position, we used *G. scitula* gr. abundance fluctuations. Therefore maxima abundances of *G. scitula*, in study area, marked the southward shift of AF, during glacial stages (MIS 6, 4 and 2). This latter front represents also the northern boundary of Azores Current, which position and strength, has been monitored through the subtropical *G. truncatulinoides* fluctuations. This species testified strengthening of this current during MIS 5, end part of 3.3 and MIS 1. Finally our model shows how *G. ruber* gr. (white) marked northward expansion of the Subtropical Gyre (STG) during interglacials, especially during MIS 5.5 and Holocene.

Appendix

Table 1. List of the recognised and censed planktonic foraminiferal species of the ATA13OF-KT1 and ATA13OF-KT18 core records. The species are grouped on the basis of the zoogeographical provinces classifications proposed by Bé and Torderlund (1971), Bé (1977), Vincent and Berger (1981), Ottens (1991) and Kucera (2007).

Polar-Subpolar sp.:
• *Neogloboquadrina pachyderma dx* (Ehrenberg, 1861)
• *Neogloboquadrina pachyderma* sx (Ehrenberg, 1861)
• *Neogloboquadrina incompta* dx (Cifelli, 1961)
• *Neogloboquadrina incompta* sx (Cifelli, 1961)
• *Turborotalita quinqueloba* (Natland, 1938)

Temperate-cold sp.:
• *Globigerina bulloides* d'Orbigny, 1826
• *Globigerina megastoma* Earland, 1934
• *Globorotalia scitula* dx (Brady, 1882)
• *Globorotalia scitula* sx (Brady, 1882)
• *Globorotalia scitula* cf. 1
• *Globorotalia scitula* cf. 2
• *Globigerinita glutinata* (Egger, 1893)
• *Globorotalia inflata* dx (d'Orbigny, 1839)
• *Globorotalia inflata* sx (d'Orbigny, 1839)
• *Globigerinita uvula* (Ehrenberg, 1861)

Cold-Subtropical sp.:
• *Globigerina* sp. 2
• *Globigerina falconensis* Blow, 1959
• *Globigerinita parkerae* Bermudez, 1961
• *Globorotalia bermudezi* dx Rogl & Bolli, 1973
• *Globorotalia bermudezi* sx Rogl & Bolli, 1973
• *Globorotalia cavernula* Bé, 1967
• *Globorotalia crassaformis crassaformis* (Galloway & Wissler, 1927)
• *Globorotalia crassaformis hessi* Bolli & Premoli Silva, 1937
• *Globorotalia crassaformis imbricata* Krasheninnikov & Bylinskaya, 2002
• *Globorotalia crassaformis ronda* Blow, 1969
• *Globorotalia crassaformis viola* Blow, 1969
• *Globorotalia crassula* Cushman & Stewart, 1930
• *Globorotalia hirsuta* dx (d'Orbigny, 1839)
• *Globorotalia hirsuta* sx (d'Orbigny, 1839)
• *Globorotalia hirsuta eastropacia* Boltovskoy, 1974
• *Globorotalia praehirsuta* cf. Blow, 1969
• *Globorotalia theyeri* Fleisher, 1974
• *Globorotalia tosaensis* cf. Takayanagi & Saito, 1962
• *Globorotalia truncatulinoides* dx (d'Orbigny, 1839)
• *Globorotalia truncatulinoides* sx (d'Orbigny, 1839)
• *Turborotalita cristata* (Heron-Allen & Earland, 1929)
• *Turborotalita humilis* (Brady, 1884)
• *Tenuitella iota* (Parker, 1962)

Warm-Subtropical sp.:

• *Beella digitata* (Brady, 1879)
• *Orbulina bilobata* d'Orbigny, 1846
• *Orbulina suturalis* Broennimann, 1951
• *Orbulina universa* d'Orbigny, 1839
• *Globigerinella siphonifera* (d'Orbigny, 1839)
• *Globigerinella calida* (Parker, 1962)
• *Globigerinella obesa* (Bolli, 1957)
• *Globoturborotalita rubescens* (Hofker, 1956)
• *Globoturborotalita tenella* (Parker, 1958)
• *Globoturborotalita* sp.1
• *Globigerinoides conglobata* (Brady, 1979)
• *Globigerinoides elongatus* (d'Orbigny, 1839)
• *Globigerinoides pyramidalis* (van den Broeck, 1876)
• *Globigerinoides cyclostomus* (Galloway and Wissler, 1927)
• *Globigerinoides ruber* alba (d'Orbigny, 1839)
• *Neogloboquadrina acostaensis* cf. (Blow, 1959)
• *Neogloboquadrina dutertrei* (d'Orbigny, 1839)
• *Dentagloborotalia anfracta* (Parker, 1967)
• *Tenuitella atlantisae* (Cifelli & Smith, 1970)
• *Tenuitella* sp.
• *Tenuitella* sp. 2
• *Tenuitella* sp. 3
• *Tenuitella* sp. 4

Tropical sp.:

• *Candeina nitida* d'Orbigny, 1839
• *Globoturborotalita rubescens* pink variety (Hofker, 1956)
• *Globigerinoides ruber* rosea (d'Orbigny, 1839)
• *Globigerinoides quadriloba* (d'Orbigny, 1846)
• *Globigerinoides sacculifera* (Brady, 1977)
• *Globigerinoides triloba* Reuss, 1850
• *Globorotalia menardii* gr. dx (d'Orbigny in Parker, Jones & Brady, 1865)
• *Globorotalia menardii* gr. sx (d'Orbigny in Parker, Jones & Brady, 1865)
• *Globorotalia tumida* dx (Brady, 1877)
• *Globorotalia tumida* sx (Brady, 1877)
• *Hastigerina pelagica* (d'Orbigny, 1839)
• *Pulleniatina obliquiloculata* (Parker & Jones, 1862)
• *Sphaeroidinella dehiscens* (Parker & Jones, 1865)

PLATE 1

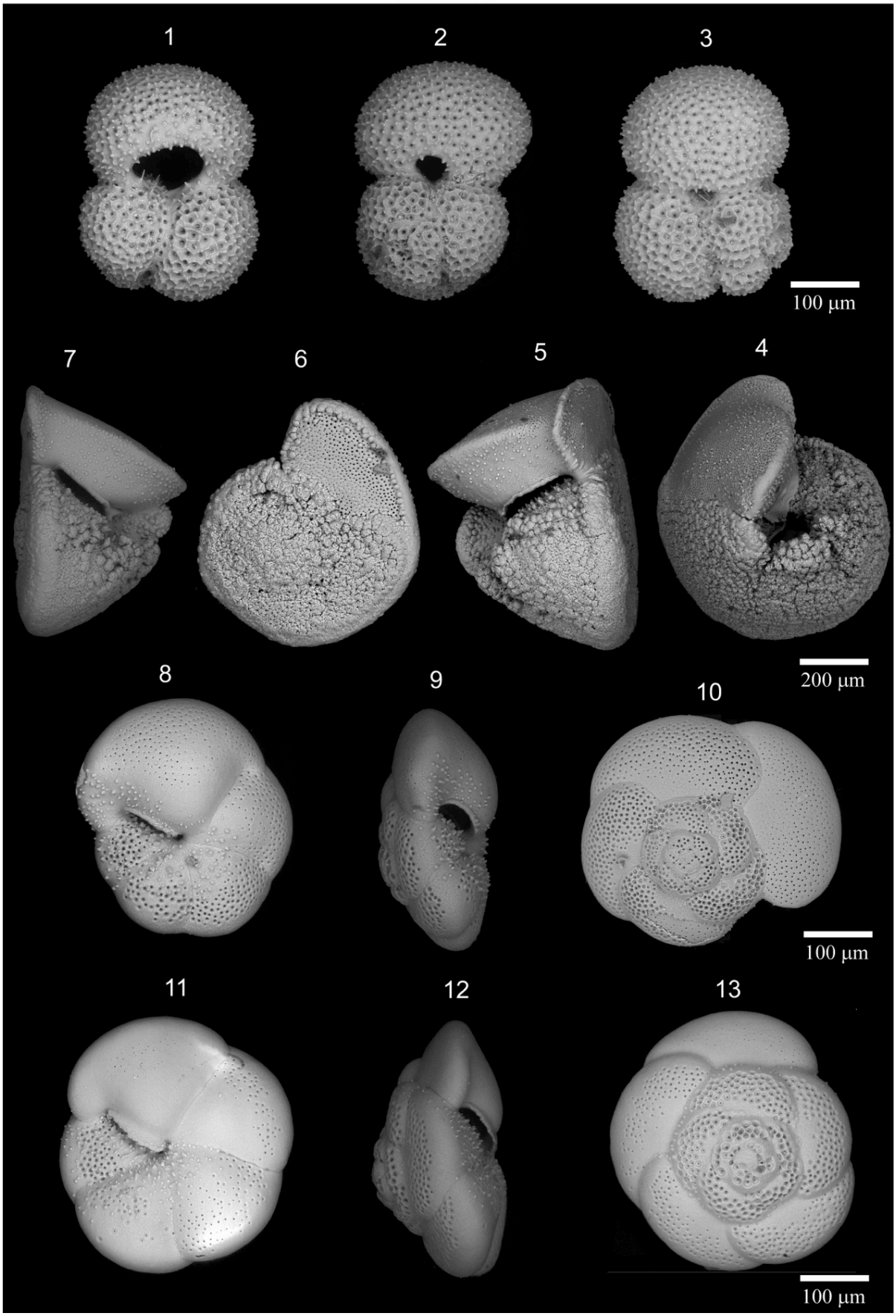

PLATE 2

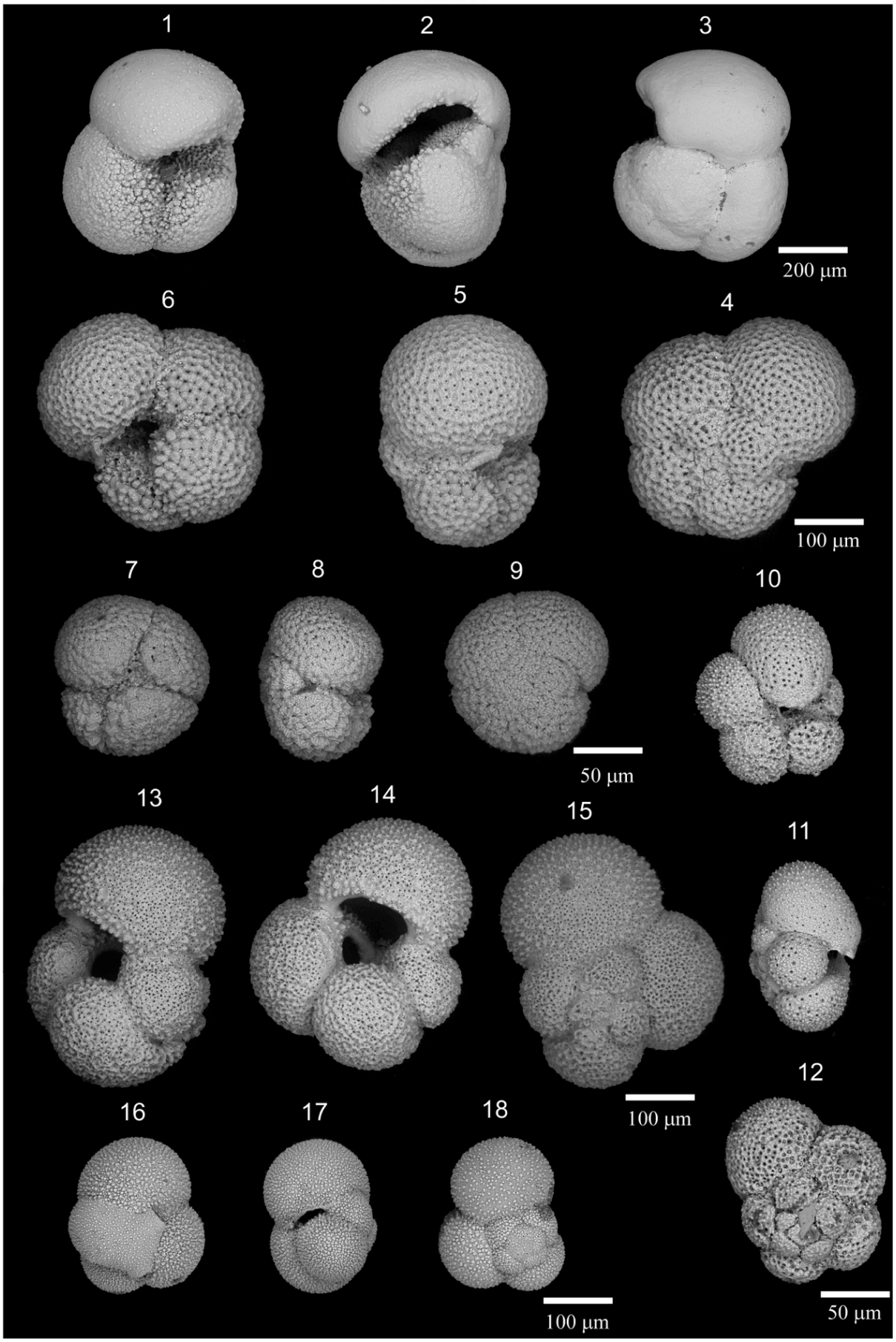
1
2
3
200 µm
6
5
4
100 µm
7
8
9
10
50 µm
13
14
15
11
12
16
17
18
100 µm
50 µm

Plate 1

Figures 1-3. *Globigerinoides ruber* (d'Orbigny, 1839). *G. ruber* s.s.-a variety (Bonfardeci et al., this thesis) - Figure 1. Umbilical view. 2. Side view. Figure 3. Spiral view.

Figure 4-7. *Globorotalia truncatulinoides* (d'Orbigny, 1839). Sinistral coiling variety - Figure 4. Umbilical view. 5. Side view. Figure 6. Spiral view. Dextral coiling variety - Figure 7. Side view.

Figures 8-13. *Globigerinoides scitula* (Brady, 1882). Dextral coiling variety - Figures 8 and 11. Umbilical view. Figures 9 and 12. Side view. Figures 10 and 13. Spiral view.

Plate 2

Figures 1-3. *Globorotalia inflata* (d'Orbigny, 1839). Figure 1. Umbilical view. 2. Side view. Figure 3. Spiral view.

Figure 4-6. *Neogloboquadrina incompta* (Cifelli , 1961). Dextral coiling variety - Figure 4. Umbilical view. 5. Side view. Figure 6. Spiral view.

Figures 7-9. *Neogloboquadrina pachyderma* (Ehrenberg, 1861). Dextral coiling variety - Figure 7. Umbilical view. 8. Side view. Figure 9. Spiral view.

Figures 10-12. *Turbototalita quinqueloba* (Natland, 1938). Figure 10. Umbilical view. 11. Side view. Figure 12. Spiral view.

Figures 13-15. *Globigerina bulloides* d'Orbigny, 1839. Dextral coiling variety - Figure 13. Umbilical view. 14. Side view. Figure 15. Spiral view.

Figures 16-18. *Globigerinita glutinata* (Egger, 1893). Dextral coiling variety - Figure 16. Umbilical view. 17. Side view. Figure 18. Spiral view.

References

Alley, R.B. Macayeal, D. R., 1994 Ice-rafted debris associated with binge/purge oscillations of the Laurentide Ice Sheet. Paleoceanography 9 (4), 503-511

Alves, M.L.G.R., DeVerdière, A.C., 1999. Instability dynamics of a subtropical jet and applications to the Azores Front current system: Eddydriven mean flow. Journal of Physical Oceanography 29, 837-864.

Barker, S., Diz, P., Vautravers, M.J., Pike, J., Knorr, G., Hall, I.R., Broecker, W. S., 2009. Interhemispheric Atlantic seesaw response during the last deglaciation. Nature 457(7233), 1097-1102.

Barker, S., Knorr, G. Edwards, R.L., Parrenin, F. Putnam, A.E., Skinner, L.C., Wolff, E., Ziegler, M., 2011. 800,000 years of abrupt climate variability. Science 334(6054), 347–351.

Bé, A.W.H., 1977. An ecological, zoogeographic and taxonomic review of recent planktonic foraminifera, in: A.T.S. Ramsey (Eds.), Oceanic micropaleontology. London: Academic Press, Vol. 1, pp. 1–100.

Bé, A.W.H., Tolderlund, D.S., 1971. Distribution and ecology of living planktonic foraminifera in surface waters of the Atlantic and Indian Oceans. In The Micropalaeontology of the Oceans (eds. B. H. Funnell and W. R. Riedel). Cambridge Univ. Press, London, pp. 105–149.

Billups, K., Hudson, C. Kunz, H., Rew, I., 2016. Exploring Globorotalia truncatulinoides coiling ratios as a proxy for subtropical gyre dynamics in the northwestern Atlantic Ocean during late Pleistocene Ice Ages. Paleoceanography 31, 553–563.Bolli et al. 1985

Billups, K., Scheinwald, A., 2014. Origin of millennial-scale climate signals in the subtropical North Atlantic. Paleoceanography 29, 612–627.

Bond, G., Broecker, W., Johnsen, S., McManus, J., Labeyrie, L., Jouzel, J., Bonani, G., 1993. Correlations between climate records from North Atlantic sediments and Greenland ice. Nature 365, 143-147.

Bond, G.C., Lotti, R., 1995. Iceberg discharges into the North Atlantic on millennial time scales during the last glaciation. Science 267, 1005 – 1010.

Brand, L.E., 1994. Physiological ecology of marine coccolithophores. In: Winter, A., Siesser,W.G. (Eds.), Coccolithophores. CambridgeUniversity Press, UK, pp.

39e49Broecker, W.S., 1994. Massive iceberg discharges as trigger for global climate change. Nature 372, 421-424.

Cayre, O., Edith, V., Yves. L., Hall, M.A., 1999. Paleoceanographic reconstructions from planctonic foraminifera off the Iberian Margin: temperature, salinity and Heinrich Events. Paleoceanography 14(3), 384-396.

Chapman, M.R., Shackleton, N.J., Duplessy, J.C., 2000. Sea surface temperature variability during the last glacial-interglacial cycle: assessing the magnitude and pattern of climate change in the North Atlantic. Palaeogeography, Palaeoclimatology and Palaeoecology 157, 1-25.

Cifelli, R., 1961. Globigerina incompta, a new species of pelagic foraminifera from the North Atlantic. Contributions from the Cushman Laboratory for Foraminiferal Research 12 (3), 83-86.

Cooke, S., Rohling, E., 2001. Stable isotopes in foraminiferal carbonate. Southampton Oceanography Centre

Cortijo , E., Duplessy, J.C., Labeyrie, L., Duprat, J., Paillard D., 2005. Heinrich events: Hydrological impact, C. R. Geosci. 337(10–11), 897-907.

Crowley, T., 1981. Temperature and circulation changes in the eastern north Atlantic during the last 150,000 years: Evidence from the planktonic foraminiferal record, Mar. Micropaleontology 6, 97-129.

Cullen, J.I., 1982. The deep chlorophyll maximum comparing vertical profiles of chlorophyll a. Can. J. Fish. Aquat. Sci. 39, 791-803

Darling, K.F., Kucera, M., Kroon, D., Wade, C.M., 2006. A resolution for the coiling direction paradox in Neogloboquadrina pachyderma. Paleoceanography 21, PA2011.

de Abreu, L., Shackleton, N., Schönfeld, J., Hall, M., Chapman, M., 2003. Millenial-scale oceanic climate variability off the western Iberian margin during the last two glacial periods. Marine Geology 196, 1-20.

Delworth, T.L., Clark, P.U., Holland, M., Johns, W.E., Kuhlbrodt, T., Lynch-Stieglitz, J., Morrill, C., Seager, R., Weaver, A.J., Zhang, R., 2008. The potential for abrupt change in the Atlantic Meridional Overturning Circulation. In: Abrupt Climate Change. A Report by the U.S. Climate Change Science Program and the Subcommittee on Global Change Research. U.S. Geological Survey, Reston, VA, pp. 117–162. Dickson,Duplessy et al., 1988

Eynaud, F., de Abreu, L., Voelker, A., Schoenfeld, J., Salgueiro, E., Turon, J.L., Penaud, A.,

Toucanne, S., Naughton, F., Goni, M.F.S., Malaize, B., Cacho, I., 2009. Position of the Polar Front along the western Iberian margin during key cold episodes of the last 45 ka. Geochem. Geophys. Geosyst. 10, Q07U05.

Gould, W.J., 1985. Physical oceanography of the Azores front. Progress in Oceanography 14, 167-190.

Haddam N. A. Haddam, E. Michel, G. Siani, G. Cortese, H. C. Bostock, J. M. Duprat, and G. Isguder, 2016. Improving past sea surface temperature reconstructions from the Southern Hemisphere oceans using planktonic foraminiferal census data. Paleoceanography 31(6), 822–837.

Hagen, S., Keigwin, L.D., 2002. Sea-surface temperature variability and deep water reorganization in the subtropical North Atlantic during Isotope Stage 2–4. Marine Geology 189, 145-162.

Heinrich, H., 1988. Origin and consequences of cyclic ice rafting in the northeast Atlantic Ocean during the past 130,000 years. Quaternary Research 29, 142-152.

Hemleben, C., Spindler, M., Anderson, O.R., 1989. Modern Planktonic Foraminifera. New York, Springer.

Hodell, D., Evans, H.F., Channell, J.E.T., Curtis, J.H., 2010. Phase relationships of North Atlantic ice-rafted debris and surface-deep climate proxies during the last glacial period. Quaternary Science Reviews 29, 3875-3886.

Hodell, D.A., Channell, J.E.T., Curtis, J.H., Romero, O.E., Röhl, U., 2008b. Onset of "Hudson Strait" Heinrich events in the eastern North Atlantic at the end of the middle Pleistocene transition (w640 ka)? Paleoceanography 23, PA4218.

Hulbe, C.L., MacAyeal, D.R., Denton, G.H., Kleman, J., Lowell, T.V., 2004. Catastrophic Ice Shelf Breakup as the Source of Heinrich Event Icebergs. Paleoceanography 19, PA1004.

Hutson, W.M., 1980. Bioturbation of deep-sea sediments: oxygen isotopes and stratigraphic uncertainty. Geology 8, 127-130.

Irval, N, Ninnemann, US, Galaasen, EV, Rosenthal, Y, Kroon, D, Oppo, DW, Kleiven, HF, Darling, K & Kissel, C 2012, 'Rapid switches in subpolar North Atlantic hydrography and climate during the Last Interglacial (MIS 5e). Paleoceanography 27(2), PA2207.

Johnson, J., Stevens, I., 2000. A fine resolution model of the eastern North Atlantic between the Azores, the Canary Islands and the Gibraltar Strait, Deep Sea Res. Part I, 47(5), 875-899.

Kase, R.H., Zenk, W., Sanford, T.B., Hillier, W., 1985. Currents, fronts and eddy fluxes in the Canary Basin, Progress in Oceanography 14, 231-257.

Kennett, J.P., Srinivasan, M.S., 1983. Neogene planktonic foraminifera: a phylogenetic atlas. Hutchinson Ross Publishing Company. Stroudsburg, Pennsylvania.

Klein, B., Siedler, G., 1989. On the origin of the Azores Current. Journal of Geophysical Research 94, 6159-6168.

Kucera, M., Schönfeld, J., 2007. The origin of modern oceanic foraminiferal faunas and Neogene climate change. In: Williams,M., Haywood, A.M., Gregory, F.J., Schmidt, D.N (Eds.), Deep-Time Perspectives on Climate Change: Marrying the Signal from Computer Models and Biological Proxies. TheGeological Society, London, pp. 409-426.

Kucera, M., Weinelt, M., Kiefer, T., Pflaumann, U., Hayes, A., Weinelt, M., Chen, M.-T., Mix A. C., Barrows, T.T., Cortijo, E. Duprat, J., Juggins, S., Waelbroeck, C., 2005. Reconstruction of sea-surface temperatures from assemblages of planktonic foraminifera: Multi-technique approach based on geographically constrained calibration datasets and its application to glacial Atlantic and Pacific Oceans. Quaternary Science Reviews 24, 951-998.

Kuhlbrodt, T., Griesel, A., Montoya, M., Levermann, A., Hofmann, M., Rahmstorf. S., 2007. On the driving processes of the Atlantic Meridional Overturning Circulation. Reviews of Geophysics, 45, RG2001.

Kuroyanagi, A., Kawahata H., 2004. Vertical distribution of living planktonic foraminifera in the seas around Japan. Mar. Micropaleontol. 53, 173–196.

Laskar, J., Robutel, P., Joutel, F., Gastineau, M. Correia, A.C.M., Levrard, B., 2004. A long term numerical solution for the insolation quantities of the Earth, Astron. Astrophys. 428, 261-285.

LeGrande, A., Lynch-Stieglitz, J., 2007. Surface currents in the western North Atlantic during the Last Glacial Maximum, Geochem. Geophys. Geosyst. 8, Q01N09.

Lirer, F., Sprovieri, M., Vallefuoco, M., Ferraro, L., Pelosi, N., Giordano, L., Capotondi, L., 2014. Planktonic foraminifera as bio-indicators for monitoring the climatic changes that have occurred over the past 2000 years in the southeastern Tyrrhenian Sea. Integr. Zool. 9, 542-554.

Lisiecki, L.E., Stern, J.V., 2016. Regional and global benthic $\delta^{18}O$ stacks for the last glacial cycle. Paleoceanography 31, 1368-1394.

Locarnini, R. A., Mishonov, A. V., Antonov, J. I., Boyer, T. P., Garcia H. E., 2010, in: S. Levitus, U.S. Gov. Print. Off., Washington, D.C, World Ocean Atlas 2009, 1: Temperature, NOAA Atlas NESDIS, 68.

Lourens, L.J., Hilgen, F.J., Gudjonsson, L., Zachariasse, W.J., 1992. Late Pliocene to early Pleistocene astronomically forced sea surface productivity and temperature variations in the Mediterranean. Marine Micropaleontology 19, 49-78.

Lynch-Stieglitz, J., Curry, W.B., Slowey, N., 1999. Weaker Gulf Stream in the Florida Straits during the Last Glacial Maximum. Nature 402, 644-648.

Macedo, M.F., Duarte, P., Ferreira, J.G., Alves, M., Costa, V., 2000. Analysis of the deep chlorophyll maximum across the Azores Front. Hydrobiologia 441, 155-172.

Marino, M., Maiorano, P., Tarantino, F., Voelker, A., Capotondi, L., Girone, A., Lirer, F., Flores, J.A., Naafs, B.D.A., 2014. Coccolithophores as proxy of seawater changes at orbital-to-millennial scale during middle Pleistocene Marine Isotope Stages 14–9 in North Atlantic core MD01-2446, Paleoceanography 29, 518-532.

McClain, C.R., Firestone, J., 1993. An investigation of Ekman upwelling in the North Atlantic. Journal of Geophysical Research 98, 12327–12339.

Mortlock, R.A., Charles, C.D., Froelich, P.N., Zibello, M.A., Saltzman, J., Hays, J.D., Burckle, L.H., 1991. Evidence for lower productivity in the Antarctic Ocean during the last glaciation. Nature 351, 220-22

Naafs, B.D.A., Hefter, J., Grützner, J., Stein, R., 2013b. Warming of surface waters in the mid-latitude North Atlantic during Heinrich Events. Paleoceanography 28 (1), 153-163.

Ottens, J.J., 1991. Planktic foraminifera as North Atlantic water mass indicators. Oceanol. Acta 14(2), 123-140.

Parker, A.O., Schmidt, M.W., Chang, P., 2015. Tropical North Atlantic subsurface warming events as a fingerprint for AMOC variability during Marine Isotope Stage 3. Paleoceanography, 30, 1425-1436.

Pflaumann, U., Duprat, J., Pujol, C., Labeyrie, L., 1996. SIMMAX: A modern analog technique to deduce Atlantic sea surface temperatures from planktonic foraminifera in deep-sea sediments, Paleoceanography 11, 15-35.

Prell, W., Martin, A., Cullen, J., Trend, M., 1999. The Brown University Foraminiferal Data Base. IGBP PAGES/World Data Center-A for Paleoclimatology, Data Contribution Series, 1999-2027. NOAA/NGDC Paleoclimatology Program, Boulder, CO, USA.

Prell,W., 1985. The stability of low-latitudes sea surface temperatures: an evaluation of the

CLIMAP reconstruction with emphasis on the positive SST anomalies, p. 60, Technical Report. TR025, United States Department of Energy,Washington, DC.

Pujol, 1980. Les foraminifères planctoniques de 1'Atlantique nord au Quaternaire. Ecologie, Stratigraphie, Environnement. Mem. Inst. Géol. Bassin d'Aquitaine, 10.

Ravelo, A. C., Fairbanks, R.G. 1995. Carbon isotopic fractionation in multiple species of planktonic foraminifera from core tops in the tropical Atlantic. J. Foramineferal Res. 25(1), 53-74.

Repschläger, J., Weinelt, M., Kinkel, H., Anderesen, N., Garbe-Schönberg, D., 2015. Response of the subtropical North Atlantic surface hydrography on deglacial and Holocene AMOC changes. Paleoceanography 30 (5), 456-476.

Rigual-Hernández, A.S., Sierro, F.J., Bárcena, M.A., Flores, J.A., Heussner, S., 2012. Seasonal and interannual changes of planktic foraminiferal fluxes in the Gulf of Lions (NW Mediterranean) and their implications for paleoceanographic studies: two 12-year sediment trap records, Deep-Sea Res. Pt. I 66, 26–40.

Rogerson, M., Rohling, EJ, Weaver, P.P.E, Murray, J.W., 2004. The Azores Front since the Last Glacial Maximum. Earth and Planetary Science Letters 222, 779-789.

Rogl, F., Bolli, H.M., 1973. Holocene to Pleistocene planktonic foraminifera of Leg 15, Site 147 (Cariaco Basin (Trench), Caribbean Sea) and thier climatic interpretation, in : N.T. Edgar, Initial Reports of the DeepSea Drilling Project, Washington, D.C., U.S., Government Printing Office 15, 553-616.

Rohling, E.J., Mayewski, P.A., Challenor, P., 2003. On the timing and mechanism of millennial-scale climate variability during the last glacial cycle. Climate Dynamics 20, 257-267.

Saito, T., Thompson, P. R., and Breger, D., 1981. Systematic Index of Recent and Pleistocene Planktonic Foraminifera. University of Tokyo Press.

Schiebel, R., and Hemleben, C., 2005. Modern planktic foraminifera. Pala¨ontologische Zeitschrift 79, 135–148

Schiebel, R., Bijma, J., Hemleben, C., 1997. Population dynamics of the planktic foraminifer Globigerina bulloides from the eastern North Atlantic. Deep-Sea Res. 44, 1701-1713.

Schiebel, R., Hemleben, C., 2000. Interannual variability of planktic foraminiferal populations and testfluxinthe easternNorth Atlantic Ocean (JGOFS), Deep Sea Res., Part II, 47, 1809-1852.

Schiebel, R., Schmuker, B., Alves, M., Hemleben, C., 2002b. Tracking the recent and late

Pleistocene Azores front by the distribution of planktic foraminifers, J. Mar. Syst. 37(1-3), 213-227.

Schiebel, R., Waniek, J., Bork, M., Hemleben, C., 2001. Planktic foraminiferal production stimulated by chlorophyll redistribution and entrainment of nutrients. Deep-Sea Research I 48 (3), 721-740.

Schiebel, R., Waniek, J., Zeltner, A., Alves, M., 2002a. Impact of the Azores Front on the distribution of planktic foraminifers, shelled gastropods, and coccolithophorids. Deep Sea Res. Part II 49(19), 4035–-4050.

Schiebel, R., Zeltner, A., Treppke, U.F., Waniek, J.J., Bollmann, J., Rixen, T., Hemleben, C., 2004. Distribution of diatoms, coccolithophores and planktic foraminifers along a trophic gradient during SW monsoon in the Arabian Sea. Marine Micropaleontology 51, 345-371.

Schmitz, W.J., McCarthy, M.S., 1993. On the North Atlantic circulation, J. Geophys. Res. 31, 29-49.

Schneider, R.R., Muller, P.J., Wefer, G., 1994. Late Quaternary paleoproductivity changes off the Congo deduced from stable isotopes of planktonic foraminifera. Palaeogeography, Palaeoclimatology, Palaeoecology 110, 255-274.

Schwab, C., Kinkel, H. Weinelt, M., Repschläger, J., 2012. Coccolithophore paleoproductivity and ecology response to deglacial and Holocene changes in the Azores Current System, Paleoceanography 27, PA3210.

Shackleton N.J., Hall, M.A., Line, J., Shuxi, C., 1983. Carbon isotope data in core V19-30 confirm reduced carbon dioxide concentrations in the ice age atmosphere. Nature 306, 319-322.

Siedler, G., Zenk,W., Emery, W.J., 1985. Strong current events related to a subtropical front in the Northeast Atlantic. Journal of Physical Oceanography 15, 885-897.

Stanford, J.D., Rohling, E.J., Bacon, S., Roberts, A.P., Grousset, F.E., Bolshaw, M., 2011. A new concept for the paleoceanographic evolution of Heinrich event 1 in the North Atlantic. Quaternary Science Reviews 30, 1047-1066.

Stolz, K., Baumann, K.H., 2010. Changes in paleoceanography and paleoecology during Marine Isotope Stage (MIS) 5 in the eastern North Atlantic (ODP Site 980) deduced from calcareous nannoplankton observations. Palaeogeogr. Palaeoclimatol. Palaeoecol. 292 (1-2), 295-305.

Storz, D., Schulz, H. Waniek, J.J. Schulz-Bull, D.E., Kucera M., 2009. Seasonal and

interannual variability of the planktic foraminiferal flux in the vicinity of the Azores Current, Deep Sea Research Part I 56(1), 107-124.

Therón, R., Paillard, D., Cortijo, E., Flores, J.A., Vaquero, M., Sierro, F.J., Waelbroeck, C., 2004. Reconstruction of paleoenvironmental features using a new multiplatform program, Micropaleontology 50(4), 391-395.

Vincent, E., Berger W.H., 1981. Planktonic foraminifera and their use in Paleoceanography. In: C. Emiliani (Ed.), The oceanic lithosphere. The sea (Vol. 7, pp. 1025–1119). Hoboken, N. J.: Wiley-Interscience.

Volkov, D.L., Fu, L.L., 2010. On the reasons for the formation and variability of the Azores Current, J. Phys. Oceanogr. 40 (10), 2197-2220.

8. Distribution and ecology of the *G. ruber – G. elongatus* eco-morphotypes in the Azores region during Late Pleistocene-Holocene

Bonfardeci A.[1-2], Caruso A.[1], Bartolini A.[2], Blanc-Valleron M.M.[2]

1- Dipartimento di Scienze della Terra e del Mare, Università degli studi di Palermo, via Archirafi 20-22, 90123 Palermo, Italy

2- CNRS – UMR 7207 CR2P, MNHN, 8, rue Buffon, 75005 Paris, France

Keywords: *Globigerinoides ruber*, *Globigerinoides elongatus,* eco-morphotypes, stable isotopes, multivariate statistic, Azores, late Quaternary, STG/AFCS boundary.

8.1 Abstract

Quantitative data and stable isotope records of the ATA13OF-KT1 core, collected south-west-ward to the Azores islands, were used to analyse the ecology and distribution of the *G. ruber* - *G. elongatus* population, during the interval between late Pleistocene and the Holocene. First of all, the contribution of *G. ruber* gr. (*alba* and *rosea*) in planktonic foraminiferal assemblage of the Azores region were evaluated. This analysis highlighted as these taxa dominated the North Atlantic Subtropical Gyre during the late Quaternary and that their cyclic oscillations have been primarily linked to the obliquity signal. The new taxonomic characterization of *G. ruber* - *G. elongatus* plexus have allowed to distinguish ten eco-morphotypes and also to review the previous classification, mainly based on the differentiation between *G. ruber* sensu stricto and sensu lato. The approach based on quantitative, multivariate statistical and stable isotopes analyses, highlighted that each of these eco-morphotype occupied a precise position in the Azores region water column, during the interval between MISs 5.1 and 1. Therefore, new important insights on ecological preferences of the selected eco-morphotypes have provided, especially as regards to the poorly studied *G. cyclostomus*, *G. pyramidalis* and *G. elongatus cf.1*. The data suggested that the *G. ruber* - *G. elongatus* eco-morphotypes distribution in the Azores region, linked to the temperature and nutrient availability of the water column, cyclically oscillated, during the last 85.6 ka. In this sense, the proportion between the eco-morphotypes were used to monitor the northward/southward shifts of the Subtropical Gyre/Azores Front Current System (STG/AFCS) boundary. The ratio between *G. ruber*-b and *G. cyclostomus* has been used as index of the STG/AFCS boundary fluctuations. *G. ruber*-b, together with *G. ruber*-d, clearly dominated the *G. ruber* - *G. elongatus* population during the MISs 5.1 and 1, marking the

northward displacement of the STG/AFCS boundary. On the contrary, *G. cyclostomus* and also *G. ruber*-k, reached their maxima abundance during glacials (MISs 4 and 2), attested the southward shifted position of the STG/AFCS boundary.

8.2 Introduction

Studies on distribution and ecology of the recent planktonic foraminifera represent a powerful tool to paleoclimatic and paleoceanographic reconstructions (Kucera, 2007). *Globigerinoides ruber* (d'Orbigny, 1839), is a common and ubiquitary species in tropical/subtropical biogeographic provinces (Bé and Torderlund, 1971) that preferentially inhabites warm surfaces waters (Bé, 1977; Kucera, 2005) and is extensively used to reconstruct past sea-surface temperature and salinity variations. However, *G. ruber* exhibits two chromotypes (*alba* and *rosea*) as well as a significant morphological variability. Thus, the taxonomical concept to classify *G. ruber* species have been subject to revisions over time (Aurhas et al., 2011). In particular, due to the reddish colouration of its test *G. ruber* was initially classified by d'Orbigny (1839) as *Globigerina rubra*, then according to Cushman (1927) was included in the genus *Globigerinoides*. Successively, to the species *G. ruber* was also attributed the *alba* variety.

According to Kennett and Srinivasan (1983) *G. ruber* includes 4 phenotypes (i.e. G. *elongatus*, *G. pyramidalis* and *G. cyclostomus*). On the contrary, Parker (1962) considered these latter species as morphotypes and/or ecophenotypic variants of the same species, because they show distinct latitudinal distribution and ecological preferences, but at the same time they are characterized by a continuum of transitional forms between the morphotypes.

Finally, molecular genetic investigations showed the presence of two distinct phylogenetic lineages within the *G. ruber* plexus (Aurahs et al. 2011). One lineage includes the chromotypes pink and white of *G. ruber* s.s. , and the other one representing a distinct lineage of *G. ruber* s.l. (Wang, 2000), closer related to *Globigerinoides conglobatus* (Brady, 1879). Intriguingly, *G. ruber* s.l. is morphologically consistent with the species definition of *Globigerinoides elongatus* (d'Orbigny 1826), whereby Aurahs et al. (2011) recommended to reinstate the name *G. elongatus* as an extant distinct species and not only as ecophenotypic variant of *G. ruber*. Furthermore, all the more several geochemical studies showed different stable isotopic composition and Mg/Ca geochemistry between the two genotypes (i.e *G. ruber* white s.s. and sensu lato, *G. elongatus*) (Steinke et al., 2005; Sadekov et al., 2009). Studies have implied different calcifying habitat conditions and ecological preferences, or a species-

specific signal (Wang, 2000; Kuroyanagi and Kawahata 2004; Lowemark et al. 2005; Kawahata 2005; Steinke et al. 2005; Antonarakou et al. 2015, and reference therein). These results may have evident critical implications for paleoceanographic and paleoclimatic reconstructions, using a non-selective mixture of these species/morphotypes. However, Thirumalai et al. (2014) in a recent study conducted with sediment traps located in the Gulf of Mexico, showed statistically indistinguishable geochemical variability between *G. ruber* white s.s. and s.l., stressing for no evidence for their own seasonal preferences and/or calcifying depth habitat. In the Mediterranean basin was founded a correlation between morphology and depth habitat of different types of *G. ruber* (white), related to alternation of glacial/interglacial conditions (Numberger et al., 2009).

In synthesis, despite a large number of works in the last years focused on the *G. ruber-G. elongatus* plexus, the link between genotype, morphological variants and ecological preferences and their calcification habitat, is still far from well understood.

Here, we present an "alternative" paleoceanographic-paleoclimatic approach to test the relationship between *G. ruber-G. elongatus* morphological variability and environmental-climatic conditions, taking advantage of very high resolution sampling of the last 85.6 ka downcore sediments (ATA13OF-KT1 core, Oceanograflu 2013 cruise) from the Azores region. A fine identification and characterization of each eco-morphotype/morphospecies has been adopted, above all for those poorly studied forms such as *G. pyramidalis* and *G. cyclostomus*. High time resolution strategy allowed to observe the sensitive of the *G. ruber - G. elongatus* morphotypes/morphospecies abundance fluctuations to astronomically-forced climatically variability at glacial-interglacial scale, and even also to rapid millennial-scale climatic changes. The Azores region is indeed particularly adapted area, because *G. ruber* gr *alba* is considered the dominant taxon in the North Atlantic Subtropical Gyre oceanic cell (Bé and Torderlund, 1971; Bé, 1977), nowadays limited northward by the Azores current (Schiebel et al., 2002b; Rogerson et al., 2004; Schwab et al., 2012; Repschläger et al., 2015; Billups et al., 2016; Bonfardeci et al., this thesis). It has already showed that *G. ruber* gr *alba* distribution/abundance is sensitive to recent and late Pleistocene Azore Front Current System dynamic (Schiebel et al., 2002b). In this work, we test for the first time if this was the case for individual morphotypes/morphospecies of *G. ruber - G. elongatus* plexus. Finally, we show that, especially *G. elongatus* and *G. cyclostomus* abundance fluctuations represent indeed a powerful tool for paleoceanographic-paleoclimatic reconstructions in the central North Atlantic.

8.3 Oceanographic setting

The North Atlantic hydrography is characterised by the North Atlantic Meridional Overturning Circulation (AMOC) system (Lynch-Stieglitz et al., 2007), that regulates the surface and deep waters movements in the Atlantic basin. In particular, the central sector of the North Atlantic is characterised by surface front/current systems that isolate well distinct water masses (Fig.1). The Azores Current, as eastern branch of the Gulf Stream, flows throughout the year, south to the Azores archipelago (Schiebel et al., 2002a; Storz et al., 2009), even if it is strongest in spring (Alves and DeVerdière, 1999; Rogerson et al., 2004).

Today this water masses is centred at 34°N, reaching the depth of about 1,000 m and 50 km of width (Schiebel et al., 2002a). The Azores Current is limited to the north by the so-called Azores Front (Schiebel et al. 2002a-b; Rogerson et al., 2004; Schwab et al. 2012; Repschläger et al. 2015).

The Azores front separates the saltier southern 18°C Mode Water, belonging to the Subtropical Gyre (STG) and characterised by a shallow summer mixed layer, from the northernmost colder and fresher Eastern North Atlantic Central Water (ENACW), with a deeper winter mixed layer (Gould, 1985; Schiebel et al. 2002a-b; Schwab et al. 2012; Repschläger et al. 2015).

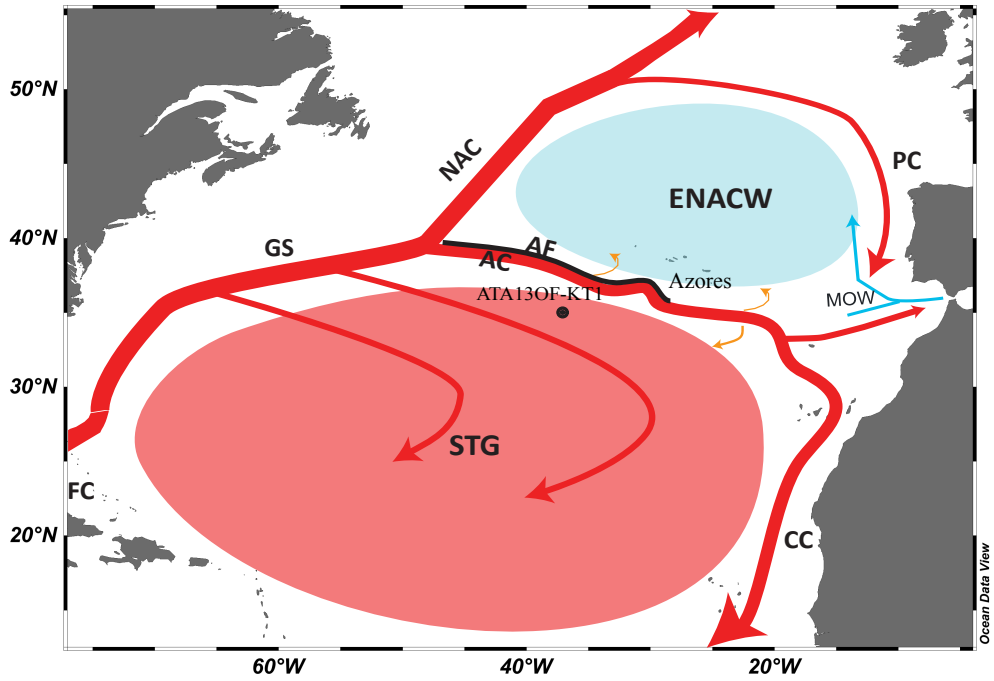

Figure 1. Surface circulation in the North Atlantic at the present day and ATA13OF-KT1 location. STG=SubTropical Gyre; ENACW=Eastern North Atlantic Central Water; FC=Florida Current; GS=Gulf

Stream; NAC=North Atlantic Current; AC=Azores Current; AF=Azores Front; PC=Portugal Current; CC=Canary Current; MOW=Mediterranean Outflow Water.

Therefore the Azores Front represents one the most important hydrographic element, in the Azores region (Fig. 2). In order to track its position in central North Atlantic waters, some Authors used the position of the 15°C isotherm (Gould, 1985; Ottens et al., 1991; Schiebel et al., 2002a-b).

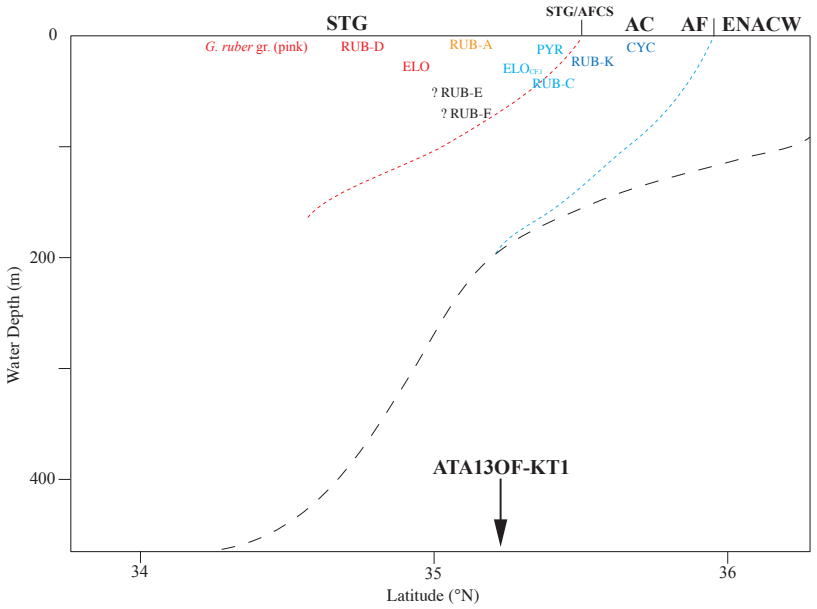

Figure 2. Distribution of the recognised eco-morphotypes and *G. ruber* gr. (pink), south-westward of the Azores archipelago. The latitudinal and vertical position, in the water column, is derived by the data of Wang (2000), Schiebel et al. (2002a-b), Numberger et al. (2009), Storz et al. (2009), Antonarakou et al. (2015). The section has been calculated at the longitude of the studied core (37,15 °W). The coarse dashed line is related to the 15°C isotherm position, reconstructed by Schiebel et al. (2002a) in the same region. The blue fine dashed line is related to the estimated depth position of the Azores Front, whereas the red fine dashed line is related to the surface considered as the boundary between the Subtropical Gyre and Azores Front Current System waters. RUB-A=*G. ruber s.s.-a*; RUB-B=*G. elongatus*; RUB-C=*G. ruber-kum c*; RUB-D=*G. ruber*-d; RUB-E=*G. ruber*-e; RUB-F=*G. ruber*-f; RUB-K=*G. ruber*-k; ELO=*G. elongatus* cf.1; CYC=*G. cyclostomus*; PYR=*G. pyramidalis*. STG=Subtropical Gyre; ENACW=Eastern North Atlantic Central Water; STG/ACFS=Subtropical Gyre/ Azores Front Current System boundary; AC=Azores Current; AF=Azores Front.

According to this reconstruction, waters north of the front are identified where the 15°C isotherm is shallower of 200 m, whereas the central zone of AF is identified where this isotherm lies between 200 and 300 m depth. Finally, the water masses south of the front are identified where the 15°C isotherm is located below 300 m depth.

8.4 Materials and Methods

8.4.1 ATA13-OF-KT1 core location and sample preparation

ATA13OF-KT1 gravity core was collected during the Oceanograflu 2013 cruise, southwestward of Azores archipelago (35°24.956'N; 37°15.749'W). This core (bathymetry=3,431 m; length=4.03 m), collected in proximity of the Mid-Atlantic Ridge, is constituted by a continuous sedimentary record, characterized by the alternation of high-carbonate content and marly levels (Bonfardeci et al., this thesis). The ATA13OF-KT1 core has been studied every 1 cm with a total of 402 samples. We used previously processed samples to pick and analyse the *G. ruber* - *G. elongatus* plexus variability.

8.4.2 Micropaleontological analyses

Micropaleontological dataset consists on quantitative analyses of the *G. ruber* - *G. elongatus* morphotypes, conducted on two different size-fractions. To measure the relatives proportions of *G. ruber* gr. *alba* and *G. ruber* gr. *rosea* respect with the whole planktonic foraminiferal assemblages the size-fraction > 125 μm was used. All these analyses were performed every centimetre.

Furthermore, the relative abundance of each morphotype/morphospecies of *G. ruber* gr. *alba* have been performed in the sediment fraction between 250 and 315 μm. A total of 202 samples have been analysed, with the resolution of 1 sample every 2 cm. The total number of specimens was between 50 and 100 for sample. Just two levels have been discarded because have been recognised less than 20 specimens in total (samples at 334 and 338 cm bsf).

In order to distinguish morphotypes/morphospecies, we follow the taxonomic classification proposed by Saito et al. (1981), and Kenneth and Srinivasan (1983). Furthermore, the recognised taxa were compared to those present at the Paleontological collection of the *Muséum National d'Histoire Naturelle* of Paris. In particular, the lectotype and paralectotype of *Globigerinoides ruber* (d'Orbigny), 1839 and the lectotype of *Globigerina elongata* d'Orbigny, 1826, were analysed. The morphology and the other the features of the test were compared to those of the analysed *G. ruber-G. elongatus* plexus.
(for details visit the site of the micropaleontological collections of the MNHN of Paris: https://science.mnhn.fr/institution/mnhn/collection/f/item/fo302?listIndex=1&listCount=231; https://science.mnhn.fr/institution/mnhn/collection/f/item/fo246?listIndex=2&listCount=6; https://science.mnhn.fr/institution/mnhn/collection/f/item/fo307?listIndex=16&listCount=23;).

The identification has been performed on the basis of classical principles of classification: 1.shape and coiling mode of the test; 2.wall texture; 3.number and shape of the chambers in the last whorl; 4.shape of the sutures; 5.shape, dimension and position of the primary and supplementary apertures. The spinose wall texture and the typical cancellate "honeycomb" wall surface have been recognised for all types, thus these features are not included in the following descriptions. Ten distinct morphotypes have been recognised (Plates 1 and 2):

- *Globigerinoides cyclostomus* (Galloway and Wissler, 1927) (Plate 1 – photos 1-2a, 1-2b, 1-2c). Test small, low to medium height trochospire with three ovoid to subspherical chambers in the last whorl, increasing moderately in size but closely packed giving the test a rectangular outline; sutures radial and depressed; wall thick, sometimes with a secondary calcite crust, surface coarsely perforate; primary aperture umbilical, interiomarginal, oval to small rounded opening; two reduced supplementary apertures, situated at spiral side at intersections of spiral and intercameral sutures. *G. cyclostomus* differs from *G. ruber* s.s. from its more compact chamber arrangement, thick wall test and small aperture relative to the chamber size. Up today no molecular genetic data are available for *G. cyclostomus*, so it is not possible to assess if is a phenotypic variants of *G. ruber* s.s. (Saito et al., 1981), or if is a separate species as proposed by Galloway and Wissler (1927).

- *G. ruber* s.s.-a. (Plate 1 – photos 3a, 3b, 3c). Test medium, low to high trochospire with three subspherical chambers in the last whorl, increasing slowly in size, symmetrical over the previous sutures; sutures radial and depressed; surface coarsely perforate; primary aperture umbilical, interiomarginal, large, wide arched opening; two distinct supplementary apertures, moderately high-arched rounded situated at spiral side at intersections of spiral and intercameral sutures. This form corresponds to the genotype Type I (Kuroyanagi et al., 2008) and Type Ia, Ib, Ib2 (Aurahs et al., 2011), and informally defined morphotype *G. ruber* gr *alba* s.s. (Wang 2000), or type a "normal" (Numberger et al., 2009).

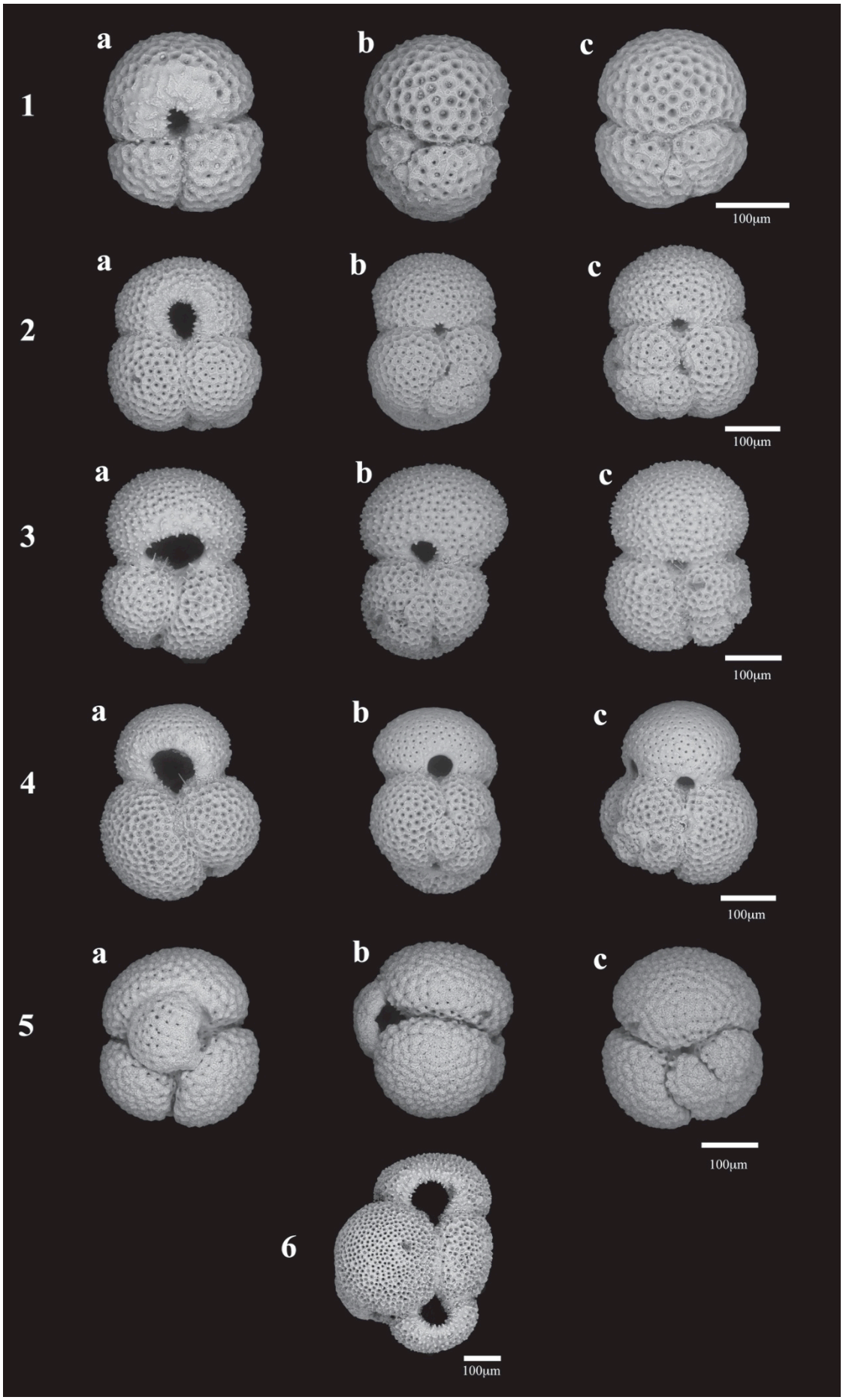
a
b
c
1
100µm
a
b
c
2
100µm
a
b
c
3
100µm
a
b
c
4
100µm
a
b
c
5
100µm
6
100µm

Figure 3. Plate 1. (a: umbilical side view; b: side view; c: dorsal side view). 1-2. *Globigerinoides cyclostomus*. 3. *Globigerinodes ruber*-a. 4. *Globigerinodes ruber*-d. 5. *Globigerinodes ruber*-c. 6. *Globigerinodes ruber*-e (only umbilical side view).

- *G. ruber*-d (Plate 1 – photos 4a, 4b, 4c). Test medium, low to high trochospire with three subspherical chambers in the last whorl, with the last chamber decreased in size compared to the penultimate, slightly asymmetrical over the previous sutures; sutures radial and depressed; surface coarsely perforate; primary aperture umbilical, interiomarginal, large, wide arched opening; two distinct supplementary apertures, high-arched rounded, situated at spiral side at intersections of spiral and intercameral sutures and bordered by a rim. This type is morphologically close to *G. ruber* s.s., but it presents a larger primary aperture, compared to the reduced size of the last chamber.

- *G. ruber*-kum c. (Plate 1 – photos 5a, 5b, 5c). Test small, low to medium height trochospire with three ovoid to subspherical chambers in the last whorl, increasing moderately in size; sutures incised; wall thick, sometimes with a secondary calcite crust, surface coarsely perforate; primary aperture umbilical, interiomarginal, totally or partially covered by a distinct chamber-like structure; narrow supplementary apertures on spiral side, formed at intersections of spiral and intercameral sutures.

- *G. ruber*-e. (Plate 1 – photo 6). Morphology very close to *G. elongatus*; it possesses a diagnostic, but anomalous, additional chamber, very similar in the shape to the last one. This form was labelled by Saito et al. (1981) as "helicina".

- *G. elongatus* (d'Orbigny, 1826). (Plate 2 – photos 7a, 7b, 7c). Test medium to large, low to medium high trochospire; three chambers in the last whorl, ovoid to rectangular, asymmetrical over the previous sutures; typically flattened the last chamber; sutures distinctly depressed; wall thick, surface coarsely to medium densely perforate; primary aperture umbilical, interiomarginal, normally small to medium rounded opening, bordered by a rim; secondary supplementary apertures on spiral side circular, formed at intersections of spiral and intercameral sutures. That morphotype corresponds to the informally defined morphotype *G. ruber* s.l. (Wang, 2000) and type b "platys" (Numberger et al., 2009). It corresponds to the genetic Type IIa (Aurahs et al., 2009; 2011) and it is consistent to the morphological concept of *G. elongatus* species of d'Orbigny (1826).

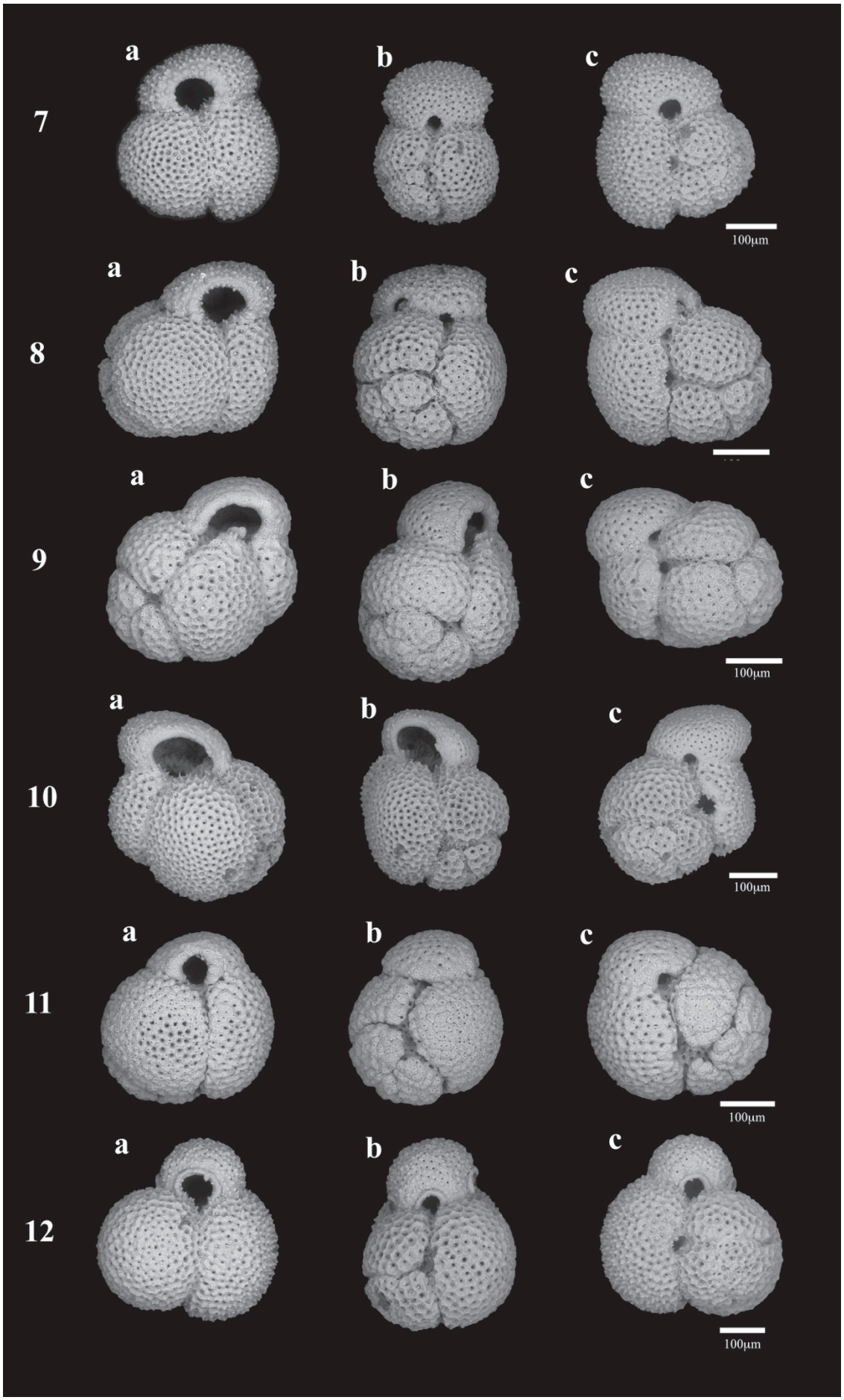
7
a
b
c
100µm
8
a
b
c
9
a
b
c
100µm
10
a
b
c
100µm
11
a
b
c
100µm
12
a
b
c
100µm

Figure 4. Plate 2. (a: umbilical side view; b: side view; c: dorsal side view). 7. *Globigerinodes ruber*-b. 8. *Globigerinodes elongatus* cf.1. 9-10. *Globigerinodes pyramidalis.* 11. *Globigerinodes ruber*-k. 12. *Globigerinodes ruber*-f.

- *G. elongatus* cf.1. (Plate 2 – photos 8a, 8b, 8c). Test medium to large, high trochospire; three chambers in the last whorl, ovoid to rectangular, asymmetrical over the previous sutures; sometimes flattened radially the last chamber; sutures depressed; wall thick, surface coarsely to medium densely perforate; primary aperture umbilical, interiomarginal, rounded or medium arched opening, bordered by a rim; secondary supplementary apertures on spiral side circular, formed at intersections of spiral and intercameral sutures. That type corresponds with that recognised as *G. elongatus* by Rogl and Bolli (1973). Furthermore, it partially corresponds with that labelled as type c "elongate" by Numberger et al. (2009), although these Authors believed this type consistent with the Saito et al. (1981) concept of *G. pyramidalis*. *G. elongatus* cf.1 differs from *G. elongatus* (d'Orbigny, 1826) for the higher coiled trochospire and for the shape of the last chamber not always flattened. We distinguish *G. elongatus* cf.1 from *G. pyramidalis* on the basis of the number of the chambers in the last whorl, 3 in *G. elongatus* cf.1 and 4 in *G. pyramidalis* and for the shape of the primary aperture (wide-arched opening in *G. pyramidalis*, sub-rounded in *G. elongatus* cf.1).

- *G. pyramidalis* (van den Broeck, 1876). (Plate 2 – photos 9-10a, 9-10b, 9-10c). Test medium to large, very high trochospire, with a typical pyramid shape; four chambers in the last whorl, initially subspherical to flattened radially, especially the last one, asymmetrical over the previous sutures; sutures radial to slightly curved and depressed; wall thick, surface coarsely to medium densely perforate; primary aperture umbilical, interiomarginal, very large to medium, wide-arched opening, sometimes with a tooth-like structure present; secondary supplementary apertures on spiral side also large, circular, formed at intersections of spiral and intercameral sutures. That type partially corresponds with the description of Saito et al. (1981) and Rogl and Bolli (1973), but has been differentiated and distinguished by *G. elongatus* cf. 1, because it has four than three chambers in the last whorl and a larger and wide-arched primary aperture. In some samples we have observed rare intermediate forms, mostly between *G. elongatus* cf.1 and G. *pyramidalis*.

- *G. ruber*-k. (Plate 2 – photos 11a, 11b, 11c). Test medium, high trochospire; three chambers in the last whorl, ovoid to subspherical, asymmetrical over the previous sutures; last

chamber significantly smaller and flattened than the previous; sutures deep; wall thick, sometimes with a secondary calcite crust, surface coarsely perforate; primary aperture umbilical, interiomarginal, rounded opening; narrow supplementary apertures on spiral side, formed at intersections of spiral and intercameral sutures. That type corresponds to *G. ruber* Kummerform, identified and described by Numberger et al. (2009). We agree with them that it could represent the terminal ontogenetic stage and/or a morphologic variation in response to environmental stress.

- *G. ruber*-f. (Plate 2 – photos 12a, 12b, 12c). Test medium, high trochospire; three subspherical chambers in the last whorl, asymmetrical over the previous sutures; last spherical chamber significantly smaller than the previous; sutures depressed; medium to thick wall, surface coarsely perforate; primary aperture umbilical, interiomarginal, rounded opening, bordered by a distinct rim; supplementary apertures rounded opening on spiral side, formed at intersections of spiral and intercameral sutures, bordered by a distinct rim. This morphotype is also a Kummerform, but it differs from *G. ruber*-k for the less thick wall, the more spherical shape of the chambers and especially for the rounded and rimmed apertures.

The morphotypes with abundance of about 90 %, such as *G. elongatus*, *G. ruber* ss, *G. elongatus* cf.1 and *G. cyclostomus* have been included in the group here named Greater Contributors (GC), whereas the others with percentages less abundant than 10 % have been considered as Minor Contributors (MC).

8.4.3 *Stable isotope analyses*

Stable isotope analyses were performed at LSCE (Laboratoire des Sciences du Climat et de l'Environnement – Gif sur Yvette) using an Elementar Isoprime mass spectrometer, directly coupled to an automated carbonate preparation device. All values are given in δ-notation versus VPDB Vienna Pee Dee Belemnite. The used standard (UCD-SM92) was a Carrara marble, prepared at the beginning of 1990s for the University of California. The adopted values of this standard are –1.91 ‰ (V-PDB) for $\delta^{18}O$ and +2.09 ‰ (V-PDB) for $\delta^{13}C$. The analytical precision and the reproducibility for repeated measurements of the laboratory reference calcite is ± 0.05 ‰ for $\delta^{18}O$ and ± 0.03 ‰ for $\delta^{13}C$. Prior to analysis the foraminifers have been cleaned in a methanol ultrasonic bath for 10 seconds and then naturally dried in fume hood. The $\delta^{18}O$ and $\delta^{13}C$ *G. ruber* s.s.-a curves came from Bonfardeci

et al. (this thesis). The *G. ruber* s.s. were picking in the size-fraction 250-315 μm. The sampling resolution was one centimetre. In the present work, we have been carried out additional $\delta^{18}O$ and $\delta^{13}C$ analyses from coeval morphotypes/morphospecies coming from two strategic intervals. *G. elongatus* and *G. elongatus* cf.1 have been handpicked from part of interglacial MIS1 interval (0-18.5 cm bsf) and *G. cyclostomus* and *G. elongatus* cf.1 from part of glacial MIS 2 interval (42-60 cm bsf) (fig.). Ten individuals for each morphotypes/morphospecies have been analysed from the same samples (size-fraction 250-315) where *G. ruber* s.s. have been handpicked.

8.4.4 Multivariate statistical analyses

In order to understand how the climate forcing control the distribution of the *G. ruber* - *G. elongatus* eco-morphotypes, a multivariate statistical treatment has been performed through the studied interval. These analyses allow to identify the statistical proximity and/or distance between the recognised morphotypes, as well as representing a very powerful tool to summarize and ordinate the micropaleontological data. In particular, the Principal Component Analysis (PCA), the Principal Coordinate Analysis (PCoA) and the Cluster Analysis (CA) have been carried out, using the PAST version 3.11 (Hammer et al., 2001). Moreover, the similarity (Bray-Curtis) and distance (Euclidean) indexes for the *G. ruber* - *G. elongatus* plexus distribution have been calculated.

PCA allows to linearly combine two new hypothetical variables (components) (Davis, 1986; Harper, 1999), presents in the *G. ruber* - *G. elongatus* eco-morphotypes of the ATA13OF-KT1 dataset. For this analysis the input data is a matrix with ten recognised eco-morphotypes (rows) and samples (column). The analysis has been firstly performed for the entire core and then focused in each Marine Isotope Stages obtaining different PCA for these intervals. To ordinate the analysed data PCoA based on the algorithm of Davis (1986) has been used as supplementary method. To this method a Bray-Curtis similarity index has been applied that permits to explore similarities of the analysed data. Finally, *G. ruber* - *G. elongatus* eco-morphotypes have been clustered using CA.

Method using the Single Linkage (SL) through the Bray-Curtis similarity index (Gower and Ross, 1968) and Ward's algorithm (Ward, 1963) have been used. This latter method operates through the Euclidean dissimilarity index and joins groups to minimize the within-group variance increase. In order to assess the robustness of the specimens grouping, dendrograms obtained by the two different clustering methodologies have been compared,.

8.5 ATA13OF-KT1 core chronology

The ATA13OF-KT1 core chronology, derived by the study of Bonfardeci et al. (this thesis), has been developed combining four AMS ^{14}C analyses, concentrated in the first 40 cm bsf, and the synchronization of $\delta^{18}O_{\text{G. ruber s.s.-a}}$ with MD95-2042 $\delta^{18}O_{\textit{G. bulloides}}$ record, re-tuned by Lisiecki and Stern (2016). Thirty-four additional age control points have been established through the alignment of ATA13OF-KT1 $\delta^{18}O_{\textit{G.ruber}\ \text{s.s.-a}}$ maxima/minima with those correspondent in the MD95-2042 $\delta^{18}O_{\textit{G. bulloides}}$ (LS16) record (Bonfardeci et al., this thesis). According to the developed age model the time interval recorded by ATA13OF-KT1 core goes from 81.94 to 2.75 ka (MIS 5.1 – MIS 1). The mean sedimentation rate for this sedimentary record results of 5.08 cm/kyr. Considering the sampling rate of one sample every two centimetre, adopted in this work, a temporal resolution of 0.394 years between samples have been calculated.

8.6 Results

8.6.1 Stable isotope data

The stable oxygen isotope of *G. ruber* s.s. shows a typical Azores region glacial/interglacial pattern (Bonfardeci et al. this thesis) during the last 81.94 ka (Fig. 9). The $\delta^{18}O_{\text{G. ruber s.s.-a}}$ was heavier during glacial periods of MIS 4 and 2 with values between 2.1and 0.8 ‰, whereas it showed clear lightening during warm and temperate-warm phases (1.7-0.4 ‰).

In $\delta^{18}O_{\text{G. ruber s.s.-a.}}$ curve several high frequency/low intensity fluctuations, probably linked sub-orbital climatic phases (see reference therein Bonfardeci et al., this thesis), have been individuated. These climatic phases coincide with the coolest events (“H”1 to “H”7), marked by abrupt increases > 0.7-1 ‰ in $\delta^{18}O_{\text{G. ruber s.s.-a.}}$ record. Moreover, twenty Dansgaard/Oeschger interstadials, in correspondence of 0.5-1 ‰ $\delta^{18}O_{\text{G. ruber s.s.-a.}}$ lightening, are present in the studied oxygen isotope record.

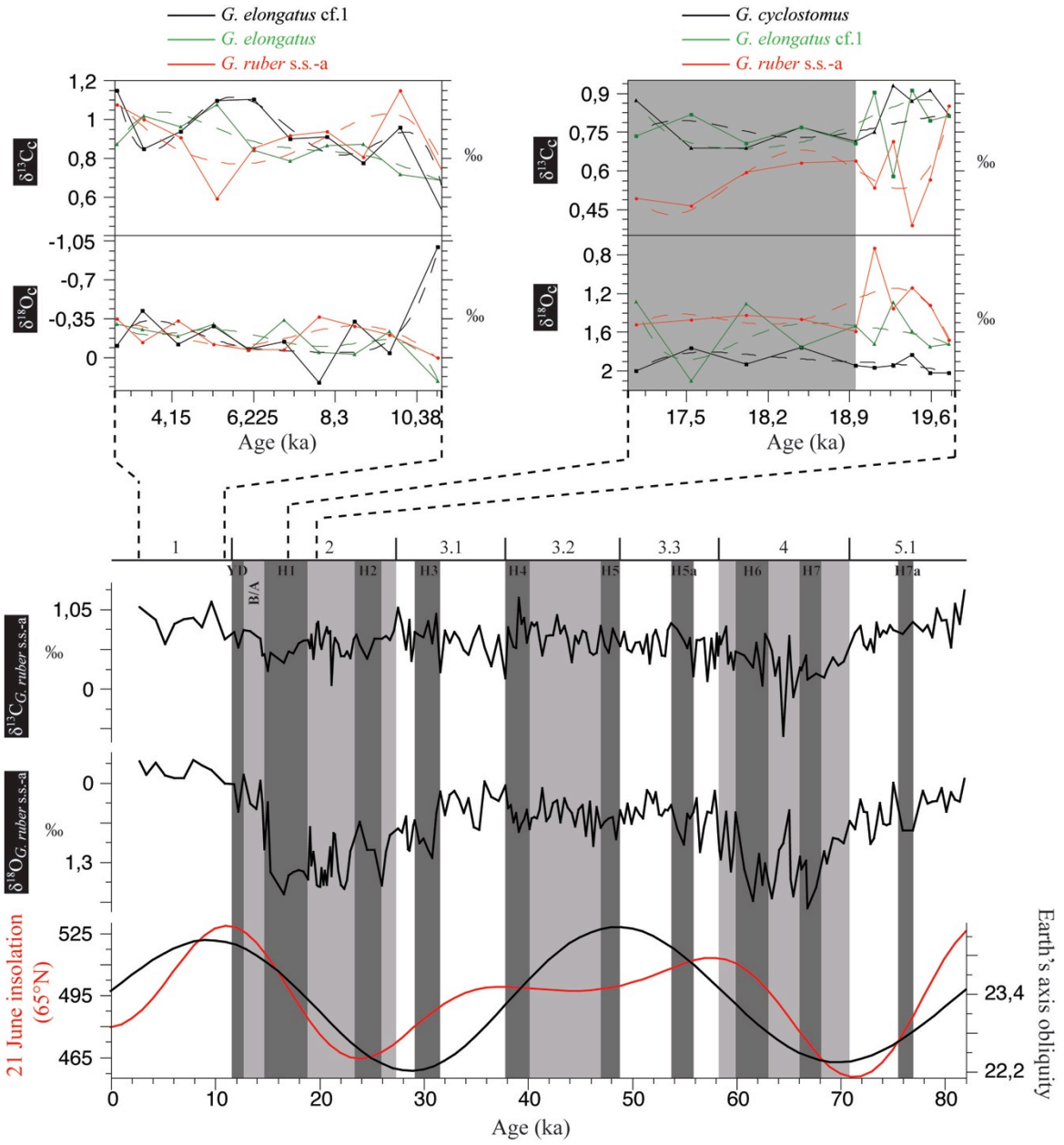

Figure 5. $\delta^{18}O$ *G. ruber* s.s.-a and $\delta^{13}C$ *G. ruber s.s.-a* fluctuations of ATA13OF-KT1 core record. The abundances fluctuation data are plotted respect to the 21 June insolation at 65°N (red curve) and obliquity (black curve) signals, calculated for the interval between 82 to 0 ka (Laskar et al., 2004). Light gray vertical bars refer to the glacial stages (MIS 2 and 4) and cool-temperate periods (MIS 3.2). White vertical bars are related to the interglacials (MIS 1 and 5.1) and temperate-warm periods (MIS 3.1 and 3.3). Dark gray vertical bars identify the intervals correspondent to the Heinrich events, proposed by Lisiecki and Stern (2016), here labelled as H1 to H12. YD=Younger Dryas stadial; B/A=Bølling/Allerød interstadial.

As regard to the $\delta^{13}C$ G. ruber-s.s-a. data, the lowermost values have been registered during the glacial periods, especially during the MIS 4. In this latter stage a marked lightening of $\delta^{13}C$ G. ruber-s.s-a., down to -0.65 ‰ has been measured. On the contrary, the heavier $\delta^{13}C$ G. ruber-s.s.-a values, between 0.13 and 1.3 ‰, were registered during MIS 5.1, MIS 3 and Holocene. High-

frequency fluctuations are present also in the $\delta^{13}C_{G.\ ruber\ s.s.-a}$ record, with shifts between 0.5 and 1 ‰, on average.

The $\delta^{18}O$ and $\delta^{13}C$ data of individual morphotypes for two selected intervals (Holocene and LGM/"H"1 transition) are showed in Figure 9 and Table 1 and 2.

Depth (cm bsf)	**Age (ka)**	***G. elongatus***	***G. elongatus* c.f.1**	***G. ruber s.s.*-a**
0.50	2.75	-0.30	-0.11	-0.35
2.50	3.42	-0.25	-0.42	-0.13
4.50	4.32	-0.19	-0.12	-0.33
6.50	5.21	-0.30	-0.28	-0.12
8.50	6.11	-0.06	-0.08	-0.07
10.50	7.00	-0.34	-0.14	-0.07
12.50	7.89	-0.05	0.23	-0.37
14.50	8.79	-0.03	-0.33	-0.28
16.50	9.68	-0.23	-0.04	-0.21
18.50	10.51	0.22	-1.00	0.01
Average value		-0.15	-0.23	-0.19

Depth (cm bsf)	**Age (ka)**	***G. cyclostomus***	***G. elongatus* c.f.1**	***G. ruber s.s.*-a**
42.50	16.11	2.00	1.28	1.52
44.50	16.57	1.77	2.10	1.47
46.50	17.03	1.93	1.30	1.43
48.50	17.49	1.76	1.75	1.46
50.50	17.95	1.95	1.53	1.59
52.50	18.41	1.96	1.72	0.73
54.50	18.87	1.95	1.29	1.36
56.50	19.33	1.83	1.59	1.14
58.50	19.79	2.02	1.75	1.32
60.50	20.25	2.02	1.72	1.68
Average value		1.92	1.60	1.37

Table 1. $\delta^{18}O$ data (in ‰) of the analyses carried out on *G. elongatus*, *G. elongatus* cf.1, *G. cyclostomus and G. ruber* s.s.-a.The intervals 2.75-10.51 ka and 16.11-20.35 ka have been analysed.

Depth (cm bsf)	Age (ka)	*G. elongatus*	*G. elongatus* c.f.1	*G. ruber s.s.*-a
0.50	2.75	0.87	1.15	1.08
2.50	3.41	1.02	0.85	1.00
4.50	4.30	0.96	0.94	0.91
6.50	5.20	1.08	1.10	0.59
8.50	6.10	0.84	1.10	0.85
10.50	6.99	0.79	0.90	0.92
12.50	7.89	0.87	0.91	0.94
14.50	8.79	0.87	0.78	0.81

16.50	9.69	0.72	0.96	1.15
18.50	10.91	0.68	0.44	0.65
Average value		0.87	0.91	0.89
Depth (cm bsf)	Age (ka)	*G. cyclostomus*	*G. elongatus* c.f.1	*G. ruber s.s.*-a
42.50	17.07	0.87	0.73	0.49
44.50	17.54	0.69	0.82	0.47
46.50	18.01	0.69	0.71	0.59
48.50	18.48	0.77	0.77	0.63
50.50	18.95	0.71	0.71	0.64
52.50	19.11	0.75	0.90	0.54
54.50	19.27	0.93	0.58	0.72
56.50	19.43	0.87	0.91	0.39
58.50	19.59	0.91	0.80	0.57
60.50	19.75	0.82	0.81	0.85
Average value		0.80	0.77	0.59

Table 2. $\delta^{13}C$ data (in ‰) of the analyses carried out on *G. elongatus*, *G. elongatus* cf.1, *G. cyclostomus and G. ruber* s.s.-a.The intervals 2.75-10.51 ka and 16.11-20.35 ka have been analysed.

This approach allows to estimate the response of the selected eco-morphotypes to different climatic settings. For this reason, additional stable isotope analyses have been performed in correspondence of the current interglacial (Holocene) and a part of the last glacial phase (MIS 2). It is evident that in the Holocene interval the averages values of $\delta^{18}O$ and $\delta^{13}C$ between the different morphotypes are very small, and virtually indistinguishable, being in the error range of the measures (for more detail see Table 1 and 2). In a part of the MIS 2 between 16.1 and 20.2 ka, $\delta^{18}O$ and $\delta^{13}C$ morphotypes values are more pronounced, especially between *G. ruber* s.s.-a and *G. cyclostomus* (0,55 ‰ and 0,21 ‰), *G. ruber* s.s.-a and *G. elongatus* cf.1 (0,23 ‰ and 0,18 ‰), and *G. elongatus* cf.1 and *G. cyclostomus* (0,32 ‰ and 0,03 ‰).

8.6.2 Quantitative data on G. ruber - G. elongatus morphotypes

G. ruber gr. *alba* shows a clear increase during warm climate phases (MIS 5.1 and MIS 1) (Fig. 5) with maxima percentages (10-20 %), especially during the Holocene (Fig. 6). On the contrary, it shows minima abundance (2-12.5 %) during MIS 4 and during the preglacial stage of the MIS 3.1 (3-9.5 %).

During the last glacial stage (MIS 2), *G. ruber* gr. *alba* reaches an anomalous medium abundance (13 %), except the coldest periods correspondent to the "Heinrich" related event 1 and "Heinrich" related event 2, where it decreases below 3.5 % (Fig. 6). This latter trend has

also been described in the central-eastern North Atlantic by Chapman et al. (2000) and Rogerson et al. (2004).

G. ruber gr. *rosea* variety is low abundant (0-1.6 %), even if shows significant high frequency "incursions", in particular during MIS 3.3, MIS 3.2 and MIS 1, probably linked to Dansgaard-Oeschger cycles (Fig. 6). Moreover, it shows an evident increase in abundance during the Bølling/Allerød warm period (14.7 – 12.76 ka) and during the Holocene. This chromotype is near to absent in correspondence of the coldest glacials MIS 4 and MIS 2. The different eco-morphotypes have been grouped on the basis of their contribution to the *G. ruber* - *G. elongatus* plexus, considering the entire studied record. The fluctuations of the eco-morphotypes, especially those of GC, show distinct patterns linked to insolation and obliquity curves (Fig. 6).

G. elongatus is the most abundant taxon and become dominant (up to 50 %) during warm periods (MIS 5.1, 3.3, 3.1 and 1) and during the Bølling/Allerød-Younger Dryas interval. Furthermore, it seems strictly linked to the northern Hemisphere summer daily insolation (35°N). Thus, *G. elongatus* can be considered a warm affinity species (Margaritelli et al., 2016) that increased during insolation maxima and decreased during insolation minima (Fig. 5).

On the other hand, fluctuations of *G. cyclostomus* show an anticorrelative behaviour with the insolation (Fig. 5), since maxima percentages in abundance are in phase with insolation minima and glacial periods (MIS 4 and MIS 2), highlighting its affinity with cooler water habitats.

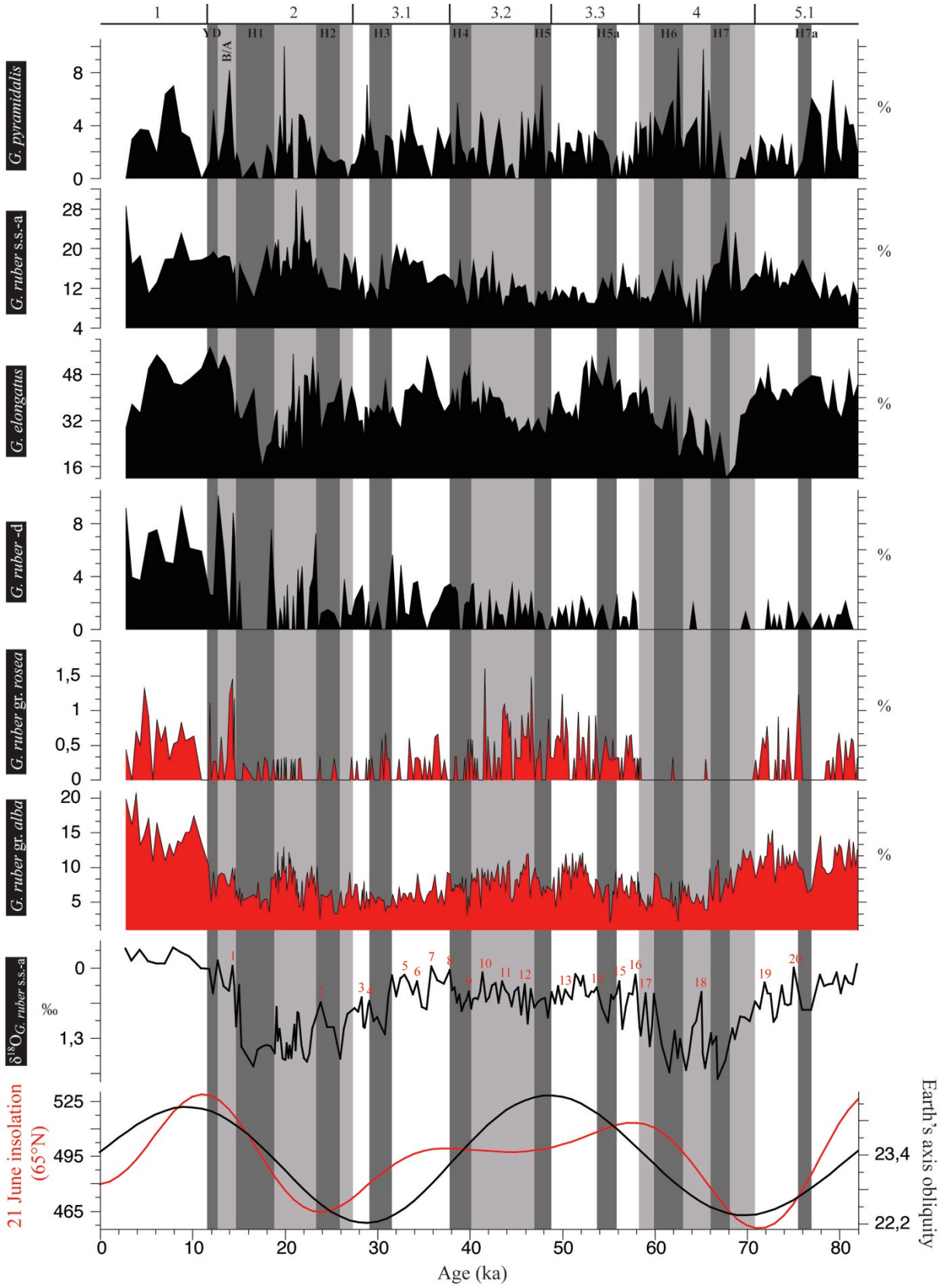

Figure 6. Abundance fluctuation data of the *G. ruber* – *G. elongatus* population (first part). The graphs with red fill are referred to the relative abundance of *G. ruber* gr. (white) and *G. ruber* gr. (pink) in the total planktonic assemblage of ATA13OF-KT1 (125 μm). The graphs with black fill are referred (from below to above) to *G. ruber*-d, *G. elongatus*, *G. ruber s.s.-a*, *G pyramidalis* (250-315 μm). The abundances fluctuation

data are plotted respect to the 21 June insolation at 65°N (red curve) and obliquity (black curve) signals, calculated for the interval between 82 to 0 ka (Laskar et al., 2004), as well as to the $\delta^{18}O$ *G. ruber* s.s.-a record (Bonfardeci et al., this thesis). Light gray vertical bars refer to the glacial stages (MIS 2 and 4) and cool-temperate periods (MIS 3.2). White vertical bars are related to the interglacials (MIS 1 and 5.1) and temperate-warm periods (MIS 3.1 and 3.3). Dark gray vertical bars identify the intervals correspondent to the Heinrich events, proposed by Lisiecki and Stern (2016), here labelled as H1 to H12. YD=Younger Dryas stadial; B/A=Bølling/Allerød interstadial. Red numbers associated to $\delta^{18}O$ *G. ruber* s.s.-a record are referred to the Dansgaard/Oeschger interstadial phase (D/O) (Barker et al., 2011; Billups et al., 2016; Bonfardeci et al., 2016).

G. cyclostomus was near to absent in interglacial MIS 5.1 and especially in MIS 1. *G. cyclostomus*, *G. elongatus* cf.1 and *G. ruber* s.s.-a oscillations appear in phase with the obliquity (Figs. 6 and 7), even if their signals are more noisy and less clear than those of *G. elongatus* and *G. cyclostomus*. As regards to the morphotypes belonging to the "Minor Contributors", it is noticeable a sharp increase of *G. ruber*-d during the last deglacial (MIS 1), especially during the Bølling/Allerød and the Holocene (Fig. 6). *G. ruber*-K variability appears to be linked to the orbital-forcing (Fig. 7). In particular, increases in abundance of *G. ruber*-K are clearly in phase with insolation minima, showing similar behaviour to *G. cyclostomus*. Morphotypes *G. ruber*-e and *G. ruber*-f are very rare in the assemblages (respectively 0.29 and 0.23 %, on average), therefore it is not evident to depict a significant distribution pattern and their curves are not discussed here.

It is important to note that the best marker for "Heinrich" related events is the *G. cyclostomus*, especially those occurred during the glacial stages ("H" 7, 6, 2 and 1). Hence, in correspondence of these climatic cooling this species increased clearly in abundance, in the Azores region.

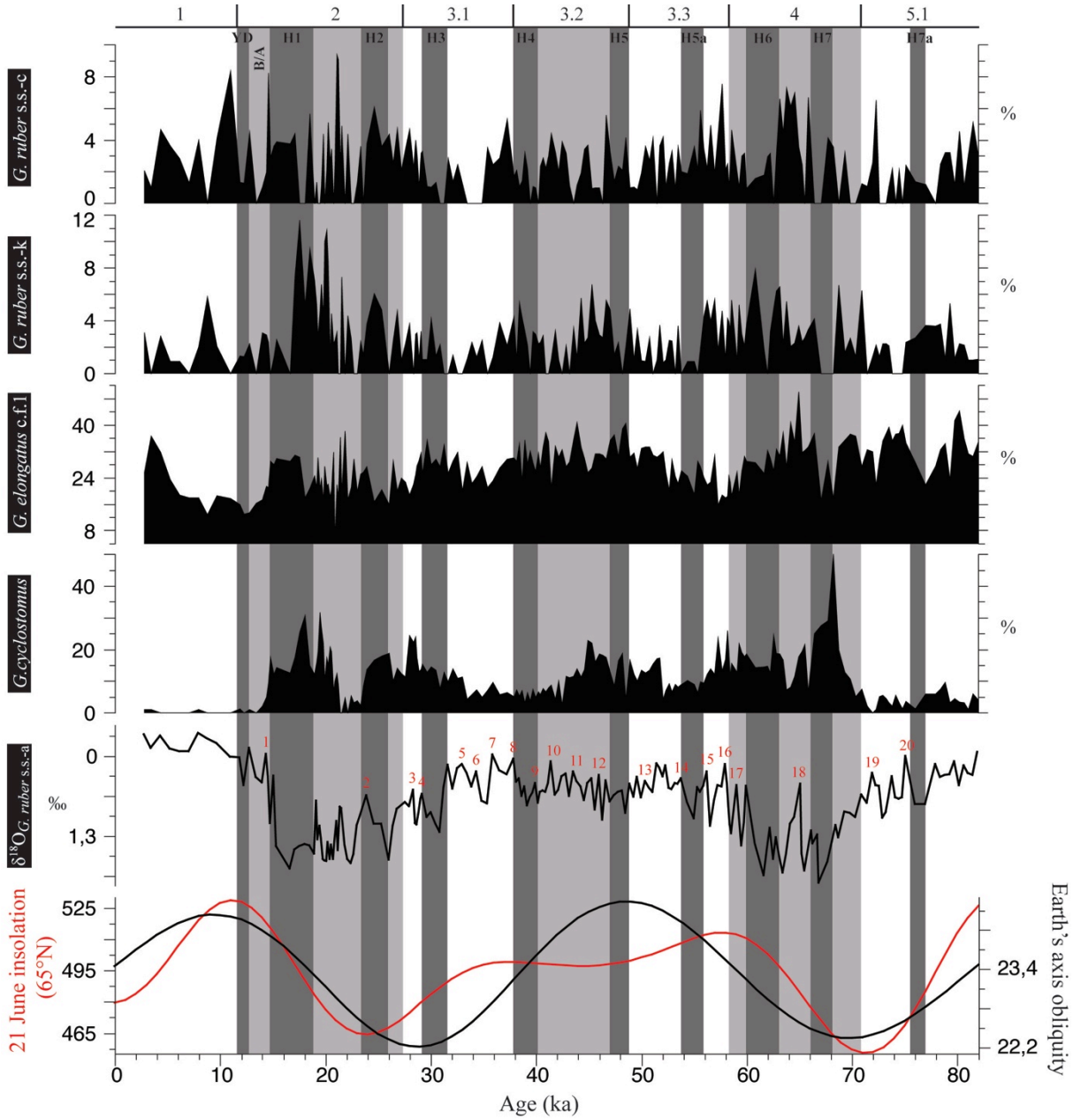

Figure 7. Abundance fluctuation data of the *G. ruber* – *G. elongatus* population (second part). The graphs with black fill are referred (from below to above) to *G. cyclostomus*, *G elongatus* cf.1, *G. ruber*-k, *G. ruber*-kum c (250-315 μm). The abundances fluctuation data are plotted respect to the 21 June insolation at 65°N (red curve) and obliquity (black curve) signals, calculated for the interval between 82 to 0 ka (Laskar et al., 2004), as well as to the $\delta^{18}O$ *G. ruber* s.s.-a record (Bonfardeci et al., this thesis). Light gray vertical bars refer to the glacial stages (MIS 2 and 4) and cool-temperate periods (MIS 3.2). White vertical bars are related to the interglacials (MIS 1 and 5.1) and temperate-warm periods (MIS 3.1 and 3.3). Dark gray vertical bars identify the intervals correspondent to the Heinrich events, proposed by Lisiecki and Stern (2016), here labelled as H1 to H12. YD=Younger Dryas stadial; B/A=Bølling/Allerød interstadial. Red numbers associated to $\delta^{18}O$ *G. ruber* s.s.-a record are referred to the Dansgaard/Oeschger interstadial phase (D/O) (Barker et al., 2011; Billups et al., 2016; Bonfardeci et al., 2016)

8.6.3 Multivariate statistical data

Quantitative data of *G. ruber* - *G. elongatus* morphotypes have been statistically treated into two different phases. During the first phase quantitative data of all morphotypes have been analysed. This analysis allowed to establish the statistical proximity of each type, in term of its distribution and ecology. The similarity (Bray-Curtis) and distance (Euclidean) indexes calculated for the *G. ruber* - *G. elongatus* plexus has been reported in Table 3.

Similarity index (Bray-Curtis)										
	G. elongatus cf.1	*G. ruber* s.s.-a	*G. elongatus*	*G. ruber*-k	*G. ruber*-f	*G. ruber* kum-c	*G. ruber*-e	*G. ruber*-d	*G. pyramidalis*	*G. cyclostomus*
G. elongatus cf.1		0.65	0.81	0.17	0.01	0.16	0.02	0.11	0.17	0.54
G. ruber s.s.-a	0.65		0.52	0.32	0.03	0.31	0.04	0.22	0.31	0.69
G. elongatus	0.81	0.52		0.12	0.01	0.12	0.01	0.08	0.12	0.42
G. ruber-k	0.17	0.32	0.12		0.12	0.61	0.16	0.42	0.58	0.36
G. ruber-f	0.01	0.03	0.01	0.12		0.11	0.20	0.13	0.13	0.03
G. ruber kum-c	0.16	0.31	0.12	0.61	0.11		0.18	0.48	0.57	0.33
G. ruber-e	0.02	0.04	0.01	0.16	0.20	0.18		0.15	0.17	0.05
G. ruber-d	0.11	0.22	0.08	0.42	0.13	0.48	0.15		0.48	0.18
G. pyramidalis	0.17	0.31	0.12	0.58	0.13	0.57	0.17	0.48		0.33
G. cyclostomus	0.54	0.69	0.42	0.36	0.03	0.33	0.05	0.18	0.33	
Distance index (Euclidean)										
	G. elongatus cf.1	*G. ruber* s.s.-a	*G. elongatus*	*G. ruber*-k	*G. ruber*-f	*G. ruber* kum-c	*G. ruber*-e	*G. ruber*-d	*G. pyramidalis*	*G. cyclostomus*
G. elongatus cf.1		201.81	199.67	317.10	342.34	316.84	341.28	327.26	316.22	240.16
G. ruber s.s.-a	201.81		332.27	138.88	163.42	138.77	162.25	145.02	138.59	109.85
G. elongatus	199.67	332.27		456.88	481.89	455.13	480.57	463.98	454.81	381.10
G. ruber-k	317.10	138.88	456.88		36.96	30.17	35.85	36.70	32.31	125.39
G. ruber-f	342.34	163.42	481.89	36.96		35.86	8.77	31.58	35.72	150.94
G. ruber kum-c	316.84	138.77	455.13	30.17	35.86		34.89	32.88	32.43	129.41
G. ruber-e	341.28	162.25	480.57	35.85	8.77	34.89		31.50	35.31	149.36
G. ruber-d	327.26	145.02	463.98	36.70	31.58	32.88	31.50		35.11	144.23
G. pyramidalis	316.22	138.59	454.81	32.31	35.72	32.43	35.31	35.11		131.56
G. cyclostomus	240.16	109.85	381.10	125.39	150.94	129.41	149.36	144.23	131.56	

Table 3. Similarity index (Bray-Curtis) and Distance index (Euclidean) referred to the ATA13OF-KT1 core record.

Single linkage clustering (Fig. 8c), obtained through the similarity index of Bray-Curtis, revealed that *G. ruber*-e and *G. ruber*-f have similar distributions and they appear clearly separated from the other types due to their low abundances. The Bray-Curtis analysis produced a supercluster formed by *G. ruber*-d, *G. ruber*-k, *G. ruber-kum c* and *G. pyramidalis*, which highlights the statistical similarity of these morphotypes. The distributions of *G. ruber*-s.s.-a and *G. cyclostomus* result very close and associated to another cluster formed by *G. elongatus* cf.1 and G. *elongatus*.

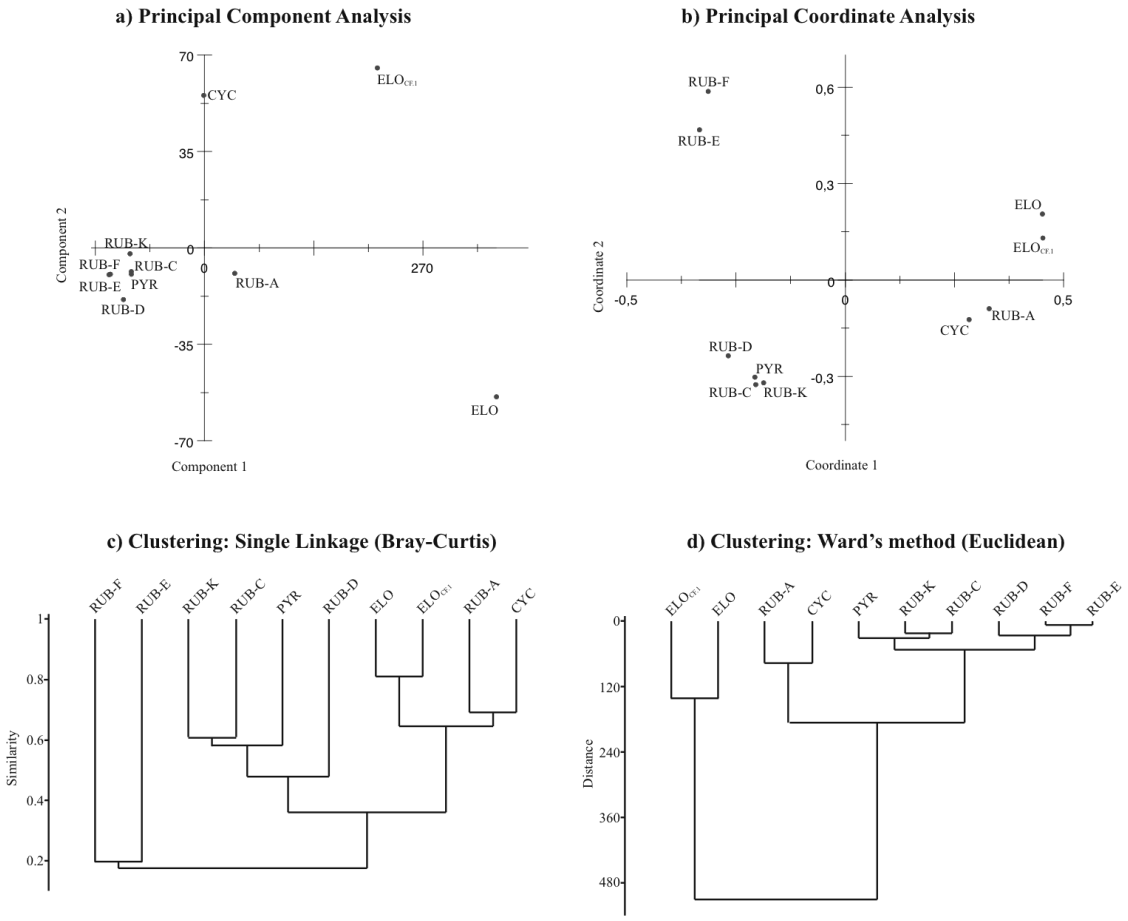

Figure 8**.** Multivariate statistical analyses performed on quantitative data. a) Principal Component Analysis (PCA) performed on the entire ATA13OF-KT1 core record. b) Principal Coordinate Analysis (PCoA) performed on the entire ATA13OF-KT1 core record. c) Single linkage cluster analysis obtained through the similarity index of Bray-Curtis. d) Cluster analysis based on the Ward's algorithm. RUB-A=*G. ruber s.s.-a*; ELO=*G. elongatus*; RUB-C=*G. ruber-kum c*; RUB-D=*G. ruber*-d; RUB-E=*G. ruber*-e; RUB-F=*G. ruber*-f; RUB-K=*G. ruber*-k; $ELO_{CF.1}$=*G. elongatus* cf.1; CYC=*G. cyclostomus*; PYR=*G. pyramidalis.*

The second clustering method, based on the Ward's algorithm (Fig. 8d), shows almost the same results of the single linkage method, even if based on the statistical distance between the morphotypes. Therefore, *G. elongatus* cf.1 – *G. elongatus* result belonging to an independent group probably because together represent up to 65 % (on average) of the *G. ruber* - *G. elongatus* assemblages. For this reason, the cluster formed by the latter morphotypes results very distant by *G. ruber*-d, *G. ruber*-e and *G. ruber*-f cluster.

a) Principal Component Analysis - MIS 1

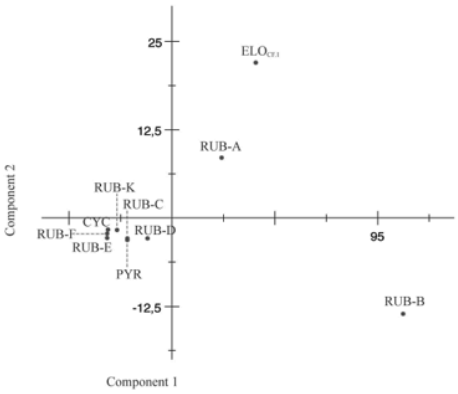

b) Principal Component Analysis - MIS 2

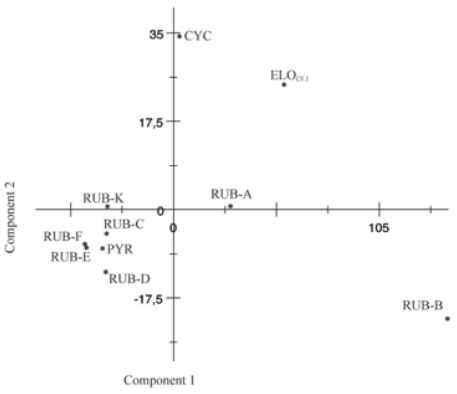

c) Principal Component Analysis - MIS 3.1

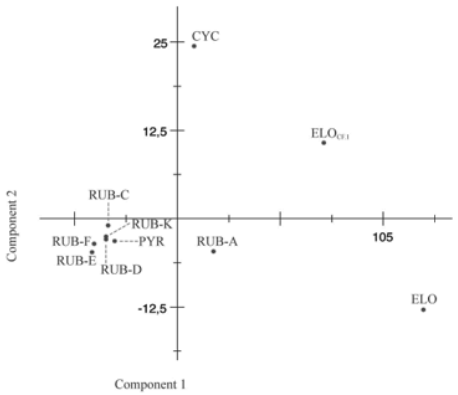

d) Principal Component Analysis - MIS 3.2

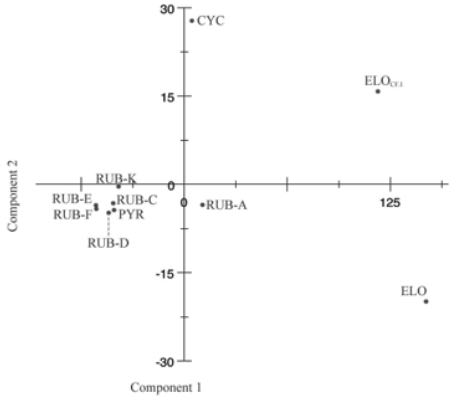

e) Principal Component Analysis - MIS 3.3

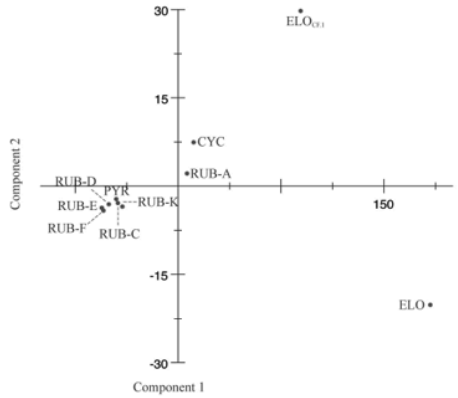

f) Principal Component Analysis - MIS 4

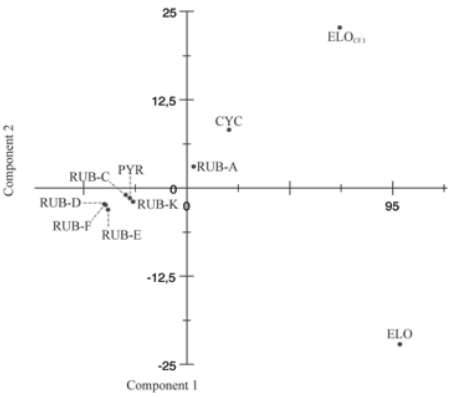

g) Principal Component Analysis - MIS 5.1

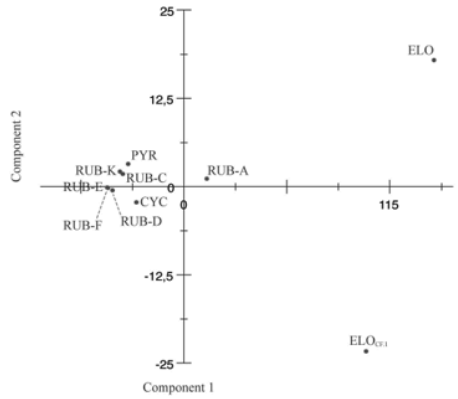

Figure 9**.** Multivariate statistical analyses performed on quantitative data. a) Principal Component Analysis performed on the interval of MIS 1. b) Principal Component Analysis performed on the interval of MIS 2. c) Principal Component Analysis performed on the interval of MIS 3.1. d) Principal Component Analysis performed on the interval of MIS 3.2. e) Principal Component Analysis performed on the interval of MIS 3.3. f) Principal Component Analysis performed on the interval of MIS 4. g) Principal Component Analysis performed on the interval of MIS 5.1. RUB-A=*G. ruber s.s.-a*; ELO=*G. elongatus*; RUB-C=*G. ruber-kum c*; RUB-D=*G. ruber*-d; RUB-E=*G. ruber*-e; RUB-F=*G. ruber*-f; RUB-K=*G. ruber*-k; $ELO_{CF.1}$=*G. elongatus* cf.1; CYC=*G. cyclostomus*; PYR=*G. pyramidalis.*

Thus, in the Azores region *G. ruber*-s.s.-a/*G. cyclostomus* and *G. ruber*-k/*G. ruber-kum c*/*G. pyramidalis* clusters show a similar behaviour (Fig. 8d). The PCA proved to be very useful to sort and reduce the variables into two components. The Component 1 has been considered as an expression of the relative abundance of each eco-morphotype. The contribution in term of abundance of each type increases from the left to the right (Fig. 8a). On the contrary, the component 2 has been correlated to the climatic affinity or at least to the preferential distribution of each morphotype in a determinate interval (MIS). Therefore, in the PCA plot the morphotypes with positive values of component 1 are considered as always presents in the studied samples, whereas the negative values are referred to those not always present (Fig. 8a). Thus, *G. elongatus* cf.1, *G. elongatus*, *G. ruber*-ss, and *G. cyclostomus* share a more continuous record. The more negative values of the component 1 are relatives to *G. ruber*-e and *G. ruber*-f, which record is highly discontinuous. *G. elongatus* cf.1 and *G. cyclostomus* reach the most positive values in the component 2, whereas the distribution of *G. ruber*-s.s.-a and above all *G. elongatus* have negative values. On the contrary, the MC group of *G. ruber - G. elongatus* plexus is not well represented in the component 2. Results of the PCoA (Fig. 8b) support the high statistical similarity of *G. elongatus* cf.1 and *G. elongatus*, such as *G. ruber*-ss and *G. cyclostomus*.

In order to better reconstruct the behaviour of the *G. ruber - G. elongatus* plrxus, the PCA has been repeated for each Marine Isotope Stage (Fig. 9). These analyses confirmed what has been observed in the abundance fluctuation curves and allow to summarize the features of *G. ruber - G. elongatus* population in each period.

8.7 Discussion

8.7.1 Does the isotopical signal from morphotypes inform about their calcification habitat preference?

Previously geochemical works on *G. ruber* s.s. and *G. ruber* s.l. (in this work *G. elongatus* and *G. elongatus* cf.1) have hypothesized differences in seasonal preferences or calcification depth, suggesting that *G. ruber* s.l. calcifies in colder and/or deeper waters than *G. ruber* s.s.-a (Wang, 2000, Steinke et al., 2005). In this work, we wanted to test if this was the case in the Azores area, choosing an interglacial (MIS 1) and glacial (MIS 2) intervals. As showed in Figure 9, it is evident that *G. ruber* s.s.-a, *G. elongatus* and *G. elongatus* cf.1 do not show significant offset in stable isotope values during MIS 1. On the contrary, the high-frequency fluctuating curves intersect each other. This imply that during the Holocene there are not evident differences in the Azores region in habit preferences between these three morphotypes/morphospecies. During the MIS2 *G. ruber* s.s.-a presents lower stable isotope values respect to *G. cyclostomus*, but again no evident $\delta^{18}O$ offsets respect to *G. elongatus* cf.1, a part in three points (Fig. 5). It is worth to note that during the Holocene, *G. ruber* s.s.-a, G. *elongatus* and *G. elongatus* cf.1 fluctuate within a narrow band of values comprises between -0.1 and -0.4 ‰. Furthermore, during the Holocene the differences of stable isotopes values in the morphotypes are indistinguishable and fall within the error range of measures (Tab. 1 and 2). Whereas the differences in $\delta^{18}O$ between *G. ruber s.s.*-a and *G. cyclostomus* during glacial MIS 2 interval are wider between 0.5 and 1.1 ‰. The carbon isotope signals are not so trivial by explain, this also because *G. ruber* s.s.-a is a symbiont-bearing species, and the $\delta^{13}C$ signal could be not mirror those of dissolved inorganic carbon in seawater (Ravelo and Fairbanks, 1995; Ravelo and Hillaire-Marcel, 2007). Our data are in agreement with those proposed by Thirumalai et al. (2014) that suggests there are not differences in *G. ruber* s.s. and *G. elongatus* and *G. elongatus* cf.1 calcifying processes depending by differences in habitat or during seasonality alternation. The habitat preferences of the studied morphotypes/morphospecies may vary regionally and can depend by sea water stratification, salinity or local productivity as described by Numberger et al. (2009) in the eastern Mediterranean Sea. While in South China Sea, the difference in geochemical signal between the two morphospecies/morphotypes is much more marked due to a strong seasonality linked to monsoon regime (Wang, 2000; Steinke et al. 2005). However, during the MIS2 *G. ruber* s.s. and *G. cyclostomus* show dissimilar isotopical behaviours in the Azores area. Different

hypothesis could explain such behaviour, i.e. water depth habitats, water masses and vital effect. The higher $\delta^{18}O$ values of G. *cyclostomus* than *G. ruber* s.s.-a may explain difference in water depth habitats, deeper and colder waters being characterized by higher $\delta^{18}O$ values than to shallow and warmer waters. But the higher values of carbon isotope are difficult to conciliate with this hypothesis, because generally in a well-stratified water column, the $\delta^{13}C$ values tend to become lower with depth, due to increase of nutriments and organic matter (ref.). On the other hand, we can not exclude that such anomalous high carbon isotope values for *G. cyclostomus* may be linked to vital effect. Alternatively, a most plausible explication is that *G. cyclostomus* prefers cooler and likely saltier seawater habitats (or currents) explaining both the heavier stable isotope values.

8.7.2 Significance of G. ruber gr. alba and G. ruber gr. rosea fluctuations

The variability of *G. ruber* gr. *alba* is directly forced by Earth' orbital parameters, and particularly their fluctuations are controlled by the obliquity signal. The maxima abundances of this group occur when the insolation is in phase with the obliquity signal during MIS 5.1 and MIS 1 (Fig. 6). However, the weaker increase in abundance of *G. ruber* group during MIS 3.3/3.2 passage occurs in obliquity maximum and insolation minima. Therefore, the interplay between these different astronomical periodicities produces a modest increase of temperatures and abundance of warm surface species respect to the warmest periods (MIS 5 and 1). In the same way, the increase of the *G. ruber* gr. *alba* during the middle part of the last glacial stage (MIS 2), corresponds with a period of insolation minimum slightly contrasted by obliquity/eccentricity increasing. In our opinion, the astronomical periodicities control the expansion and reduction of the North Atlantic STG, causing the migration of the *G. ruber* gr. *alba* towards north and southward. Today, *G. ruber* gr. *rosea* variety is present in the Atlantic Ocean and in the Mediterranean Sea (Numberger et al., 2009), whereas disappeared in the Indo-Pacific at ~ 120 ka (Thomson et al., 1979). This chromotype is most abundant near the land and prefers higher summer sea surface temperatures from August to October, opposed to the white variety that lives throughout the year, with maximum from the winter to the early spring (Bé and Torderlund, 1971). Schiebel et al. (2002b) in their study on living planktonic foraminifera of the Azores region, confirmed that *G. ruber* gr. *rosea* variety is limited to the summer season and to the shallowest part of water column. Storz et al. (2009) instead suggest that both *G. ruber rosea* and *alba* varieties prevail from the end of July to the end of January, in the Azores area. In the Mediterranean Sea, this chromotype is rare in western sector and

abundant in its eastern part. According to Pujol and Vergnaud-Grazzini, (1995), it proliferates at the end of summer when surface water are well stratified.

The phase of maxima expansion of the STG, in the Azores region, especially during the Bølling/Allerød (14.64 – 12.75 ka) and the Holocene, were marked by evident increase in abundance of the *G. ruber* gr. *rosea* variety. During that period, the pink chromotype migrated from the tropical North Atlantic to the Azores region, favoured by the high and stable SSTs of that period. On the hand, the relative higher percentages of *G. ruber* gr. *rosea* may be controlled by higher salinity and/or oligotrophism as suggest by Caruso et al., (unpublished data). During the Holocene the maximum strengthening of the AMOC system was observed (Repschläger et al., 2015; Bonfardeci et al., this thesis), causing the northward expansion of the Subtropical Gyre and the reinforcement of the Azores Front/Current System. During this latter period, the group of *G. ruber* reached maxima abundances suggesting that highly warm, stratified and oligotrophic upper water column persisted at the studied site.

8.7.3 Position of the different eco-morphotypes within the Subtropical Gyre

The abundance fluctuations of the ten eco-morphotypes, belonging to the *G. ruber* - *G. elongatus* plexus, shows very particular trends. In particular, this study provided insights on the new eco-morphotypes, such as *G. ruber*-d, *G. ruber*-kum c and *G-ruber*-f and high-detailed informations about their ecology and distribution in the Azores region. The results provide by quantitative data have been confirmed and clear resumed through the multivariate analyses. The multivariate statistical treatment of quantitative data have highlighted some important features of these eco-morphotypes, above all as regard to their response to the climatic and hydrographic changes occurred in the Azores region, between the MISs 5.1 and 1. All multivariate statistical data (PCA, PCoA, Cluster analysis, similarity/distance indexes) indicate that especially *G. elongatus*, but also *G. ruber* s.s., *G. elongatus* cf.1 and G. *cyclostomus*, here labelled as greater contributors, are dominant in the *G. ruber* - *G. elongatus* plexus during the last 81.94 ka. Moreover, these data have highlighted as *G. elongatus* and *G. elongatus* cf.1 have an anti-correlative behaviour, but similar relative abundances in their assemblages. This pattern is very similar to those of *G. ruber* s.s.-a and *G. cyclostomus* and it could be related to different ecological nikes, strictly tied to different temperatures in surface waters as well shown by stable isotopes measured in the different morphotypes. In these sub-clusters, in fact, *G. elongatus* cf.1 and *G. cyclostomus* show a higher affinity for cooler temperatures. This hypothesis seems to be supported by the morphological evidences of these two couples. *G. elongatus* cf.1 presents indeed a test shape very close to *G. elongatus*, even if

is more robust and has a higher trochospire. *G. cyclostomus* might represent the cool/temperate eco-phenotypic variant of *G. ruber* s.s.-a, characterized by a more compact and robust test, as well as by a small and rounded aperture.

Infact, *G. cyclostomus* was present almost exclusively during glacial and temperate-warm climate periods (from the MISs 4 to 2), whereas *G. elongatus* cf.1 has a similar trend except for the MIS 5.1. On the contrary, *G. elongatus*, represents the most abundant eco-morphotype and increases during the interglacial stages more than *G. ruber* s.s.-a. This latter increases from the MIS 3.2/3.1 boundary, in Azores region.

As regards to the Minor Contributors, *G. ruber*-k resulted to be a cold-tolerant eco-morphotype, whereas *G. pyramidalis* and *G. ruber*-kum c show affinity for cool-temperate climatic conditions. On the contrary, *G. ruber*-d prefers warmer climate conditions occurred during the MIS 1. In particular, this latter eco-morphotype reached maxima abundance in the warm, stratified and oligotrophic water masses that characterised the Azores region during the Bølling/Allerød and the Holocene periods. Although the morphologic features of *G. ruber*-d are close to *G. ruber* s.s.-a, its distribution is very similar to that of *G. ruber* gr. *rosea*. Due to the very low abundance *G. ruber*-f and *G. ruber*-e no particular ecological preferences have been hyphotesized.

As regard the *G. ruber* - *G. elongatus* plexus, each morphotype inhabits a specific latitudinal position within the Subtropical Gyre strictly tied to SST, even if some Authors (Hemleben et al., 1989; Numberger et al., 2009; Storz et al., 2009; Antonarakou et al., 2015) have pointed out their connection to the trophic chain. In particular, *G. ruber* s.s.-a is commonly accepted as oligotrophic surface water symbiont-bearing taxon, whilst *G. elongatus* (reported as *G. ruber* s.l. by the previous authors) might prefer higher productivity waters.

8.7.4 Tracking Subtopical Gyre / Azores Front Current System water masses dynamic by G. ruber - G. elongatus plexus morphotypes

Variations in abundance of *G. ruber* gr. *alba* in the studied record can be used to reconstruct the width of the Subtropical Gyre (Repschläger et al 2015), and consequently its northern boundary represented by the AFCS. As reported by Schiebel et al. (2002a-b), Storz et al. (2009) and Repschläger et al. (2015) *G. ruber* gr. *alba* has its maxima abundance within the STG. Our data point out as it has a greater affinity for warmer climatic stages, such as the last part of the MIS 5.1 and the Holocene. Today, *G. ruber* gr. *alba* prefers warm, stratified and oligotrophic surface water masses of the Azores region. This environmental conditions

were similar during MIS 5.1. We suppose that during the last 81.94 ka the expansion and reduction of the STG, controlled by 21 June insolation (65°N), caused the migration of the *G. ruber* gr. *alba* towards north and south, respectively. In addition, *G. cyclostomus* is the best tracer for the northern boundary between the Subtropical Gyre and the Azores current, whilst *G. elongatus* and *G. ruber*-d (this latter during the Holocene) could be used as tracers of the central body of the North Atlantic Subtropical Gyre and consequent intensification of the AMOC system. Therefore, the *G. elongatus* and *G. cyclostomus* ratio percentages may be used as index of the northward/southward displacement of the STG/AFCS boundary (Fig. 10).

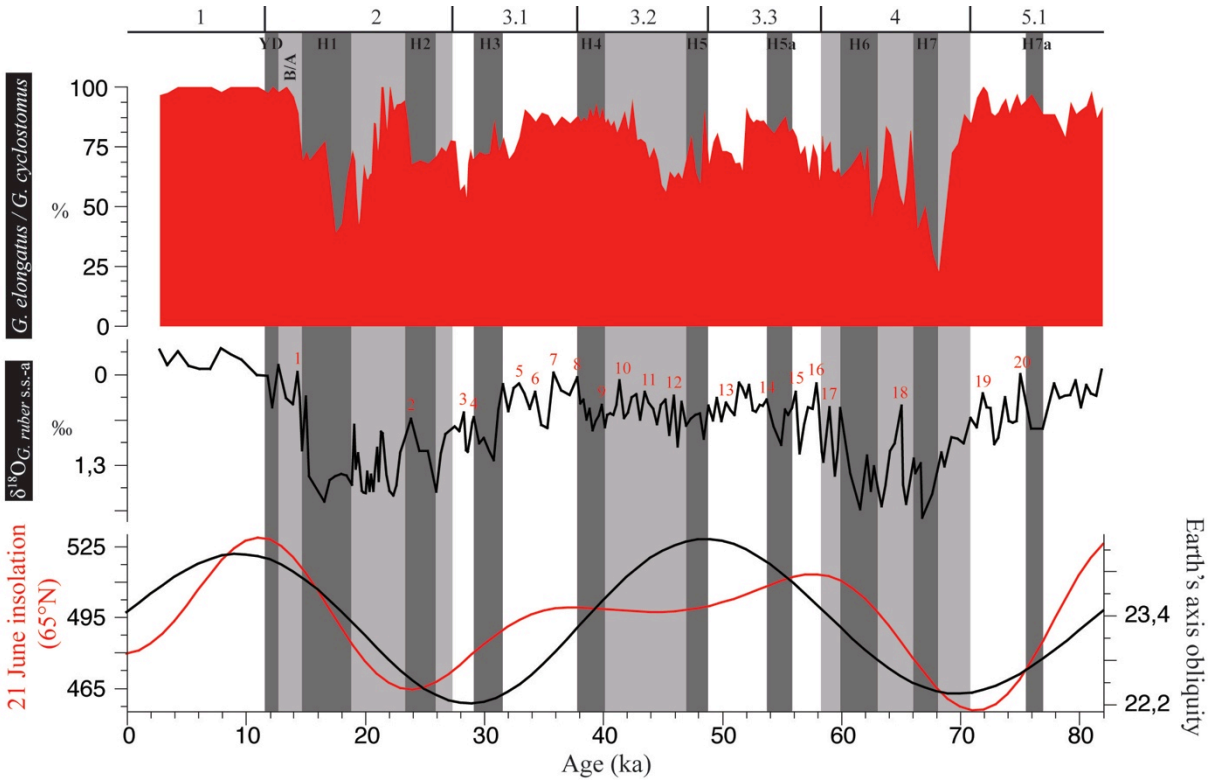

Figure 10. STG/AFCS boundary index, calculated through the ration between the relative percentage of *G. elongatus* against the totality of *G. elongatus* + *G. cyclostomus*. Red filled area indicates the proportion of *G. elongatus* in the Azores region waters, during the last 81.94 ka. The intervals in which *G. elongatus* dominate are linked to the northward displacement of the STG/AFCS boundary, whereas intervals in which *G. cyclostomus* increases in abundance (bluer) are linked to the southward shifts of this surface. The abundances fluctuation data are plotted respect to the 21 June insolation at 65°N (red curve) and obliquity (black curve) signals, calculated for the interval between 82 to 0 ka (Laskar et al., 2004), as well as to the $\delta^{18}O_{\ G.\ ruber\ s.s.-a}$ record (Bonfardeci et al., this thesis). Light gray vertical bars refer to the glacial stages (MIS 2 and 4) and cool-temperate periods (MIS 3.2). White vertical bars are related to the interglacials (MIS 1 and 5.1) and temperate-warm periods (MIS 3.1 and 3.3). Dark gray vertical bars identify the intervals correspondent to the Heinrich events, proposed by Lisiecki and Stern (2016), here labelled as H1 to H12. YD=Younger Dryas stadial; B/A=Bølling/Allerød

interstadial. Red numbers associated to $\delta^{18}O_{\textit{G. ruber}\ \text{s.s.-a}}$ record are referred to the Dansgaard/Oeschger interstadial phase (D/O) (Barker et al., 2011; Billups et al., 2016; Bonfardeci et al., 2016)

In detail, during MIS 5.1 high abundance of G. *elongatus* testifies warm and well productive surface waters with the STG/AFCS boundary positioned north to the coring site. Whilst, high abundances of *G. elongatus* cf.1 are related to the cooling trend culminated in the MIS 4. During this latter stage, higher abundances of cooler morphotypes mark a period during which the STG/AFCS boundary was southwards displaced, due to the expansion of the Polar-Subpolar front (for detail see Bonfardeci et al. this thesis). On the contrary, during MIS 3.3 and 3.2 the STG/AFCS boundary reached the northernmost position in the Azores region respect to the MIS 4, testifying a restoration of the AMOC system. The STG/AFCS boundary shifted cyclically in latitudes due to the forcing of insolation/obliquity cycles that were out of phase. The beginning of the last glacial stage was firstly characterised by high abundances of *G. ruber*-s.s.-a and *G. elongatus*, which suggest that the STG/AFCS boundary was at the same latitudinal position respect to that reached during MIS 3.1. Afterwards, during the central and terminal part of MIS 2, the *G. ruber - G. elongatus* plexus assemblages was dominated by *G. elongatus* cf.1, *G. ruber*-k and *G. cyclostomus* which mark the southernmost displacement of the STG/AFCS and the relative AMOC weakening.

The rapid increase in SST during the Bølling/Allerød probably caused the northward shift of the STG/AFCS boundary testified by the very rare presence of *G. cyclostomus* and the coeval increase of *G. ruber*-d. Apart the short interruption, caused by the Younger Dryas, the STG/AFCS boundary was progressively displaced toward north, reaching approximately the actual position. The interval of MIS 1, especially for the Holocene, is characterised by high abundance of warm morphotypes.

8.8 Conclusions

In the *G. ruber-G. elogantus* plexus, ten eco-morphotypes have been recognised and their taxonomic classification have been here discussed. The group composed by *G. elongatus*, *G. ruber* s.s.-a, *G. elongatus* cf.1 and *G. cyclostomus*, constitutes about the 90 % of the *G. ruber - G. elongatus* assemblages, whereas the remaining 10% of *G. ruber*-kum c, *G. ruber*-d, *G. ruber*-k, *G. ruber*-e, *G. ruber*-f and *G. pyramidalis* represent the rest. For the greater part of them, the astronomical periodicities control their abundance fluctuations, and they are strictly tied to the environmental of surface waters (i.e, temperature, salinity and food supply). Each

morphotype occupies a precise ecological niche in the Subtropical Gyre of the North Atlantic Ocean. *G. cyclostomus* and *G. ruber*-k are most abundant in correspondence of MIS from 4 to 2 and represent the best indicators of cold climatic conditions. On the contrary, *G. elongatus* and *G. ruber*-d may be considered the best indicators of warm water in the Azores region, since reached their maxima abundances during interglacial periods (MISs 5.1 and 1). *G. elongatus* cf.1 and *G. ruber* s.s.-a are here considered as cool-temperate and warm-temperate, respectively. Thus, they represent an important element for the paleoclimatic and paleoceanographic recostrunction of the central North Atlantic (Azores region) between 81.94 and 2.75 ka. Furthermore, the *G. elo*ngatus and *G. cyclostomus* ratio may be considered as index of the periodic fluctuations of the STG/AFCS boundary. In particular, the maxima southward shifts, referred to the MIS 4 and 2, caused the dominance of cold and cool-temperate tolerant eco-morphotypes at the latitude of the coring site, whereas the northermost position reached by STG/AFCS boundary, have been observed in correspondence of MISs 5.1 and 1. In addition, *G. elongatus* and *G. cyclostomus* are those that better respond to the astronomical forcing, especially insolation. In conclusion, a good use of the percentage of abundance of these morphotypes provide new tools for paleoclimatic/paleoceanographic reconstruction and how the Subtropical Gyre/Azores Front Current System boundary shifted at different latitudes.

References

Alves, M.L.G.R., de Verdière, A.C., 1999. Instability dynamics of a subtropical jet and applications to the Azores Front Current System: eddy-driven mean flow. Journal of Physical Oceanography 29, 837-864.

Antonarakou, A., Kontakiotis, G., Mortyn, P.G., Drinia, H.,Sprovieri, M., Besiou, E., Tripsanas, E., 2015. Biotic and geochemical (δ18O, δ13C, Mg/Ca, Ba/Ca) responses of Globigerinoides ruber morphotypes to upper water column variations during the last deglaciation, Gulf of Mexico. Geochimica et Cosmochimica Acta 170, 69-93.

Aurahs, R., Grimm, G.W., Hemleben, V., Hemleben, C., Kucera, M., 2009a. Geographical distribution of cryptic genetic types in the planktonic foraminifer Globigerinoides ruber. Mol. Ecol. 18, 1692-1706.

Aurahs, R., Treis, Y., Darling, K. Kucera, M., 2011. A revised taxonomic and phylogenetic concept for the planktonic foraminifer species Globigerinoides ruber based on molecular and morphometric evidence. Marine Micropaleontology 79, 1-14.

Barker, S., Knorr, G. Edwards, R.L., Parrenin, F. Putnam, A.E., Skinner, L.C., Wolff, E., Ziegler, M., 2011. 800,000 years of abrupt climate variability. Science 334(6054), 347–351.

Bé, A.W.H., Tolderlund, D.S., 1971. Distribution and ecology of living planktonic foraminifera in surface waters of the Atlantic and Indian Oceans. In The Micropalaeontology of the Oceans (eds. B. H. Funnell and W. R. Riedel). Cambridge Univ. Press, London, pp. 105–149.

Bé, A.W.H., 1977. An ecological, zoogeographic and taxonomic review of Recent planktonic Foraminifera, in: A.T.S. Ramsey (Eds.), Oceanic micropaleontology. London: Academic Press, Vol. 1, pp. 1-100.

Berger, W.H., Killingley, J., Vincent, E., 1978. Sable isotopes in deep-sea carbonates-box core ERDC-92, west equatorial Pacific. Oceanol. Acta 1(2), 203-216.

Billups, K., Hudson, C. Kunz, H., Rew, I., 2016. Exploring Globorotalia truncatulinoides coiling ratios as a proxy for subtropical gyre dynamics in the northwestern Atlantic Ocean during late Pleistocene Ice Ages. Paleoceanography 31, 553-563.

Bolli, H. M., Bermudez, P. J., 1965. Zonation based on planktonic foraminifera of Middle Miocene to Pliocene warm-water sediments. Assoc. Ven. Geol. Min. Petrol., Bol. Inf. 8 (5), 119.

Bond, G., Broecker, W., Johnsen, S., McManus, J., Labeyrie, L., Jouzel, J., Bonani, G., 1993. Correlations between climate records from North Atlantic sediments and Greenland ice. Nature 365, 143-147.

Brady, H.B., 1879. Notes on some of the reticularean Rhizopoda of the Challenger Expedition, Part II. Additions to the knowledge of the porcellanous and hyaline types. Q. J. Microsc. Sci. 19

Broecker, W.S., 1994. Massive iceberg discharges as trigger for global climate change. Nature 372, 421-424.

Chapman, M.R., Shackleton, N.J., Duplessy, J.C., 2000. Sea surface temperature variability during the last glacial-interglacial cycle: assessing the magnitude and pattern of climate change in the North Atlantic. Palaeogeography, Palaeoclimatology and Palaeoecology 157, 1-25.Cordey, W.G., 1967. The development of Globigerinoides ruber (D'Orbigny 1839) from the Miocene to recent. Paleontology 10, 647-659.

Cushman, J.A., 1927. Some new genera of the Foraminifera. Contr. Cushman Lab. Foramin. Res. Sharon Mass. 2, 77-81.

d'Orbigny, A.D., 1826. Tableau méthodique de la classe de céphalopodes. Ann. Des Sci. Nat.

14, 1-277.

d'Orbigny, A.D., 1839. Voyage dans l'Amerique Meriodionale. Strasbourg, France.

Davis, J.C., 1986. Statistics and Data Analysis in Geology. John Wiley & Sons.

Galloway, J.H., Wissler, S.G., 1927. Pleistocene foraminifera from the Lomita Quarry, Palos Verdes Hills, California. J. Paleontol. 1, 35-87.

Gould, W.J., 1985. Physical oceanography of the Azores front. Progress in Oceanography 14, 167-190.

Gower, J.C., Ross, G.J.S., 1968. Minimum Spanning Trees and Single Linkage Cluster Analysis. Journal of the Royal Statistical Society. Series C (Applied Statistics) 18, (1), 54-64.

Hammer, Ø, Harper, D.A.T., and P. D. Ryan, 2001. PAST: Paleontological Statistics Software Package for Education and Data Analysis. Palaeontologia Electronica 4(1), 9.

Harper, D.A.T., 1999. Numerical Palaeobiology. John Wiley & Sons.

Hecht, A.D., 1974. Intraspecific variation in recent populations of Globigerinoides ruber and Globigerinoides trilobus and their application to paleoenvironmental analyses. J. Paleontol. 48, 1217-1234.

Heinrich, H., 1988. Origin and consequences of cyclic ice rafting in the northeast Atlantic Ocean during the past 130,000 years. Quaternary Research 29, 142-152.

Hemleben, C., Spindler, M., Anderson, O.R., 1989. Modern Planktonic Foraminifera. Springer Verlag, New York.

Kawahata, H., 2005. Stable isotopic composition of two morphotypes of Globigerinoides ruber (white) in the subtropical gyre in the north Pacific. Paleontol. Res. 9, 27-35.

Kennett, J.P., Srinivasan, M.S., 1983. Neogene Planktonic Foraminifera: A Phylogenetic Atlas. Hutchinson Ross Publishing Co., Stroudsburg, PA. 265 pp.

Kucera, M., Weinelt, M., Kiefer, T., Pflaumann, U., Hayes, A., Weinelt, M., Chen, M.-T., Mix A. C., Barrows, T.T., Cortijo, E. Duprat, J., Juggins, S., Waelbroeck, C., 2005. Reconstruction of sea-surface temperatures from assemblages of planktonic foraminifera: Multi-technique approach based on geographically constrained calibration datasets and its application to glacial Atlantic and Pacific Oceans. Quaternary Science Reviews 24, 951-998.

Kucera, M., Schönfeld, J., 2007. The origin of modern oceanic foraminiferal faunas and Neogene climate change. In: Williams,M., Haywood, A.M., Gregory, F.J., Schmidt, D.N (Eds.), Deep-Time Perspectives on Climate Change: Marrying the Signal from Computer Models and Biological Proxies. TheGeological Society, London, pp. 409-

426.

Kuroyanagi, A., Kawahata H., 2004. Vertical distribution of living planktonic foraminifera in the seas around Japan. Mar. Micropaleontol. 53, 173–196.

Kuroyanagi, A., Tsuchiya, M., Kawahata, H., Kitazato, H., 2008. The occurrence of two genotypes of the planktonic foraminifer Globigerinoides ruber (white) and paleoenvironmental implications. Mar. Micropaleontol. 68, 236–243.

Laskar, J., P. Robutel, F. Joutel, M. Gastineau, A. C. M. Correia, and B. Levrard (2004), A long term numerical solution for the insolation quantities of the Earth, Astron. Astrophys. 428, 261-285.

Loewemark, L., Hong, W.L., Yui, T.F., Hung, G.W., 2005. A test of different factors influencing the isotopic signal of planktonic foraminifera in surface sediments from the northern South China Sea. Mar. Micropaleontol. 55, 49-62.

Lynch-Stieglitz, J., Adkins, J.F., Curry, W.B., Dokken, T., Hall, I.R., Herguera, J.C., Hirschi, J.J. M., Ivanova, E.V., Kissel, C., Marchal, O., Marchitto, T.M., McCave, I.N., McManus, J.F., Mulitza, S., Ninnemann, U., Peeters, F., Yu, E.-F., Zahn, R., 2007. Atlantic meridional overturning circulation during the Last Glacial Maximum. Science 316, 66-69.

Margaritelli, G., Vallefuoco, M., Di Rita, F., Capotondi, L., Bellucci, L.G., Insinga, D.D., Petrosino, P., Bonomo, S., Cacho, I., Cascella, A., Ferraro, L., Florindo, F., Lubritto, C., Lurcock, P.C., Magri, D., Pelosi, N., Rettori, R., Lirer, F., 2016. Marine response to climate changes during the last five millennia in the central Mediterranean Sea. Global and Planetary Change 142, 53-72.

Mortlock, R.A., Charles, C.D., Froelich, P.N., Zibello, M.A., Saltzman, J., Hays, J.D., Burckle, L.H., 1991. Evidence for lower productivity in the Antarctic Ocean during the last glaciation. Nature 351, 220-223.

Numberger, L., Hemleben, C., Hoffmann, R., Mackensen, A., Schulz, H., Wunderlich, J.M. Kucera, M., 2009. Habitats, abundance patterns and isotopic signals of morphotype of the planktonic foraminifer Globigerinoides ruber (d'Orbigny) in the eastern Mediterranean Sea since the Marine Isotopic Stage 12. Mar. Micropaleontol. 73, 90-104.

Ottens, J.J., 1991. Planktic foraminifera as North Atlantic water mass indicators. Oceanol. Acta 14(2), 123-140.

Parker, F.L., 1962. Planktonic foraminiferal species in Pacific sediments. Micropaleontology 8, 219-254.

Pujol, C., Vergnaud-Grazzini, C., 1995. Distribution patterns of live planktic fora- minifera as related to regional hydrography and productive systems of the Mediterranean sea. Marine Micropaleontology 25, 187-217.

Ravelo, A. C., Fairbanks, R.G. 1995. Carbon isotopic fractionation in multiple species of planktonic foraminifera from core tops in the tropical Atlantic. J. Foramineferal Res. 25(1), 53-74.

Ravelo, C., Hillaire-Marcel, C., 2007. The Use of Oxygen and Carbon Isotopes of Foraminifera in Paleoceanography, in: Hillaire-Marcel, C., de Vernal, A., Methods in Late Cenozoic Paleoceanography, Elsevier (Eds), Amsterdam (NL).

Repschläger, J., Weinelt, M., Kinkel, H., Anderesen, N., Garbe-Schönberg, D., 2015. Response of the subtropical North Atlantic surface hydrography on deglacial and Holocene AMOC changes. Paleoceanography 30 (5), 456-476.

Robbins L.L., Healy-Williams, N., 1991. Toward a classification of planktonic foraminifera based on biochemical, geochemical and morphological criteria. Journal of Foraminiferal Research 21(2), 159-167.

Rogerson, M., Rohling, EJ, Weaver, P.P.E, Murray, J.W., 2004. The Azores Front since the Last Glacial Maximum. Earth and Planetary Science Letters 222, 779-789.

Rogl, F., Bolli, H.M., 1973. Holocene to Pleistocene planktonic foraminifera of Leg 15, Site 147 (Cariaco Basin (Trench), Caribbean Sea) and thier climatic interpretation, in : N.T. Edgar, Initial Reports of the DeepSea Drilling Project, Washington, D.C., U.S., Government Printing Office 15, 553-616.

Sadekov, A., Eggins, S.M., De Deckker, P., Ninnemann, U., Kuhnt, W., Bassinot, F., 2009. Surface and subsurface seawater temperature reconstruction using Mg/Ca microanalysis of planktonic foraminifera Globigerinoides ruber, Globigerinoides sacculifer, and Pulleniatina obliquiloculata. Paleoceanography 24, 17.

Saito, T., Thompson, P.R., Breger, D., 1981. Systematic Index of Recent and Pleistocene Planktonic Foraminifera. University of Tokyo Press, Tokyo, pp. 1–190.

Schiebel, R., Waniek, J., Zeltner, A., Alves, M., 2002a. Impact of the Azores Front on the distribution of planktic foraminifers, shelled gastropods, and coccolithophorids. Deep Sea Res. Part II 49(19), 4035-4050.

Schiebel, R., Schmuker, B., Alves, M., Hemleben, C., 2002b. Tracking the recent and late Pleistocene Azores front by the distribution of planktic foraminifers, J. Mar. Syst. 37(1-3), 213-227.

Schwab, C., Kinkel, H. Weinelt, M., Repschläger, J., 2012. Coccolithophore

paleoproductivity and ecology response to deglacial and Holocene changes in the Azores Current System, Paleoceanography 27, PA3210.

Sprovieri, R., Di Stefano, E., Incarbona, A., Gargano, M.E., 2003. A high-resolution of the last deglaciation in the Sicily Channel based on foraminiferal and calcareous nannofossil quantitative distribution. Palaeogeography, Palaeoclimatology, Palaeoecology 202, 119-142.

Steinke, S., Chiu, H.Y., Yu, P.S., Shen, C.C., Loewemark, L., Mii, H.S., Chen, M.T., 2005. Mg/Ca ratios of two Globigerinoides ruber (white) morphotypes: implications for reconstructing past tropical/subtropical surface water conditions. Geochem. Geophys. Geosyst. 6.

Storz, D., Schulz, H. Waniek, J.J. Schulz-Bull, D.E., Kucera M., 2009. Seasonal and interannual variability of the planktic foraminiferal flux in the vicinity of the Azores Current, Deep Sea Research Part I 56(1), 107-124.

Thirumalai K., Richey J.N., Quinn T.M., Poore R.Z., 2014. Globigerinoides ruber morphotypes in the Gulf of Mexico: a test of null hypothesis. Sci. Rep. 4, 6018.

Tolderlund, D.S., Bé, A.W.H., 1971. Seasonal distribution of planktonic foraminifera in the western North Atlantic. Micropaleontology 17, 297–329.

Van den Broeck, E., 1876. Etude sur les Foraminiferes de la Barbade (Antilles). Soc. Belge Microsc. An. 1, 55-152.

Wang, L.J., 2000. Isotopic signals in two morphotypes of Globigerinoides ruber (white) from the South China Sea: implications for monsoon climate change during the last glacial cycle. Palaeogeogr. Palaeoclimatol. Palaeoecol. 161, 381–394.

Ward, J.H., 1963. Hierarchical grouping to optimize an objective function. Journal of the American Statistical Association 58, 236-244.

9. Conclusive remarks

Cyclical fluctuations of ATA13-OF-KT1 and ATA13-OF-KT18 proxy records allowed recognising the climatic and hydrographic variability of the central North Atlantic, during the last 144 ka.

The obtained data have clearly shown that the carbonate content of sediments and the planktonic foraminiferal response, in terms of relative abundance and oxygen isotope composition of the tests, are controlled by insolation and obliquity forcing during the last climatic cycle.

In order to develop a correct age model for ATA13-OF-KT1 and ATA13-OF-KT18, two different approaches were used. The insolation-based tuning was compared to an age model based on the synchronization of the $\delta^{18}O_{G.\ ruber}$ of both cores with the MD95-2042 $\delta^{18}O_{G.\ bulloides}$ (LS16) record. The wavelet analysis performed on carbonate content and $\delta^{18}O_{G.\ ruber}$ records, developed with the two different approaches, revealed ~~as~~ that the proxies oscillations are forced by the summer insolation maximum (65°N) and obliquity signals. Hence, these two forcings are considered as the main trigger for the climatic and oceanographic changes that occurred in the Azores region. In this work, the LS16-based model has been selected and used to interpret the proxies oscillations of both cores studied. In fact, the LS16-based method allows to globally correlate the studied records, because the Lisiecki and Stern (2016) model takes into account the ice volume effect and the related sea level variations that, as proven, induce a delay in the recording of the climatic response, on marine proxies, to the orbital forcing (Imbrie and Imbrie, 1980).

According to this approach, a time lag of 4.72-2.3 kyr for $\delta^{18}O_{G.\ ruber}$ and of 4.94-4.8 kyr for carbonate content, to summer insolation at 65°N, was estimated.

Therefore, the ATA13-OF-KT1 core records the time interval 2.75 to 81.94 ka (MIS 1 to 5.1), and the ATA13-OF-KT18 core the interval 3.36 to 143.79 ka (MIS 1 to 6). The periodicities of the dominant forcing are related to the precession cycles, attested respectively at 21.17 and 23.46 kyr for ATA13-OF-KT1 and ATA13-OF-KT18 carbonate content records. Likewise, for the ATA13-OF-KT1 and ATA13-OF-KT18 $\delta^{18}O_{G.\ ruber}$ records, the response to insolation forcing is recorded respectively in 21.22 and 23.51 kyr cycles .

Over the last 144 ka, increases in the carbonate content and decreases in the $\delta^{18}O_{G.\ ruber}$ were forced by the summer insolation maximum (65°N). These conditions mark the onset of climatic warm/interglacial phases of MIS 5.5 and 1. On the contrary, insolation minima

caused climate cooling, well marked by minima percentages in the carbonate content and heavier $\delta^{18}O_{G.\ ruber}$ values.

According to the age model, based on MD95-2042 $\delta^{18}O_{G.\ bulloides}$ (LS16) record, in ATA13-OF-KT1 oxygen isotope record, the D/O interstadials phases (Barker et al., 2011) ~~from~~ 1 to 20 have been observed. In the same manner, in the ATA13-OF-KT18 coring site signal, the D/O events 1 to 22 were recorded in~~to~~ the $\delta^{18}O_{G.\ ruber}$ signal. Likewise, the "Heinrich" related events ~~from~~ 1 to 7a (Lisiecki and Stern, 2016) have been recognised in the ATA13-OF-KT1 studied proxies, whereas in the ATA13-OF-KT18 coring site, the "Heinrich" related events 1 to 12 (Lisiecki and Stern, 2016) have been traced through the $\delta^{18}O_{G.\ ruber}$ high-frequency increases.

In the Azores region the carbonate content of deepsea sediments shows the typical "Atlantic-Style" behaviour and reflects the interplay between surface biogenic production and deep carbonate dissolution. The vertical displacements of the calcite lysocline have been traced during the last 144 ka, through the Resistant Species Percentage analysis. During interglacials the estimated position of the lysocline was 4,500 m deep, in central North Atlantic, reaching shallower positions during glacial phases. The lysocline reached its shallowest position~~s~~ in central North Atlantic during "Heinrich" related events 7 and 1, as well as during the Last Glacial Maximum, when it was likely 1000 m shallower than today. The rise of the lysocline corresponds probably to the AMOC system shut down.

SSTs reconstruction based on Modern Analog Technique, together with Warm/Cold species index, highlighted that the climatic and hydrographic variability of the last 144 kyr have been differently recorded in the two coring sites. During colder climatic phases, the AMOC system slowed down, inducing a decrease in SST, well recorded in ATA13-OF-KT1 planktonic foraminiferal record. At the same time, the persistent activity of Gulf Stream and the activity of STG and ENACW induced warming of the surface water masses at the ATA13-OF-KT18. This contrasting reaction between the two sites is particularly evident during the most extreme "Heinrich" related events.

The cyclical fluctuations of selected species provided powerful tools to reconstruct the climatic and hydrographic variability of the central North Atlantic, linked to orbitally-forced AMOC weakening/strengthening, during the last 144 Kyr.

G. bulloides, *T. quinqueloba* and *G. glutinata* relative abundances have been used as paleoproductivity proxies, showing that more high-productivity surface water masses have characterized the north-westernmost site. During glacial MIS 4 and, in less extent during MIS

3, high abundances of *G. glutinata* may suggest diatom dominated primary productivity. Such highest siliceous biogenic productivity, especially during extreme glacials, was probably fed by Polar-Subpolar water masses.

Downcore abundance fluctuations of key species have been used to trace the latitudinal and longitudinal migrations of these water masses and current front/current systems, as well as their intensification linked to climatic orbital forcing.

N. pachyderma dx, has been used to trace a south-southeastern shift of Subpolar Gyre and the related Subpolar Front, linked to the Laurentide-Greenland ice sheets expansion, during glacials MIS 6 and 2 periods. The temperature and productivity effects related to this southeastern displacement of SPG are more evident in the north-westernmost sector of the study area. This difference, between the two core records, especially during glacial stages and millennial-scale cold events ("Heinrich" related events), may indicate that the main polar-subpolar water source was positioned between Canadian and Greenland margins (Hudson area).

N. incompta dx and *G. inflata* have been recognized as good proxies of the northeast-flowing North Atlantic Current (NAC) position and strength, linked to the Gulf Stream fluctuations. Moreover *N. incompta* dx probably occupied preferentially northwestern part of NAC, whereas *G. inflata* was more abundant in correspondence of the central body of this current. Hence, they together marked the period in which NAC was reduced and located south-east of its actual position. These conditions, in Azores region, marked the onset and the persistence of cold climate phases, in correspondence with MIS 6, 4, 3.2 and 2.

The *G. scitula* gr. abundance fluctuations were used to trace the extension of the ENACW water masses and therefore the AF position as their maxima abundances marked the southward shift of AF, during glacial stages (MIS 6, 4 and 2). This latter front represents also the northern boundary of Azores Current, which position and strength have been monitored through the subtropical *G. truncatulinoides* fluctuations. This species testified strengthening of AC during MIS 5, and part of 3.3 and MIS 1. Finally our model shows how *G. ruber* gr. (white) marked northward expansion of the Subtropical Gyre (STG) during interglacials, especially during MIS 5.5 and Holocene.

Finally, the focus on *G. ruber* - *G. elongatus* plexus of ATA13-OF-KT1 core, provides new insights on taxonomy of this group. In *G. ruber* - *G. elongatus* population, ten eco-morphotypes have been recognised and censed (in the size-fraction between 250 and 315 μm). The taxonomic revision of this important group of surface eco-morphotypes has allowed improving the ancient informal classification based on *G. ruber* s.s. and s.l.

The analyse of the relative abundances of *G. ruber* gr. *alba* and *rosea*, in the Azores planktonic foraminiferal assemblages, shows ~~as~~ that their cyclic oscillations were primarily forced by the obliquity and that their maxima abundances occurred when obliquity and insolation maxima are in phase.

The abundance fluctuations data, confirmed by multivariate statistical analyses, highlight that each of these eco-morphotypes occupies a specific ecological niche in the North Atlantic Subtropical Gyre (STG) .

Relative abundance fluctuations of the different eco-morphotypes, during the interval between MISs 5.1 and 1, have shown that *G. cyclostomus* and *G. ruber*-k are the best indicators of cold-temperate climatic conditions. These eco-morphotypes are most abundant in correspondence with MIS from 4 to 2, especially during glacials, whereas they are almost absent during the interglacials (MISs 5.1 and 1). This latter observation suggests that these forms inhabited waters north and/or in proximity of the Azores Front Current System (AFCS). On the contrary, *G. ruber*-d and especially *G. elongatus* are considered as the best surface warm water indicators, in the Azores region, being more abundant during interglacial periods. Thus, these latter eco-morphotypes can be considered typical of the STG water masses. Finally, *G. elongatus* cf.1 and *G. ruber* s.s.-a, show respectively cool-temperate and warm-temperate affinities.

The variations in abundance of these eco-morphotypes have been used to track the position occupied by the Subtropical Gyre/Azores Front Current System (STG/AFCS) boundary, during the last 82 ka. Especially the ratio between the two best climatic indicators, *G. elongatu*s and *G. cyclostomus*, is usefull for monitoring the periodic latitudinal displacement of STG/AFCS boundary during time.

References

Alley, R.B. Macayeal, D. R., 1994 Ice-rafted debris associated with binge/purge oscillations of the Laurentide Ice Sheet. Paleoceanography 9 (4), 503-511.

Barker, S., Knorr, G. Edwards, R.L., Parrenin, F. Putnam, A.E., Skinner, L.C., Wolff, E., Ziegler, M., 2011. 800,000 years of abrupt climate variability. Science 334(6054), 347–351.

Bé, A.W.H., Tolderlund, D.S., 1971. Distribution and ecology of living planktonic foraminifera in surface waters of the Atlantic and Indian Oceans. In The Micropalaeontology of the Oceans (ds. B. H. Funnell and W. R. Riedel). Cambridge Univ. Press, London, pp. 105–149.

Bé, A.W.H., 1977. An ecological, zoogeographic and taxonomic review of recent planktonic foraminifera, in: A.T.S. Ramsey (Eds.), Oceanic micropaleontology. London: Academic Press, Vol. 1, pp. 1–100.

Beier, C., Turner, S.P., Plank, T., and White, W., 2010, A preliminary assess- ment of the symmetry of source composition and melting dynamics across the Azores plume: Geochemistry Geophysics Geosystems, v. 11, Q02004, doi: 10 .1029 /2009GC002833 .

Beier, C., Haase, K.M., Abouchami, W., Krienitz, M.-S., and Hauff, F., 2008, Magma genesis by rifting of oceanic lithosphere above anomalous mantle : Terceira Rift, Azores: Geochemistry Geophysics Geosystems, v. 9, Q12013, doi: 10 .1029 /2008GC002112 .

Bolli, H.M., Saunders, J.B., 1985. Oligocene to Holocene low latitude planktic foraminifers, in: Bolli, H.M., Saunders, J.B., Perch-Nielsen, K., Plankton Stratigraphy, Cambridge Earth Sciences Series, Cambridge University Press, pp. 165-262.

Bond, G., Broecker, W., Johnsen, S., McManus, J., Labeyrie, L., Jouzel, J., Bonani, G., 1993. Correlations between climate records from North Atlantic sediments and Greenland ice. Nature 365, 143-147.

Bradshaw, J.S., 1959. Ecology of living plank- tonic foraminifera in the North and equatorial Pacific Ocean, Contrib. Cushman Found. For- aminiferal Res., 10, 25–64.

Broecker, W.S., 1994. Massive iceberg discharges as trigger for global climate change. Nature 372, 421-424.

Dansgaard, W., Johnsen, S.J., Clausen, H.B., Dahl-Jensen, D., Gundestrup, N.S., Hammer, C.U., Hvidberg, C.S., Steffensen, J.P., Sveinbjörnsdottir, A.E., Jouzel, J.,

Bond, G., 1993. Evidence for general instability of past climate from a 250-kyr ice-core record. Nature 364, 218-220.

Detrick, B., Needham, H.D., Renard, V., 1995. Gravity anomalies and crustal thickness variations along the Mid-Atlantic Ridge between 33°N and 40°N. J. Geophys. Res. 100, 3767-3787.

Duplessy, J.C., 1999. Climate and the Gulf Stream. Nature 402, 593-595.

Emiliani, C., 1955. Pleistocene temperatures. Journal of Geology 63, 538-578.

Fox P.J., Lowrje, J.R., Heezen, B.C., 1969. Oceanographer fracture zone. Deep Sea Research 16, 59-66.

Guest, J.E., Gaspar, J.L., Cole, P.D., Queiroz, G., Duncan, A.M., Wallenstein, N., Ferreira, T., Pacheco, J.M., 1999. Volcanic geology of Furnas volcano, S. Migeul, Azores. J. Volcanol. Geotherm. Res. 92, 1–29.

Haug, G.H., Tiedemann, R., 1998. Effect of the formation of the Isthmus of Panama on Atlantic Ocean thermohaline circulation. Nature 393, 673-676.

Hays, J.D., Imbrie, J., Shackleton, N.J., 1976. Variations in the Earth's Orbit: Pacemaker of the Ice Ages. Science 194 (4270), 1121-1132.

Heinrich, H., 1988. Origin and consequences of cyclic ice rafting in the northeast Atlantic Ocean during the past 130,000 years. Quaternary Research 29, 142-152.

Hemleben, C., Spindler, M., Anderson, O.R., 1989. Modern Planktonic Foraminifera. New York, Springer.

Imbrie, J., Imbrie, J.Z., 1980. Modeling the climatic response to orbital variations. Science 207, 943-953.

Kucera, M., Schönfeld, J., 2007. The origin of modern oceanic foraminiferal faunas and Neogene climate change. In: Williams,M., Haywood, A.M., Gregory, F.J., Schmidt, D.N (Eds.), Deep-Time Perspectives on Climate Change: Marrying the Signal from Computer Models and Biological Proxies. TheGeological Society, London, pp. 409-426.

Kucera, M., Weinelt, M., Kiefer, T., Pflaumann, U., Hayes, A., Weinelt, M., Chen, M.-T., Mix A. C., Barrows, T.T., Cortijo, E. Duprat, J., Juggins, S., Waelbroeck, C., 2005. Reconstruction of sea-surface temperatures from assemblages of planktonic foraminifera: Multi-technique approach based on geographically constrained calibration datasets and its application to glacial Atlantic and Pacific Oceans. Quaternary Science Reviews 24, 951-998.

Kurase, D., Watkins, N., 1970. North atlantic crustal genesis in the vicinity of the Azores. Geophys. J. Astron. Soc. 19, 261-283.

Lisiecki, L.E., Stern, J.V., 2016. Regional and global benthic $\delta^{18}O$ stacks for the last glacial cycle. Paleoceanography 31, 1368-1394.

Lourenço, N., Luis, J.F., Miranda, J.M., Ribeiro, A., Victor, L.A.M., 1998. Morpho-tectonic analysis of the Azores volcanic plateau from new bathymetric compilation of the area.Mar. Geophys. Res. 20, 141–156.

Martrat, B., Grimalt, J.O., Shackleton, N.J., de Abreu, L., Hutterli, M.A., Stocker, T.F., 2007. Four climate cycles of recurring deep and surface water destabilizations on the Iberian Margin. Science 317, 502-507.

Milankovitch, M., 1930. Mathematische Klimalehre und astronomische Theorie der Klimaschwankungen, in: Handbuch der Klimatologie, edited by: Köppen, W. and Geiger, R., Vol. 1, Gebrüder Bornträger, Berlin 1-176.

Ottens, J.J., 1991. Planktic foraminifera as North Atlantic water mass indicators. Oceanol. Acta 14(2), 123–140.

Rabain, A., Cannat, M., Escartìn, J., Pouliquen, G., Deplus, C., Rommevaux-Jestin, C., 2001. Focused volcanism and growth of a slow spreading segment (Mid-Atlantic Ridge, 35°N). Earth and Planetary Science Letters 185, 211-224.

Rogl, F., Bolli, H.M., 1973. Holocene to Pleistocene planktonic foraminifera of Leg 15, Site 147 (Cariaco Basin (Trench), Caribbean Sea) and thier climatic interpretation, in : N.T. Edgar, Initial Reports of the DeepSea Drilling Project, Washington, D.C., U.S., Government Printing Office 15, 553-616.

Saito, T., Thompson, P.R., Breger, D., 1981. Systematic Index of Recent and Pleistocene Planktonic Foraminifera. University of Tokyo Press, Tokyo, pp. 1–190.

Schiebel, R., and Hemleben, C., 2005. Modern planktic foraminifera. Pala¨ontologische Zeitschrift 79, 135–148.

Schiebel, R., Waniek, J., Zeltner, A., Alves, M., 2002a. Impact of the Azores Front on the distribution of planktic foraminifers, shelled gastropods, and coccolithophorids. Deep Sea Res. Part II 49(19), 4035–-4050.

Schiebel, R., Schmuker, B., Alves, M., Hemleben, C., 2002b. Tracking the recent and late Pleistocene Azores front by the distribution of planktic foraminifers, J. Mar. Syst. 37(1-3), 213-227.

Schiebel, R., Waniek, J., Bork, M., Hemleben, C., 2001. Planktic foraminiferal production stimulated by chlorophyll redistribution and entrainment of nutrients. Deep-Sea Research I 48 (3), 721-740.

Shakleton, N.J., Opdyke, N.D., 1977. Oxygen isotope and paloeomagnetic evidence for early northern hemisphere glaciation. Nature 270, 216-219

Storz, D., Schulz, H. Waniek, J.J. Schulz-Bull, D.E., Kuçera M., 2009. Seasonal and interannual variability of the planktic foraminiferal flux in the vicinity of the Azores Current, Deep Sea Research Part I 56(1), 107-124.

Tolderlund, D.S., Bé, A.W.H., 1971. Seasonal distribution of planktonic foraminifera in the western North Atlantic. Micropaleontology 17, 297–329.

Vincent, E., Berger W.H., 1981. Planktonic foraminifera and their use in Paleoceanography. In: C. Emiliani (Ed.), The oceanic lithosphere. The sea (Vol. 7, pp. 1025–1119). Hoboken, N. J.: Wiley-Interscience.

White, W.M., Schilling, J.G., Hart, S.R., 1976. Evidence for the Azores mantle plume from strontium isotope geochemistry of the Central North Atlantic. Nature 263, 659-663.

Yang, T., Shen, Y., van der Lee, S., Solomon, S.C., Hung, S.H., 2006. Upper mantle structure beneath the Azores hotspot from finite-frequency seismic tomography. Earth and Planetary Science Letters 50 (1–2), 11–26..